Analysis of tunnel segment connection selection under differential settlement using a multi-criteria decision-making approach

Master Thesis Report

Wouter Wagenaars

Delft University of Technology



TU Delft

Analysis of tunnel segment connection selection under differential settlement using a multi-criteria decision-making approach

Master Thesis Report

by

Wouter Wagenaars





Thesis Committee:	Prof.dr.ir. E.O.L. Lantsoght	TU Delft
	Dr.ir. P.C.J. Hoogenboom	TU Delft
	Willem Smetsers	WSP Nederland

Faculty:	Faculty of Civil Engineering and Geoscience, Delft
Student Number:	55886619
Company:	WSP Nederland

Date:	11-08-2026
Status:	Final 7.0
Cover:	Image from NASA [1]

Preface

For the completion of the Master Civil Engineering at Delft University of Technology, I was looking for a graduation research that aligned well with my Structural Engineering track and specialization in concrete structures. At the same time, I wanted to explore possible directions for my future career. WSP provided me with this opportunity by supervising my graduation research and integrating me into the structural engineering team at the office in Breda.

This research provided me with the opportunity to further deepen my knowledge of tunnel structures while simultaneously developing my modeling skills in SCIA Engineer. The research also allowed me to incorporate geotechnical aspects through the use of PLAXIS.

Finally, I would like to thank several people who contributed to the completion of this thesis. First and foremost, I would like to express my gratitude to my daily supervisor, Willem Smetsers, for his knowledge, commitment, and valuable guidance throughout the project. I would also like to thank my thesis supervisors, Prof. dr. ir. E.O.L. Lantsoght and Dr. ir. P.C.J. Hoogenboom, for their supervision, feedback, and support during the graduation process.

I would also like to thank several colleagues at WSP for their valuable contributions to this research. I would like to thank Mark Hermans for our initial discussions and for introducing me to WSP. I am grateful to Niels van der Zee for his support regarding the geotechnical aspects of the research. In addition, I would like to thank Bram Erkelens and Johan Fokkinga for their assistance with structural engineering challenges. I am also grateful to Marco Flipse for sharing his knowledge and experience regarding construction practices and cost estimation.

Wouter Wagenaars
Delft, August 2026

Summary

Tunnels founded on shallow foundations experience settlements during their service life. As tunnel structures consist of multiple tunnel segments, differential settlements may occur and must be accommodated by tunnel segment connections. Various connection techniques are available for this purpose, each with its own characteristics. In addition, no standardized method currently exists for the design and selection of tunnel segment connections. This study therefore focuses on integrating settlement modeling, the determination of connection forces, the structural validation of connection variants, and the structured and reproducible selection of tunnel segment connections. The Oosterweelknoop project is used as a case study, considering the connections between four tunnel segments.

The study started with a literature review aimed at identifying decision-making methods, potential tunnel segment connections, and the associated design requirements. As a basis for the decision model, the Multi-Criteria Decision Analysis (MCDA) methods AHP and TOPSIS were selected. Based on the literature review, four connection concepts were identified for further development: a shear key, collar construction, dowel connection, and free-settlement joint.

Subsequently, an optimization study was carried out on the current design of the four Oosterweelknoop tunnel segments to compare the resulting connection forces. Particular attention was given to the application of lightweight EPS as embankment fill material. The connection forces were determined using the design methodology applied within the Oosterweelknoop project, which combines coupled PLAXIS 2D and SCIA Engineer 3D models. The results show that reducing the surcharge load leads to smaller differential settlements. At the same time, the stiffness of the subgrade decreases, resulting in lower force transfer to the foundation soil. Ultimately, this leads to a reduction in the connection forces compared with the existing design.

Next, a variant study was conducted in which the four selected connection concepts were further developed. Based on hand calculations, strut-and-tie models, and supplier information, the connections were designed and assessed against the applicable design requirements. The results demonstrate that all investigated variants satisfy the specified design criteria.

To compare the connection variants, a decision model was developed based on the two selected MCDA methods. The variants were evaluated with respect to structural safety, robustness, constructability, sustainability, service life, and costs. The assessment was based on project data from the case study, engineering input from WSP, and literature.

Based on the results, it is concluded that the dowel connection is the most suitable connection variant for the investigated tunnel segments within the Oosterweelknoop project. Compared to the current shear key design, the dowel connection requires less reinforcement detailing, is easier to integrate into the wall reinforcement layout, and reduces modelling complexity during the design process. As a result, it provides a more practical solution while maintaining the required structural performance. The developed methodology enables tunnel segment connections to be designed, evaluated, and compared in a transparent and reproducible manner.

Contents

Preface i

Summary ii

1 Introduction 1

1.1 Background and Context . . . 1
1.2 Research Problem . . . 2
1.3 Research Question . . . 2
1.4 Scope . . . 3
1.5 Methodology . . . 5

2 Literature review 7

2.1 Multi-Criteria Design Analysis (MCDA) methods . . . 7
2.2 Connection Variants . . . 8
2.3 Design Boundary Conditions . . . 12

3 Connection Force Analysis and Optimization 14

3.1 Flowchart . . . 14
3.2 EPS-Design . . . 16

4 Connection variants 21

4.1 Longitudinal Model . . . 22
4.2 Shear Key . . . 24
4.3 Collar Construction . . . 28
4.4 Dowel Connection . . . 30
4.5 Free-Settlement Joint . . . 32

5 Decision Model 35

5.1 MCDA Method . . . 35
5.2 Model . . . 36

6 Results 41

7 Discussion 44

8 Conclusion 45

References 47

A Case Study Oosterweelknoop **50**
A.1 Geological and Geotechnical Profile . . . 51

B AHP & TOPSIS Calculation Steps **53**

C Structural and Geotechnical Design Principles **57**
C.1 Structural Design Principles . . . 57
C.2 Geotechnical Design Principles . . . 65

D Methodology Optimization Analysis **67**
D.1 Plaxis 2D model . . . 67
D.2 SCIA 3D model . . . 70

E SCIA Longitudinal Model **76**
E.1 STD tunnel elements . . . 77
E.2 Shear Key Model . . . 82
E.3 Collar Construction Model . . . 88
E.4 Dowel Connection Model . . . 91
E.5 Free-Settlement Joint Model . . . 93

F Strut and Tie Models **94**

G Fatigue Spreadsheet Reinforcement **101**

H Elastomer Bearing Block **104**

I Detailing of Hanger Reinforcement in Consoles **106**

J Fatigue Spreadsheet Dowels **108**

K Design Dowel Connection **111**

L Joint Displacements without Structural Connection **116**
L.1 Vertical Displacements . . . 116
L.2 Horizontal Displacements . . . 117
L.3 Traffic Contribution . . . 119

M Properties Joint **121**

N Pairwise Comparison **123**

O Criteria Scoring **125**
O.1 Robustness . . . 125
O.2 Modeling Reliability . . . 129
O.3 Feasibility . . . 130
O.4 Sustainability . . . 132

O.5 Durability 137
O.6 Costs 139

P Decision Model A3 **140**

Q MCDA Method Validation **142**
Q.1 Sensitivity Analysis 142
Q.2 AHP Replaced by PSI 143
Q.3 TOPSIS Replaced by WSM 144
Q.4 TOPSIS Replaced by VIKOR 144
Q.5 Conclusion 145

1

Introduction

1.1. Background and Context

In urban areas where space for infrastructure is limited, underground infrastructure such as tunnel constructions can provide a solution for accommodating traffic flows while minimizing the impact on the above-ground environment. One possible foundation method for tunnels is a shallow foundation in which differential settlements over the service life of the tunnel must be taken into account.

To accommodate shrinkage, creep, and temperature effects, tunnels are constructed in segments with lengths ranging from 20 to 30 m. As a result, adjacent tunnel segments can undergo differential settlements over time due to:

- Construction phasing
- Varying subsoil conditions
- Varying surface loads at ground level
- Differences in geometry of the segments, such as width and length
- Differences in the depth of the segments

To ensure structural continuity, connections between tunnel segments are designed to resist differential settlements [2]. The relative displacements generate connection forces between adjacent segments. Several connection types are available to transfer these forces and control the differential settlements between the tunnel segments. Each connection type has specific advantages and disadvantages depending on the project conditions, deformation requirements, and magnitude of the connection forces.

The Oosterweelknoop, part of the Oosterweelverbinding project in Antwerp, is an ongoing infrastructure project involving the construction of a cut-and-cover tunnel on a shallow foundation. For this project, WSP and the client Lantis selected a concrete shear key connection for the tunnel segment connections. During the design and construction phases several challenges and engineering questions arose. These challenges form the basis of this research.

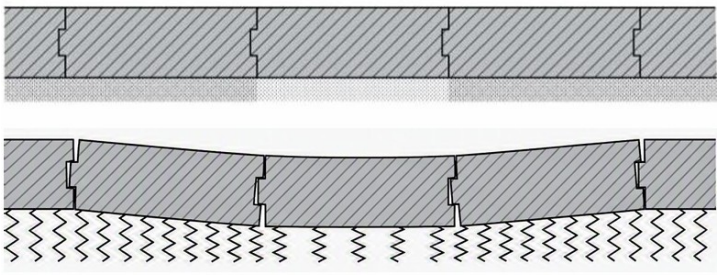

Figure 1.1: Differential settlements on tunnel segments with shear key construction [2]

1.2. Research Problem

The connections between tunnel segments in cut-and-cover tunnels are typically project-specific solutions. Variations in geometry, load conditions, construction phasing, and environmental factors mean that similar projects do not necessarily adopt the same connection type. In addition, significant freedom exists in the modeling approach used to determine settlements and the resulting connection forces. As a result, there is currently no standardized methodology that integrates the modeling of connection forces, the structural verification of connection variants, and the systematic assessment of alternatives within a single framework. This makes it difficult to objectively compare connection variants based on relevant criteria and to transparently justify design choices. Consequently, the design process becomes more complex and increases the likelihood of suboptimal solutions or solutions with an increased risk profile.

The tunnel at the Oosterweelknoop provides a relevant case study for investigating this engineering problem. Variations in subgrade stiffness, phased construction, and the availability of multiple connection types create a design environment in which a structured decision-making framework would be valuable. The concrete shear key adopted in the current design introduces challenges related to both constructability and modelling. The high reinforcement content required around the connection is difficult to integrate into the wall reinforcement detailing. Uncertainties also remain regarding the most appropriate modelling approach for the shear key and the resulting determination of the connection forces. Furthermore, opportunities exist to optimize the connection forces, allowing an analysis of the current shear key design. These optimizations may also create additional opportunities for alternative connection variants by reducing the governing connection forces [3].

1.3. Research Question

This research focuses on the research questions that guide the further exploration of the topic. The main question serves as the starting point, supported by several sub questions which together define the full scope of the research.

Main question

How can a systematic decision-making approach be used to determine the most suitable tunnel segment connection for the Oosterweelknoop?

Sub questions

1) *What requirements and design conditions apply to tunnel segment connections in cut-and-cover tunnels founded on shallow foundations?*

2) *What connection techniques are described in literature for cut-and-cover tunnels founded on shallow foundations, what are their characteristic properties, and which structural checks are required to verify their safety?*

3) *How do changes in surface loading influence the differential settlements and the resulting connection forces between tunnel segments?*

4) *How can a multi-criteria decision analysis model be developed to evaluate and rank tunnel segment connections based on cost, feasibility, technical performance and sustainability?*

1.4. Scope

For this study, project parameters including the geotechnical data, construction phasing, and geometry of tunnel segments STD-10, STD-11, STD-12, and STD-13, which form part of the Oosterweelknoop project in Antwerp (Appendix A), were used. These tunnel segments define the scope of the study and serve as the basis for answering the research questions. The tunnel segments are 25 m long and, together with the STD tunnel tube, form an access road from the port area to the R1. The location of these tunnel segments within the combined tunnel alignment is shown in Figure 1.2.

The four selected tunnel segments form a representative and feasible section of the Oosterweelknoop within the scope of this research. They are founded using the same foundation method and are subjected to similar load transfer mechanisms and force distributions as the other tunnel segments. The selected segments therefore provide a suitable basis for the development and evaluation of alternative segment connection variants.

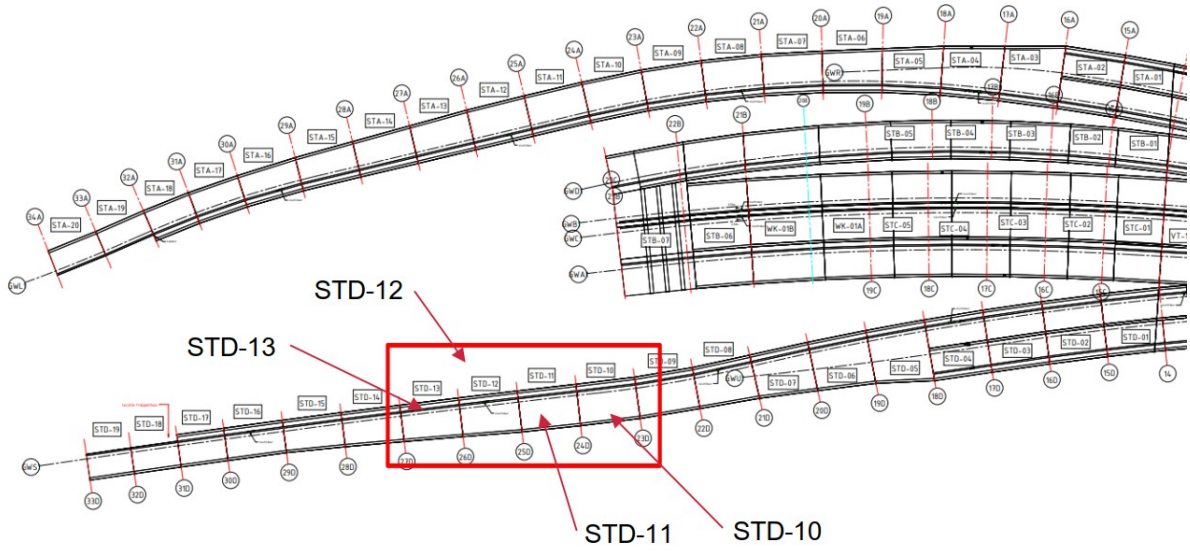

Figure 1.2: Top view of the combined tunnels showing tunnel segments STD-10 to STD-13 [4]

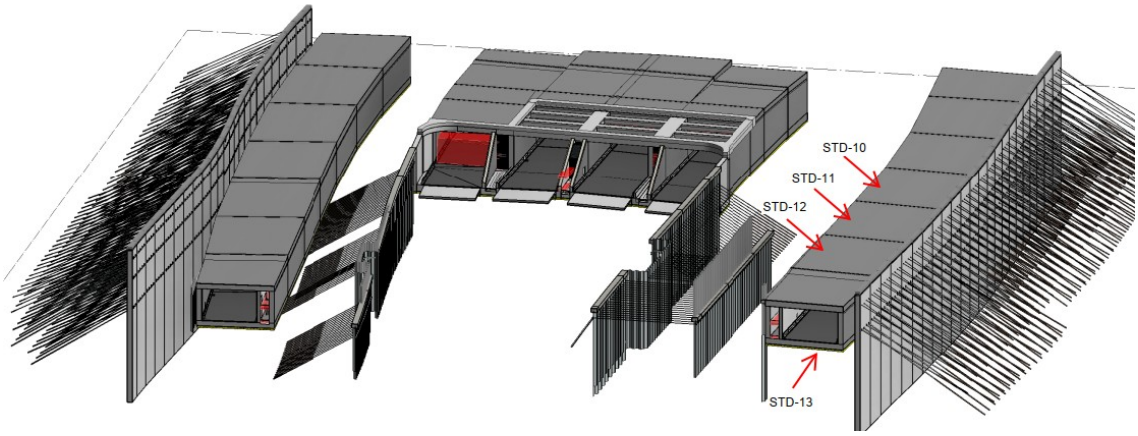

Figure 1.3: 3D cross-section of a part of the combined tunnels showing tunnel segments STD-10 to STD-13 [5]

The tunnel elements are founded on shallow foundations and are connected by a structural connection consisting of a shear key in the walls (Figure 1.4a) and a shear key extending across the full width of the floor. For this research the wall shear key is considered in particular. This connection mainly transfers the transverse forces that arise from long-term actions, such as soil settlement and other permanent loads. Due to the relatively stiff behavior of the tunnel walls, these shear forces are concentrated primarily in the wall shear key.

The STD tunnel tube consists of a traffic lane and an emergency passage separated by an intermediate wall. A concrete overhang is provided along the northern side of the tunnel roof to retain the soil above the structure. The geometry and dimensions of tunnel segments STD-10 to STD-13 are shown in Figure 1.4.

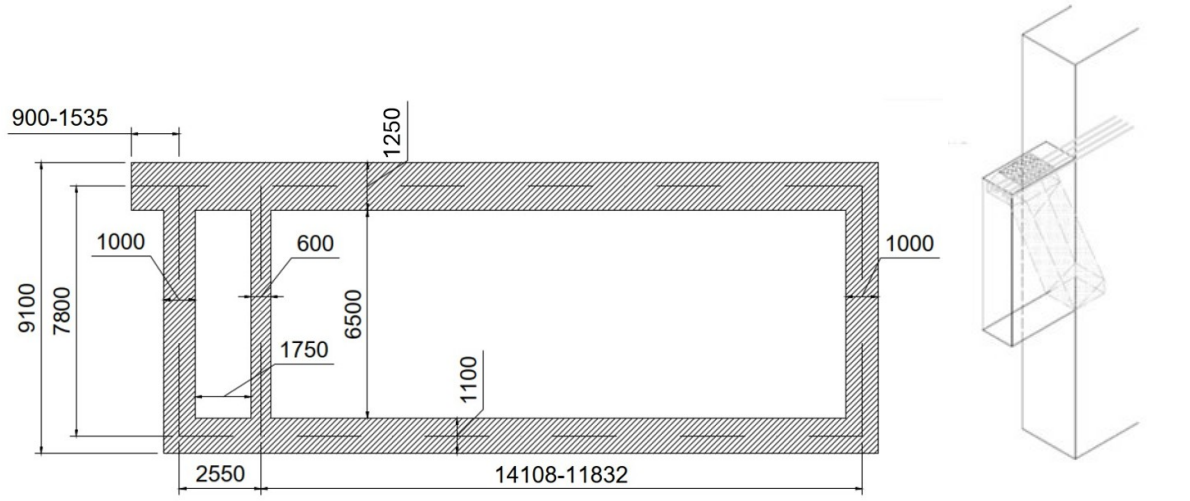

(a) Cross–section of the STD tunnel segment

(b) 3D visualization of the wall shear key connection

Figure 1.4: Overview STD tunnel tube [4]

1.4.1. Existing design information

Existing analyses and design documentation from the Oosterweelknoop project have been used as an information source. The following project information has been consulted:

- *SCIA Engineer 3D longitudinal analysis*: Determination of the global force distribution and structural deformations.
- *PLAXIS 2D cross-sectional analyses*: Geotechnical assessment of settlements and subgrade stiffnesses beneath the tunnel segments for various soil parameter sets.
- *Structural Design Basis Report*: Design principles, structural concepts and design guidelines for the Oosterweelknoop tunnel structures.
- *Shear Key Calculation Report*: Structural design and verification of the existing shear key connection based on a strut-and-tie model in accordance with EN 1992-1-1.

1.5. Methodology

A research approach was followed to answer the main and sub-research questions. This approach is visualized in the flowchart shown in Figure 1.5. The research methodology consists of four interconnected research steps that are explained in Chapters 2 to 5.

1.5.1. Flowchart

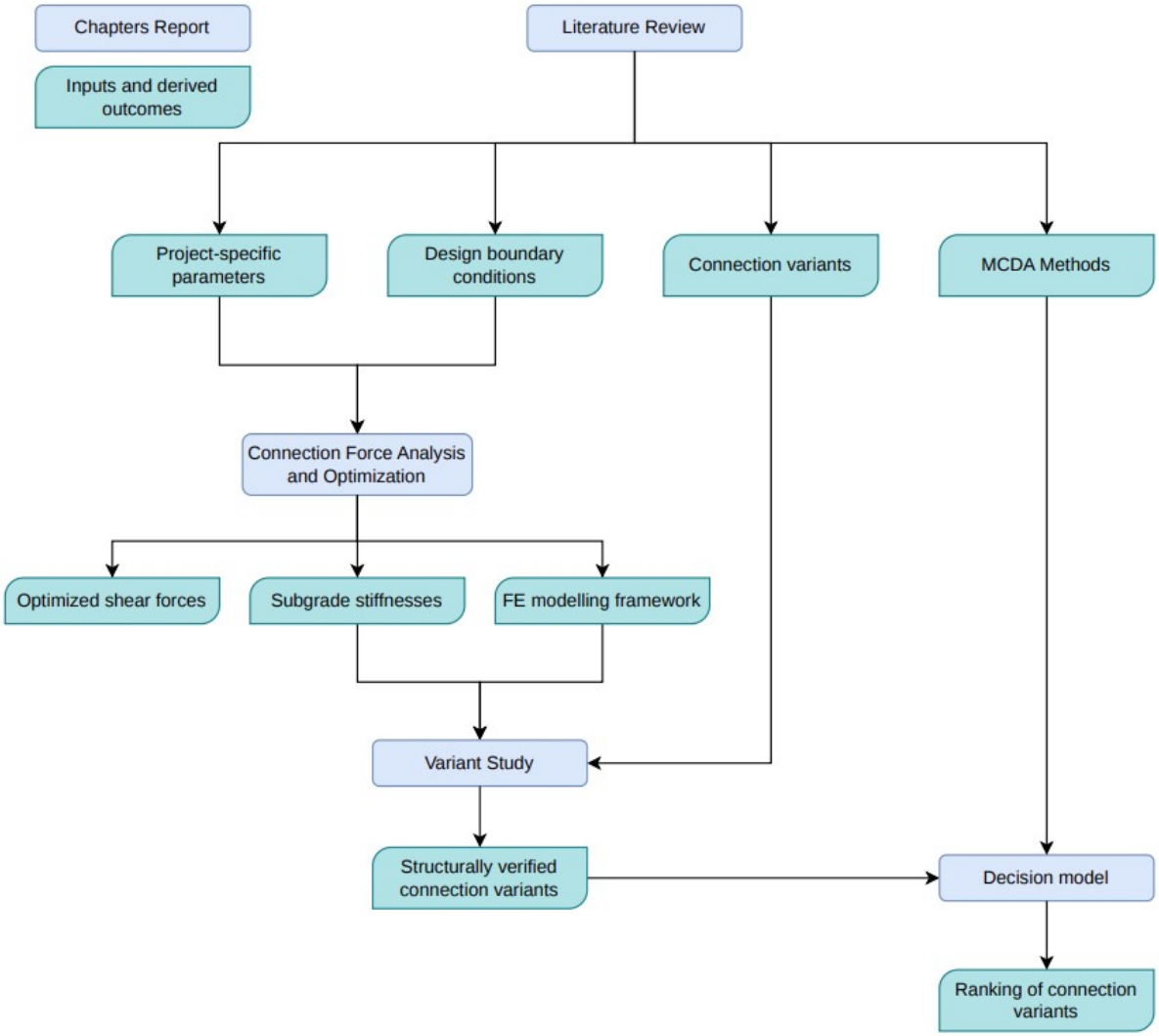

Figure 1.5: Flowchart

1.5.2. Description of the flowchart

Literature Review (Chapter 2)

The literature review forms the basis of the research. This includes:

- Research into suitable MCDA methods for various tunnel segment connections.
- Identification of possible variants for the segment connection for tunnels on shallow foundations.
- Collection of relevant structural and geotechnical parameters from standards, guidelines, and project documentation.

The literature review results in documented input that guides further analysis, modeling, and variant development. The focus is on identifying, selecting, and organizing the information needed for the following steps of the research.

Connection Force Analysis and Optimization (Chapter 3)

The optimization analysis investigates the effect of a lightweight fill material on the shear forces in the segment connections of the STD tunnel segments. To evaluate this optimization measure, existing finite element models developed for the Oosterweelknoop project in PLAXIS and SCIA Engineer are used and adapted.

The analysis provides insight into the influence of the optimization measure on the soil–structure interaction, expressed in terms of subgrade stiffnesses and shear forces between the tunnel segments. In addition, the optimization analysis establishes a finite-element modeling framework for assessing the force transfer in the segment connections. These outputs are subsequently used in the variant study for the development and evaluation of the connection variants.

Variant Study (Chapter 4)

In the variant study, the connection concepts identified in the literature review are translated into practical and structurally verifiable designs. The objective is to gain insight into the structural behavior, required dimensions, and material quantities of the different connection variants.

The finite element modeling framework developed during the optimization study is used to determine the subgrade stiffness and develop a finite element model for each variant. The resulting designs are verified in both the Ultimate Limit State (ULS) and Serviceability Limit State (SLS).

Decision Model (Chapter 5)

The decision model evaluates the structurally verified connection variants using two MCDA methods selected during the literature review. The model follows a hierarchical structure consisting of the variants, main criteria, and subcriteria. The assessment of the criteria is based on information obtained from the literature, project-specific data, and engineering judgment. The output is a ranking of the variants and the identification of the preferred connection for the Oosterweelknoop case study.

2

Literature review

This chapter describes the literature review conducted for this research. The review consist the selection of a suitable MCDA method, the identification of potential connection concepts for shallow-founded tunnels, and the collection of relevant structural and geotechnical parameters from standards, guidelines, and project documentation. The results provide the input for the development, modeling, and assessment of the connection variants.

2.1. Multi-Criteria Design Analysis (MCDA) methods

Various MCDA methods were reviewed for application in the decision model for tunnel segment connections. The methods were evaluated based on their characteristics, complexity, and suitability for engineering decision-making problems involving both qualitative and quantitative criteria. The reviewed methods included VIKOR, PSI, Fuzzy AHP, DEMATEL, EA-FAHP, the Analytic Hierarchy Process (AHP), and the Technique for Order Preference by Similarity to Ideal Solution (TOPSIS). From these methods, AHP and TOPSIS were identified as the most suitable approaches for this research. These methods can be applied individually or combined in a hybrid framework. The calculation steps and formulas of the two methods are provided in Appendix B.

2.1.1. Analytical Hierarchy Process (AHP)

The Analytic Hierarchy Process (AHP) was developed by Saaty (1980) and is a widely used MCDA method for decision-making problems involving multiple qualitative and quantitative criteria. The method structures the problem into a hierarchy consisting of the goal, the criteria (and any sub criteria) and the alternatives [6].

AHP uses pairwise comparisons, whereby elements within the same level are compared in pairs. These comparisons are expressed on a numerical scale from 1 to 9, where 1 means equal importance and 9 means extremely greater importance. The method is based on four principles: reciprocity, consistency, dependence between levels, and re-evaluation in the event of changes in the hierarchy [7].

2.1.2. Technique for Order Preference by Similarity to Ideal Solution (TOPSIS)

The Technique for Order Preference by Similarity to Ideal Solution (TOPSIS) was developed by Hwang and Yoon (1981) and works according to the principle of the ideal solution. The method is based on the principle that the best choice is the alternative that is closest to the positive ideal solution (PIS) and furthest from the negative ideal solution (NIS) [8].

The PIS represents the best possible performance on all criteria (maximisation of benefit criteria and minimisation of cost criteria), while the NIS represents the worst possible performance. By determining the relative distance of each alternative to these two reference points, TOPSIS can identify the most suitable option in a transparent and intuitive manner. The method is explained in the following steps, supplemented with the corresponding mathematical formulations [7] [9].

2.2. Connection Variants

To identify suitable connection concepts for shallow-founded tunnel segment joints, the Tunnel Construction Handbook (Handboek Tunnelbouw), SATO, and various reference projects were reviewed. Based on this review, three connection concepts were selected that are capable of transferring connection forces between adjacent tunnel segments:

1. Collar construction
2. Shear key
3. Dowel connection

Finally, there is the option of allowing settlements to occur. In this case, settlements are accepted and must be accommodated by other structural components, such as the waterproofing and expansion joint systems.

2.2.1. Shear key

The shear key connection consists of a console side and a recess side that interlock at the location of the tunnel segment joint. The connection can be constructed in either steel or concrete. In practice, a concrete solution is often adopted because the connection can be easily integrated into the tunnel element and compressive forces can be efficiently transferred through the concrete.

The connection forces are transferred through concrete compression struts that distribute the forces from the shear key into the surrounding structure. The geometry of the concrete console allows connection forces to be transferred both upwards and downwards. In many cases, the consoles are provided with bearing blocks that ensure controlled force transfer and allow limited rotations between adjacent tunnel segments. When the shear key connection is applied in the tunnel walls, it offers considerable design flexibility because the available wall height can be used to adjust the dimensions and load-carrying capacity of the console to the applied loads. A disadvantage of this connection is that the bearing blocks require inspection, maintenance, and fire protection [2].

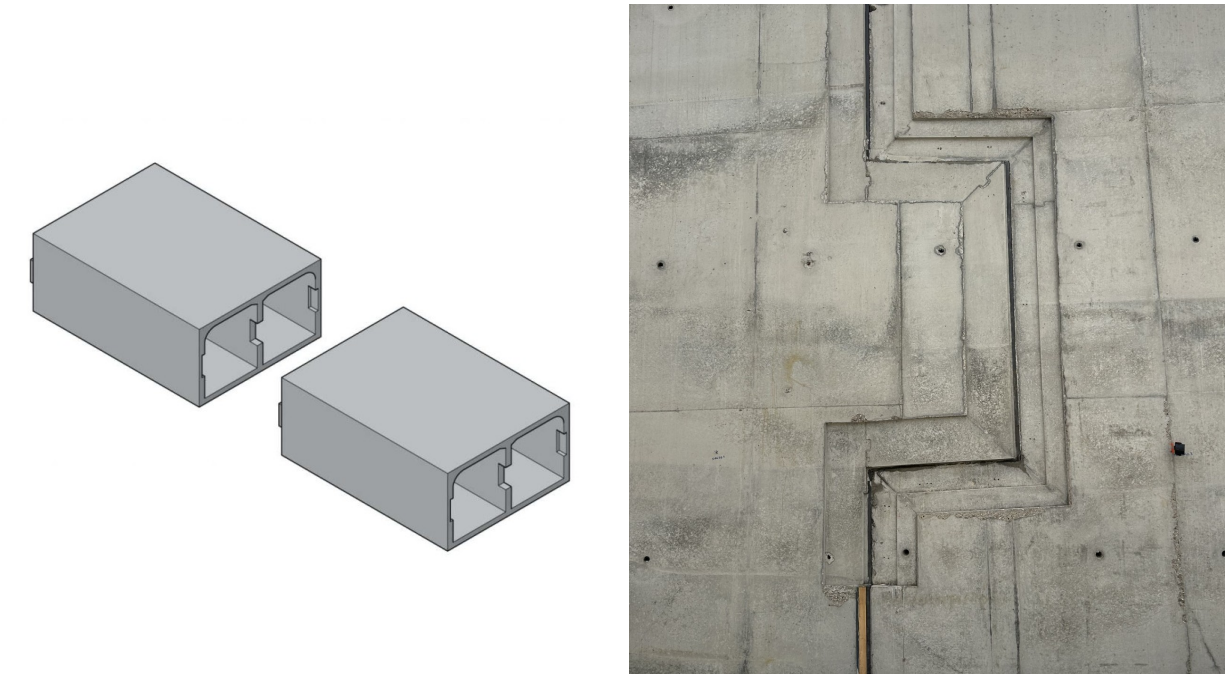

Figure 2.1: Illustration of a shear key connection between two tunnel segments (left) [2] and the implementation of a shear key connection in the Oosterweelknoop project (right)

2.2.2. Collar construction

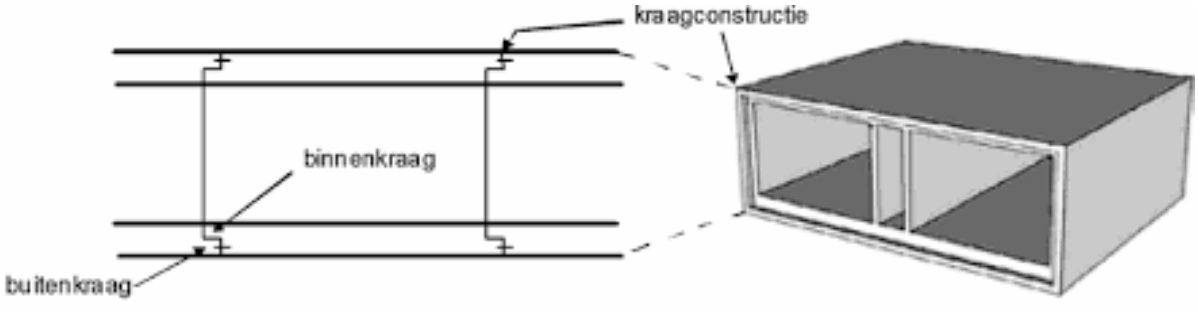

Figure 2.2: Tunnel segment joint with a collar connection around the entire cross-section [10]

The collar connection consists of a connection integrated into the perimeter of the tunnel and therefore extends through the floor, outer walls, and roof of the tunnel. The connection consists of an inner collar and an outer collar that interlock along the entire perimeter. This allows shear forces to be transferred between adjacent tunnel segments. Load transfer takes place through the bearing surface between the inner and outer collar, resulting in compressive stresses in the concrete [10].

When differential settlements occur between two tunnel segments, only one of the two collars can be activated. If segment A settles relative to segment B, the collar connection in the floor will transfer the shear force while the collar connection in the roof does not transfer any force. In the case of settlement in the opposite direction, the collar connection in the roof is activated instead. As a result, only one of the two collar connections governs the load transfer at any time (Figure 2.3).

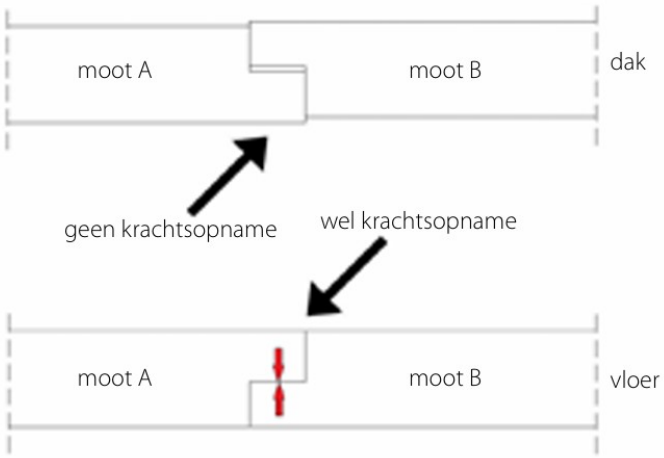

Figure 2.3: Force transfer in a collar connection when segment A settles relative to segment B [10]

The collar connection has the disadvantage that a concentrated pressure point develops at the top or bottom of the wall during the transfer of shear forces. Due to the high stiffness of the walls, a large portion of the shear force is transferred through this cross-section. As a result, high local stresses occur and a significant amount of reinforcement is required in the collar connection. In addition, the waterproofing profile must be installed in the same zone, meaning that waterproofing and force transfer are integrated into a single detail. Crack formation may therefore directly lead to leakage into the tunnel. Furthermore, the design freedom is limited because both the connection and the waterproofing detail must be accommodated within the same available structural depth [2].

2.2.3. Dowel connection

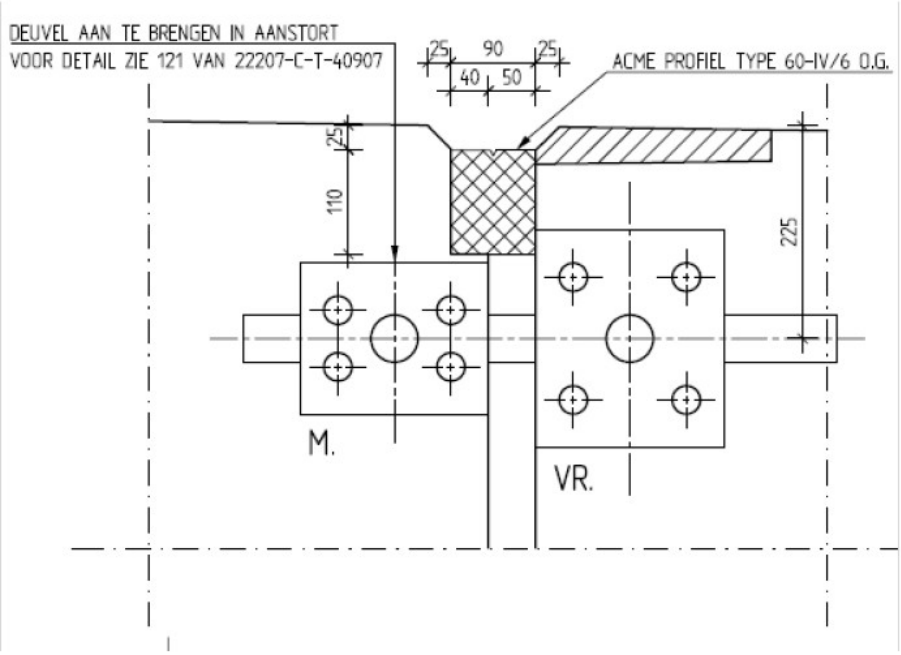

Figure 2.4: Steel dowel connection in the tunnel floor [2]

The dowel connection consists of stainless steel pins that are cast into the tunnel structure across the joint. To anchor the dowels, they are provided with steel anchor plates and transverse anchors. Due to this detailing, the bending point of the dowel is located outside the concrete, allowing the forces to be transferred into the concrete through a punching mechanism [11]. The dowel connection can accommodate deformations resulting from temperature variations, shrinkage, and limited settlements [12]. Various configurations and suppliers of dowel connections are available. An example is the Double Shear Dowel Type Q (DSDQ) supplied by Leviat and Hakron (Figure 2.5).

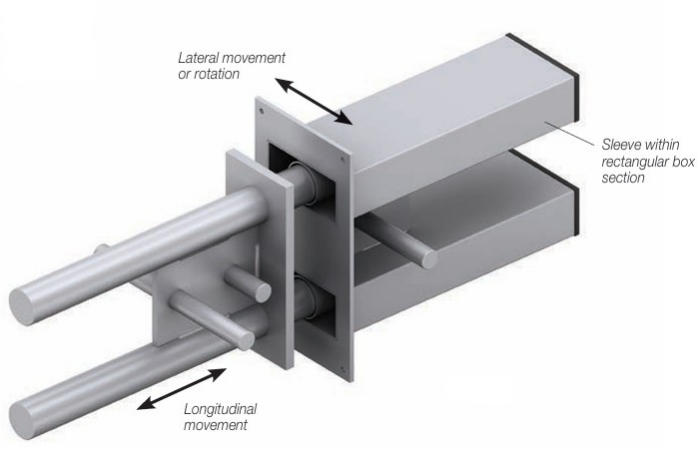

Figure 2.5: 3D visualization DSDQ dowel [12]

2.2.4. Free-settlement joint

In contrast to structural connections, the free-settlement joint allows relative displacements between adjacent tunnel segments. As a result, no connection forces are transferred between tunnel segments. The joint therefore only needs to accommodate the occurring displacements through other structural components, such as the joint system and the waterproofing profile.

Because the tunnel segments are free to settle and rotate, not only the usual deformations resulting from temperature effects and shrinkage but also the relative vertical and horizontal displacements between tunnel segments must be accommodated. In this regard, the joint in the road surface is governing. The relative displacements may lead to differences in asphalt level, requiring a joint system that can accommodate these movements throughout the design service life. In addition, the joint profile and waterproofing profile must remain capable of accommodating the expected displacements.

2.2.5. Overview

Table 2.1: Connection variants – advantages, disadvantages, practice examples

Connection variant	**Advantages**	**Disadvantages**	**Practice examples**
Shear Key	Applicable in tunnel walls with high design flexibility	Bearing blocks require inspection, maintenance, and fire protection	Scheldetunnel; Oosterweelknoop
	Connection forces can be transferred in both directions within the same detail	Sensitive to stress concentrations at the shear key	
	Suitable for accommodating rotations		
Collar connection	Very stiff connection	Waterproofing and force transfer integrated into a single detail	Drechtunnel; Noordtunnel
	Simple force transfer through concrete compression	High local stresses caused by a concentrated bearing point at the top or bottom of the wall	
		Limited design flexibility due to integration within the wall and roof structure	
Dowel connection	Prefabricated systems can be directly integrated into the formwork	Hard to inspect or replace (fixed after installation)	A2 tunnel at Maastricht
	Accommodates horizontal displacements such as shrinkage and temperature effects	Limited rotational capacity	
Free-settlement joint	No transfer of connection forces	Asphalt joints have a limited service life and require frequent maintenance	HSL (Northern Holland)
	Ensures smooth driving comfort (e.g. through transition plates or asphalt joints)	Displacement may affect tunnel free profile	

2.3. Design Boundary Conditions

The design of the connection variants starts with defining the design requirements. The codes and guidelines are determined based on the location of the case study. Some design parameters fall outside the scope of this study and are therefore adopted from the Oosterweelknoop project. These include structural and geotechnical parameters. Together the codes and project-specific parameters define the boundary conditions within which the connection variants are designed.

2.3.1. Normative standards and guidelines

As for the Oosterweelknoop, Standaardbestek 260 (SB260) is used for this research. SB260 is the Flemish Standaardbestek for engineering structures and hydraulic engineering constructions and brings together all the common provisions for implementation. SB260 supplements the NBN EN series of Eurocodes, which cannot be viewed separately from each other. Within this study, only Chapter 21 – Design, study and calculation notes is relevant, as it sets out the structural requirements and principles for the tunnel connection [13].

Version 2a (2021) of SB260 is adopted because the current Oosterweelknoop design is based on this version. In addition, the client Lantis has specified project-specific requirements that supplement Chapter 21 of SB260 [14]. These requirements are adopted as leading design criteria within this study.

Finally, the ROK (Richtlijnen Ontwerp Kunstwerken) is used in the Netherlands as a national supplement to the Eurocodes. The ROK has no normative status in Belgium and is therefore not applicable within this study. However, where relevant, the ROK is used as a guideline to support design choices [15]. The following ranking order is used for this study:

1. Additions to Standaardbestek 260 (SB260–C.4.3.2.21)
2. Standaardbestek 260 (SB260–21.), Eurocodes (EN 1990 – EN 1999)
3. Richtlijnen Ontwerp Kunstwerken (ROK)

2.3.2. Structural design principles

This section provides an overview of the structural design principles and requirements adopted throughout this research. A detailed overview, including references to the relevant SB260 chapters, is provided in Appendix C.1.

The following structural design principles are considered:

- Material properties of concrete and steel, including strength class, concrete cover, maximum crack width, and exposure and environmental classes
- Safety level (CC3)
- Settlement requirements, including a maximum total settlement of 50 mm and a maximum relative displacement of 5 mm for connections without structural coupling and transition plates in the SLS quasi-permanent load combination
- Joint movements, including the current expansion and watertightness design of the Oosterweelknoop project
- Loads, including traffic load models LM1 and LM3, shrinkage, temperature effects, and permanent surface loads
- Load combinations and partial factors

2.3.3. Geotechnical design principles

This section provides an overview of the geotechnical parameters that are used in the designing of the tunnel segment connection variants. Since the determination of these parameters falls outside the scope of this research, project-specific parameters from the Oosterweelknoop project are used. These parameters are used as input for the finite element software Plaxis to determine the soil behavior over the service life of the STD tunnel segments. A detailed overview of the geotechnical parameters that are adopted for the design an analysis of the connection variants is provided in Appendix C.2.

The following geotechnical design principles are adopted from the Oosterweelknoop:

- Soil layers and their properties, including unit weight, density, and strength parameters
- Compressibility parameters
- Stiffness parameters of the Hardening Soil Small Strain (HS-Small) model
- Horizontal subgrade stiffness
- Two subsoil behavior variants (UA1 and UA3) with a factor of $\sqrt{2}$ applied to permeability and stiffness to account for geotechnical uncertainty

Table 2.2: Governing geotechnical parameters of the soil layers supporting the STD tunnel segments

Layer	γ_{unsat} [kN/m^3]	ϕ' [°]	c' [kPa]	E_{50}^{ref} [MPa]	E_{oed}^{ref} [MPa]	m [-]
Kd	17.0	37.5	1	96.0	96.0	0.5
BK0 UA1	20.0	26.0	20	10.0	7.0	0.0
BK0 UA3	20.0	26.0	20	5.0	3.5	0.0
BK1 UA1	20.0	26.0	20	15.0	10.0	0.7
BK1 UA3	20.0	26.0	20	7.5	5.0	0.7

3

Connection Force Analysis and Optimization

This chapter examines the extent to which optimizing the tunnel structure can help reduce the shear forces in the joints between the STD tunnel segments. These shear forces are critical for the detailing of the segment joints.

Several potential optimization measures were identified, including changes to the installation sequence of the connection, soil preloading, soil improvement, and the use of longer tunnel segments [3]. Of these measures, only the application of lightweight backfill material above the tunnel tube was further investigated. This optimization reduces the surface load acting on the tunnel structure and its influence on the resulting connection forces is evaluated in this chapter.

On the one hand, the optimization analysis aims to reduce the shear forces in the connections between the STD tunnel segments, thereby enabling the design of the connections to be optimized. This could lead to more efficient detailing, such as reducing reinforcement or increasing safety. The second aim of the analysis is to gain insight into the origin and transfer of shear forces between the tunnel segments. By evaluating a single optimization, a reference framework is created for the development of alternative variants. The insights gained into the influence of relevant parameters and mechanisms contribute to the modeling and evaluation of variants that can ultimately be incorporated into the decision-making model.

3.1. Flowchart

The procedure for the optimization analysis is shown schematically in Figure 3.1. The flowchart provides an overview of the consecutive steps followed to quantify the effect of an optimization measure.

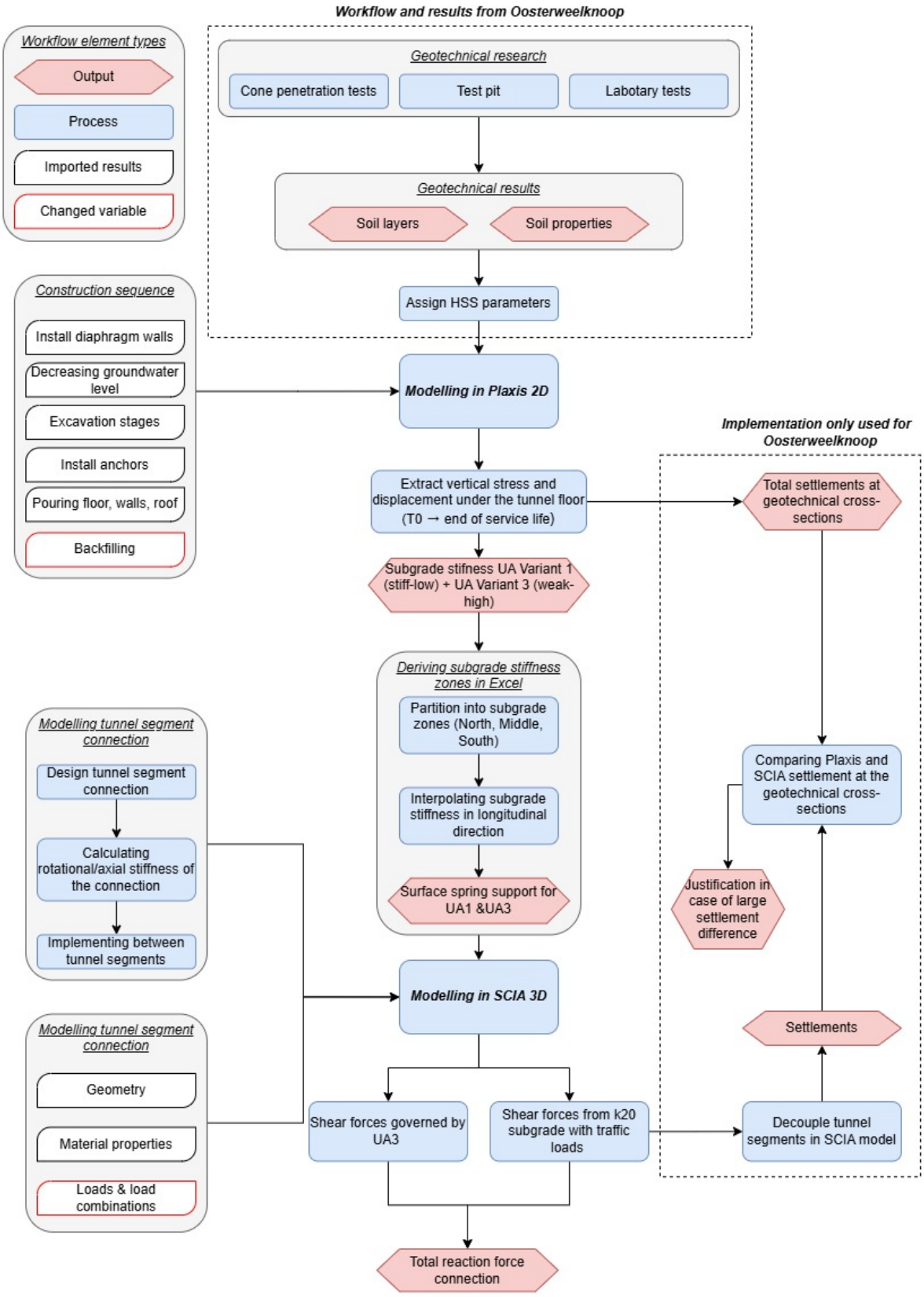

Figure 3.1: Flowchart optimization analysis of the connection forces

Scope and Application of the Models

The geotechnical analysis is built on existing numerical models developed within the Oosterweelknoop project. For the Plaxis 2D cross-section model, in consultation with the geotechnical engineer [16], the applied phasing with corresponding time intervals, the soil structure beneath the tunnel, and the tunnel geometry were adopted. These components were not re-modeled.

Within this existing model, the upper soil layers and the associated time-dependent loads were modified so that they matched the optimization model. The modified variants were then recalculated. The resulting stress and displacement developments were extracted and processed in Excel to obtain and visualize the required subgrade stiffnesses.

Within the SCIA model, the subsoil and the static loads were re-modeled. The subgrade stiffnesses derived from Plaxis 2D were applied to describe the interaction between the structure and the subsoil. The geometry of the tunnel segments was directly imported from an existing model from the Oosterweelknoop project. The results were analyzed and interpreted in this chapter.

For a detailed description of the relationship between the Plaxis 2D and SCIA 3D models, refer to Appendix D.

3.2. EPS-Design

In the final configuration, the tunnel tube will be covered by a layer of soil approximately 5 meters thick. In the original design, sand with a unit weight of 18 kN/m^3 was selected for the backfill. Because an embankment has been designed along the longitudinal direction of tunnel segments STD-9 to STD-16, there are opportunities to significantly reduce the dead load on the tunnel roof by using lightweight backfill material such as EPS.

Standard EPS100 is frequently used in practice as a lightweight backfill material due to its low mass density of 0.40 kN/m^3 [17]. In combination with a top layer of one meter of sand, EPS offers an option to significantly reduce the dead weight of the backfill. The design of the cross-section of STD–10 is shown in Figure 3.2 where the EPS backfill is indicated in pink.

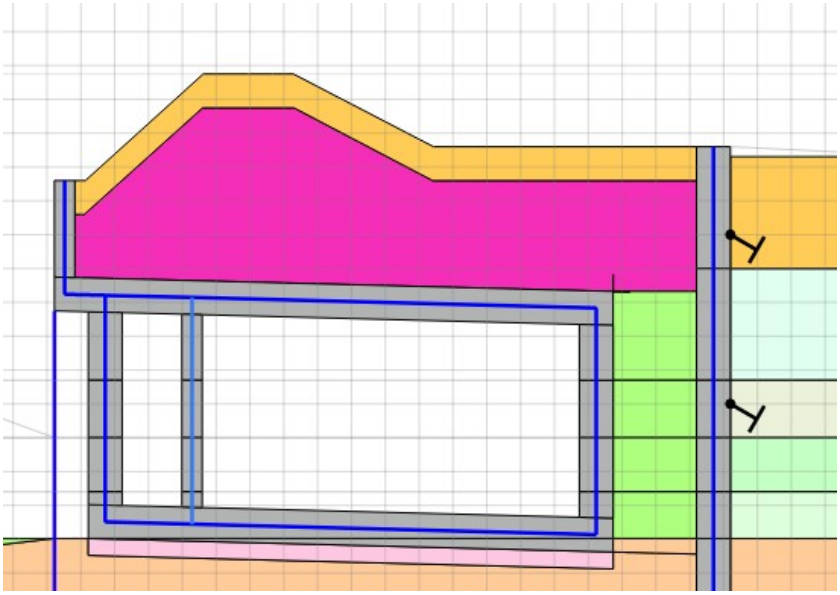

Figure 3.2: Cross-section of tunnel segment STD-10 with EPS design (north on the left, south on the right)

Plaxis Model

The EPS100, with its corresponding material properties from the literature [17], was implemented in the Plaxis 2D models at the geotechnical cross-sections S01 and S06B. The soil was modeled using the governing UA3 HSS parameters, representing the most critical stiffness conditions for assessing the resulting transverse forces.

The EPS layer was activated in the relevant construction phase, fully consistent with the provided execution sequence. In this phase, the original sand backfill was replaced by the lightweight EPS material so that the influence of the reduced vertical loading can be analyzed for stresses and deformations beneath the tunnel floor.

The vertical stresses and displacements directly beneath the tunnel floor are then extracted from the Plaxis results to determine the subgrade stiffness across the width of the cross-section. The resulting subgrade stiffnesses for both S06B and S01 are shown in Figure 3.3 for the original situation (green) and the optimized situation (orange) with EPS.

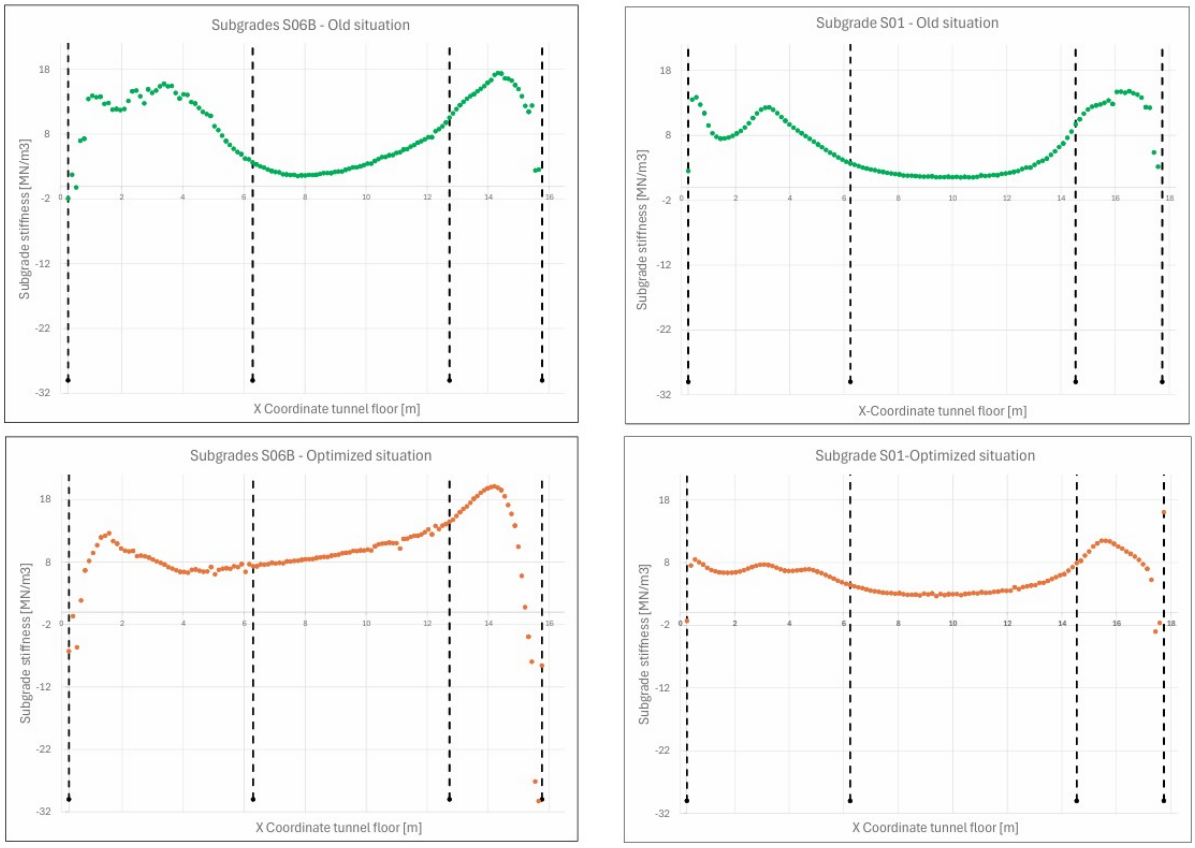

Figure 3.3: Subgrade stiffness at geotechnical cross-sections S06B and S01 for the original and optimized (EPS) situations

A change is noticeable in the subgrade stiffness values for tunnel segments STD-9 to STD-15. Specifically, the subgrade stiffness decreases beneath the zones located under the two walls (north and south from Figure 3.2), while the subgrade stiffness in the central zone increases.

This behavior can be explained by the reduction in vertical load acting on the tunnel walls as a result of the decreased dead load on the tunnel roof. Due to this load reduction, the vertical displacement of the tunnel walls decreases. At the same time, the reduced vertical loading leads to smaller bending deformations of the tunnel walls, which in turn results in less upward bending of the tunnel floor. As a consequence, the calculated subgrade stiffness beneath the central part of the floor increases compared to the reference situation.

Finally, for the tunnel segments that do not lie directly on the geotechnical cross-sections S06B and S01, the subgrade stiffnesses were determined by linear interpolation between the two sections. The geotechnical cross–sections located beneath other STD tunnel segments, such as the adjacent cross–sections S06A and S02, were retained from the original model, as they fall outside the scope of this study. Consequently, no extrapolation of subgrade stiffness values beyond the range defined by the cross–sections S06B and S01 was performed. A complete overview of the subgrade stiffness values is shown in Figure 3.4.

Subgrade stifnses current design [MN/m3]

Segment	geotechnical cross	Tunnel tube 5		
		N	M	S
STD-1		9,15	3,25	9,65
STD-2	S07	8,80	2,10	7,70
STD-3		6,75	1,90	6,75
STD-4	S03	4,70	1,70	5,80
STD-5		3,70	1,50	6,55
STD-6	->S05	2,70	1,30	7,30
STD-7		4,25	1,55	9,60
STD-8	S02	5,80	1,80	11,90
STD-9		6,80	2,17	12,07
STD-10		7,80	2,53	12,23
STD-11	S01	8,88	2,90	12,40
STD-12		9,95	3,45	13,05
STD-13	S06B	11,10	4,00	13,70
STD-14		9,63	5,17	11,33
STD-15		8,17	6,33	8,97
STD-16	S06A	6,70	7,50	6,60

Subgrade stifnses optimized design [MN/m3]

Segment	geotechnical cross	Tunnel tube 5		
		N	M	S
STD-1		9,15	3,25	9,65
STD-2	S07	8,80	2,10	7,70
STD-3		6,75	1,90	6,75
STD-4	S03	4,70	1,70	5,80
STD-5		3,70	1,50	6,55
STD-6	S05	2,70	1,30	7,30
STD-7		4,25	1,55	9,60
STD-8	S02	5,80	1,80	11,90
STD-9		***6,09***	***2,48***	***11,11***
STD-10		***6,37***	***3,17***	***10,33***
STD-11	S01	***6,66***	***3,85***	***9,54***
STD-12		***7,37***	***6,95***	***10,27***
STD-13	S06B	***8,08***	***10,06***	***11,01***
STD-14		***7,62***	***9,21***	***9,54***
STD-15		***7,16***	***6,14***	***6,36***
STD-16	S06A	6,70	7,50	6,60

Figure 3.4: Overview of subgrade stiffness values (UA3 variant) for the current and optimized EPS design

SCIA Model

In the SCIA model, the subgrades are modeled in the vertical direction beneath the tunnel segments as surface spring supports. To prevent tensile forces from being transmitted into the ground, a manually defined F-u function has been applied to these springs, ensuring that the spring can only generate compressive forces. In the horizontal and longitudinal directions, 10% of the vertical subgrade stiffness is used as a friction component, in accordance with engineering judgment from the Oosterweelknoop project.

In addition to the subgrade stiffnesses, the application of lightweight backfill material also changes the soil load on the roof of the tunnel segments. In the SCIA model, this load is divided into a surface load and a free surface load, distributed over the width of the embankment. The width of the free surface load is taken as 3 m, in accordance with the embankment slope geometry. In the original situation, the surface load is approximately 90 kN/m^2, combined with a live load of 22.0 kN/m^2. After optimization using lightweight backfill material, this load is reduced to approximately 19.60 kN/m^2 for the surface load and 0.49 kN/m^2 for the free surface load.

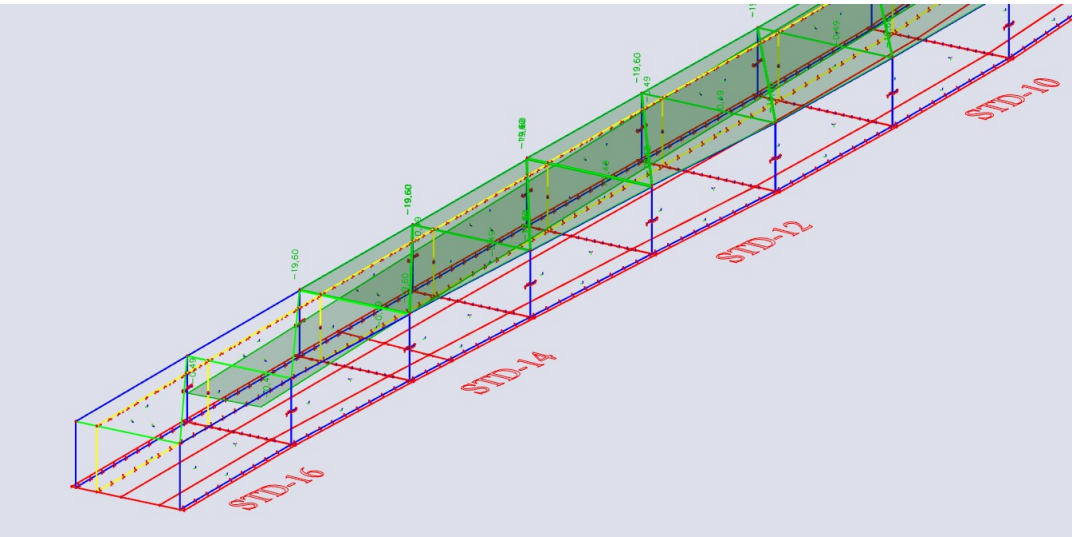

Figure 3.5: SCIA model with surface and free surface loads

In addition to these soil pressures, permanent loads such as the tunnel's own weight and the ground surface load with a value of 10 kN/m^2 are also included. The ULS load combination that determines the shear forces is as follows:

$$Q = Q_{\text{self-weight}} \cdot 1.5 + Q_{\text{soil-pressure}} \cdot 1.6 + Q_{\text{ground surface-load}} \cdot 1.6 \tag{3.1}$$

This ULS combination and the applied partial safety factors are consistent with the load combinations used in the structural design of the Oosterweelknoop tunnel segments to determine governing shear forces.

Results

Absolute value shear forces current design [kN]

Connection	Tunnel tube 5		
	Wall-N	Floor	Wall-S
STD-9 - STD-10	1866,24	190,31	869,64
STD-10 - STD-11	1593,27	148,44	920,51
STD-11 - STD-12	1545,46	180,53	749,76
STD-12 - STD-13	1642,25	188,96	1027,00
STD-13 - STD-14	1452,28	117,75	814,65
STD-14 - STD-15	2640,81	229,27	2072,09
STD-15 - STD-16	511,17	73,91	634,30

Absolute value shear forces optimized design [kN]

Connection	Tunnel tube 5		
	Wall-N	Floor	Wall-S
STD-9 - STD-10	1300,59	129,85	815,38
STD-10 - STD-11	922,06	100,81	1142,78
STD-11 - STD-12	1288,35	167,11	1005,85
STD-12 - STD-13	1146,52	153,34	1018,72
STD-13 - STD-14	600,75	80,98	555,32
STD-14 - STD-15	1088,06	136,72	862,32
STD-15 - STD-16	412,03	61,99	586,42

Connection	Tunnel tube 5		
	Wall-N	Floor	Wall-S
STD-9 - STD-10	30,3%	31,8%	6,2%
STD-10 - STD-11	42,1%	32,1%	-24,1%
STD-11 - STD-12	16,6%	7,4%	-34,2%
STD-12 - STD-13	30,2%	18,9%	0,8%
STD-13 - STD-14	58,6%	31,2%	31,8%
STD-14 - STD-15	58,8%	40,4%	58,4%
STD-15 - STD-16	19,4%	16,1%	7,5%

Figure 3.6: Results

Figure 3.6 presents the resulting shear forces in the shear keys of both the tunnel walls and the floor. Overall, the use of lightweight fill material results in a clear reduction of the vertical load acting on the tunnel roof. Although this initially appears favorable for the shear forces between the tunnel segments, the load reduction also leads to a decrease in the effective vertical stress in the subsoil. As a consequence, the vertical subgrade stiffness beneath the tunnel tube (k_v) is reduced, which negatively affects the structural behavior.

To explain this mechanism, a simplified 2D SCIA longitudinal model was developed. In this model, the tunnel cross-section is explicitly represented, while the loading is derived from a longitudinal slice through the 3D model, taken at deck level near the south wall as a representative example. Hinges are modeled between the tunnel segments to ensure longitudinal continuity.

The results show that when the subsoil responds more softly, vertical loads are transferred less directly to the foundation. Instead, a larger portion of the load is redistributed through the structural connections between the tunnel segments. As a result, a reduction in subgrade stiffness leads to an increase in shear demand in these connections.

In general, the application of EPS leads to a reduction in shear forces in the tunnel walls. Since the embankment is located on the north side, this positive effect is more pronounced at the north wall, where a reduction of approximately 30% to 60% occurs.

Further along the STD tunnel tube, in the region where the slope has fully disappeared (starting at STD-7), the use of EPS leads to more balanced shear forces between the segment connections. In this area, however, the advantage of load reduction is largely offset by the accompanying decrease in subgrade stiffness. Moreover, the abrupt change in soil loading at tunnel segment STD-7 induces larger differential settlements, which locally increase the shear forces. This effect limits the achievable optimization in this transition zone.

4

Connection variants

In the literature review (Chapter 2), four possible shear force connections have been identified: the collar connection, the shear key connection, the dowel connection, and a solution in which no structural connection is applied and free settlement is allowed. This chapter represents the next step, in which these concepts are translated into practical and structurally safe connection variants for the connections between tunnel segments STD-10 through STD-13. During the design process, the following boundary conditions are taken into account:

- The global shear forces and deformations of the STD tunnel segments, determined based on the methodology as described in Chapter 3. This includes the modeling of two longitudinal models for each variant.
- The loads and subgrade stiffness as derived from the EPS infill design, as described in Section 3.2.
- Connections in the walls are combined with the existing shear key connection in the floor from the Oosterweelknoop design (Figure 4.1).
- Based on the results from Oosterweelknoop reports, it is established that connections in the walls are only applied in the inner wall and the southern outer wall, as application in other walls results in excessive forces in the floor shear keys.
- The design guidelines and requirements are based on SB260 and the associated additions, as described in Section 2.3.2.

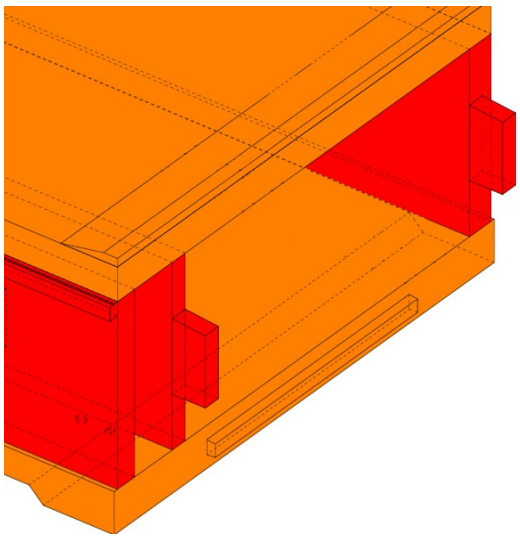

Figure 4.1: Current design of the shear key connection in the floor and walls for the Oosterweelknoop project [18]

The objective of this chapter is to structurally verify the four variants and to determine the associated material quantities, so that the connections can be assessed in the following chapter based on the criteria of the MCDA model.

4.1. Longitudinal Model

As part of the methodology of the optimization study, two longitudinal models are developed in order to determine the resulting shear forces that must be transferred by the connection variants. In both longitudinal models, the tunnel segments STD-06 to STD-16 are included to capture the longitudinal behavior of the tunnel around the connections. The two models differ only in their support conditions and applied loads. The following two longitudinal models are defined:

1. **UA3 longitudinal model**, including permanent loads, in which the subgrade stiffness is derived from the UA3 soil parameters (Section 2.3.3: Geotechnical design principles);
2. **k20 longitudinal model**, including traffic loads, assuming a uniform subgrade stiffness of 20 MN/m^2 over the entire tunnel length.

The complete description of the longitudinal model, including the associated geometry, material properties, support conditions, loads, and modeling assumptions of the structural elements forming the STD tunnel segments, is provided in Section E.1. To determine the shear force for each variant, all variants are modeled as described in Table 4.1. The full description of the modeling of the four variants is included in Appendix E.2 to E.5. Together, Appendix E provides a comprehensive description of the model, including all parameters required to reproduce the analyses and obtain the same results.

Table 4.1: Overview of modeling approach for the connection variants

Variant	Element type	Description	Appendix
Shear Key	1D beam elements (2 per console) with hinge	Console modeled as two eccentric beam elements; one end of each beam is connected via rigid line links to an internal edge in the wall over the height of the console, while the other end is connected via rigid line links to an internal edge at the centerline of the console within the adjacent wall (Figure 4.2).	E.2
Collar construction	Multiple 1D beam elements distributed across the width of the floor slab, each assigned a hinge with a nonlinear force-displacement relationship.	Beam elements with hinges are placed at 1 m intervals and connect the adjacent 2D elements in both the floor and the roof; Hinges are coupled to nonlinear translational springs, allowing shear force transfer in one direction only (Figure 4.3).	E.3
Dowel	1D beam element	Dowels are modeled as a single equivalent beam element with combined diameter; the beam is aligned with the wall axis and can displace in the longitudinal direction at one end (Figure 4.2).	E.4
Free-settlement joint	No elements	Model without structural connection between segments, used to determine relative displacements and rotations.	E.5

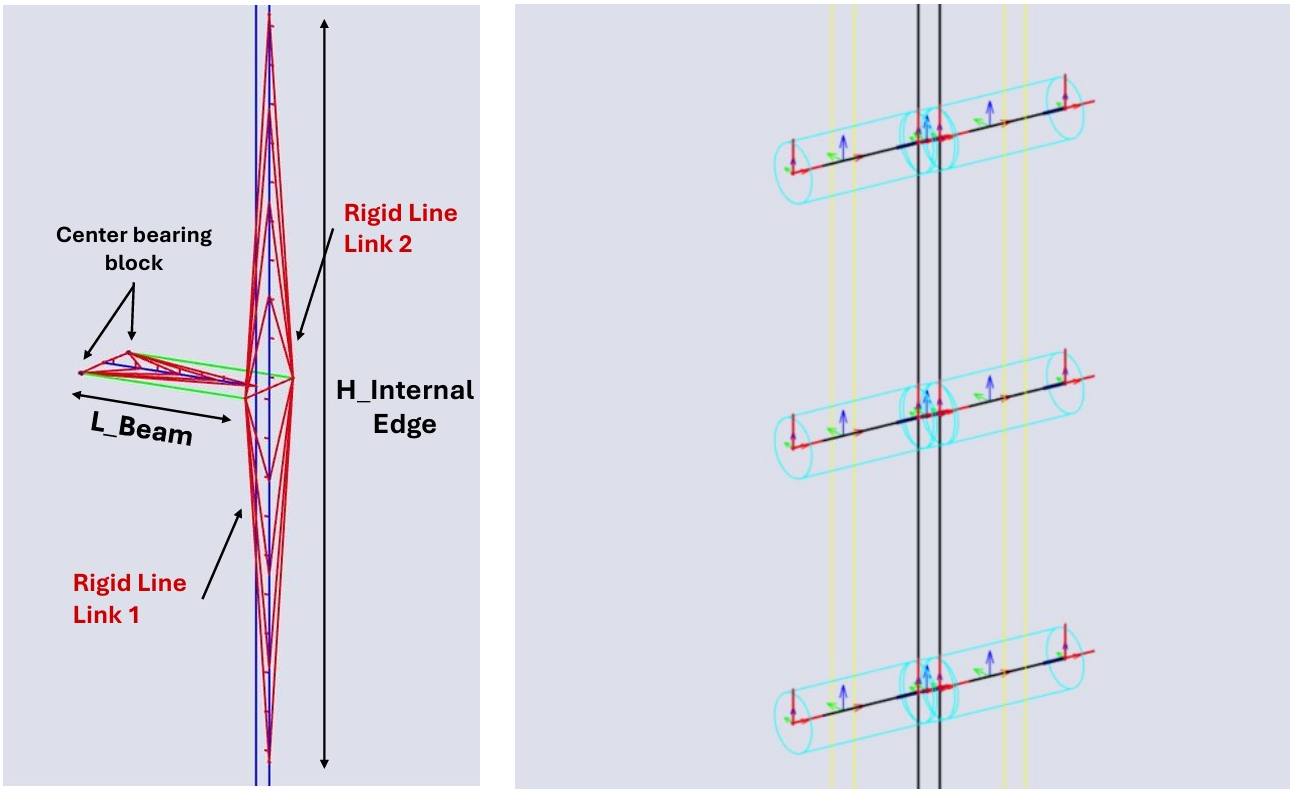

Figure 4.2: Model of shear key (left) and dowel (right) connection

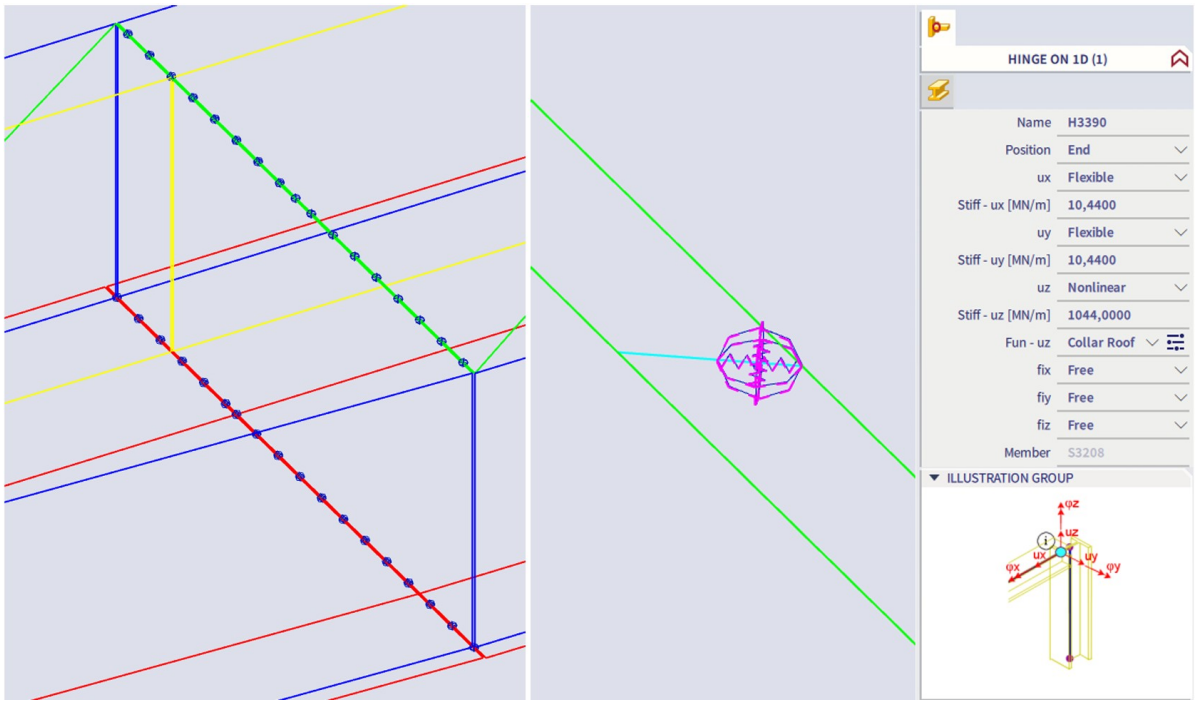

Figure 4.3: Model of collar construction

4.2. Shear Key

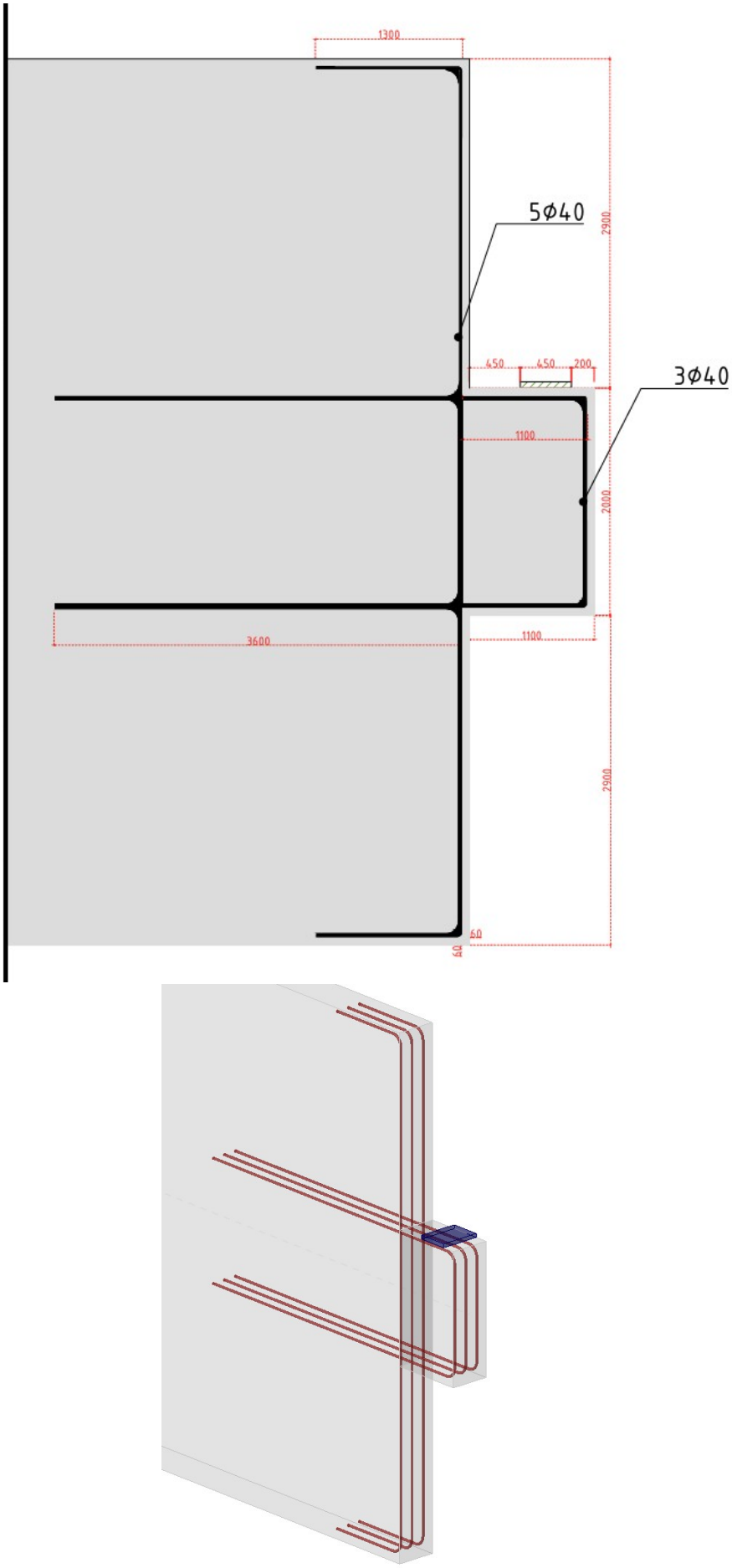

Figure 4.4: Geometry and reinforcement layout of the shear key connection (male part)

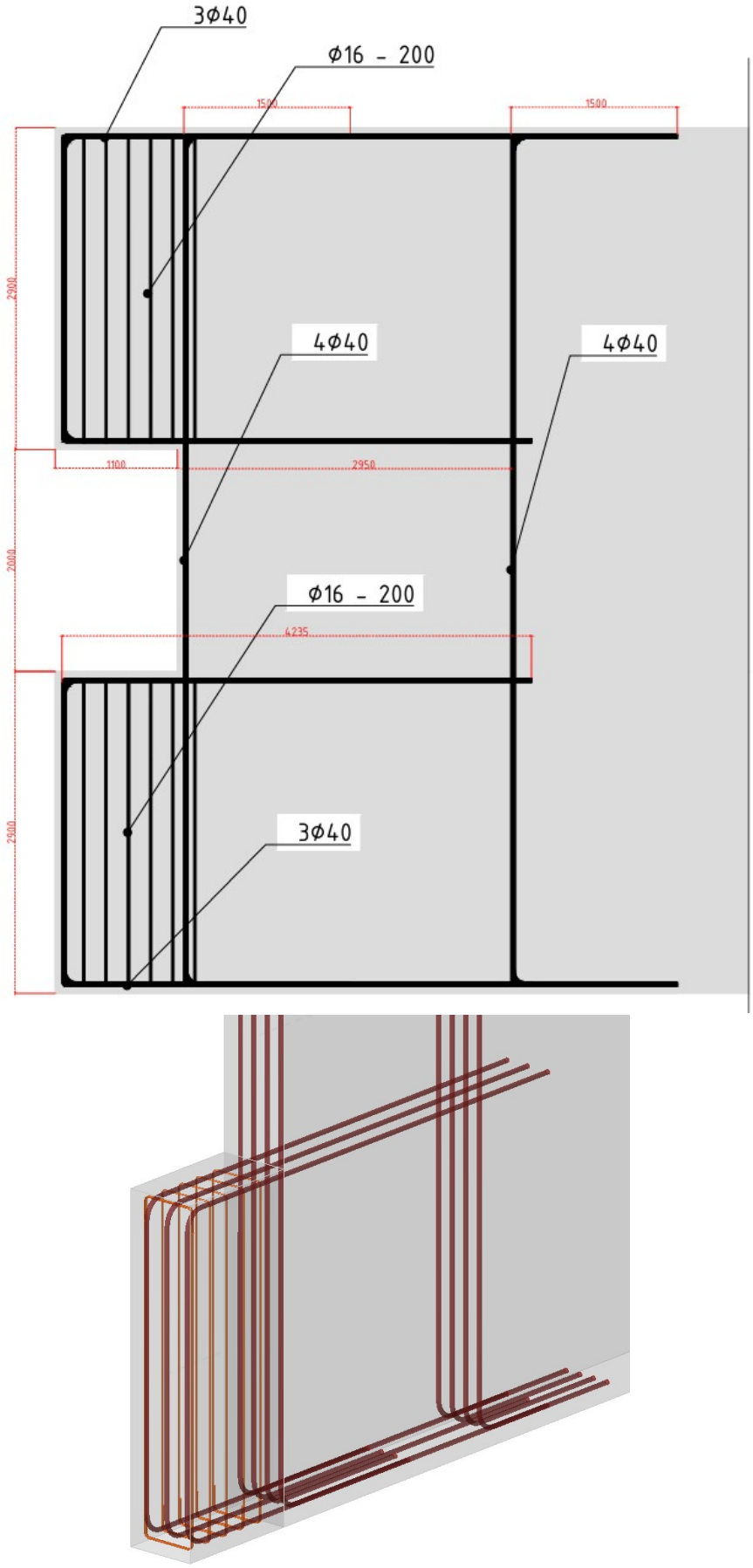

Figure 4.5: Geometry and reinforcement layout of the shear key connection (female part)

The design of the shear key connection consists of two concrete components in the wall: a male part, consisting of a concrete console, and a female part, consisting of an opening with overhangs at the top and bottom of the wall (Figure 4.4 and 4.5). Bearing blocks are placed between these concrete components to transfer the forces. The shear keys are applied in the northern inner wall and the southern outer wall. The consoles are positioned at the vertical center of the inner wall. In the outer wall, the consoles are placed eccentrically with an eccentricity of 200 mm relative to the wall centerline. In total, six shear keys are applied for the connection between the STD tunnel segments.

The shear key is designed in concrete strength class C35/45 (according design assumptions). The reinforced bearing block is consists of a laminated bearing made up of elastomer layers with embedded steel reinforcement plates. The dimensions of the console are 2000 mm in height, 600 mm in transverse direction, and 1100 mm in longitudinal direction. The dimensions of the console are determined based on the required space around the bearing block for reinforcement detailing and anchorage, in accordance with the strut-and-tie approach. In combination with the selected height, this results in a favorable compressive strut angle of approximately $68°$, thereby limiting the tensile forces in the reinforcement. This geometry also provides sufficient space for the development of the nodal zones within the strut-and-tie model.

The design of the bearing block is based on supplier tables [19] and the design guidelines in NEN-EN 1337-3. The bearing block has a width of 350 mm, a length of 450 mm, and a thickness of 57 mm. The complete overview of the parameters and the verification according to NEN-EN 1337-3 is presented in Appendix H. The bearing block has been verified for the shear forces from the longitudinal models and rotations derived from Appendix L.

The resulting shear forces in the connections are determined using the longitudinal models and the shear key modeling approach described in Appendix E.2. Table 4.2 provides an overview of the maximum resulting shear forces in the ULS at the connections between the tunnel segments, distinguishing between the contribution from permanent loads (UA3) and traffic loads (k20).

Table 4.2: Shear forces in shear keys from UA3 and k20 longitudinal models (ULS and SLS)

	South outer wall			**North inner wall**		
Connection	**UA3**	**k20**	**Total**	**UA3**	**k20**	**Total**
			ULS			
STD-10 – STD-11	904	697	1601	885	586	1471
STD-11 – STD-12	760	664	1424	1034	572	1606
STD-12 – STD-13	945	644	1589	1216	564	1780
			SLS			
STD-10 – STD-11	608	436	1044	589	366	955
STD-11 – STD-12	504	433	937	699	368	1067
STD-12 – STD-13	634	433	1067	781	369	1150

For the reinforcement design, the shear key is verified in accordance with EN 1992-1-1 using a strut-and-tie model (STM). For the total of six shear keys between the tunnel segments, a single representative design is developed based on the maximum shear forces in both the ULS and SLS. Within this study, only the reinforcement required to resist the connection forces and transfer them to the tunnel walls is designed. In the ULS, the design is based on the resulting stresses, while in the SLS, the crack width is verified. The complete elaboration of the STM is included in Appendix F. Finally, the reinforcement is checked for fatigue in accordance with NEN-EN 1992-1-1, Article 6.8 (Appendix G).

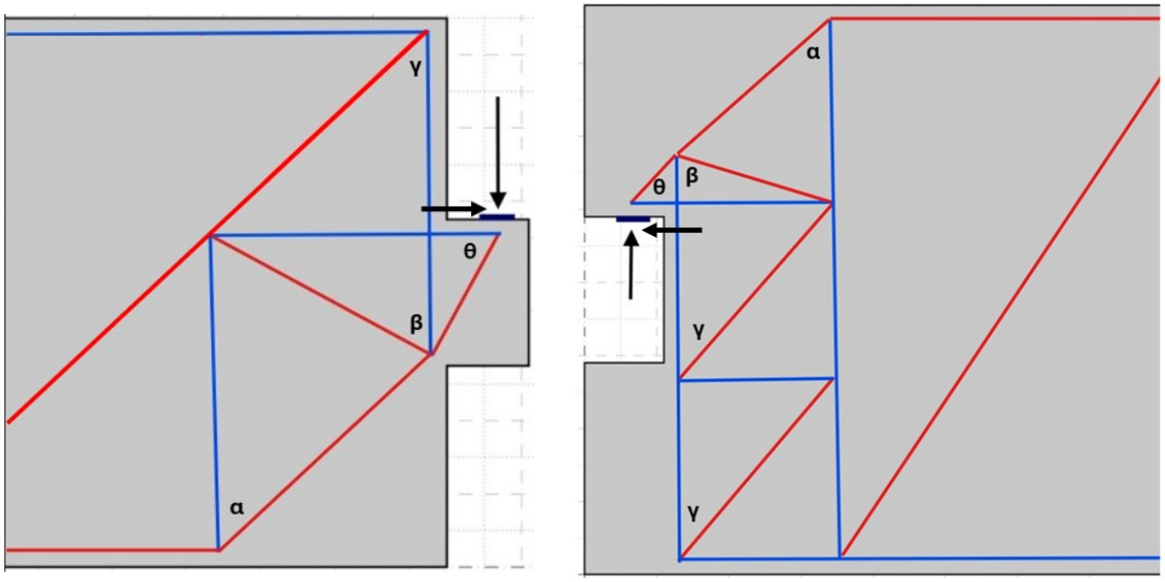

Figure 4.6: Strut-and-tie models of male (left) and female (right) segment of the shear key connection

4.3. Collar Construction

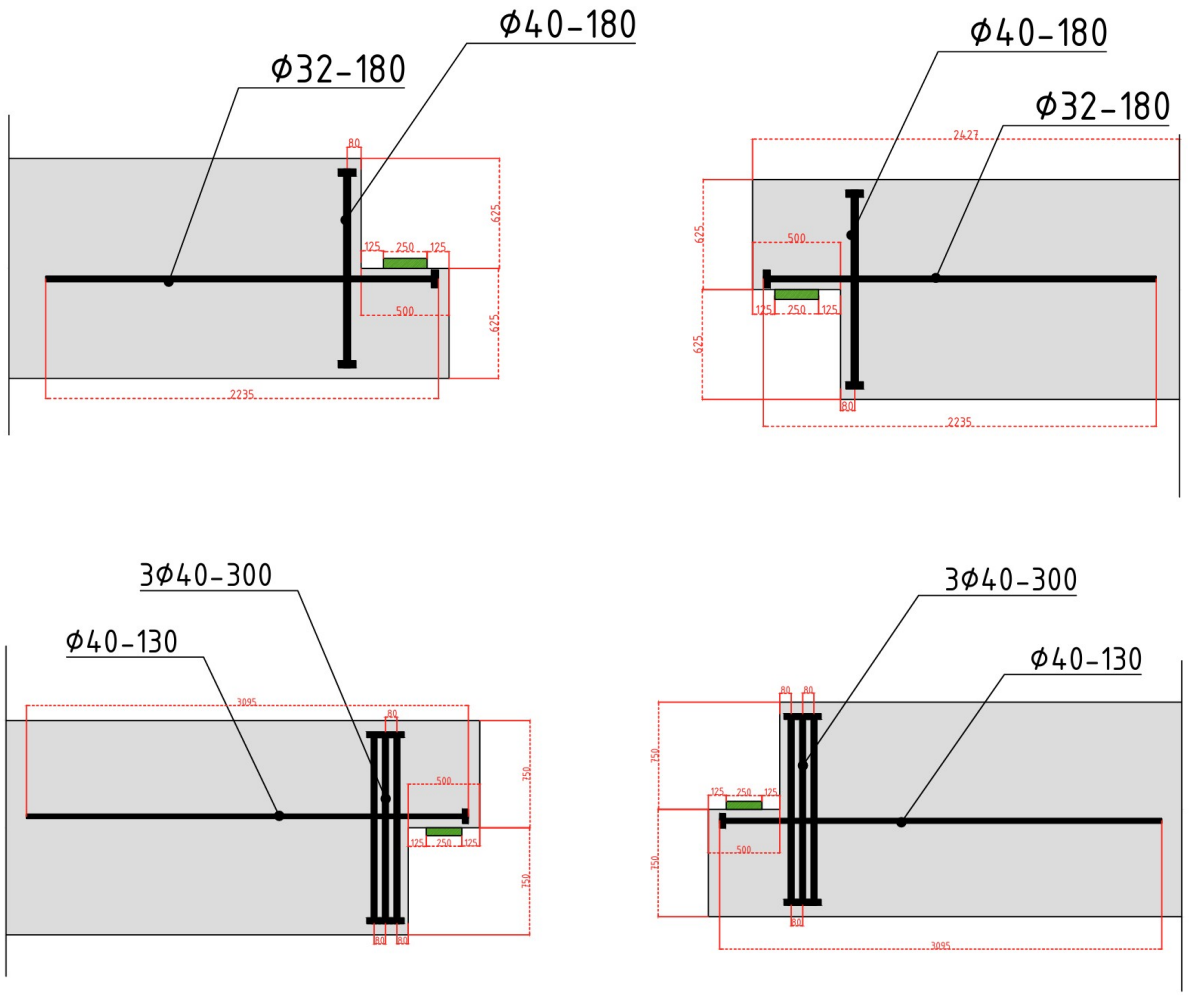

Figure 4.7: Geometry and reinforcement layout of the collar connection in the roof (top) and floor (bottom)

The design of the collar connection consists of an inner and outer collar in both the floor and the roof (Figure 4.7). For the initial design, the construction thicknesses of the STD tunnel segments are adopted, with a floor thickness of 1100 mm and a roof thickness of 1250 mm. Based on this, the floor initially results in a collar configuration consisting of two segments of approximately 625 mm in height. However, the reinforcement design shows that a local thickening of the floor to 1500 mm is required to provide sufficient space for the necessary reinforcement and detailing. The final design of the collar connection in the floor therefore consists of two segments of 750 mm each. In both the floor and the roof, an elastomer strip with a width of 350 mm is applied between the inner and outer collar over the full length of the connection.

Finally, in the detailing of the hanger reinforcement, account is taken of findings from shear key structures in recent years [20]. The traditional practice of bending reinforcement bars results in shear action rather than pure tension tie behavior, leading to an overestimation of the shear capacity of the collar. Therefore, the hanger reinforcement is detailed as shear dowels. Full explanation of the experimental and theoretical findings is provided in Appendix I. Based on these insights, the hanger reinforcement is not implemented using bent bars, but is instead detailed as discrete shear transfer elements (dowels), ensuring a clear and verifiable force transfer mechanism.

To determine the resulting shear forces in the connection, two longitudinal models are established, based on the load cases UA3 and k20. The modeling of the collar connection is described in Appendix E.3. Table 4.3 provides an overview of the maximum resulting shear forces in both the ULS and SLS at the connections between the tunnel segments. The results are presented in kN/m, where the reported value represents the maximum over the width. These forces are used for the dimensioning of the reinforcement and the geometry of the collar connection.

Table 4.3: Shear forces in collar connection in kN/m

	Floor			Roof		
Connection	**UA3**	**k20**	**Total**	**UA3**	**k20**	**Total**
			ULS			
STD-10 – STD-11	320	16	338	577	15	592
STD-11 – STD-12	4336	0	4336	415	50	465
STD-12 – STD-13	0	58	58	1548	7	1555
			SLS			
STD-10 – STD-11	213	10	223	381	9	390
STD-11 – STD-12	2870	0	2870	232	30	262
STD-12 – STD-13	0	36	36	1024	4	1028

The maximum shear forces occur at the locations of the walls. The higher shear forces at the tunnel walls are caused by rotations in the transverse direction. This is due to variations in the geometry and the subgrade stiffness (three zones) of the structure in the UA3 longitudinal model. In combination with the higher stiffness of the walls, this leads to a local concentration of forces.

For the reinforcement design of both collars, strut-and-tie models (STM) are developed in accordance with NEN-EN 1992-1-1 for the inner collars in the floor and roof (Figure 4.8). The reinforcement is determined per meter length of the collar. Since the collars are symmetric, only the inner collar is analyzed in detail, and the reinforcement is subsequently applied to the outer collar. Consequently, the reinforcement quantities in the outer collar are identical to those in the inner collar. The hanger reinforcement consists of three rows of shear dowels. The centers of these rows coincide with the location of the vertical tie in the STM model. The complete elaboration of the strut-and-tie model of the inner collar is included in Appendix F. Finally, the reinforcement is checked for fatigue in accordance with NEN-EN 1992-1-1, Article 6.8 (Appendix G).

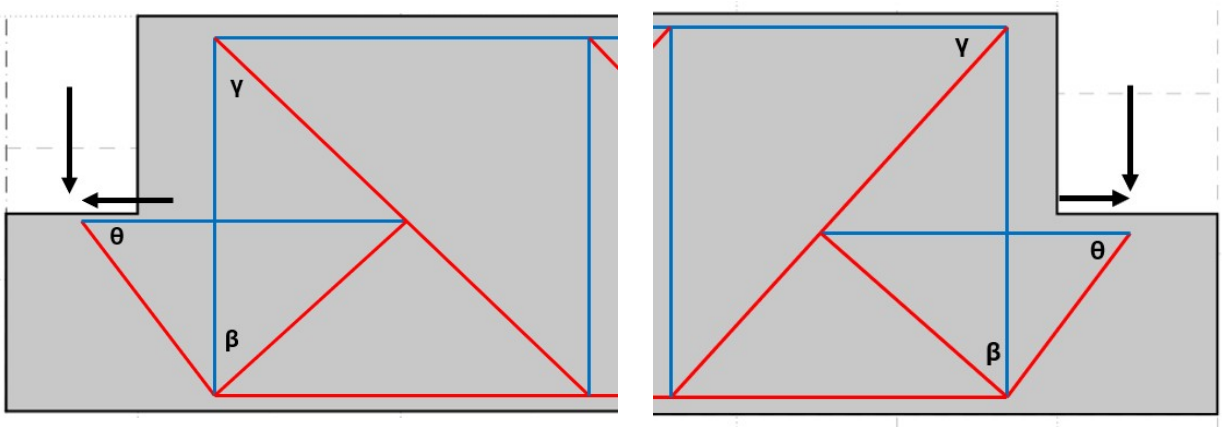

Figure 4.8: Strut-and-tie model of the collar inner collar segments floor(left) and roof (right)

4.4. Dowel Connection

For the dowel connection, multiple Double Shear Dowel Type Q (DSDQ) units will be designed in the north inner wall and the south outer wall. This system is commonly applied in concrete structures and is designed to transfer high shear forces while allowing relative movement between adjacent concrete elements in two directions [12].

The material properties and geometric characteristics of the DSDQ-450 dowels are presented in Table 4.4. The final design of the dowel connection consists of three DSDQ-450 dowels distributed over the height of the wall. The complete design of the connection in the inner and outer walls of the STD tunnel elements, including all dimensions and spacings, is presented in Appendix K.

Table 4.4: Properties of DSDQ 450 dowel connection [12]

Property	**DSDQ 450**
Steel grade	RVS-INOX W.NR.1.4429
f_t	650 MPa
$f_{0.2}$	355 MPa
Elongation A_{10}	25%
Overall length	690 mm
Dowel diameter	65 mm
Dowel centers	180 mm
Dowel projection	360 mm
Anchor bar position	80 mm
Anchor bar lengths	130/300 mm
Minimum center-to-center spacing	1000 mm

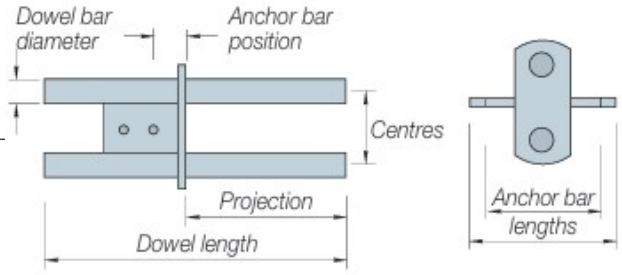

Figure 4.9: Cross-section and side view of DSDQ dowel geometry [12]

To verify the capacity, the dowel design is modeled in the two SCIA longitudinal models (k20 and UA3), as described in Appendix E.4. From these models, the shear forces per dowel are obtained, as presented in Table 4.6.

These values are compared with the design tables provided by the suppliers Hakron and Leviat (Figure 4.10). The capacity of the dowels depends not only on the type, but also on the joint width between the tunnel elements. The joint width is determined based on the deformation contributions due to temperature and shrinkage, as calculated in Appendix L. In addition, the contribution of traffic loads and the initial joint width are taken from the Oosterweelknoop design assumptions [21]. Traffic effects include braking and acceleration forces, resulting in a contribution of 0.25 mm. The initial joint width is taken as 20 mm. The resulting deformations of the STD tunnel segments are presented in Table 4.5.

Table 4.5: Overview of longitudinal deformations Δx in mm

Load / combination	**Δx**		**Total Δx**	
	min	**max**	**min**	**max**
Temperature	0.00	2.50	0.00	5.00
Traffic	0.00	0.25	0.00	0.50
Shrinkage t_0	-0.25	-0.25	-0.50	-0.50
Shrinkage t_∞	-2.75	-2.75	-5.50	-5.50
SLS_short (t_0)	–	–	-1.00	5.00
SLS_long (t_∞)	–	–	-5.50	-0.50
SLS total		**10.50**		
ULS (1.2× SLS)		**12.60**		
Initial joint width		**20.00**		
Joint width dowels		**32.60**		

Table 4.6: Results (ULS) of shear forces in dowels from the UA3 and k20 longitudinal models

	South outer wall			**North inner wall**		
Connection	**UA3**	**k20**	**Total**	**UA3**	**k20**	**Total**
STD-10 – STD-11	410	303	713	424	280	704
STD-11 – STD-12	359	290	649	472	258	730
STD-12 – STD-13	391	515	906	364	290	654

Slab Thickness (mm)	Product Reference	Maximum Width of Joint (mm) 10	20	30	40	50	60
600*	DSD/DSDQ 450	549.8	549.8	549.8	549.8	549.8	549.8
650		584.2	584.2	584.2	584.2	584.2	584.2
700		636.2	636.2	636.2	636.2	636.2	586.9
800		741.7	741.7	741.7	741.7	684.7	586.9
900		847.6	847.6	847.6	811.4	684.7	586.9
1000		952.1	952.1	941.1	811.4	684.7	586.9

* Refers to the minimum slab depth H_{min} for each connector type.

Figure 4.10: V_{Rd} Design Resistance (kN) for Various Joint Widths (mm) and Slab Thickness (mm) using C30/37 Concrete [12]

The design capacity of a DSDQ-450 dowel with a joint width of 32 mm is 915 kN. This value is obtained by linear interpolation between the capacities for joint widths of 30 mm and 40 mm. The maximum resulting shear force is 909 kN when three dowels are applied per wall. This corresponds to a unity check of 1.0, indicating that the DSDQ-450 dowel satisfies the requirements in the ULS for shear.

The hanger reinforcement is based on the total shear force per wall, which is obtained by summing the forces in the three dowels. The governing total shear force amounts to 1983 kN in the ULS and 1252 kN in the SLS. This results in a required hanger reinforcement of 4∅40, anchored at the top and bottom over a length of 1300 mm, in accordance with NEN-EN 1992-1-1, Article 8.7.3.

Finally, the governing dowel, namely the connection between tunnel segments STD-12 and STD-13, is verified for fatigue in accordance with NEN-EN 1993-1-9. For this purpose, a spreadsheet was developed (Appendix J), in which the moments are derived from the k20 longitudinal model, based on Load Model 1 for fatigue [22] (LM1fat). This load model is based on the characteristic load model 1 for fatigue (LM1fat), where the axle loads are taken as $0.7 \cdot Q_{ik}$ and the uniformly distributed load as $0.3 \cdot q_{ik}$. As the DSDQ dowels are modeled as 1D

bar elements with an equivalent diameter, the normal and shear stresses are calculated using half of the applied moment and shear force. The normal force in the dowel is equal to zero, as it is free to move in the longitudinal direction. The dowels are classified in detail category 80, due to the presence of intermittent fillet welds between the steel plates in the DSDQ-450 connection.

4.5. Free-Settlement Joint

The final connection concept is the free-settlement joint, which allows adjacent tunnel segments to move freely relative to each other. For this concept, the joints in the floor, walls, and roof must be designed to accommodate the required horizontal and vertical displacements and to ensure watertightness. The joint profile in the floor must be capable of accommodating both the relative movements and differences in asphalt level that develop as a result of the free movement of adjacent tunnel segments. For the joints in the wall and roof the FMS and ACME profiles of the current Oosterweelknoop design (Appendix C.1) must be verified.

In Appendix L the vertical (Δz) and longitudinal displacements (Δx) between the STD tunnel segments are determined. Rotation effects are found to be negligible and are therefore not considered in the determination of the joint displacements. As a result, the displacements in the floor and roof are assumed to be equal. A traffic contribution of 0.25 mm is taken into account due to braking and acceleration forces [21]. The governing joint displacements between STD-10 and STD-13 are summarized in Table 4.7.

Table 4.7: Load effects on joint displacements (SLS)

Load case	$\Delta x_{\min}$ [mm]	$\Delta x_{\max}$ [mm]	$\Delta z_{\max}$ [mm]
Self-weight / soil	–		4.20
Temperature	0.00	2.50	–
Traffic	0.00	0.25	–
Shrinkage (t_0)	-0.25	-0.25	–
Shrinkage (t_∞)	-2,75	-2,75	–
Total_short	-0.50	5.00	4.20
Total_long	-5.50	-0.50	4.20

The maximum deformation amounts to 10.50 mm in the longitudinal direction and 4.20 mm in the vertical direction in the SLS quasi-permanent load combination. The maximum joint displacements satisfy the requirements specified in SB260 in the SLS quasi-permanent load combination (Section 2.3.2). The calculated relative displacements therefore remain within the limit value of 0.005 m for both the horizontal and vertical directions.

For the dimensioning of the joints, the ULS combination is adopted, in which the design value of the joint displacement is determined based on:

$$u_{\text{joint,d}} = 1{,}2 \cdot u_{\text{joint,k}} \tag{4.1}$$

This results in a design value of approximately 12.60 mm for the horizontal displacement (Δx) and approximately 5.00 mm for the vertical displacement (Δz). The displacement in the transverse direction (Δy) is negligible due to the symmetric transverse loading on both sides of the tunnel.

The free-settlement joint was selected using the Rijkswaterstaat expansion joint selection matrix shown in Figure 4.11. The selection was based on the expected joint movements and the functional requirements of a highway expansion joint.

The floor joint consists of a Type 1.2 a2 Nosing Joint, which is suitable for noise-reducing joint transitions on asphalted highways (Figure 4.12). The elastomer joint profile provides watertightness and accommodates the horizontal and vertical displacements. Differences in pavement level can be accommodated by varying the thickness of the steel edge plates at the top of the joint against which the asphalt pavement is cast. The nosing joint consists of steel edge profiles that are mechanically anchored into the underlying concrete structure. The nosing joint has an expected service life of approximately 40 years, while the elastomer joint profile requires periodic replacement approximately every 10 years [23].

De matrix geeft een beoordeling van prestaties op basis van functies en kwaliteit. De beoordeling is als volgt geklassificeerd: -- Slecht - Matig + Redelijk ++ Goed Ontbrekende volgnummers betreffen de niet in deze matrix opgenomen factsheets, door onvoldoende significante ervaringsgegevens.		Functies voegovergangen										
		1				2	3	4		5	6	
		bewegingsvrijheid				mechanische weerstand		gebruiksvriendelijkheid en veiligheid		geluid	waterdichtheid	
Familie	Concept (zie factsheets)	Δx [mm]	Δy [mm]	Δz [mm]	kruisingshoek (gon)	uit de constructie	uit het verkeer	oneffenheid	stroefheid	GLW bij 120 km/u		
1. Nosing Joints												
1.2 Stalen randprofielen met ingeklemde voegprofielen in verankerde onderbouw van de constructie met en zonder voegovergangsbalken zonder (a1/b1) en met (a2/b2) geluidbeperkende maatregelen.	1.2 a1	+/-40	+/- 40	+/- 10	20-100	++	++	-	++	87.6	++	
	1.2 a2	+/-40	+/- 4 tot +/- 40	+/- 10	65-100	++	+	+	++	81.7	++	
	1.2 b1	+/-40	+/- 40	+/- 10	20-100	++	++	-	++	87.6	++	
	1.2 b2	+/-40	+/- 40	+/- 10	65-100	++	+	+	+/++	81.7	++	

De matrix geeft een beoordeling van prestaties op basis van functies en kwaliteit. De beoordeling is als volgt geklassificeerd: -- Slecht - Matig + Redelijk ++ Goed Ontbrekende volgnummers betreffen de niet in deze matrix opgenomen factsheets, door onvoldoende significante ervaringsgegevens.		Kwaliteit (RAMS)										Opmerkingen
		betrouwbaarheid					beschikbaarheid	onderhoud-baarheid			veiligheid	
Familie	Concept (zie factsheets)	levensduur onderdelen	levensduur constructie	uitvoerings ongevoeligheid	slijtvastheid	aantastings ongevoeligheid	beschikbaarheid	vast onderhoud	vervangen onderdelen	vervangen constructie	risicio op letselschade	
1. Nosing Joints												
1.2 Stalen randprofielen met ingeklemde voegprofielen in verankerde onderbouw van de constructie met en zonder voegovergangsbalken zonder (a1/b1) en met (a2/b2) geluidbeperkende maatregelen.	1.2 a1	10	40	++	++	+	-	++	++	--	++	GLW bij 100 gon
	1.2 a2	10	40	+	++	+	-	++	++	--	-	GLW bij 100 gon
	1.2 b1	10	25	+	++	+	-	++	+/++	--	++	GLW bij 100 gon
	1.2 b2	10	25	+	++	+	-	++	+/++	--	-	GLW bij 100 gon

Figure 4.11: Multi-criteria decision matrix for joint systems [23]

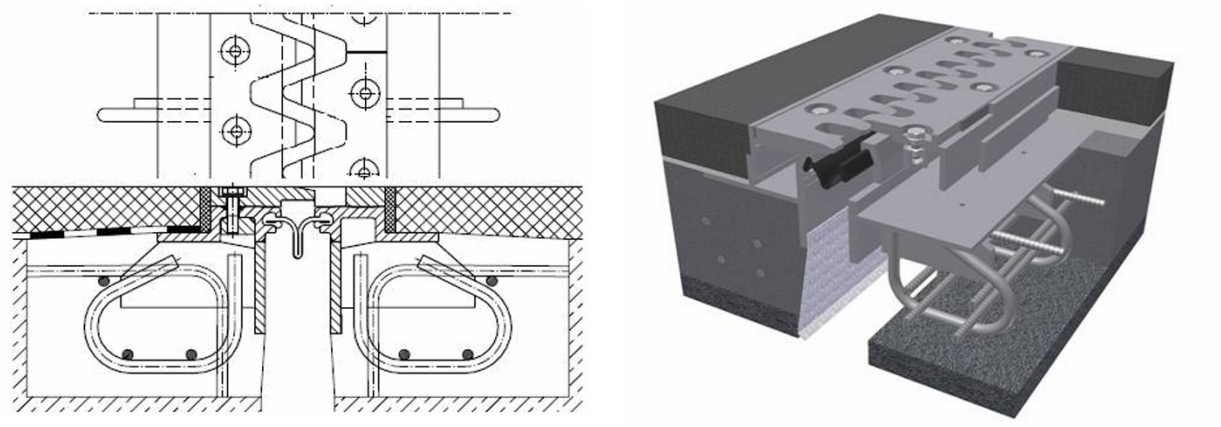

Figure 4.12: Nosing joint type 1.2 a2 [23]

Finally, the joint profiles in the walls and roof of the reference design are verified against the displacement capacity specified by the manufacturers. The applied FMS350 and ACME 35 profiles can accommodate a total displacement of 45 mm and 55 mm, respectively [24, 25]. Both joint profiles have a design service life of 100 years.

$$V_r = \sqrt{v_x^2 + v_y^2 + v_z^2} = \sqrt{12.6^2 + 0^2 + 5^2} = 13.6mm \tag{4.2}$$

The resulting relative displacement is 13.6 mm and therefore remains within the displacement capacity of both joint profiles. As a result, the profiles are suitable for application in combination with a connection concept without a structural connection. Figure 4.13 shows a detail of the expansion joint in the tunnel roof, in which the ACME profile and the FMS350 profile are applied in combination.

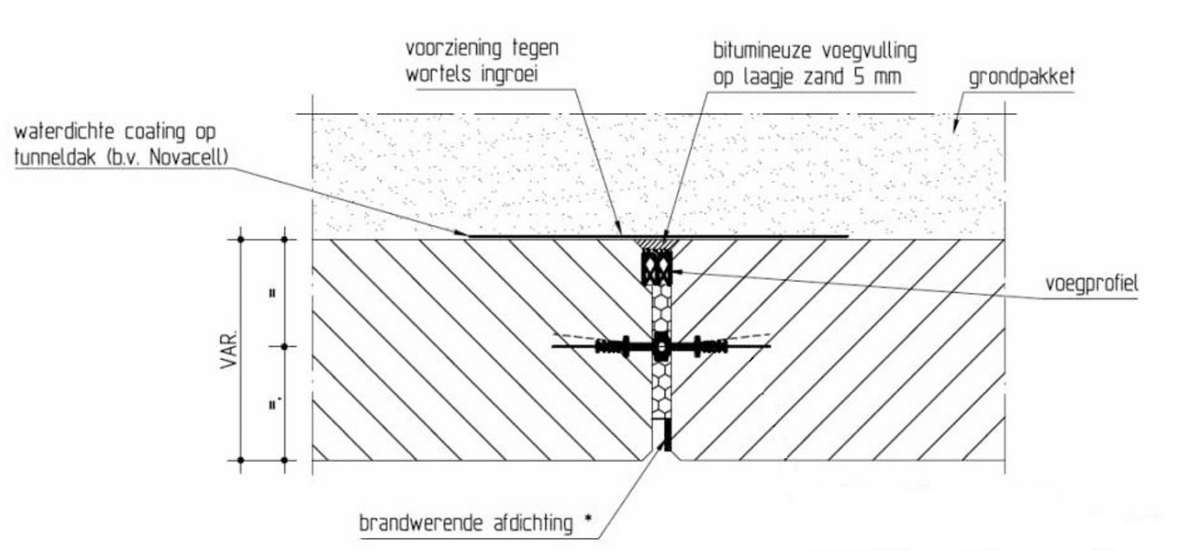

Figure 4.13: Roof expansion joint detail [2]

5

Decision Model

In Chapter 4, several variants have been developed for the connection between tunnel segments STD 10 through STD 13. In this chapter, the decision model is established and applied to the considered variants. First, the applied methodology is explained and justified, after which the criteria are presented and evaluated.

The decision model consists of 15 subcriteria, divided into 6 main criteria. The applied methodology is based on a combination of the Analytic Hierarchy Process (AHP) method and the Technique for Order Preference by Similarity to Ideal Solution (TOPSIS) method. The model is developed and implemented in Excel.

5.1. MCDA Method

The decision model is based on a combination of the AHP and TOPSIS methods that are explained in the Literature Review (Section 2.1). The AHP method is applied to determine the weights of the subcriteria. In this approach, the relative importance of the main criteria is established using pairwise comparisons. These comparisons are evaluated using the Saaty scale (1–9), where a value of 1 indicates equal importance and a value of 9 indicates a strong preference for one of the two criteria (Table 5.1). The final weights are derived from the normalized pairwise comparison matrix A. Within each main criterion, the subcriteria are considered equally important and are therefore assigned equal weights.

Table 5.1: Saaty scale for pairwise comparisons [6]

Value of a_{ij}	**Definition**
1	i and j are equally important
3	i is slightly more important than j
5	i is more important than j
7	i is strongly more important than j
9	i is absolutely more important than j
2, 4, 6, 8	Intermediate values between two adjacent judgments

The final score of the variants will be calculated using the TOPSIS method. Qualitative subcriteria are assessed using a discrete scale ranging from 1 to 5 where a higher score represents a more favorable evaluation. Quantitative subcriteria are evaluated in their original units such as costs in euros (€). Based on the weighted normalized matrix, the positive ideal solution (PIS) and the negative ideal solution (NIS) are determined for each subcriterion. After that the distance to both the PIS and the NIS is calculated across all subcriteria for each variant. This results in the distances D^+ and D^-. The final performance score C ranges between 0 and 1 and is determined based on the relative distance to these ideal solutions, where a higher value corresponds to a better-performing variant [8].

Table 5.2: Qualitative rating scale for TOPSIS

Score	Definition
1	Very unfavorable performance with significant deficiencies
2	Unfavorable performance with multiple shortcomings
3	Neutral performance meeting minimum requirements
4	Favorable performance with limited shortcomings
5	Very favorable performance with excellent characteristics

The Saaty scale is an appropriate scale for application within the AHP method, as it enables both qualitative and quantitative criteria to be systematically translated into numerical ratios. By ranking the variants using the TOPSIS method, a relatively simple and transparent decision model is obtained. In addition, the method is well suited for situations involving conflicting criteria, where an improvement in one criterion often comes at the expense of another. TOPSIS is therefore a widely used and well-established method in multi-criteria decision making, with applications in engineering as well as other domains [7].

Finally, the motivation for using a scale from 1 to 5 for qualitative subcriteria within the TOPSIS method is based on its compactness. The use of a limited scale prevents false precision and contributes to a more robust evaluation of the variants.

5.2. Model

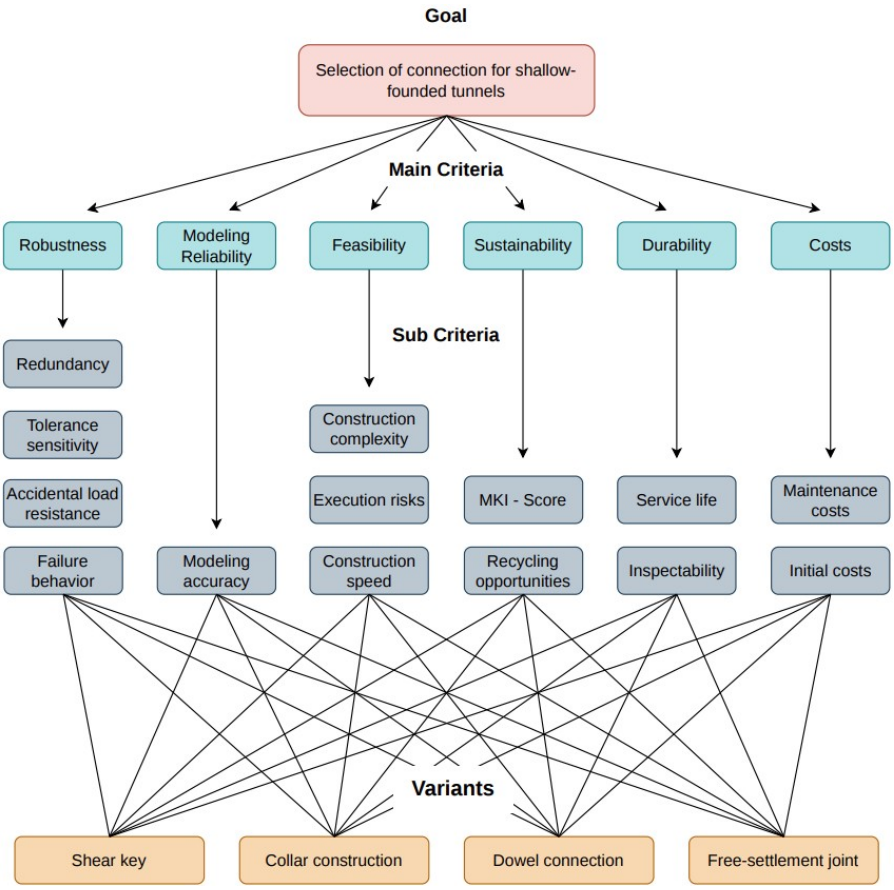

Figure 5.1: Hierarchal structure of decision model

The decision model follows a hierarchical structure consisting of connection variants, main criteria and subcriteria. The selected criteria reflect both project-specific challenges within the Oosterweelknoop project, such as constructability and structural uncertainty, and aspects commonly considered in structural engineering and civil engineering decision-making, including cost and sustainability. These criteria were used in the pairwise comparison to determine the relative criterion weights. Combined with the quantitative and qualitative assessment scores, they form the input of the decision model.

Table 5.3: Description of the main assessment criteria

Main criterion	Description
Robustness	Ability of the connection to maintain its structural function under unforeseen conditions. Regular ULS and SLS checks are included as boundary conditions in the model.
Modeling Reliability	Degree to which the structural behavior of the connection can be reliably modelled and predicted.
Feasibility	Degree to which the connection can be constructed easily, safely and quickly during execution.
Sustainability	Environmental performance of the connection over its entire life cycle.
Durability	Degree to which the connection maintains its performance during the design life and the extent to which its condition can be inspected and monitored.
Costs	Economic performance of the connection based on initial construction costs and maintenance costs.

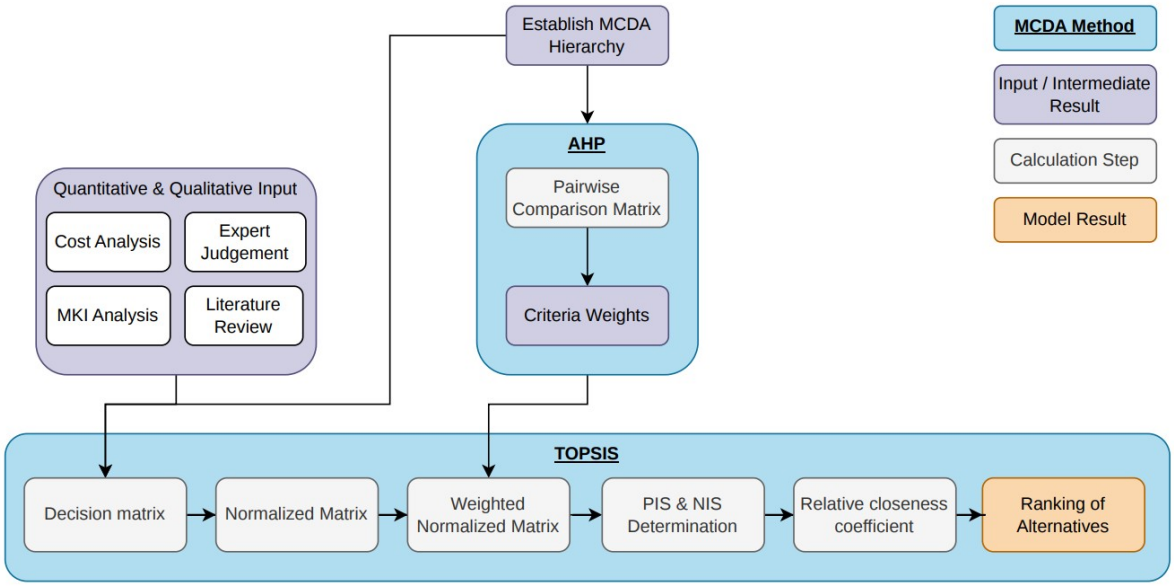

Figure 5.2: Flowchart of decision model

Figure 5.2 presents the workflow of the decision model. The workflow is implemented in Excel and consists of multiple worksheets:

- Pairwise Matrix (AHP method)
- Quantitative Input
- Decision Matrix (TOPSIS method)
- Model Overview

The operation of the decision model is as follows:

1. The criterion weights are determined in the ‘Pairwise Matrix’ worksheet using AHP. The underlying justification is provided in Appendix N. The resulting weighting factors are applied in the ‘Decision Matrix’ worksheet and are presented in the ‘Model Overview’ worksheet.
2. The quantitative input data are entered in the ‘Quantitative Input’ worksheet. These values are derived from the design of the four variants for the connection between tunnel segments STD-10 through STD-13 within the Oosterweelknoop project. The values are automatically processed in both the ‘Decision Matrix’ and the ‘Model Overview’ worksheets.
3. The qualitative assessments are part of the decision model and are based on engineering input from WSP and findings from the literature review. The justification of both the qualitative and quantitative criteria is provided in Appendix O.
4. In the ‘Decision Matrix’ worksheet, the assessments are combined with the criterion weights, and the calculation steps are carried out according to the TOPSIS methodology and results in the ranking of the alternatives.
5. The ‘Model Overview’ worksheet presents the variants, the applied evaluation method, and the final score for each variant.

The subcriteria are assessed using predefined assessment points, which are summarized in Table 5.4. Within the TOPSIS methodology, benefit criteria are considered preferable when higher values are achieved, whereas cost criteria are considered preferable when lower values are achieved. These assessments are subsequently incorporated into the calculation of the distances to the positive ideal solution (PIS) and negative ideal solution (NIS). The justification of the scores assigned to each variant and the corresponding assessment points is provided in Appendix O.

Table 5.4: Overview of assessment points for each subcriterion

Subcriterion	Assessment based on	TOPSIS Type	Value Determination
Redundancy	Ability of the connection to carry load after local failure through alternative load transfer mechanisms and load redistribution	Benefit (Qualitative)	Literature on load redistribution in shear key [26] and collar connections [10, 20]
Tolerance Sensitivity	Extent to which tolerances can be accommodated within the connection concept and how these tolerances influence stresses and connection capacity	Benefit (Qualitative)	DSDQ design graphs from supplier [12], literature and analyses on strut-and-tie modeling [27]
Accidental Load Resistance	Ability of the connection to maintain its structural performance under accidental loading conditions like fire	Benefit (Qualitative)	Literature on fire resistance of tunnel joints [28], fire performance of elastomer bearings [29], and expansion joint fire protection systems [30] supplemented with expert judgment from WSP
Failure Behavior	Failure mechanism of the connection and the consequences of failure for the connection and tunnel system.	Benefit (Qualitative)	Literature on ductility, cracking behavior and failure mechanisms of reinforced concrete, dowels and joint profiles [10, 31, 23]
Model Accuracy	Ability of the SCIA Engineer model to represent the actual behavior of the connection and the modeling effort required, assessed based on representation of physical behavior, modeling assumptions and simplifications, sensitivity and robustness, and complexity and risk of errors	Benefit (Qualitative)	Model verification and validation studies presented in Appendix E
Construction Complexity	Overall technical difficulty of construction, assessed based on geometric configuration, reinforcement ratio and detailing, and degree of prefabrication	Benefit (Qualitative)	WSP expert judgment and practical experience with reinforcement detailing, formwork and tunnel segment construction [32]
Execution Risks	Extent to which external conditions, controllability and recoverability affect successful execution of the connection	Benefit (Qualitative)	WSP expert judgment and project experience from tunnel construction projects [32]
Construction Speed	Relative construction duration, considering all required on-site activities before and during realization of the connection	Benefit (Qualitative)	WSP expert judgment and experience with construction sequencing and execution planning [32]
MKI Score	Environmental impact of the connection expressed as an MKI score	Cost (Quantitative)	Calculation of material quantities for each variant and multiplication with MKI values using DuboCalc (Rijkswaterstaat database) [33]
Recycling Opportunities	Extent to which components can be separated into individual materials at the end of their service life and the potential for reuse of these materials	Benefit (Qualitative)	Literature on recycling and reuse of reinforced concrete and steel [34, 35] supplemented with expert judgment from WSP [32]
Service Life	Design service life of the connection concept expressed in years	Benefit (Quantitative)	Literature, supplier information for asphalt joint systems [23] and expert judgment from WSP [32]
Inspectability	Extent to which the connection can be inspected during its service life for deterioration, damage and degradation	Benefit (Qualitative)	WSP expert judgment regarding the inspectability of structures, connection details and their finishing systems within tunnel constructions [32]
Initial Costs	Material and construction costs expressed in euros	Cost (Quantitative)	Calculation of required material quantities and multiplication with unit prices obtained from supplier information and expert judgment from WSP [36]
Maintenance Costs	Expected maintenance and replacement costs over the service life expressed in euros	Cost (Quantitative)	Supplier information on maintenance intervals of asphalt joint systems and WSP cost estimates for maintenance interventions and tunnel closures [32, 36]

Finally, the model operates under the following boundary conditions:

- The assessment is performed in accordance with Standaardbestek 260 (SB260) and the supplementary comments provided by the client Lantis for the Oosterweelknoop project, including a maximum allowable deformation of 5 mm in the quasi-permanent load combination for the settlement-free joint
- The project-specific quantified criteria apply to three joint transitions: STD-10-STD-11, STD-11-STD-12 and STD-12-STD-13.
- All considered variants have been structurally verified at both the ULS and SLS levels.
- The application of the connections is limited to the inner wall and the outer wall.
- The connections in the wall are considered for a wall thickness of 600 mm.
- The connections in the wall are considered in combination with a shear connection in the tunnel floor, which is primarily responsible for transferring traffic-induced loads.

The complete decision model is presented in Figure 5.3 and in Appendix P in A3 format. The decision model is presented as a overview table in which the connection variants, methodology, weightings, assessments, and results are integrated. The columns represent the four connection variants, while the rows contain the different criteria. The final score of each variant is displayed at the bottom of the model.

At the top of the model, the four connection variants are briefly described and illustrated with an image. The applied MCDA methods and scoring legend are then presented. For the qualitative criteria, a brief explanation of the assessment is included. The quantitative criteria are presented as numerical scores highlighted in grey. The model also displays the intermediate results for each main criterion. These results ultimately lead to the overall score and ranking of the variants.

TU Delft

MCDA decision model for connection variants between tunnel segments STD-10 through STD-13

Author: Wouter Wagenaars

Date: 20-7-2026

Variant	Shear Key	Collar Connection	Dowel Connection	Free-Settlement Joint
Variant Description	Connection consisting of a concrete key (male part) and an opening (female part) in the inner and outer wall. Transfers shear forces in two directions using a bearing block.	Connection consisting of an inner and outer collar in the floor and roof. Transfers shear forces in one direction using a bearing block.	Connection with three DSDQ-450 steel dowels per wall in both the inner and outer wall, where each dowel consists of two stainless steel bars that only transfer shear forces. Through the application of a sliding sleeve, displacements in both longitudinal and transverse directions are enabled.	Joint without structural coupling (reking joint) that can accommodate displacements in longitudinal direction (±40 mm) and vertical direction (±10 mm), without transfer of shear forces.
Photo for design clarification				

Qualitative criteria legend

1	Very unfavorable performance with significant deficiencies	2	Unfavorable performance with multiple shortcomings	3	Neutral performance meeting minimum requirements	4	Favorable performance with limited shortcomings	5	Very favorable performance with excellent characteristics

MCDA Method

The MCDA method combines the AHP and TOPSIS methods. Using the AHP methodology, the relative weighting of the main criteria is determined based on pairwise comparisons according to the Saaty scale (1-9). Subsequently, the variants are evaluated using the TOPSIS methodology. Qualitative criteria are scored on a scale of 1 to 5, and quantitative criteria are assessed based on project-specific input data. Based on this, a ranking is established using the TOPSIS methodology. Qualitative criteria are scored on a scale of 1 to 5, and quantitative criteria are assessed based on project-specific input data. Based on this, a ranking is established.

	Clarification	Rating	Clarification	Rating	Clarification	Rating	Clarification	Rating
Robustness Weight : 0,35								
Redundancy Weight: 0,09	Concentrated stress field and single load path; limited redistribution in case of local failure	2	Load transfer via one dominant mechanism; no alternative load path in case of failure	2	Multiple load paths through parallel working dowels allowing redistribution	4	Secondary load transfer through surrounding concrete after joint failure, but with local stress concentrations	3
Tolerance Sensitivity Weight: 0,09	Sensitive to geometry and reinforcement, but sufficient design space is available to accommodate tolerances	4	Sensitive to geometry and reinforcement. Limited design space results in a greater influence of tolerances on the force distribution and capacity	3	Highly sensitive to joint width and eccentricity; deviations directly lead to capacity loss	2	Tolerances do not hinder the joint system; vertical deviations can still be corrected in the asphalt layer	5
Accidental Load Resistance Weight: 0,09	Protected against fire by fire-resistant sheetings	4	Protected against fire by fire-resistant sheetings	4	Protected against fire by fire-resistant sheetings and extra cover through cast-in concrete	5	Joint in floor not protected against high temperatures; elastomer degrades and loss of watertightness	2
Failure Behavior Weight: 0,09	Concrete cracking followed by plastic behavior of reinforcement; ductile behavior	4	Concrete cracking followed by plastic behavior of reinforcement; ductile behavior with possible degradation to functional performance	3	Plasticization of dowels; ductile failure mechanism; local concrete damage possible around dowels	4	Ductile behavior; material degradation, wear and reduced bond to the substrate	4
Relative Performance - Robustness		**0,78**		**0,66**		**0,85**		**0,79**
Modeling Reliability Weight : 0,04	**Clarification**	**Rating**	**Clarification**	**Rating**	**Clarification**	**Rating**	**Clarification**	**Rating**
Modeling Accuracy Weight: 0,04	1D model verified with 2D model; good agreement in deformations, rotations and shear force; complex modeling	4	1D and 2D verification with good agreement; dependent on non-linear functions, numerical residual forces present	3	Simple model with conservative assumptions; rotations in transverse direction and slip not modeled	3	Load transfer does not need to be modeled; behavior directly derived from global deformations	5
Relative Performance - Modeling Reliability		**0,80**		**0,60**		**0,60**		**1,00**
Feasibility Weight : 0,35	**Clarification**	**Rating**	**Clarification**	**Rating**	**Clarification**	**Rating**	**Clarification**	**Rating**
Construction complexity Weight: 0,12	Complex geometry due to the cantilevered key profile; high reinforcement ratio	2	High reinforcement ratio at wall locations; additional formwork required over entire width of floor and roof	1	Prefabricated; locally extra reinforcement around dowel	4	Prefabricated; no additional formwork and limited reinforcement complexity	5
Execution risks Weight: 0,12	Risks before and during pouring manageable through execution measures	4	Risks before and during pouring manageable through execution measures	4	Risks before and during pouring manageable through execution measures	4	Risks before and during pouring manageable through execution measures	4
Construction speed Weight: 0,12	Custom formwork and challenging rebar placement	2	Multiple pouring phases and additional formwork; complex rebar placement at wall locations	1	Prefabricated dowels that can be easily placed in the formwork; locally challenging rebar placement	4	Prefabricated joint system; no additional pouring required	5
Relative Performance - Feasibility		**0,60**		**0,47**		**0,87**		**1,00**
Sustainability Weight : 0,05	**Clarification**	**Rating**	**Clarification**	**Rating**	**Clarification**	**Rating**	**Clarification**	**Rating**
MKI Score Weight: 0,03		€ 2590		€ 5110		€ 5150		€ 1250
Recycling opportunities Weight: 0,03	Not demountable; recycling via crushing, steel recoverable and concrete reusable as aggregate	2	Not demountable; recycling via crushing, steel recoverable and concrete reusable as aggregate	2	Not demountable due to cast-in; steel only recoverable after demolition	2	Steel edge profiles cast-in and elastomer not reusable	2
Relative Performance - Sustainability		**0,83**		**0,51**		**0,50**		**1,00**
Durability Weight : 0,10	**Clarification**	**Rating**	**Clarification**	**Rating**	**Clarification**	**Rating**	**Clarification**	**Rating**
Service Life Weight: 0,05		100 years		100 years		100 years		40 years
Inspectability Weight: 0,05	Not visible due to fire-resistant cladding; shear key in inner wall visible on one side	2	Fully covered by fire-resistant cladding; connection not visually inspectable	2	Fully embedded in concrete; inspection only possible indirectly via deformations or damage	1	Directly accessible from roadway when closed off; joint profile and steel construction visually inspectable	4
Relative Performance - Durability		**0,75**		**0,75**		**0,63**		**0,70**
Costs Weight : 0,11	**Clarification**	**Rating**	**Clarification**	**Rating**	**Clarification**	**Rating**	**Clarification**	**Rating**
Initial costs Weight: 0,06		€ 24231		€ 42781		€ 31440		€ 150000
Maintenance costs Weight: 0,06		€ 0		€ 0		€ 0		€ 525000
Relative Performance - Costs		**1,00**		**0,93**		**0,97**		**0,00**
Total score	**0,51**		**0,41**		**0,67**		**0,57**	

Figure 5.3: Decision model for tunnel connection founded on shallow foundation

6

Results

This chapter presents and analyzes the results of the MCDA decision model developed in Chapter 5. Table 6.1 shows the relative performance of the alternatives for each main criterion and the final score. Values are normalized between 0 and 1, where higher values indicate better performance compared to the other alternatives. The reported values represent relative performance scores and should not be interpreted as absolute measures of performance.

Table 6.1: Relative performance per criterion and overall TOPSIS score

Criterion	Shear Key	Collar Construction	Dowel Connection	Free-Settlement Joint	Weight
Robustness	0.78	0.66	0.85	0.79	34.97 %
Modeling Reliability	0.80	0.60	0.60	1.00	3.72 %
Feasibility	0.60	0.47	0.87	1.00	34.97 %
Sustainability	0.83	0.51	0.50	1.00	5.21 %
Durability	0.75	0.75	0.63	0.70	9.81%
Costs	1.00	0.93	0.97	0.00	11.32%
Total Score	**0.51**	**0.41**	**0.67**	**0.57**	

Shear Key

The shear key achieves a total score of 0.51. The connection performs well in terms of robustness, as the high degree of design flexibility of the console ensures that geometric deviations and construction tolerances have only a limited influence on the force transfer mechanism. In addition, the shear key performs favorably in terms of cost, as it relies solely on conventional reinforcing steel and does not require additional materials or components.

The drawback of the connection is its constructability. Due to its complex geometry, additional formwork is required, and large quantities of heavy reinforcement are needed, including long reinforcing bars that must be anchored deep into the wall.

Collar Construction

The collar connection achieves a total score of 0.41, ranking last among the considered connection variants. The connection is characterized by high stress concentrations at the top and bottom of the walls. A thickening of the tunnel floor beneath the walls is required to accommodate the extensive structural detailing. The high reinforcement ratio and increased material consumption result in a less sustainable design with limited constructability. The connection also need additional formwork across the full width of the floor and roof that will increase the complexity of the construction.

A potential drawback of the connection is the risk of unfavorable force distributions when the compression strut is not formed correctly (Appendix I). Improper detailing may also result in increased forces in the horizontal tension ties, making the structural behavior sensitive to design and construction deviations.

Dowel Connection

The dowel connection achieves the highest overall score of the considered variants with a score of 0.67. The connection is robust due to the presence of multiple dowels which allow forces to be redistributed through alternative load paths in the event of local dowel failure. The connection is also highly constructible because the dowels can be easily integrated into the casting of the tunnel walls and require only limited reinforcement detailing within the wall reinforcement.

A limitation of the connection is that the dowels are fully embedded within the concrete structure after construction which makes inspection impossible. Uncertainties also remain regarding the modeling of the interaction between the dowel, the sleeve and the surrounding concrete. The use of stainless steel results in a higher environmental impact than conventional reinforcing steel which negatively affects the sustainability of the connection.

Free-Settlement Joint

The free-settlement joint achieves a total score of 0.57. The connection is easy to construct because no structural connection between the tunnel segments is required and the joint system can be readily integrated into the tunnel structure. In addition, only a limited amount of additional material is required which keeps the environmental impact relatively low.

The main drawback of the connection is the limited service life of the joint system. As a result, maintenance and replacement are required multiple times during the design life of the tunnel which leads to high life-cycle costs. Since the other connection types do not incur maintenance costs during the design life, the free-settlement joint obtains a relative cost score of 0.00 in Table 6.1. This score results from the fact that the free-settlement joint has both the highest initial costs and the highest maintenance costs of all considered alternatives. Consequently, it coincides with the negative ideal solution for the cost criterion in the TOPSIS analysis.

Validation MCDA Method

The applied AHP-TOPSIS methodology is an existing and widely accepted MCDA method described in the literature. This research does not develop a new decision-making methodology but applies an established method to the assessment of tunnel segment connection concepts. Additional validation tests were performed to evaluate the reliability of the applied methodology.

The Consistency Ratio (CR) and the sensitivity analysis (Q.1) were used as internal validation methods. These tests assess whether the AHP calculations were performed consistently and to what extent changes in the criterion weights influence the final ranking. In addition, the results were compared with alternative weighting and ranking methods. The validation tests included replacing AHP with PSI (Q.2) and replacing TOPSIS with both WSM and VIKOR (Q.3 and Q.4).

The results of the validation tests show that the final ranking is independent of the selected ranking method and dependent on the applied criterion weights. This is consistent with the decision model, in which the AHP analysis assigns a high priority to feasibility and robustness. When equal or objectively derived weights are applied, the preferred alternative shifts to the shear key and the free-settlement joint, respectively. This shift is not considered a limitation of the decision model but rather a logical consequence of the project-specific priorities embedded in the weights. It can be concluded that the combination of AHP and TOPSIS provides a reliable methodology for the assessment of the tunnel segment connection concepts considered.

Reflection

During the design phase of the Oosterweelknoop project, the client selected a shear key as the tunnel segment connection concept at an early stage. During the subsequent design development by WSP, it became evident that considerable effort was required to detail and construct this connection. This raised the question within the project team whether alternative connection concepts could offer improved constructability.

The results of this research are consistent with these expectations. The structural validation demonstrates that multiple connection concepts are capable of transferring the required connection forces while satisfying the applicable project requirements and design standards. The results also confirm that alternative connection concepts are available that offer significantly better constructability than the shear key designed for the STD tunnel segments.

One finding that was not anticipated concerns the relatively small differential settlements calculated for the STD tunnel segments considered in this study. During the initial design phase, attention was primarily focused on the more complex tunnel segments within the project. A free-settlement joint was therefore quickly considered unsuitable due to the expected exceedance of the SB260 requirements.

The calculated differential settlements for the investigated STD tunnel segments are significantly lower. Consequently, a free-settlement joint represents a more realistic structural alternative than originally anticipated.

7

Discussion

The results of the decision model indicate that the dowel connection is the preferred alternative for the tunnel segments considered with a relative score of 0.67. This outcome depends on the adopted boundary conditions and the weighting factors applied within the model.

The reliability of the applied methodology is influenced by several factors. The AHP method is inherently subjective as the criterion weights depend directly on expert input. The validation tests performed provide confidence in the applied AHP-TOPSIS methodology and demonstrate that the final ranking is largely independent of the selected ranking method while remaining dependent on the applied weighting approach. This is consistent with the objective of the decision model in which project priorities are translated into criterion weights. Nevertheless, uncertainties remain regarding the qualitative scores. These scores are partly based on expert judgment and may therefore vary when different experts are consulted. In addition, the results have not been compared with similar cases from the literature or engineering practice. Such a comparison could provide further insight into the representativeness of the results.

For this research several limitations affect the applicability of the decision model and the uncertainty associated with the results.

- The research was conducted for tunnel segments with relatively similar geometries. For larger geometric differences between adjacent tunnel segments, the applicability of the decision model may be reduced.
- For the determination of settlements and connection forces, the same subgrade stiffness was assumed for all variants. This stiffness was derived from PLAXIS and based on the moment of roof casting. In reality, this moment differs between variants, which may result in different subgrade stiffnesses and consequently different connection forces.
- The design of the free-settlement joint was based on SB260, where traffic loads are not included in the quasi-permanent load combination. In practice, however, these loads are often considered in the SLS assessment.
- The crack width verification of the reinforced concrete connections was based on interpolation. Table 7.3N of Eurocode 2 was used, although values are only provided for crack widths of 0.20 mm and 0.30 mm.

The decision model also offers opportunities for further research to improve the reliability of the results.

- The connection variants can be further optimized with respect to material consumption by varying their geometry and positioning.
- The assessment of the qualitative criteria can be further validated by comparing the applied expert judgment with data from completed tunnel projects with a similar geometry.

8

Conclusion

During the course of this research, it became evident that the design of tunnel segment connections for tunnels on shallow foundations is a complex process. In practice, different choices are made regarding modeling approaches, decision-making methodologies, and the eventual implementation of the connection. For this reason, a methodology for selecting a connection variant was developed based on the following main research question:

How can a systematic decision-making approach be used to determine the most suitable tunnel segment connection for the Oosterweelknoop, considering settlement behavior resulting from construction phasing and structural response?

To answer this research question, a decision model was developed for four connection variants in which project-specific criteria were combined with standardized performance criteria. The decision model was linked to a methodology for modeling the connection forces using a combination of SCIA Engineer and PLAXIS. This methodology was applied to the Oosterweelknoop project for an optimized design of tunnel segments STD-10 through STD-13. Based on the performed analyses and the developed decision model, it can be concluded that the dowel connection is the most suitable solution for the considered tunnel segments. This variant provides the best balance between constructability, robustness and costs.

The research also include several important insights:

- The optimization analysis and modeling demonstrate that the interaction between SCIA Engineer and PLAXIS has a significant influence on the calculated connection forces. A reduction in the self-weight of the tunnel superstructure leads to a decrease in the effective subgrade stiffness beneath the walls, as obtained from PLAXIS. This results in an unfavorable increase in the connection forces.
- The modeling results also show that the use of 1D elements for the connections introduces additional points of attention. The calculated forces are sensitive to factors such as the selected mesh size and the adopted idealization of the connection. As a result, variations may occur in the calculated forces. This highlights the importance of careful modeling and interpretation of the results to ensure a reliable assessment of the connection forces.
- The assessment of the connection variants shows that the preferred alternative depends on the selected project priorities. The validation demonstrates that the final ranking is largely independent of the applied ranking method but remains sensitive to the adopted criterion weights. This highlights that the selection of a tunnel segment connection depends not only on the technical characteristics of the alternatives but also on the priorities established within the project.

Based on the results, the use of dowel connections in the tunnel walls is recommended for the Oosterweelknoop STD tunnel segments. The connection should be combined with a shear connection in the floor, which primarily accommodates the relative displacements caused by traffic loads. The concrete shear key adopted in the current design requires extensive reinforcement detailing and is more difficult to integrate into the existing wall reinforcement layout than the proposed dowel connection. The dowel connection requires less additional reinforcement and avoids several of the detailing challenges. Furthermore, the dowel connection reduces modeling complexity. During the development of the current Oosterweelknoop design, considerable effort was required to model the shear key and optimize the connection force. The dowel connection reduces the required modeling effort and limits the number of design iterations during the engineering process.

Although the assessment was performed for the Oosterweelknoop case study, the developed methodology is also applicable to tunnel segments that are representative of those considered in this research. Future projects involving tunnels on shallow foundations are therefore encouraged to systematically assess alternative connection variants using the developed decision model and the associated modeling methodology. The decision model can be further expanded by incorporating additional assessment criteria. To further refine the methodology, the connection variants should be structurally validated at a more detailed level before being implemented in the model.

References

[1] NASA. *Canadarm 2 robotic arm grapples SpaceX Dragon*. Image Accessed on 10-02-2026. 2016.

[2] *Handboek Tunnelbouw*. Versie 2025.1-6. Accessed at 08-01-2026. Centrum Ondergronds Bouwen (COB). 2025. URL: `https://www.cob.nl`.

[3] Johan Fokkinga. *Interview with Johan Fokkinga about the Oosterweelknoop project, challenges related to the shear key, and optimization opportunities*. Personal Interview, February 2026. 2026.

[4] Bram Erkelens and Brigitte van Kronenburg. *Rekennota Analyse Langseffecten*. Document code: OWRA-05983-RNK-REK-W60-000007. 2024.

[5] Roy Jadoenathmissie. *Tekening: Geotechnisch profiel S06B*. Document code: OWRA-06327-RNK-TEK -W60-000100. 2024.

[6] Thomas L. Saaty. *The Analytic Hierarchy Process: Planning, Priority Setting, Resources Allocation*. New York, USA: McGraw-Hill, 1980.

[7] Farhad Hosseinzadeh Lotfi et al. *Fuzzy Decision Analysis: Multi Attribute Decision Making Approach*. Vol. 1121. Studies in Computational Intelligence. Springer, 2023.

[8] C. L. Hwang and K. Yoon. *Methods for multiple attribute decision making*. New York, USA: Springer-Verlag, 1981.

[9] Irem Bayram Zumrut. "Multi-criteria decision-making approach for selecting a structural system of an industrial facility". In: *Organization, Technology and Management in Construction* (2022).

[10] A. H. J. M. Vervuurt, C. R. Braam, and I. Schols. "Zettingsgedrag en capaciteit van mootvoegen in zinktunnels". In: *Land + Water Magazine* (Dec. 2013).

[11] Hakron. *DSD-dwarskrachtdeuvels*. Productbrochure: Ter opname en overdracht van permanente en relatief hoge dwarskrachten.

[12] Leviat. *Ancon DSD/ESD Shear Load Connectors for the Construction Industry*. Product brochure, DSD/ESD shear load connectors. 2026.

[13] *Standaardbestek 260 voor kunstwerken en waterbouw. Hoofdstuk 21*. Geconsolideerde versie 2.0a. Departement Mobiliteit en Openbare Werken, Vlaanderen. Dec. 2021.

[14] *Aanvullingen standaardbestekken. Deel C – C.4.3.2.21 Ontwerp, studie en berekeningsnota's*. Revisie 1.0. Document code OWRA-00ALG-LAN-NOT-W65-000018. Lantis. Mar. 2022.

[15] *RTD 1001 Richtlijnen Ontwerp Kunstwerken*. Versie 2.0a. Rijkswaterstaat, Ministerie van Infrastructuur en Waterstaat. Dec. 2021.

[16] Niels Van der Zee. *Interview with Niels van der Zee about Plaxis cross section models S01 en S06B*. Personal Interview, March 2024. 2026.

[17] CROW. *Publicatie 150: Toepassingsrichtlijn voor EPS in de wegenbouw*. 2000.

[18] Ronnie Baardman. *Tekening: Overzicht stortnaden MOOT STA-09 (EWP7 Samengestelde en Vlechttunnel)*. Document code: OWRA-10802-RNK-TEK-W60-199999. 2025.

[19] Trelleborg. *Elastomeric Bearing Pads & Strips*. Product brochure. 2026.

[20] C. S. Kleinman. “Nokken met die Tanden!, Deel 1 t/m 4”. In: *TU Eindhoven, Faculteit Bouwkunde* (2006). Obtained via CementOnline.

[21] Niels van der Zee. *UGP Vlechttunnel Geotechniek*. Document code: OWRA-05983-RNK-ONT-W65 -000001. 2025.

[22] *NEN-EN 1991-2 (nl): Eurocode 1 – Belastingen op constructies – Deel 2: Verkeersbelastingen op bruggen*. Obtained via Briswarenhuis. Nederlands Normalisatie-instituut (NEN). 2003.

[23] Rijkswaterstaat. *Meerkeuzematrix (MKM) voegovergangen (met factsheets)*. RTD 1007-1, versie 1.0, definitief, datum: 1-4-2013. Rijkswaterstaat, Ministerie van Infrastructuur en Milieu. 2013.

[24] Sika. *Sika Waterbar® - Elastomer Type FM, FMS: Technische fiche*. Interne voegbanden voor voegafdichting in waterdichte betonstructuren conform DIN 7865-1/-2. Sika. 2020.

[25] Schrumpf Bouwstoffen BV. *SCHRUMPF ACME Voegprofiel*. Accessed:2026-07-14. 2025. URL: `https://www.schrumpf.nl/wp-content/uploads/2019/06/Acme.pdf`.

[26] Zhi-nan Hua and Yong-li Xie. “Mechanical and failure characteristics of shear keys on immersed tunnel segment joints under differential settlements”. In: *Procedia Engineering* (2016). 2nd International Symposium on Submerged Floating Tunnels and Underwater Tunnel Structures, pp. 373–378.

[27] Rob Vergossen and Eelco de Winter. “Staafwerkmodellen nader beschouwd: Keuze voor staafwerkmodel en overeenkomstige detaillering essentieel voor capaciteit tand-nokconstructies”. In: *Cement 4* (2026). Obtained via CementOnline.

[28] Zhen Huang. “Simulation of Thermomechanical Coupling and Evaluation of the Fire Resistance for the Joints of Fabricated Frame Tunnel”. In: *Fire* (2023).

[29] Massimiliano Lucon. “Experimental fire response of seismic elastomeric bearings”. In: *University of Trento* (2023).

[30] Nystrom. *Expansion Joint Fire Barriers: Essential for Building Safety and Code Compliance*. 2026. URL: `https://blog.nystrom.com/expansion-joint-fire-barrier`.

[31] Giovanni Muciaccia. *Design Approach for Lateral Capacity of Dowel-Type Steel Connections in Precast Reinforced Concrete Elements*. Accessed: 2026-06-17. 2021. URL: `https://www.frontiersin.org/journals/built-environment/articles/10.3389/fbuil.2021.640189/full`.

[32] Marco Flipse. *Interview with Marco Flipse on the feasibility, costs, and durability of the variants*. Personal Interview, June 2024. 2026.

[33] Rijkswaterstaat. *uboCalc – MKI calculation software for the Dutch GWW sector*. Software platform; MKI values used as provided in DuboCalc and sourced from the National Environmental Database (NMD). 2026. URL: `https://dubocalc.nl/`.

[34] João Pacheco. “Recycled Aggregates Produced from Construction and Demolition Waste for Structural Concrete: Constituents, Properties and Production”. In: *Materials* (2021).

[35] SteelPro Group. *Steel Structure Recycling & Reuse: Benefits, Challenges & What’s Recyclable*. 2026. URL: `https://peb.steelprogroup.com/steel-structure/sustainability/recycling-reuse/`.

[36] Johannes Woudsma. *Interview with Johannes Woudsma about costs*. Personal Interview, June 2024. 2026.

[37] Oosterweelverbinding. *DitisOosterweel Brocure*. 2025.

[38] Thomas L. Saaty and M. S. Özdemir. “Why the magic number seven plus or minus two?” In: *Mathematical and Computer Modelling* (2003), pp. 233–244.

[39] Rijkswaterstaat Bouwdienst. *SATO RWS-Deel 5.1 Dilatatievoegen*. 2005.

[40] Sander Roubos. *Tekening: Voegen bodemplaat*. Document code: OWRA-T0505-RNK-TDE-W60-000007. 2025.

[41] Sander Roubos. *Tekening: Voegen dakplaat*. Document code: OWRA-T0505-RNK-TDE-W60-000009. 2025.

[42] *NEN-EN 1992-1-1 (nl): Eurocode 2 – Ontwerp en berekening van betonconstructies – Deel 1-1: Algemene regels en regels voor gebouwen*. Obtained via Briswarenhuis. Nederlands Normalisatie-instituut (NEN). Apr. 2005.

[43] *NEN-EN 1990:2002/NB:2019 Nationale bijlage bij NEN-EN 1990*. Obtained via Briswarenhuis. Nederlands Normalisatie-instituut (NEN). Jan. 2021.

[44] Rots. *Eindrapportage proefput*. Document code: OWR-VO-RAP-OWR-GT-0003. 2015.

[45] *Richtlijnen voor de toepassing van Eurocode 7 in België: Het grondmechanisch ontwerp van kerende constructies: Beschoeiingen*. Versie 19/03/2015. studocu. 2015.

[46] Sander Roubos. *Tekening: Detailwapening console buitenwand*. Document code: OWRA-T1304-RNK-TDE-W60-000012. 2025.

[47] Nederlands Normalisatie-instituut (NEN). *NEN 6720: Voorschriften Beton TGB 1990 – Constructieve eisen en rekenmethoden (VBC)*. Second edition, September 1995. 1995.

[48] Cement & Beton. *Rekenvoorbeelden Eurocode 2*. Part 8 of Cement & Beton serie (CB8). 2010.

[49] & dr.ir. Cor van der Veen & ir. Simon Wijte ir. Jan Gijsbers. “Tandopleggingen volgens NEN6720”. In: *Cement Article* (2009). Obtained via CementOnline.

[50] J. Cees. “Tandtechniek”. In: *Cement Article* (2008). Obtained via CementOnline.

[51] Rosaria de F. S. M. Russo and Roberto Camanho. “Criteria in AHP: A Systematic Review of Literature”. In: *Information Technology and Quantitative Management* (2015). Obtained via ScienceDirect.

[52] Murat Gunduz Saman Aminbakhsh and Rifat Sonmez. “Safety risk assessment using analytic hierarchy process (AHP) during planning and budgeting of construction projects”. In: *Journal of Safety Research* (2013). Obtained via ScienceDirect.

[53] InfralImpact. *Wat is DuboCalc en hoe gebruik je het?* Accessed: 2026-07-16. 2026. URL: `https://www.infralimpact.nl/artikelen/wat-is-dubocalc-en-hoe-gebruik-je-het`.

[54] WSP. *Presentatie MKI & DuboCalc*. Internal workshop DuboCalc from WSP. 2025.

[55] GEP ECOTECH (Wendy). *Concrete Construction Waste with Reinforcement Resource Utilization Schemes*. 2026. URL: `https://www.aishred.com/release/concrete-construction-waste-with-reinforcement-resource-utilization-schemes.html`.

A

Case Study Oosterweelknoop

The Oosterweelknoop project in Antwerp is used as the case study for this research. The Oosterweelknoop forms part of the larger Oosterweelverbinding project, through which the Antwerp Ring Road (R1) will be completed by constructing a new connection beneath and alongside the River Scheldt. The Oosterweelverbinding consists of three main components (Figure A.1): a new tunnel under the Scheldt, the Oosterweelknoop, and the kanaaltunnels. Together, these components will enable the completion of the Antwerp ring road and a better distribution of traffic flows around the city [37].



Figure A.1: Overview Oosterweelverbinding [37]

The Oosterweelknoop is a cut-and-cover tunnel structure that will be constructed beneath the Oosterweeleiland. The structure forms the link between the Scheldt Tunnel on the east side and the canal tunnels on the west side. The tunnel is being constructed using the dry method between two diaphragm wall structures and will later be integrated into a landscaped polder area. The tunnel is founded on shallow foundations, with differential settlement being prevented by means of shear keys in both the walls and the floor of the tunnel.

The tunnel structure of the Oosterweelknoop can be divided into two main types: the combined tunnels and the weaving tunnels. The combined tunnels consist of separate tunnel tubes that gradually converge towards one another until they join at the weaving tunnels. The weaving tunnels transform the multiple tunnel tubes into a 2×2 stacked tunnel configuration that connects to the canal tunnels on the west side.

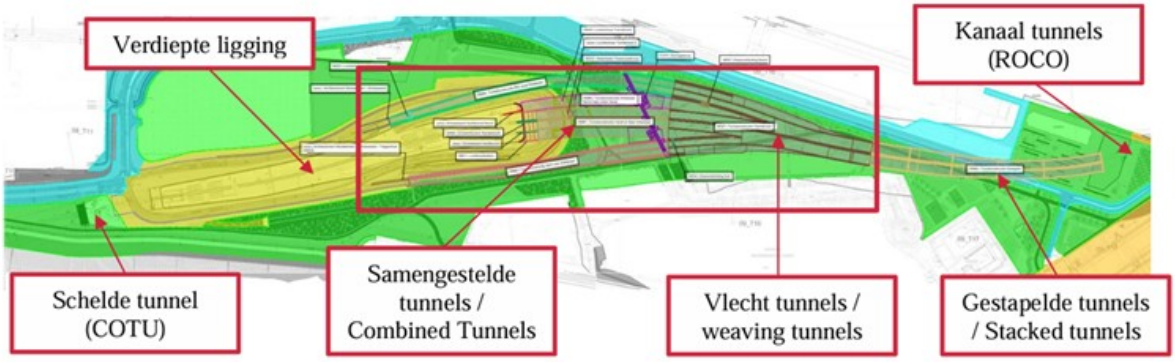

Figure A.2: Overview Oosterweelknoop [4]

A.1. Geological and Geotechnical Profile

The soil structure at the Oosterweelknoop has a direct influence on settlement behavior and determines the deformations and force distribution that may occur in the tunnel segment connections. Determining the soil structure and the associated geotechnical parameters is beyond the scope of this research. Therefore, the results of the ground investigations carried out within the Oosterweelknoop project are adopted as input and boundary conditions for the analyses performed in this research.

To establish the soil structure, cone penetration tests were carried out along the entire alignment of the combined tunnels. These investigations indicate that the soil structure within the project area is homogeneous. The tunnel elements are founded on a thin sand layer, underlain by the Boomse Clay, which is subdivided into several sublayers (BK0, BK1, BK2, BK3, BK4).

The Boomse Clay layer is a soil layer that has fully consolidated under natural geological conditions. During the construction of the tunnel, excavation between the diaphragm walls temporarily reduces the vertical effective stress. Once the tunnel structure is cast and the excavation pit is backfilled, the vertical stress is gradually restored. This unloading–reloading cycle leads to recompression and time-dependent secondary consolidation, both of which contribute to the final settlements beneath the STD tunnel elements. The complete soil structure under the combined tunnels is shown in Table A.1. The sand layer and the upper sublayers of the Boomse clay (BK0 and BK1) determine the settlement behavior beneath the STD tunnel segments.

Table A.1: Geological profile of STD tunnel tube

Formation	Abbreviation	Brief description
Kattendijk	Kd	Dense fine sand, possibly containing glauconite.
Upper layer of Boomse Clay	BK0	BK0 is between a few decimeters and 4 meters thick and is the weathered top layer of BK1
Dark grey clay	BK1	Clay with a silty and clayey layer approximately 12–17 meters thick
Black clay	BK2	High luthum content, approximately 12 meters thick
Grey clay	BK3	Clay with a silty and clayey layer approximately 25 meters thick
Sandy silty clay	BK4	Approximately 10 meters thick

B

AHP & TOPSIS Calculation Steps

This appendix presents the calculation steps and mathematical formulations of the Analytic Hierarchy Process (AHP) and the Technique for Order Preference by Similarity to Ideal Solution (TOPSIS). These methods are used in the decision-making model for tunnel segment connection variants.

Analytical Hierarchy Process (AHP)

Step I. The pairwise comparison judgment matrix:
The pairwise comparison matrix A contains the relative importance of each criterion compared to the other criteria. Each matrix element a_{ij} represents the importance of criterion i relative to criterion j, based on the Saaty scale. n is the number of criteria in the model.

$$A = \begin{bmatrix} a_{11} & a_{12} & \cdots & a_{1n} \\ a_{21} & a_{22} & \cdots & a_{2n} \\ \vdots & \vdots & \ddots & \vdots \\ a_{n1} & a_{n2} & \cdots & a_{nn} \end{bmatrix} = \begin{bmatrix} 1 & a_{12} & \cdots & a_{1n} \\ 1/a_{12} & 1 & \cdots & a_{2n} \\ \vdots & \vdots & \ddots & \vdots \\ 1/a_{1n} & \cdots & \cdots & 1 \end{bmatrix} \tag{B.1}$$

Values on the diagonal are equal to 1, as each criterion is equally important to itself. The reciprocal value $1/a_{ij}$ is assigned to the opposite comparison to ensure consistency within the matrix. The relative importance of two criteria is assessed using the Saaty scale shown in Table B.1 [9, 6].

Table B.1: Scale for pairwise comparisons

Value of a_{ij}	**Definition**
1	i and j are equally important
3	i is slightly more important than j
5	i is more important than j
7	i is strongly more important than j
9	i is absolutely more important than j
2, 4, 6, 8	Intermediate values between two adjacent judgments

Step II. Determination of weights:
To determine the weights for each criterion, the pairwise comparison matrix is normalized by dividing each matrix element by the sum of its corresponding column. Subsequently, the average value of each row is calculated. These row averages represent the weighting factors of the criteria.

$$a_{ij,\text{norm}} = \frac{a_{ij}}{\sum_{i=1}^{n} a_{ij}} \quad w_i = \frac{\sum_{j=1}^{n} a_{ij,\text{norm}}}{n} \tag{B.2}$$

Step III. Calculation of consistency ratio (CR):
To ensure the reliability of the pairwise comparison matrix, the consistency of the pairwise judgments is evaluated using the Consistency Ratio (CR). The pairwise comparison matrix is considered sufficiently consistent when $CR < 0.10$ [9, 6].

The consistency ratio is calculated as:

$$CR = \frac{CI}{RI} \tag{B.3}$$

where CI is the Consistency Index and RI is the Random Index obtained from Table B.2.

The Consistency Index is determined from the maximum eigenvalue λ_{Max} according to:

$$\lambda_i = \frac{(A \cdot w)_i}{w_i} \qquad \lambda_{Max} = \frac{1}{n} \sum_{i=1}^{n} \lambda_i \qquad CI = \frac{\lambda_{Max} - n}{n - 1} \tag{B.4}$$

where A is the pairwise comparison matrix, w is the weighting vector, and n is the matrix size.

Table B.2: The random index [38]

n	1	2	3	4	5	6	7	8	9	10	11	12
RI	0.00	0.00	0.52	0.89	1.11	1.25	1.35	1.40	1.45	1.49	1.52	1.54

Technique for Order Preference by Similarity to Ideal Solution (TOPSIS)

Step I. Normalization of the decision matrix:
The evaluation scores of all alternatives are first arranged in a decision matrix. The alternatives are represented by the rows (i), while the criteria are represented by the columns (j). Both quantitative and qualitative criteria can be included within the same matrix. The decision matrix is subsequently normalized using equation (B.5). Here, a_{ij} denotes the score of alternative i under criterion j, and x_{ij} represents the corresponding normalized score ($i = 1, 2, \ldots, m$; $j = 1, 2, \ldots, n$).

$$x_{ij} = \frac{a_{ij}}{\sqrt{\sum_{i=1}^{m} a_{ij}^2}} \tag{B.5}$$

Step II. Obtaining the weighted normalized matrix:
Multiplying the normalized matrix by the weights w_j produces the weighted normalized matrix (V_{ij}). These weights can be determined using other MCDM methods.

Step III. Determining the Positive and Negative Ideal Points:
The positive ideal solution (PIS) and negative ideal solution (NIS) are constructed from the weighted decision matrix by selecting the best and worst value for each criterion. For benefit criteria, the highest weighted score is selected as the ideal value and the lowest score as the anti-ideal value. For cost criteria, the opposite applies.

$$PIS = \left\{v_1^+, \ldots, v_j^+, \ldots, v_n^+\right\}$$
$$NIS = \left\{v_1^-, \ldots, v_j^-, \ldots, v_n^-\right\} \tag{B.6}$$

where

$$v_j^+ = \begin{cases} \max\limits_i \{v_{ij}\}, & C_j \text{ is a benefit criteria,} \\ \min\limits_i \{v_{ij}\}, & C_j \text{ is a cost criteria.} \end{cases} ;\ j = 1, \ldots, n. \tag{B.7}$$

$$v_j^- = \begin{cases} \min\limits_i \{v_{ij}\}, & C_j \text{ is a benefit criteria,} \\ \max\limits_i \{v_{ij}\}, & C_j \text{ is a cost criteria.} \end{cases} ;\ j = 1, \ldots, n. \tag{B.8}$$

Step IV. Calculation of separation distances:
For each alternative, the distance to both the PIS (D_i^+) and the NIS (D_i^-) is calculated using equations B.9.

$$D_i^+ = \sqrt{\sum_{j=1}^{n} \left(v_{ij} - v_j^+\right)^2} \qquad D_i^- = \sqrt{\sum_{j=1}^{n} \left(v_{ij} - v_j^-\right)^2} \tag{B.9}$$

Step V. Calculation of the Relative Closeness Coefficient:
The separation distances to the Positive Ideal Solution (PIS) and Negative Ideal Solution (NIS) are used to calculate the relative closeness coefficient (C_i). This coefficient represents the final TOPSIS score of an alternative and ranges between 0 and 1. A value closer to 1 indicates that the alternative is located closer to the PIS and further from the NIS, whereas a value closer to 0 indicates the opposite. The relative closeness coefficient is determined according to Equation B.10.

$$C_i = \frac{D_i^-}{D_i^- + D_i^+} \tag{B.10}$$

The alternatives are ranked based on their C_i values, where the alternative with the highest score is considered the preferred solution.

Step VI (optional). Calculation of intermediate results
As an addition to the standard TOPSIS analysis, intermediate results (I_i) can be calculated for each main criterion. This analysis determines the relative performance of the alternatives with respect to each main criterion. As a result, greater insight is obtained into the contribution of the individual main criteria to the final TOPSIS score.

To determine the intermediate result, the normalized contribution of subcriterion j (S_j) is first calculated for each alternative i. For benefit criteria, the normalized contribution is determined according to Equation B.11. For cost criteria, the normalized contribution is determined according to Equation B.12.

$$S_j = \frac{x_j}{x_{\max}} \tag{B.11}$$

$$S_j = \frac{x_{\max} - x_j}{x_{\max} - x_{\min}} \tag{B.12}$$

$x_{\max}$ and $x_{\min}$ represent the highest and lowest normalized weighted score, respectively, among all alternatives for the corresponding subcriterion.

The intermediate result for each main criterion is then calculated as the average of the normalized contributions of the associated subcriteria. This calculation is performed according to Equation B.13.

$$I_i = \frac{\sum_{j=1}^{n} S_j}{n} \tag{B.13}$$

where n is the number of subcriteria within the main criterion. The intermediate result is expressed on the same scale as the final TOPSIS score (C_i), where a value of 0 corresponds to the relatively least favorable performance and a value of 1 corresponds to the relatively most favorable performance with respect to the main criterion considered.

C

Structural and Geotechnical Design Principles

This appendix presents the structural and geotechnical design principles used for the development and verification of the connection variants.

C.1. Structural Design Principles

C.1.1. Concrete

The requirements in Table C.1 must be met for the design of concrete connections.

Table C.1: Principles concrete

Design requirement	Value	Unit	Description	SB260 [13]
Concrete strength class	C35/45	-	Strength class for tunnel structures (EE4/ES4)	21-5.2.1
Concrete cover (insitu)	60	mm	Cover in accordance with exposure class (EE4/ES4), design service life 100 years, cast in place and non-segmental	21-5.2.2.1
Concrete cover (prefab)	50	mm	Cover in accordance with exposure class (EE4/ES4), design service life 100 years, precast and non-segmental	21-5.2.2.2
Minimum thickness	≥ 300	mm	Thickness of tunnel walls, roof slab and base slab is at least 300 mm	21-5.4.7
Crack width	0,20	mm	Maximum crack width for elements in tunnel structures directly subjected to traffic at the top surface	21-6-6.1
Crack width	0,25	mm	Maximum crack width for walls and slabs with an earth-retaining function, without a watertight requirement and not subjected to traffic loading	21-6-6.1
Steel grade	B500B	-	Reinforcement	21–5.2.3.1

The exposure class prescribed by SB260 for tunnel structures is EE4/ES4. EE4 stands for an outdoor environment that is exposed to frost and de-icing salts, such as parts of road infrastructure where splashing or runoff salt water may occur. The environmental classes differ per tunnel segment and are listed below [14]:

- Ground-side walls, above water level: XC4, XD2, XA1
- Traffic-side walls: XC4, XD3, XF4
- Tunnel floor, upper side: XC4, XD3, XF2
- Tunnel floor, lower side, above groundwater level: XC4, XD2, XA1
- Tunnel roof, upper side, less than 1 m below a road: XC4, XD3, XF4
- Tunnel roof underside: XC3, XD3, XF4

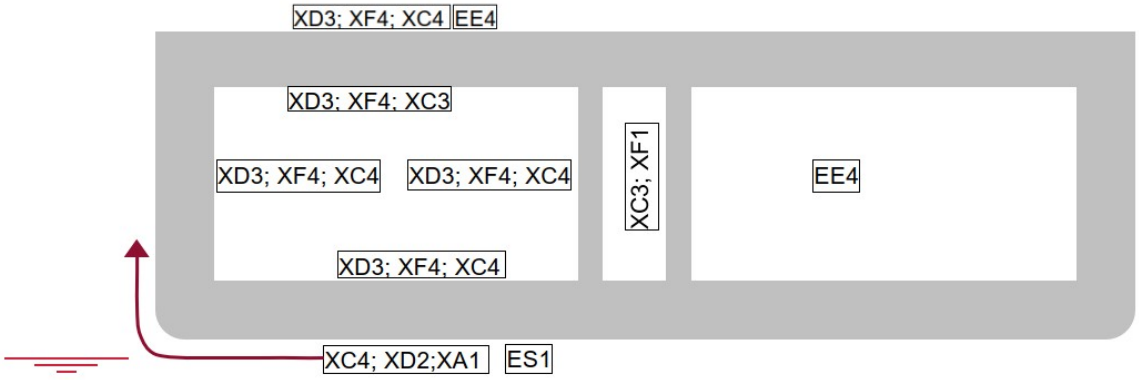

Figure C.1: Environmental and exposure classes of the tunnel within the polder

C.1.2. Steel

The physical properties of structural steel are derived from NBN EN 1993–1–1, ANB:2010, whereby the following assumptions are made for all steel connections:

- modulus of elasticity of E_s = 210,000 N/mm²
- Poisson's ratio of ν = 0.30
- Shear modulus of G = 81,000 N/mm²
- Thermal expansion coefficient of $\alpha = 1.2 \times 10^{-5}$

C.1.3. Safety level

Design life required for permanent structures is t_{ref} = 100 years (SB260-21–5.1.1.1) [13].

The tunnel connections are classified as consequence class CC3 (21–6.3) [14].

C.1.4. Settlements

According to SB260-C.4.3.2.21, Article 6.6.6.2.C, the following limit values for settlement apply to the characteristic load combination. The overall settlement may not exceed 5 cm. The differential settlement (Δz) between two elements may not exceed 1/2 of the average settlement for a foundation on solid ground, and 1/3 of the average settlement for a foundation on piles, with an absolute minimum of 1 cm. In addition, a limit value of 1/1,000 (angular deformation) applies to the differential settlement within a single element, both for each point relative to the horizontal and between two extreme points or arbitrary points within the same element [14].

According to SB260-C.4.3.2.21, Article 5.4.7, for joints without structural coupling and without the use of transition plates, a maximum permissible deformation difference of 0.005 m across the joint applies, both in the vertical direction (floor, roof) and in the horizontal direction (wall), under the quasi-permanent load combination. This requirement applies from the moment of completion until the end of the service life and is considered to be the guiding principle in the design of the connection variants [14].

This corresponds to the guidelines in the ROK, Article 6.9–NEN 9997–1, which specifies a maximum allowable settlement difference of 0.005 m between tunnel elements for connections without couplings and without transfer plates. Driving comfort can be guaranteed by using transition plates, for which a maximum gradient of 1:200 is permitted [15].

C.1.5. Joint movements

Watertightness and possible movements across the joint must also be considered in the design of the tunnel segment connection. To fulfill both requirements, a combination of an expansion profile and a waterproofing profile is applied in standard tunnel details [39].

For the calculation of joint movements SB260-H21.6.13 is used. Equation C.1 must be used to calculate the joint movement. The combination value (ψ_0) of the thermal, wind and traffic loads is set at 0.8 for all these loads for the calculation of the maximum joint movement [13].

$$\begin{aligned} u_{\text{joint1},k} &= 1.0\,u_{T,k} + 0.8\,u_{Q,k} + 0.8\,u_{w,k} + u_{cr,k} + u_{sh,k} + u_{set} \\ u_{\text{joint2},k} &= 0.8\,u_{T,k} + 1.0\,u_{Q,k} + 0.8\,u_{w,k} + u_{cr,k} + u_{sh,k} + u_{set} \\ u_{\text{joint3},k} &= 0.8\,u_{T,k} + 0.8\,u_{Q,k} + 1.0\,u_{w,k} + u_{cr,k} + u_{sh,k} + u_{set} \end{aligned} \tag{C.1}$$

Table C.2: Overview of displacement components

$u_{T,k}$	Displacements due to temperature
$u_{Q,k}$	Displacements due to traffic loading
$u_{w,k}$	Displacements due to wind loading
$u_{cr,k}$	Displacements due to creep
$u_{sh,k}$	Displacements due to shrinkage
u_{set}	Displacements due to settlement

The expansion capacity of the joint is equal to or greater than the maximum joint movement in the serviceability condition (= $u_{\text{joint},k}$ = max $(u_{\text{joint1},k}; u_{\text{joint2},k}; u_{\text{joint3},k})$). The joint continues to meet all functional requirements (including mechanical resistance, watertightness, comfort, noise).

In the ultimate limit state, no tensile forces may be caused in either the bridge or the joint itself that could lead to failure of the joint. To determine the movement capacity to be taken into account in ULS, $u_{\text{joint},d}$ is used as a basis.

$u_{\text{joint},d}$ = 1,2 x $u_{\text{joint},k}$

As an additional guideline, the Dutch Handboek Tunnelbouw recommends limiting the maximum differential displacement across a joint with rubber metal without significant joint width (<=1 mm) to approximately 20 mm.

In the design of the connection variants, it will first be assessed whether they can be implemented in combination with the current joint profiles of the Oosterweelknoop design. The design includes an FMS350 waterproofing profile and an ACME 35 joint profile in the floor, roof, and exterior walls (Figure C.2).

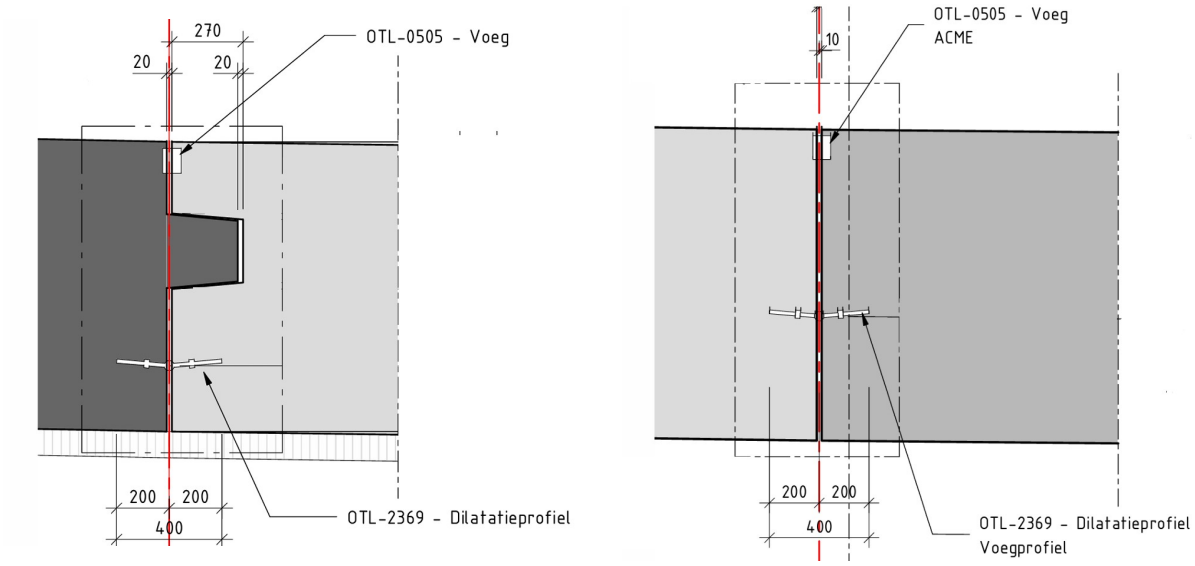

Figure C.2: Detail drawings of expansion joint in the floor with shear key (left) and the roof (right) [40] [41]

The FMS350 profile is capable of accommodating a total movement of 45 mm at a water pressure of 0 bar [24]. This applies because the STD tunnel segments are located in a permanent polder. The ACME 35 profile is capable of accommodating a total movement of 55 mm [25]. The total movement is calculated using the following equation:

$$V_r = \sqrt{v_x^2 + v_y^2 + v_z^2} \tag{C.2}$$

C.1.6. Traffic load

The traffic load on the STD tunnel segments is determined in accordance with SB260, which specifies that the traffic load must be determined in accordance with NEN-EN 1991-2 and the associated National Appendix. For the STD tunnel tube, both load model 1 (LM1) and load model 3 (LM3) must be taken into account [14]. The STD tunnel tube consists of four lanes (1a, 1b, 2, and 3).

LM1

Load Model 1 (LM1) represents the effect of regular road traffic and consists of a combination of:

- A uniformly distributed load (UDL) across the lanes
- One or more concentrated axial loads, modeled as tandem axles

For the main and primary roads of the Oosterweelverbinding the load system $Q^{1k} - Q^{1k} - Q^{2k} - Q^{3k}$ is used instead of exclusively $Q^{1k} - Q^{2k} - Q^{3k}$ [14]. This load system applies to both concentrated axial loads and uniformly distributed loads (UDL).

The geometry and positioning of the axle loads and distributed loads per lane are shown in Figure C.3.

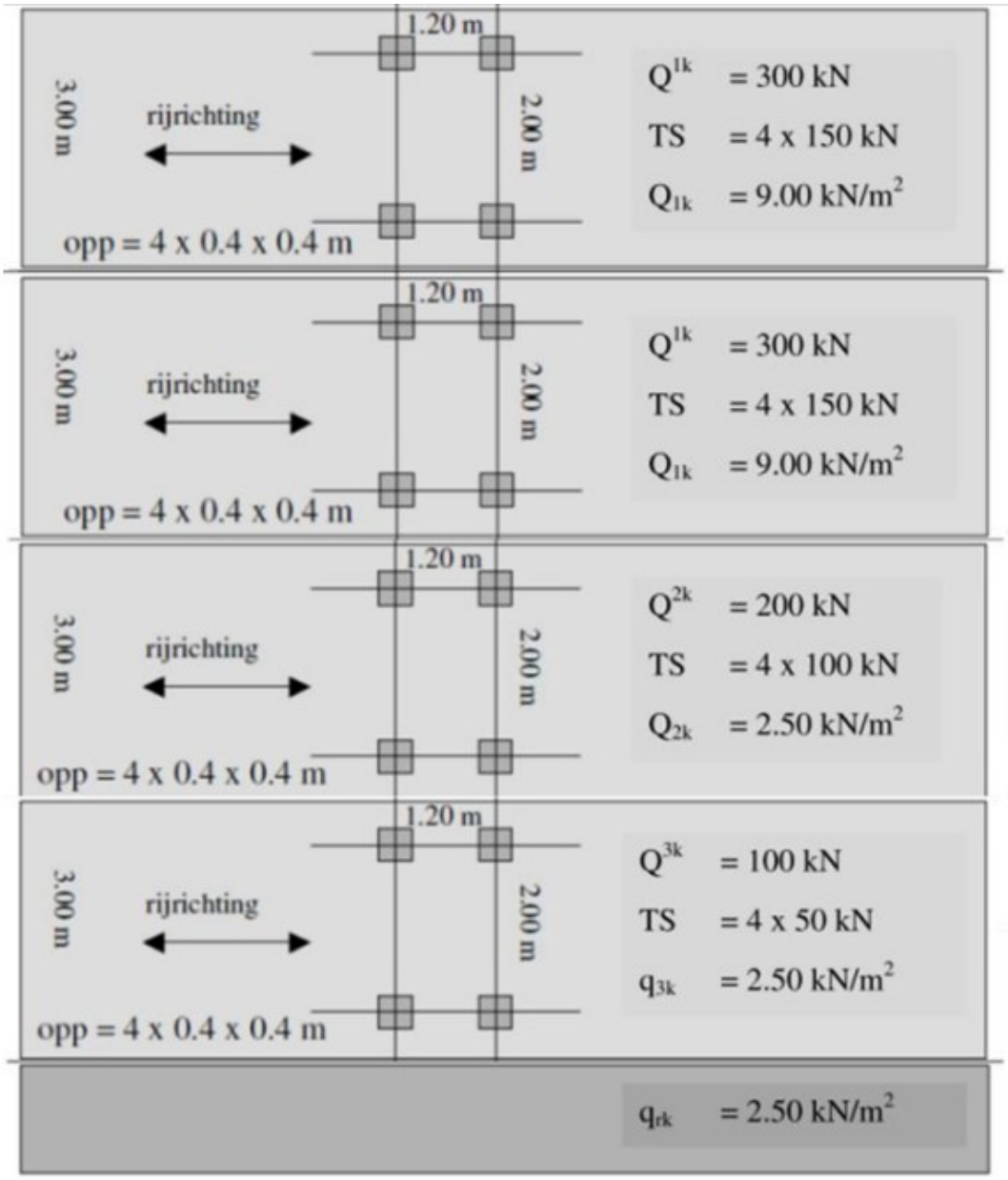

Figure C.3: LM1 traffic load configuration

LM3

Load Model 3 (LM3) describes the load resulting from special vehicles. LM3 consists exclusively of concentrated axle loads. For the STD tunnel tube, indivisible transport must be taken into account, in which case the traffic load is modeled using load model LM3. In accordance with NBN-EN 1991-2 with National Annex (ANB, Art. A.3) and SB260 (H21, Art. 4.2.3.2.A), load condition TEUV1 is used for this purpose in this study [14].

TEUV1 assumes a special vehicle traveling at a speed of 5 km/h, with the vehicle being the only object present on the structure. A dynamic amplification factor of $\phi = 1.40$ is applied to the special vehicle load. For the STD tunnel tube, indivisible transport is modeled using LM3 2400/200 at a speed of 5 km/h. This load only acts in lane 1a. The geometry is shown in Figure C.4

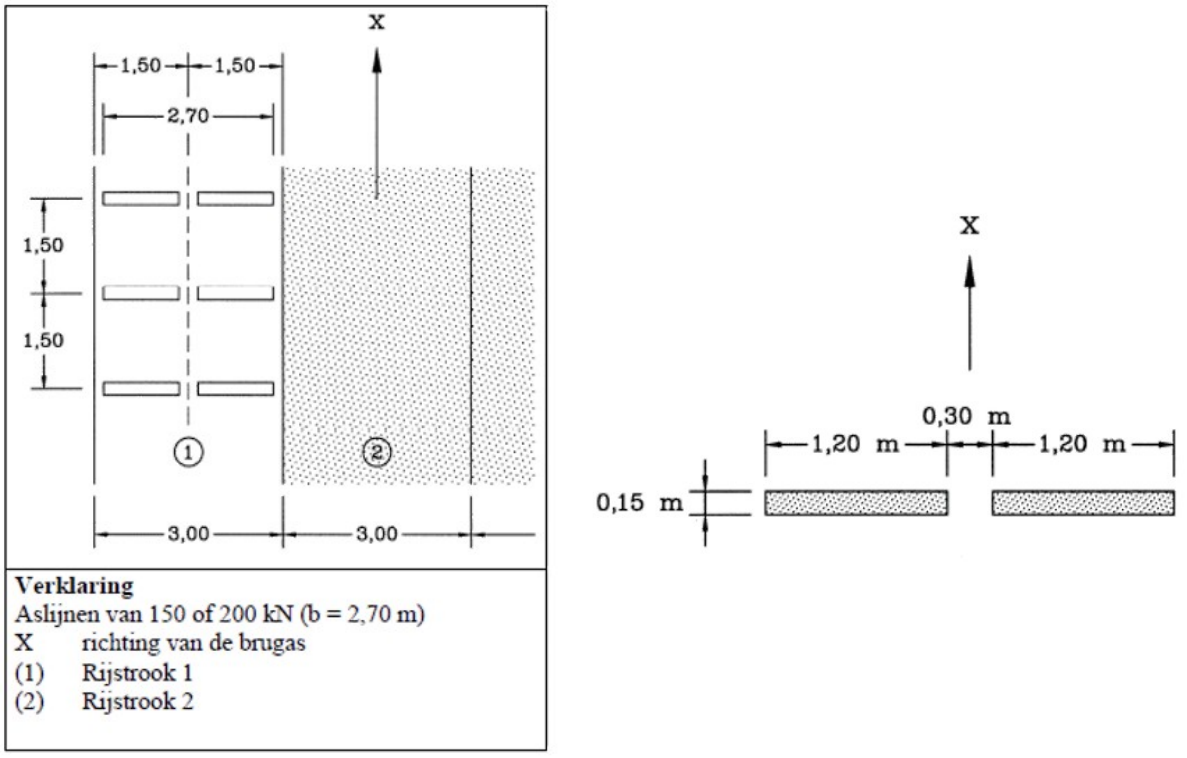

Figure C.4: LM3 traffic load configuration

Configuration

To assess the impact of traffic load on the shear forces in the tunnel segment connections, three traffic configurations were considered:

- Configuration A (Lane 1a – south side)
- Configuration B (Lane 1a – north side)
- Configuration C (Lanes 1a-1b, middle 2)

In addition, concentrated axial loads were placed at key locations to induce unfavorable shear forces in the tunnel segment joints. For modeling the concentrated axial loads from LM1 and LM3, two locations of the tandem sets were considered for each configuration. The tandem sets were placed:

- On the east side of the tunnel floor (against the edge)
- On the west side of the tunnel floor (against the edge)

These positions were chosen because concentrated axial loads close to the edge of the tunnel floor lead to an unfavorable distribution of shear forces across the cross-section of the tunnel segment. By considering both edge positions, in combination with three traffic configurations, the most unfavorable shear force in the tunnel segment joints is accounted for.

The traffic load was analyzed using two load groups in accordance with Section 4.5.1 of NEN-EN 1991-2. In load group 1a, only the LM1 load model is considered. In load group 5, a combination is applied in which the LM3 load model is amplified by a project-specific factor of 1.4 and combined with the characteristic value of LM1.

C.1.7. Shrinkage

The effect of shrinkage is taken into account in the determination of the horizontal displacements. The magnitude of shrinkage depends on environmental conditions, in particular the temperature and relative humidity at the reference time t_0.

The adopted values for t_0 are based on the Oosterweelknoop project and are used consistently in this study:

- Temperature: $10\ ^\circ\mathrm{C}$
- Relative humidity: 80%

The shrinkage strains are determined in accordance with the procedure described in Eurocode 1992-1-1 [42]. The adopted values for the shrinkage strain are taken from the project design assumptions:

- Concrete: $\varepsilon_{\mathrm{sh}} = 200 \cdot 10^{-6}$
- Asphalt: $\varepsilon_{\mathrm{sh}} = 220 \cdot 10^{-6}$

For the asphalt layer, shrinkage is considered only after 60 days. Consequently, the shrinkage effects are evaluated based on the remaining shrinkage between t_0 (60 days) and the ultimate condition t_∞.

The longitudinal shortening due to shrinkage results in an increase of the joint opening between adjacent tunnel segments.

C.1.8. Temperature

The structure is calculated for the thermal loads specified in SB 260-21-4.2.3.10. The following simplified load model may be applied for the uniform temperature component ΔT_N and the linear temperature component ΔT_{My} on walls and slabs with soil on one side.

Open toegangen	**ΔT_N (°C)**	**ΔT_{My} (°C)**
Wand < 60 cm	+30	+15
	-5	-8
Wand ≥ 60 cm	+25	+15
	-5	-8
Plaat (asfalt = 15 cm)	+25	+7
	-5	-6
Tunnel (gesloten gedeelte)	**ΔT_N (°C)**	**ΔT_{My} (°C)**
Wand + plaat (dekking D ≥ 1,5 m)	+20	+5
	0	-5

Figure C.5: Temperatures tunnel segments [13]

C.1.9. Loading on soil masses

According to SB260-4.6.3.15, soil masses above the tunnel structure that are inaccessible to motorized traffic shall be subjected to a uniformly distributed variable load of 10 kN/m^2, whereas a load of 20 kN/m^2 applies to areas accessible to motorized traffic. In the final design of the STD tunnel segments, a park area is planned above the tunnel structure that is closed to motorized vehicles. Therefore, a uniformly distributed variable load of 10 kN/m^2 is adopted.

C.1.10. Fatigue

Bent reinforcement, welded reinforcement, and dowel connections between tunnel segments may be susceptible to fatigue due to repeated traffic loading. For the fatigue assessment, the $\mathrm{BM1_{fat}}$ load combination (0.7Q + 0.3q) is applied.

For reinforcing steel, the fatigue resistance is determined in accordance with Article 6.8 of NBN EN 1992-1-1. For structural steel, the fatigue stresses and the allowable number of stress cycles are determined in accordance with NEN-EN 1993-1-9, Art. 7.1.

C.1.11. Load Combinations & Factors

For consequence class CC3, the Ultimate Limit State (ULS) load combination is determined in accordance with the fundamental combination specified in EN 1990. The partial factors applied are presented in Table C.3. The ULS load combination is defined as:

$$\sum \gamma_G \, G_k \; + \; \gamma_Q \, Q_{k,\text{lead}} \; + \; \sum \gamma_Q \, \psi_0 \, Q_{k,i} \tag{C.3}$$

For the Serviceability Limit State (SLS), the characteristic combination is defined as:

$$\sum G_k + Q_{k,1} + \sum \psi_0 Q_{k,i} \tag{C.4}$$

The frequent combination is defined as:

$$\sum G_k + \psi_1 Q_{k,1} + \sum \psi_2 Q_{k,i} \tag{C.5}$$

The quasi-permanent combination is defined as:

$$\sum G_k + \sum \psi_2 Q_{k,i} \tag{C.6}$$

The values of the combination factors ψ are given in Table C.4.

Table C.3: Partial factors for CC3 [43]

CC3 Load Case	γ_G	γ_Q
Self-weight	1.50	–
Earth pressure	1.50	–
Traffic loads	–	1.60
Special vehicles (LM3)	–	1.60

Table C.4: Combination factors ψ for road bridges [43]

Load Case	**Model**	ψ_0	ψ_1	ψ_2
gr1a (LM1)	UDL	0.40	0.40	0
gr1a (LM1)	TS	0.75	0.75	0
gr5 (LM3 – special vehicles)	TS	0.75	0.75	0

C.2. Geotechnical Design Principles

C.2.1. Soil properties

The soil parameters were determined based on a combination of cone penetration test (CPTs), measurement results from test pits at the project location [44], laboratory tests and the guidelines for the application of EC7 in Belgium [45]. The characteristic value was determined for the following basic parameters:

- Volume weights: γ_d, γ_n
- Strength parameters: φ', c', ψ, $p_{\max}$, C_u
- Compressibility parameters: C, A, CR, RR, C_α
- Stiffness parameters Hardening Soil Small Strain model: E_{50}^{ref}, $E_{\text{oed}}^{\text{ref}}$, $E_{\text{ur}}^{\text{ref}}$, p_{ref}, m, ν_{ur}, R_{inter}
- subgrade parameters: horizontal subgrade constant k_h; vertical subgrade derived from $E_{\text{oed}}^{\text{ref}}$
- Additional data: soil type, density/consistency, cone resistance q_c, friction ratio R_f

C.2.2. Stiffness parameters

The Hardening Soil Small Strain (HS-small) model is used in Plaxis to model the deformations under the tunnel supports. This model describes the stress- and strain-dependent behavior of the subsoil and uses three primary stiffness moduli:

- E_{50}^{ref} – secant shear modulus at 50% of the maximum deviatoric stress, governing the deformation behavior under primary loading
- $E_{\text{oed}}^{\text{ref}}$ – oedometer modulus, governing the vertical settlements beneath the tunnel segments
- $E_{\text{ur}}^{\text{ref}}$ – unloading–reloading modulus, describing the stiffer behavior during unloading and reloading

These stiffnesses are derived from the cone resistance q_c according to the Guidelines for the application of EC7 in Belgium, whereby the correlations have been validated with pressuremeter tests. The reference pressure ρ_{ref} is taken to be equal to the effective vertical stress at the center of the relevant soil layer, so that the stress dependence of the HSS model is correctly represented.

For calculating $E_{\text{oed}}^{\text{ref}}$ and $E_{\text{ur}}^{\text{ref}}$ the following relationships are used:

$$E_{\text{oed}}^{\text{ref}} = C \cdot \sigma_v' \qquad E_{\text{ur}}^{\text{ref}} = A \cdot \sigma_v'$$

where C and A are the compression constants determined for each soil layer, and σ_v' represents the effective vertical stress at the centre of the corresponding layer.

The exponent m determines the extent to which the stiffness increases with the stress. The project guidelines were followed for this:

- m = 0,5 for sand layers
- m = 1,0 for quaternary clay and peat layers
- m = 0 tot 0,7 for the Booms clay, depending on the results from the test pit [44].

C.2.3. Application in Plaxis modeling

The finite-element program Plaxis 2D is used to simulate the behavior of the subsoil, in which parameters such as the construction phasing and the tunnel geometry are also modeled. The geotechnical structure is modeled layer by layer. The layers are entered using the HS-small model, in which the three stiffnesses and the corresponding measured characteristic soil parameters are used for each layer. This includes both the characteristic parameters obtained from cone penetration tests and laboratory tests, as well as the stiffness parameters derived from these parameters for the HS-small model. Figure C.6 shows the input table for the BK0 layer in the Plaxis 2D program.

Two variants were considered for determining the subsoil behavior. These variants represent the extreme cases in terms of stiffness and permeability of the Boomse clay. UA variant 1 is based on high stiffness and a low permeability, causing the Boomse clay to consolidate only slowly. UA variant 3, on the other hand, uses low stiffness and high permeability, leading to faster consolidation. The factor between the UA3 and UA1 variants is $\sqrt{2}$, such that uncertainties are taken into account in a conservative manner.

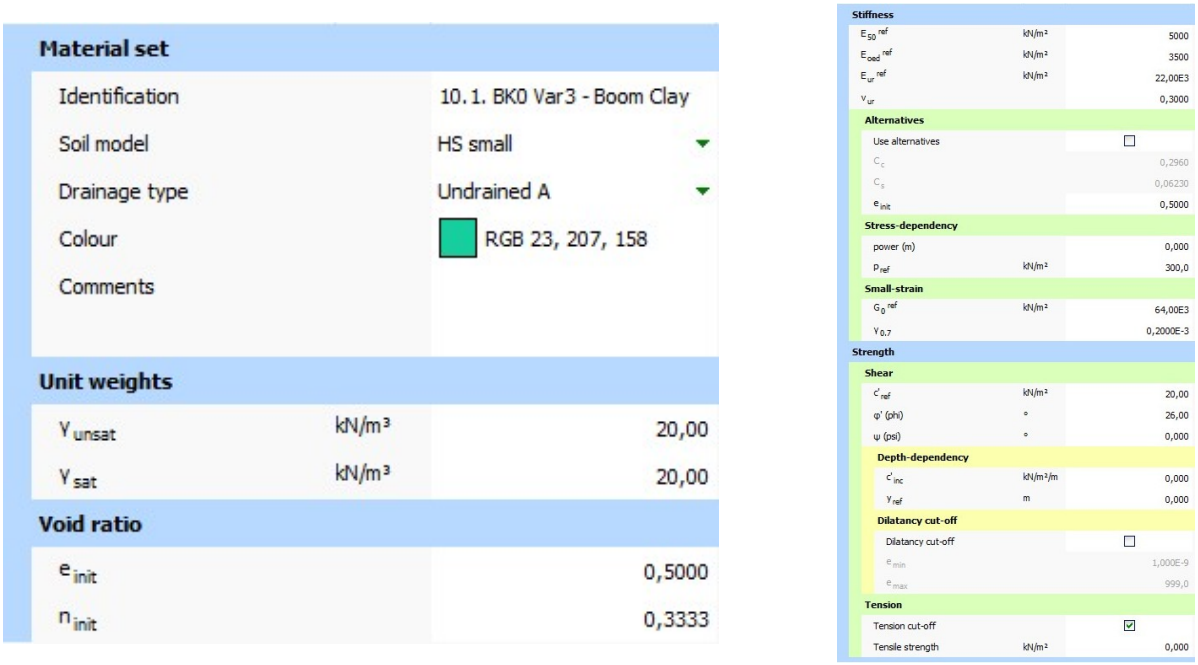

Figure C.6: Input data BK0 soil layer in Plaxis 2D

D

Methodology Optimization Analysis

This appendix provides a detailed description of the modeling and analysis steps used in the optimization analysis presented in Chapter 3. The organization of this appendix follows the structure of the workflow shown in the optimization analysis flowchart.

D.1. Plaxis 2D model

The finite element program Plaxis 2D is used to determine the subsoil support (subgrades), which are used as input for the SCIA 3D model. In this study, the existing Plaxis models for tunnel tubes STD-10 and STD-13, along with the corresponding geotechnical cross-sections S01 and S06B, are used (Figure D.1). These two models are modified in this study to enable optimization analyses of the shear force, which will be determined at a later stage. The soil structure and soil parameters used are described in section 2.3.2 and are used unchanged as input in both Plaxis models.

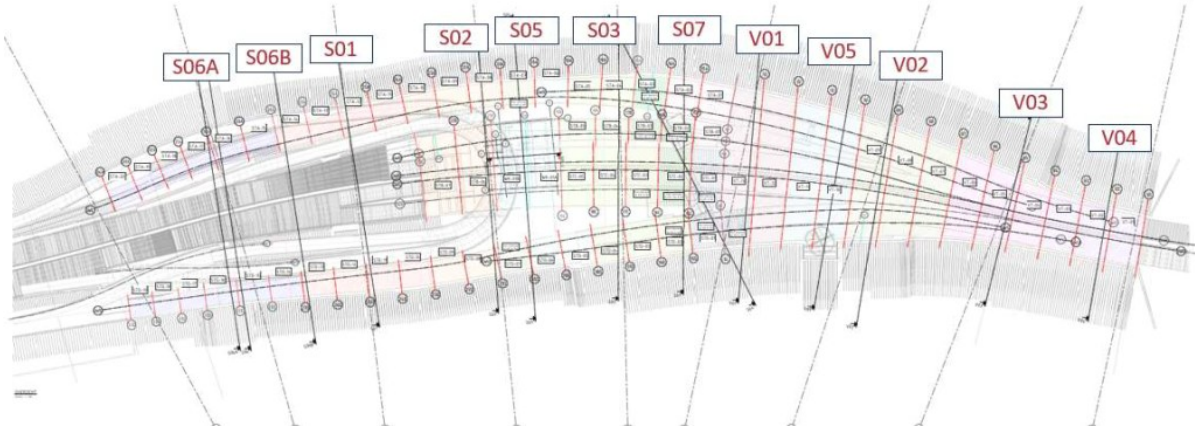

Figure D.1: Overview of geotechnical cross-sections of the combined tunnels [4]

Plaxis 2D is used as a cross-section model, in which the soil structure, water level, and construction phasing are modeled for each geotechnical section. To determine the subgrade properties, an interface is modeled directly beneath the tunnel segment, so that the displacements (settlements) and soil stresses across the entire width of the floor can be easily determined. The subgrade stiffness is then calculated as the ratio between the change in stress and the corresponding vertical displacement.

The models do not account for longitudinal effects. The interaction between tunnel segments and the resulting shear forces is therefore fully incorporated into the SCIA 3D model.

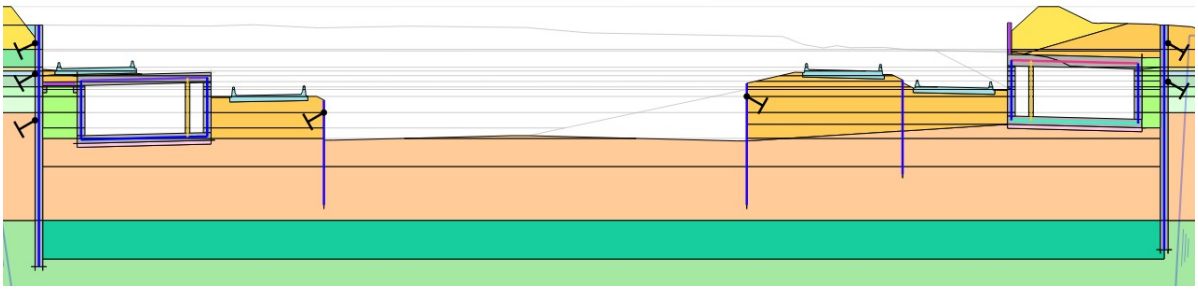

Figure D.2: Plaxis 2D model for geotechnical section S01

Construction sequence

The subgrade stiffness depends on the construction sequence that is implemented. In Plaxis, the entire construction phasing of the tunnel project is therefore modeled. Each construction phase is linked to a specific time. This phasing includes, among other things, the installation of diaphragm walls and anchors, the successive excavation steps and dewatering, the construction of the tunnel floor, walls, and roof, and the backfilling of the excavation pit with fill material after the tunnel is completed.

Each individual phase results in incremental settlement and stress. By summing these incremental contributions, the total settlement and stress per phase are calculated. The modeled construction phasing with its associated timeframe is based on input from the contractor of the Oosterweelknoop.

Finally, a uniformly distributed load of 40 kPa is applied on the tunnel floor over the entire service life (100 years). This load is introduced to represent the influence of the tunnel structure itself on the subsoil during long□term consolidation and does not represent traffic loading. The applied load serves as a simplified means of accounting for the structural presence of the tunnel in the determination of the final subgrade stiffness [21].

Subgrade stiffness

The subgrade stiffness is determined based on the ratio of the change in vertical soil stress (Normal effective stress σ'_N) to the corresponding vertical displacement (u_y (Equation D.1).

$$k_v = \frac{\Delta\sigma'_N}{\Delta u_y} \tag{D.1}$$

To determine the subgrade stiffness, the time difference is taken between the moment the tunnel roof is poured (T0) and the final state of the structure after long-term consolidation (assumed at 100 years). This choice follows directly from the modeling philosophy adopted for the SCIA model, in which the tunnel segment is represented in its final geometry and stiffness, without explicitly modeling construction phases [21].

In the Plaxis model, the tunnel structure is constructed stepwise, with floors, walls, and roof being activated in separate construction phases. As a result, the normal stress distribution beneath the tunnel floor and the associated vertical displacements vary per phase, depending on the stiffness and loading state of the tunnel structure at that stage. The subgrade stiffness therefore evolves during construction and cannot be represented by a single value during intermediate phases.

Since the SCIA model represents the tunnel segment only in its final configuration, the subgrade stiffness applied in SCIA must be consistent with this final structural state. The subgrade stiffness is therefore determined between T0, which marks the stage at which the tunnel geometry is fully realized and the complete self-weight of the tunnel structure is transferred to the subsoil, and the final consolidated state. In this way, the derived subgrade

stiffness accounts for the long-term consolidation behaviour of the subsoil under permanent loading. This ensures compatibility between the geotechnical PLAXIS model and the structural SCIA model.

Within Plaxis, both the stress distribution and the vertical displacement can be obtained over the full width of the tunnel floor. For the Oosterweelknoop project, multiple variants of soil parameters are modeled for each geotechnical section. In this research, only the following two variants are considered for the geotechnical cross-sections S01 and S06B:

- UA variant 1: stiff parameters for Boomse clay and low permeability (slow-behaving Boomse clay)
- UA variant 3: soft parameters for Boomse clay and high permeability (fast behavior of Boomse clay)

Since this study focuses on the maximum shear forces between tunnel segments, only the UA3 variant is considered. This can be explained by the fact that adopting the lower-bound stiffness parameters results in larger and faster soil deformations. Due to the relatively high permeability, settlements develop more rapidly, leading to higher differential deformations between segments.

D.2. SCIA 3D model

The SCIA 24.0 Engineer model serves as the link between the geotechnical results from the Plaxis models and the overall structural analysis of the tunnel segments in the longitudinal direction. Whereas Plaxis focuses on local cross-sections and soil-structure interaction, SCIA creates a 3D model in which the interconnection between tunnel segments and the associated force distribution is analyzed.

Two SCIA models are used to determine the total shear force in the connections. The first model incorporates the results from Plaxis using the UA3 soil parameters. In this model, the supports are defined by subgrade stiffnesses derived from the Plaxis analyses, and only permanent loads are considered. In the second model, the traffic load is applied using the k20 variant, in which the subgrade is represented by a uniform stiffness of 20 MN/m^2. The assumption of a uniform subgrade stiffness is justified by the nature of the traffic loading, which is local and short-term.

Modeling subgrade

The subgrade stiffness values obtained from Plaxis for UA3 were determined in the transverse direction across the width of the tunnel floor. In the transverse direction, the determined subgrade stiffnesses are simplified into three subgrade zones North, Central, and South, as shown in Figure D.3. This zoning results from the presence of the tunnel walls, which locally lead to higher effective earth pressures and thus higher subgrade stiffnesses.

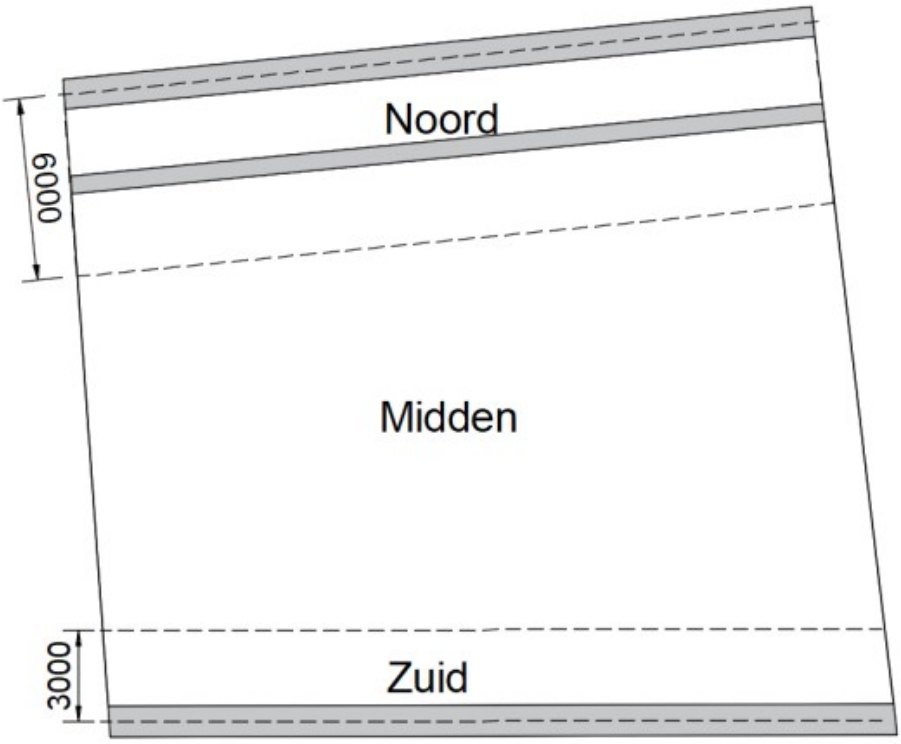

Figure D.3: Subgrade zones under STD tunnel segments [4]

Since the subgrade stiffnesses have been determined only at geotechnical cross-sections S06B and S01, an additional calculation step must be performed in the longitudinal direction. Between these two sections, the subgrade stiffnesses for all three subgrade zones are determined using linear interpolation. In doing so, it is assumed that the subgrade stiffness does not vary within a zone under the same tunnel segment.

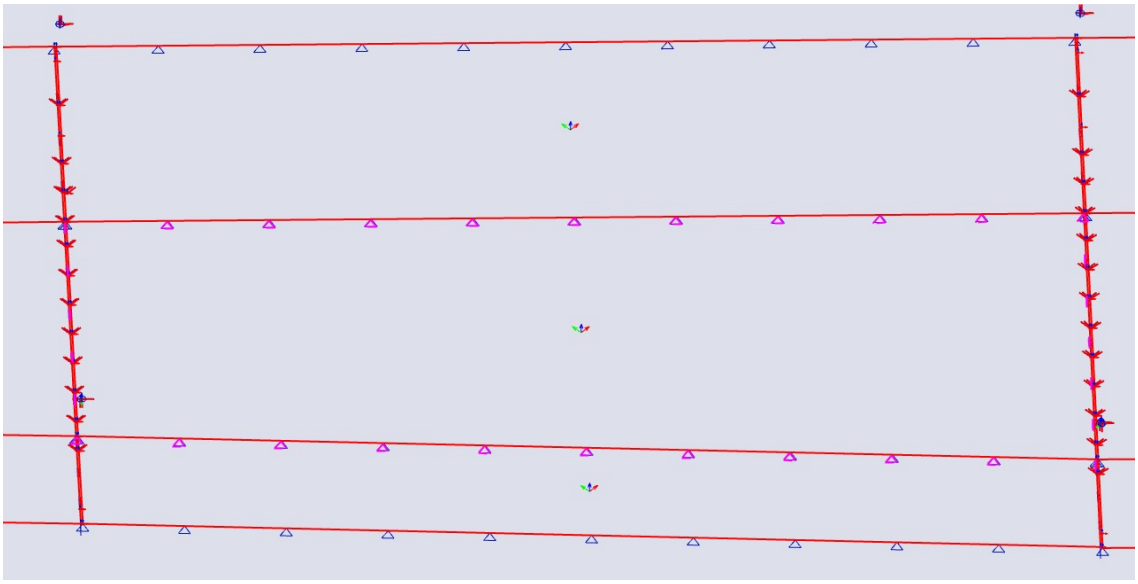

Name	STD12_buis5_M1
Decription	
C1x [MN/m^3]	0,6950
C1y [MN/m^3]	0,6950
C1z	Nonlinear function
Stiffness [MN/m^3]	6,9500
Nonlinear function C1z	STD12_bui...
C2x [MN/m]	0,0000
C2y [MN/m]	0,0000
▼ PARAMETERS FOR CHECK	
Type	Undrained
Water/air in clay sub...	
Specific weight [kg/...	0,00
Fi' [deg]	0,00
Sigma oc [MPa]	0,0
cu [kPa]	0,0
▼ PARAMETRIC INPUT	
Selector switch	

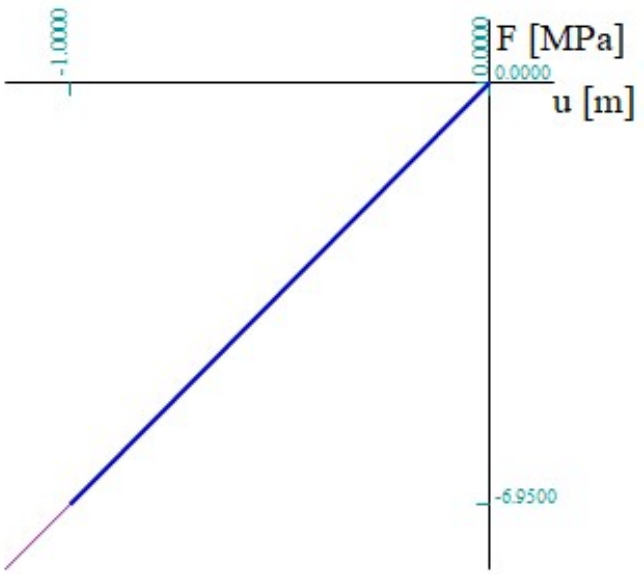

Figure D.4: Implementation of subgrade springs in the SCIA 3D Model

In the SCIA 3D model, the derived subgrade stiffnesses are implemented as vertical spring supports beneath the tunnel floor. These supports are applied as surface springs, distributed over the floor area of each tunnel segment and differentiated according to the three zones.

To realistically represent soil–structure interaction, a nonlinear force–displacement (F–u) relationship was initially applied to the subgrade springs, allowing compression-only force transfer while preventing tensile forces (see Figure D.4).

Evaluation of the model results shows that no tensile forces occur in the tunnel floor of the STD tunnel segments. As a result, the nonlinear spring formulation does not influence the calculated force transfer in this specific case. Therefore, a linear representation of the subgrade stiffnesses is considered sufficient for the subsequent analyses.

Modeling tunnel segment

Because the shear force at the segment connection is highly dependent on longitudinal effects, such as the deflection curve of the entire tunnel tube and the deformation compatibility between successive tunnel segments, the entire tunnel tube 5 (tunnel segments STD-1 through STD-16) has been modeled. This allows for the consideration of both the global stiffness distribution and the rotation and displacement transfer along the entire tunnel tube.

The tunnel segments are modeled separately and interconnected by means of an explicit representation of the connection. The tunnel walls and floor are modeled using 2D wall and plate elements. The roof of one tunnel segment is modeled using two shell elements to capture the curvature of the roof. The geometry is directly based on the design of the Oosterweelknoop. The material of all 2D elements is C35/45 cracked concrete, for which the Young's modulus is taken as one third of the original Young's modulus. In this way, the reduced stiffness of cracked concrete is correctly represented. The mesh size of the model is 1.0 m.

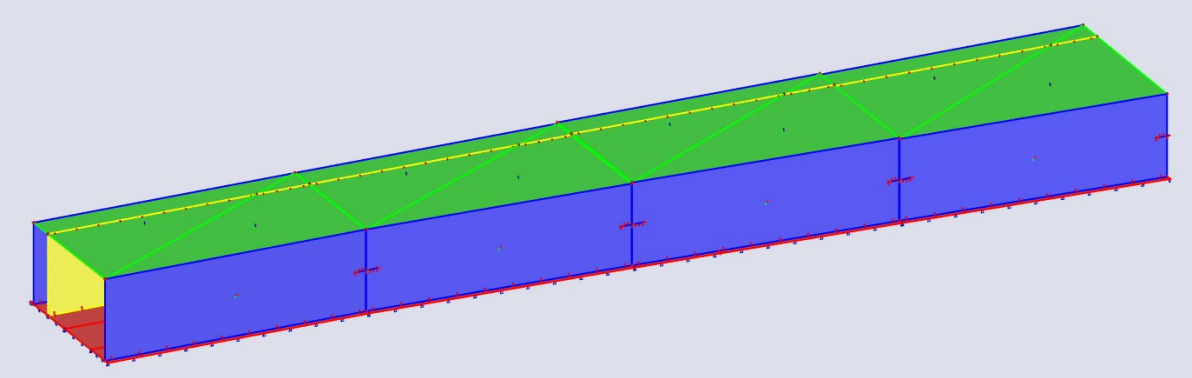

Figure D.5: Overview of the SCIA 3D model used for the longitudinal analysis of the STD tunnel segments

For both models considered in this study (the UA3 variant and the k20 traffic variant), the following loads are applied in the longitudinal analysis to determine the shear forces in the segment connections (Section 2.3.2):

- Self-weight of the tunnel segment
- Permanent soil load
- Ground surface load
- Traffic load

Modeling tunnel segment connection

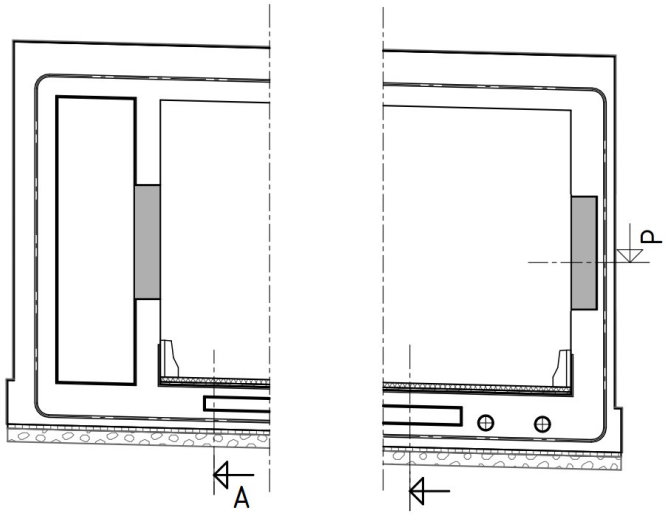

Figure D.6: Tunnel cross-section with shear key locations in the floor, inner and outer walls [46]

For the optimization, the current modeling choices for the Oosterweelknoop were studied and used as a starting point. In the current design, shear keys (consoles) are located in both the inner and outer walls of the tunnel, with a cross-section of 600 × 2500 mm. In the outer wall, there is an eccentricity between the center of the cantilever and the center of the wall, due to the presence of watertight elements. Both consoles are constructed with elastomer bearing strips (vertical stiffness of 1000 MN/m).

A shear key is also present in the tunnel floor. Since this shear-transfer connection mainly carries the traffic-induced share of the loads and only a small portion of the permanent loads, this connection falls outside the scope of the study. The modeling of the floor shear key is identical to that of the consoles in the walls. Figure D.6 provides an overview of the position of the shear keys in the current design.

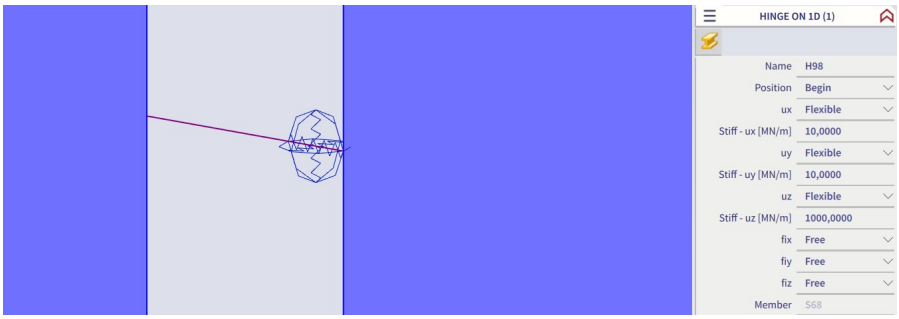

Figure D.7: Visualization model shear key in SCIA 3D model

For modeling the consoles in the walls, a connection between 2D plate elements (walls) and 1D beam elements (consoles) was chosen. The consoles are modeled as 1D beams with an infinitely rigid cross-section, where the deformation of the console and the compression of the elastomer bearing are combined into a vertical translational spring. A hinge is modeled on one side of the beam, to which the vertical translational spring is coupled. In this way, the overall behavior of the shear key connection is approximated without modeling the geometry of the console. The eccentricity in the outer wall resulting from the waterproofing elements is not included in this model.

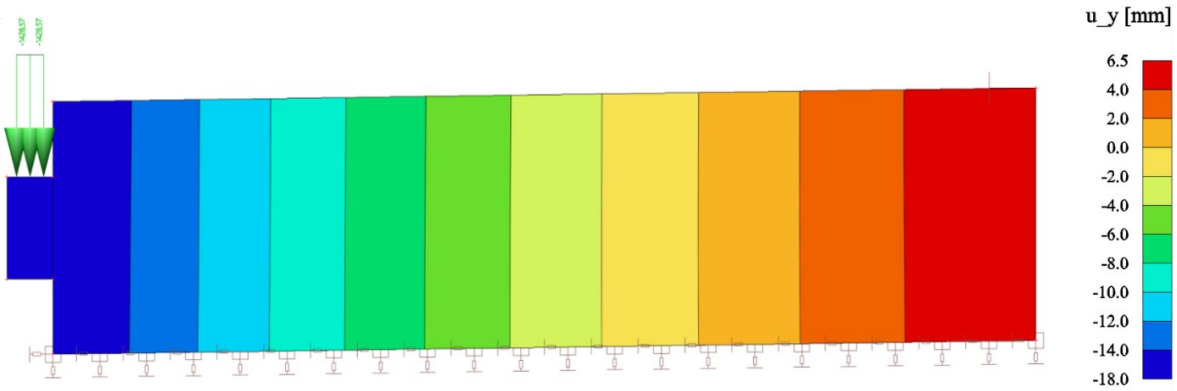

Figure D.8: 2D shear key reference model

The modeling uses a connection between a 1D beam element (console) and a 2D plate element (tunnel wall). Although this connection is geometrically point-like on the side of the beam element, the transfer of forces and displacements occurs numerically via multiple nodes in the 2D element. As a result, the deformation behavior of the cantilever is sensitive to the chosen mesh size of the wall.

A validation model was developed to enable an informed decision regarding the mesh size. In this validation model, the console is modeled as a 2D element with the same dimensions as the actual console, continuously connected to the wall over its entire height. Due to this plane coupling, the transfer of forces and deformations occurs continuously, making the deformation behavior independent of the mesh size. This model is therefore considered a realistic reference representation of the cantilever's behavior.

The 2D reference model was then compared to the model using a 1D–2D connection, in which the 1D beam element has a cross-section equal to that of the console. Since the shear forces in the console are determined by the relative displacement in combination with the stiffness of the connection, the deformation behavior was chosen as the primary validation parameter. When the deformation shape of the 1D beam element matches that of the 2D reference model, the modeling can be considered reliable.

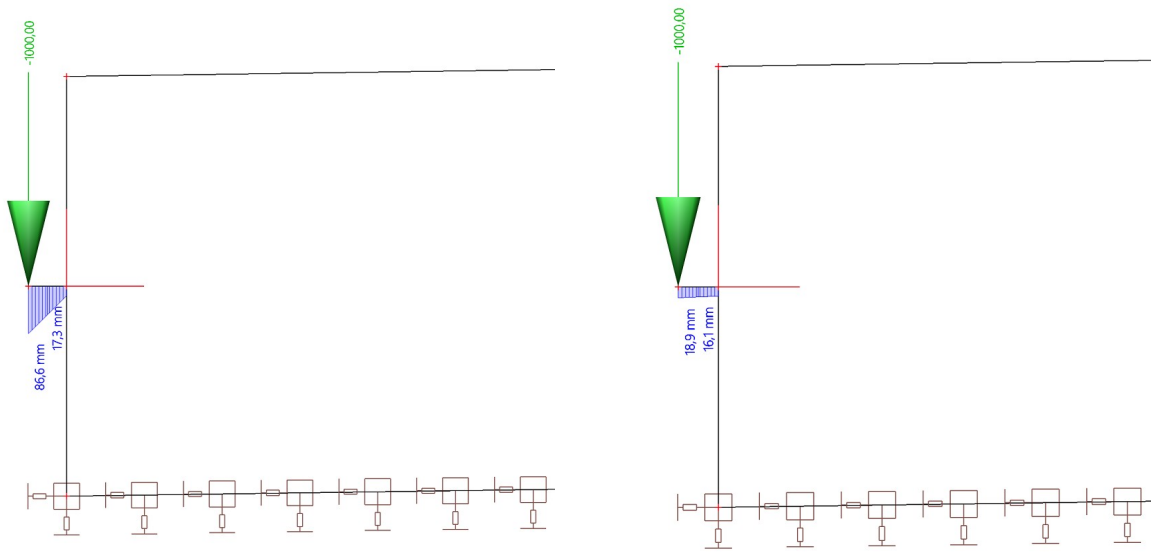

Figure D.9: Vertical displacement 1D shear key for mesh size 0.2 m (left) and 1.0 m (right)

The results of this comparison are shown in Figure D.9. With a fine mesh, many closely spaced nodes are created along the height of the wall, causing the connection between the 1D beam element and the 2D wall to become numerically very stiff. This artificial stiffness causes the deformation to concentrate primarily in the beam element, resulting in an unrealistic deformation pattern near the connection. With a coarser mesh, the vertical deflection of the cantilever is represented more realistically and aligns better with the 2D reference model. The displacements of the beam are less locally concentrated in this case.

Based on these findings, it was decided to use a mesh size of 1.0 m in the optimization study to ensure that the deformation behavior of the console remains representative.

Settlement control

Only for the Oosterweelknoop project, SCIA Engineer is also used to analyze settlements at the corner points of the geotechnical cross-sections. In this process, the tunnel segments in the model are separated from one another so that settlements can develop freely without influencing each other. These are compared one-to-one with the settlements obtained from Plaxis on geotechnical cross-sections S01 and S06B. If significant deviations occur, this is investigated further and corrected if necessary.

This verification process ensures that the input subgrade stiffnesses and the structural modeling of the tunnel segments align with the actual soil behavior as calculated in Plaxis. The reason Plaxis 3D is not used to determine the shear forces is that Plaxis is less suitable for many load combinations and therefore has very long calculation times. SCIA is considerably more efficient and user-friendly in this regard.

E

SCIA Longitudinal Model

This appendix describes the modeling of the longitudinal models and the connection variants.

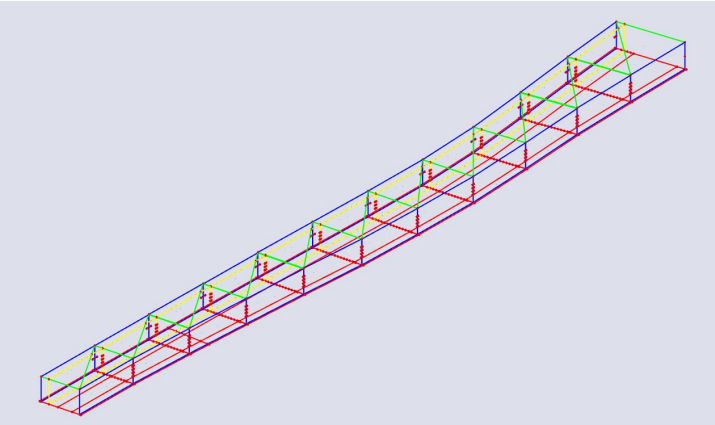

Figure E.1: SCIA 3D longitudinal model of tunnel segments STD-06 to STD-16

For designing the four connection variants between tunnel segments STD-10 and STD-13, it must be determined which shear forces need to be transferred. To determine these forces, two SCIA 3D longitudinal models were developed. Since the shear force at the segment connections is influenced by longitudinal effects, such as the global deformation shape of the tunnel and the deformation compatibility between successive segments, the tunnel segments STD-06 through STD-16 were included in the model (Figure E.1). This allows both the global stiffness distribution and the transfer of rotations and displacements along the tunnel tube to be taken into account. In both models, the tunnel segments STD-06 to STD-16 are modeled based on the geometry of the Oosterweelknoop design. The models differ only in their support conditions and applied loads. The two longitudinal models are defined as follows:

1. **UA3 longitudinal model**, including permanent loads, in which the subgrade stiffness is derived from the UA3 soil parameters (Section 2.3.3: Geotechnical design principles);
2. **k20 longitudinal model**, including traffic loads, assuming a uniform subgrade stiffness of 20 MN/m^2 over the entire tunnel length.

The assumption of a uniformly relative stiff subgrade in the k20 model is because traffic loading is local and short-term. As a result, the structural response is primarily governed by the stiffness of the tunnel structure rather than the deformation of the soil. The UA3 model is used to determine the deformation state of the tunnel under long-term conditions. Therefore, it uses the corresponding long-term subgrade stiffness. The final design shear forces in the connections are obtained by combining the results of both longitudinal models.

E.1. STD tunnel elements

The tunnel segments are modeled as separate elements and interconnected by explicitly modeled connections, with a joint width of 50 mm between adjacent segments. All 2D elements are assigned cracked concrete C35/45, with the Young's modulus taken as one third (11333 Mpa) of the uncracked value to account for cracking effects. An overview of the properties of the structural elements part of the STD-tunnel segments is provided in Table E.1, E.2 and E.3. The center-to-center distance between the inner wall and the outer wall remains constant at 2550 mm over the entire length. The exact geometry of corner points of the STD tunnel segments is presented in Table E.4 with Figure E.1 and E.3 for additional visualization.

Table E.1: General model properties

Property	Value
Mesh size [mm]	1000
Joint width [mm]	50
Concrete grade	C35/45 (cracked)

Table E.2: Support properties

Model	Distribution	Vertical stiffness	Horizontal stiffness (long./transv.)
UA3	3 zones (Figure D.3)	See subgrade stiffness Table E.6	1/100 of vertical stiffness
k20	Uniform	20 MN/m^2	0.2 MN/m^2

Table E.3: Geometry and element types

Component	Element type	Thickness [mm]	Height/width [mm]	Length [mm]
Outer wall	2D wall	1000	7750	25000
Inner wall	2D wall	1000	7750	25000
Floor	2D plate	1100	17500–20000	25000
Roof	2D plate	1250	13500–18500	25000

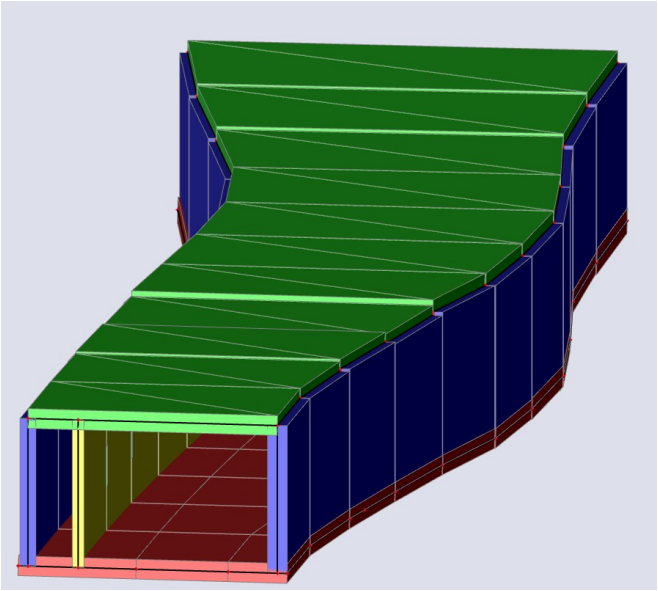

Figure E.2: Geometry and segmentation of the SCIA longitudinal model showing floor (red), walls (blue/yellow), and roof (green)

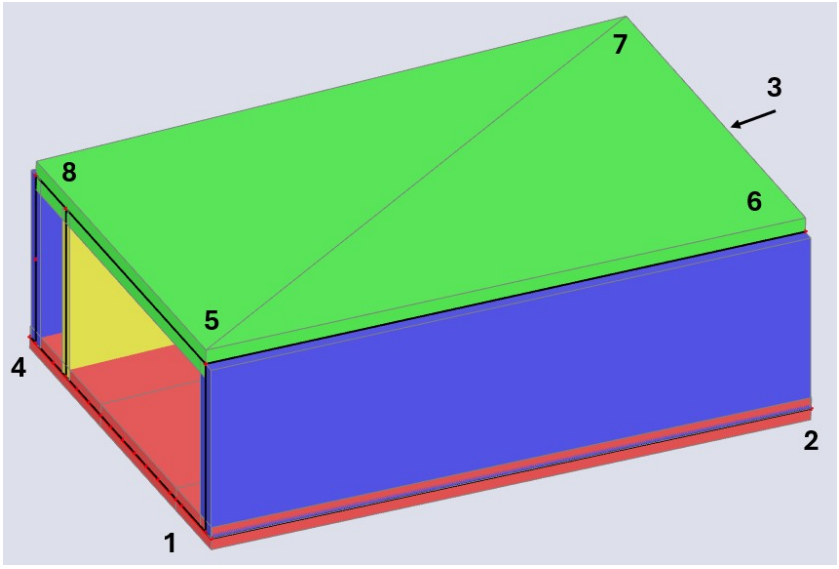

Figure E.3: Geometry points STD segments

Table E.4: Coordinates of STD tunnel segments in metres

	STD-06			STD-07			STD-08			STD-09		
Pt	x	y	z	x	y	z	x	y	z	x	y	z
1	249.2	29.4	-4.2	224.7	26.1	-4.3	199.5	21.7	-4.2	174.3	17.4	-3.9
2	273.8	32.3	-4.1	249.2	29.4	-4.3	224.6	26.1	-4.3	199.5	21.7	-4.2
3	269.5	54.7	-3.6	244.9	49.7	-3.7	220.4	44.3	-3.8	196.1	39.0	-3.7
4	245.0	49.7	-3.7	220.3	44.3	-3.8	196.2	39.0	-3.7	171.8	34.9	-3.5
5	249.1	29.9	3.8	224.5	26.6	3.6	199.4	22.2	3.6	174.2	17.9	3.8
6	273.7	32.8	3.9	249.1	29.9	3.7	224.5	26.6	3.5	199.4	22.2	3.6
7	269.6	54.2	4.4	245.0	49.2	4.2	220.5	43.8	3.9	196.2	38.5	4.0
8	245.0	49.2	4.3	220.6	43.8	4.1	196.3	38.5	4.0	162.8	34.4	4.2
	STD-10			STD-11			STD-12			STD-13		
Pt	x	y	z	x	y	z	x	y	z	x	y	z
1	149.0	14.5	-3.6	124.2	11.8	-3.1	100.2	10.0	-2.5	74.4	8.0	-1.8
2	174.2	17.4	-3.9	149.0	14.5	-3.6	124.2	11.8	-3.1	99.3	10.0	-2.4
3	171.7	34.9	-3.5	147.0	32.0	-3.1	122.2	29.2	-2.7	97.3	26.2	-2.0
4	147.1	32.0	-3.1	122.2	29.2	-2.7	97.4	26.2	-2.0	74.4	8.5	5.7
5	149.0	15.0	4.2	124.2	12.3	4.7	99.3	10.5	5.3	99.2	10.5	5.2
6	174.1	17.9	3.8	148.9	15.0	4.2	124.1	12.4	4.7	97.4	25.7	5.5
7	171.8	34.4	4.2	147.1	31.5	4.6	122.2	28.7	5.1	72.6	22.7	6.0
8	147.1	31.5	4.6	122.3	28.7	5.1	97.4	25.7	5.7	74.4	8.5	5.7
	STD-14			STD-15			STD-16					
Pt	x	y	z	x	y	z	x	y	z			
1	49.5	5.8	-1.2	24.7	3.3	-0.6	0.0	0.0	0.0			
2	74.4	8.0	-1.8	49.5	5.8	-1.2	24.6	3.3	-0.6			
3	72.5	23.2	-1.4	47.7	20.1	-0.8	22.9	16.9	-0.2			
4	47.7	20.1	-0.8	22.9	16.9	-0.2	-1.9	13.5	0.4			
5	49.5	6.3	6.4	24.6	3.8	6.9	-0.1	0.5	7.6			
6	74.3	8.5	5.8	49.4	6.3	6.3	24.6	3.8	6.9			
7	72.5	22.7	6.1	47.7	19.6	6.6	22.9	16.4	7.2			
8	47.8	19.6	6.7	23.0	16.4	7.2	-1.8	13.0	7.8			

The applied loads include the self-weight of the concrete, soil pressure, and surface loading in the UA3 model. The traffic load consists of the load models LM1 and LM3 and are only applied in the k20 model. For the k20 model the load combinations gr1a and gr5 are considered. The corresponding load values for the traffic models and load areas are provided in Appendix C.1.6. The traffic load consists of a uniformly distributed load (UDL) and a load configuration in a tandem system (TS).

Table E.5: Applied load cases and corresponding ULS and SLS factors for the longitudinal models

Load case	Model	ULS-factor	SLS-C-factor	Description
Self weight	UA3	1.5	1.0	Self-weight of the tunnel structure
Soil pressure	UA3	1.5	1.0	19.20 kN/m^2 on the roof + free surface load of 0.49 kN/m^2 at embankment level
Surface load	UA3	1.6	1.0	10 kN/m^2 on all tunnel roofs
Traffic gr1a				
LM1 UDL	k20	1.6	1.0	Distributed load on tunnel floor, values according LM1
LM1 TS	k20	1.6	1.0	4 axle loads per lane (0.4 × 0.4 m), values according LM1
Traffic gr5				
LM1 UDL	k20	0.64	0.40	Distributed load on tunnel floor, values according LM1
LM1 TS	k20	1.2	0.75	4 axle loads per lane (0.4 × 0.4 m), values according LM1
LM3 TS	k20	2.24	1.4	24 axle loads only for lane 1 (1.2 × 0.15 m), values according LM3 (Figure E.4)

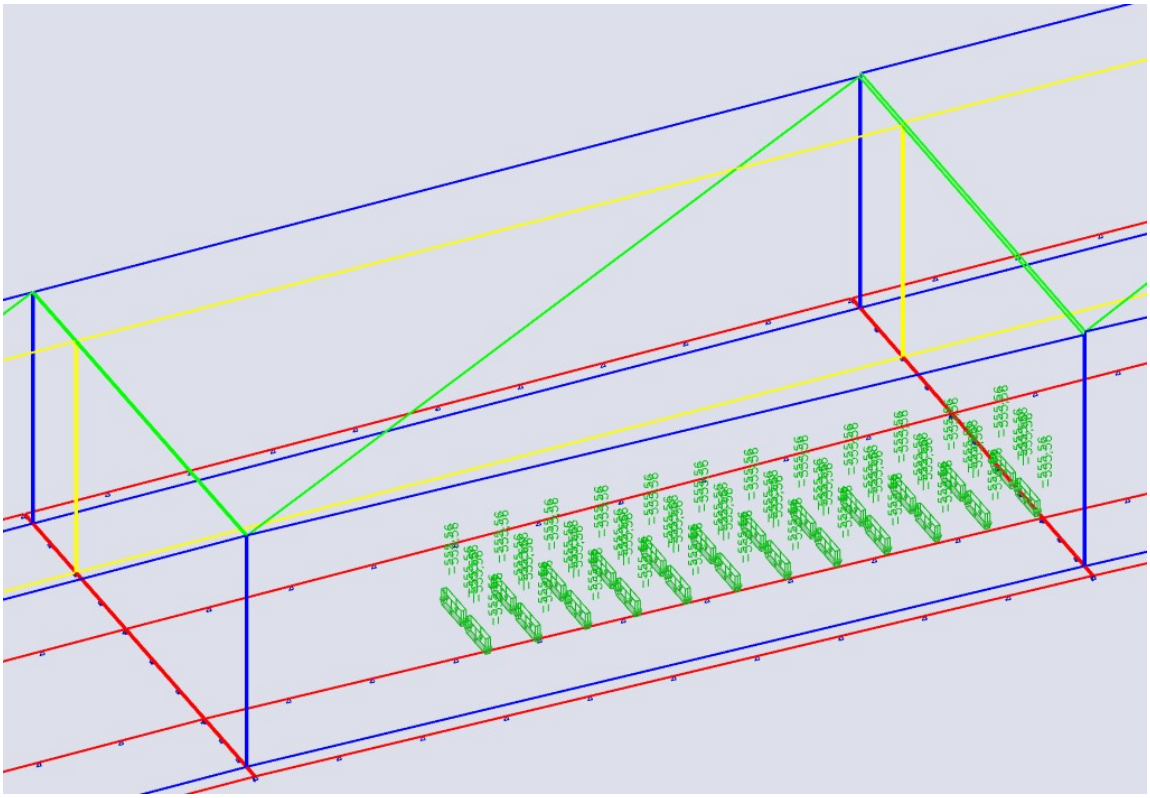

Figure E.4: Tandem system LM3

The supports in both models are modeled as uniformly distributed surface springs applied to the 2D floor elements of each tunnel segment. For each tunnel segment, three surface spring support zones are assigned based on the dimensions of the three zones that are defined in Appendix D.2. For this reason, the floor of each segment is modeled as three 2D plate elements with dimensions corresponding to the support zones. The plate elements are rigidly connected to each other in longitudinal direction. Each surface spring support is assigned stiffness properties in the vertical, longitudinal, and transverse directions.

For the UA3 model, vertical subgrade stiffness is derived from geotechnical analyses performed in Plaxis during the optimization study (Chapter 3), based on the EPS Design. The corresponding stiffness values are summarized in Table E.6. The longitudinal and transverse stiffness components are taken as 1/100 of the vertical stiffness, based on engineering judgment to represent frictional behavior.

In nonlinear analyses, a force–displacement (F–u) relationship is applied to ensure that the soil supports only compression, which reflects realistic soil behavior. For the case shown in Figure E.5, the nonlinear response is defined by two points: (0 MN, 0 m) and (-954 MN, -1 m).

Table E.6: Vertical subgrade stiffness values for tunnel segments STD-06 to STD-16 in the UA3 longitudinal model

Segment	North	Middle	South
STD-6	2.70	1.30	7.30
STD-7	4.25	1.55	9.60
STD-8	5.80	1.80	11.90
STD-9	6.09	2.48	11.11
STD-10	6.37	3.17	10.33
STD-11	6.66	3.85	9.54
STD-12	7.37	6.95	10.27
STD-13	8.08	10.06	11.01
STD-14	7.62	9.21	9.54
STD-15	7.16	6.14	6.36
STD-16	6.70	7.50	6.60

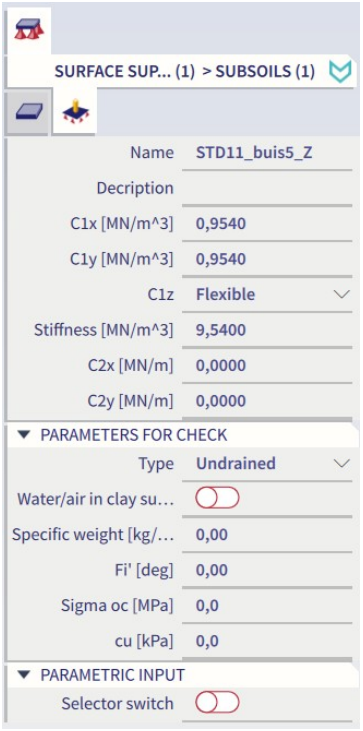

Figure E.5: Subsoil input parameters for the South floor zone of tunnel segment STD-11 in the SCIA model

In the k20 model, the three floor plate elements of each tunnel segment are assigned identical surface spring support properties. The supports have a uniform vertical stiffness of 20 MN/m^2, while the longitudinal and transverse stiffnesses are still taken as 1/100 of the vertical stiffness. This assumption represents a stiff subgrade response and reflects how the soil behaves under short-duration loading such as traffic. Due to the stiff subgrade the deformations of the tunnel segments are governed by the deformation of the segments themselves rather than by the response of the subsoil.

Finally, in the longitudinal models for the connection variants in the walls (shear key and dowels), the existing modeling of the floor shear key is directly adopted from the Oosterweelknoop design. The modeling of the floor shear key consists of a 1D rigid beam element connected to the two adjacent floor elements. This includes a hinge with a vertical translational stiffness of 140 MN/m. The elements are modeled per running meter over the total width of the floor shear key. In total there are 10 beam elements placed over a width of 11 m. The distance between the outermost beam elements and the south outer wall and north inner wall is 2.0 m. A visualization of the model is given in Figure E.6.

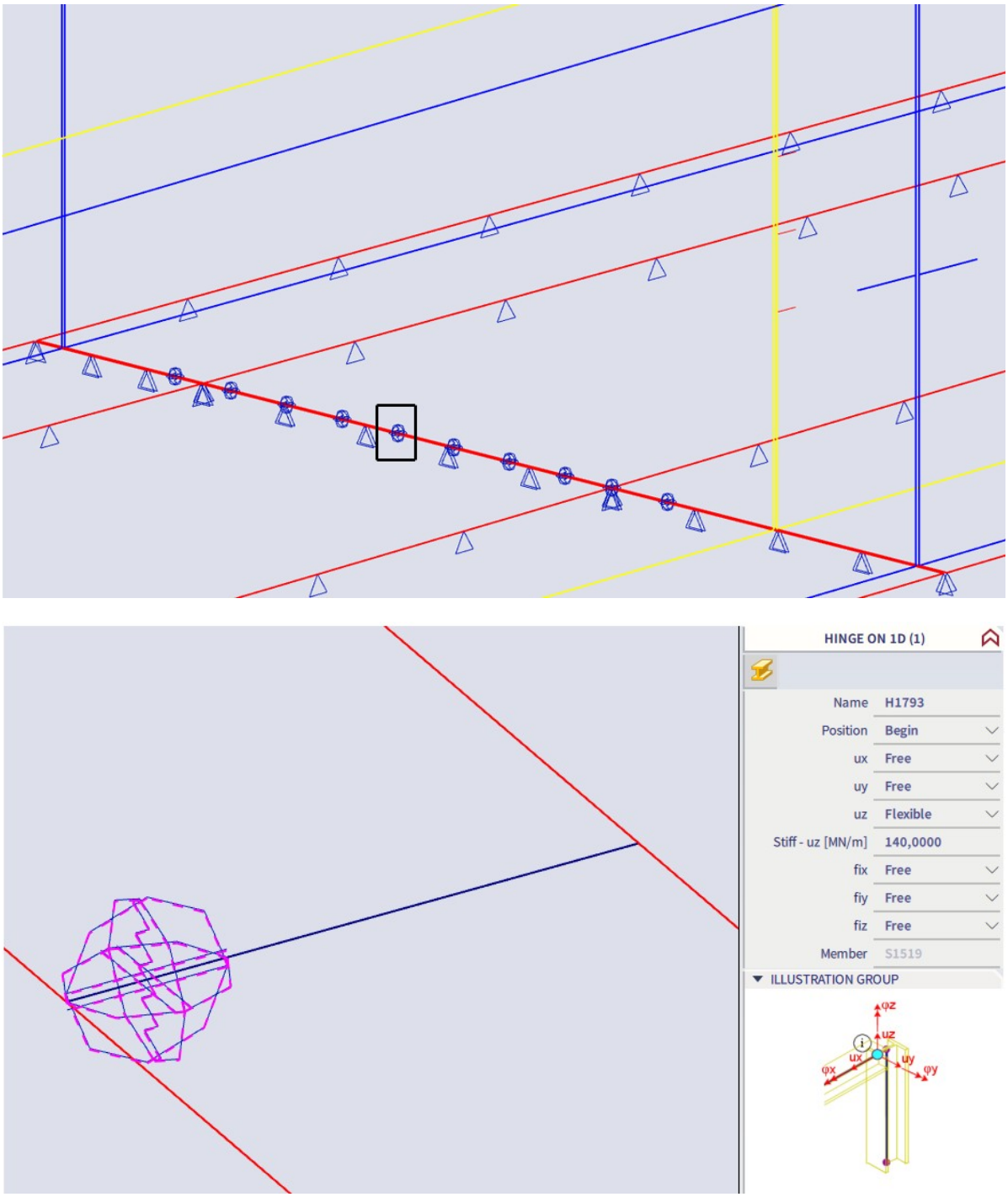

Figure E.6: Model floor shear key

E.2. Shear Key Model

During the variant study, the modeling approach of the shear key was revised compared to that used in the optimization study. The original modeling approach was adopted from the Oosterweelknoop project, where limited attention was given to the detailed behavior of the shear key. The optimization study revealed that the results for the shear key are sensitive to the chosen mesh size when it is modeled as a 1D beam element coupled to a 2D wall.

The use of 1D beams offers many advantages. In a 3D environment beam elements are easier to process, quicker to adjust, and easier to report on than 2D elements. Results such as normal forces, shear forces, moments and displacements are directly available at the element level. This simplifies the evaluation of variants and the implementation of optimizations. The use of beams also results in a less complex and more computationally efficient model, which is important in an iterative optimization process. For this reason, the shear key connection is also modeled using 1D beams in the variant study. After successful verification, the validated 1D modeling approach was adapted to the final shear key design for the connections between tunnel segments STD-10 and STD-13.

E.2.1. Design verification model

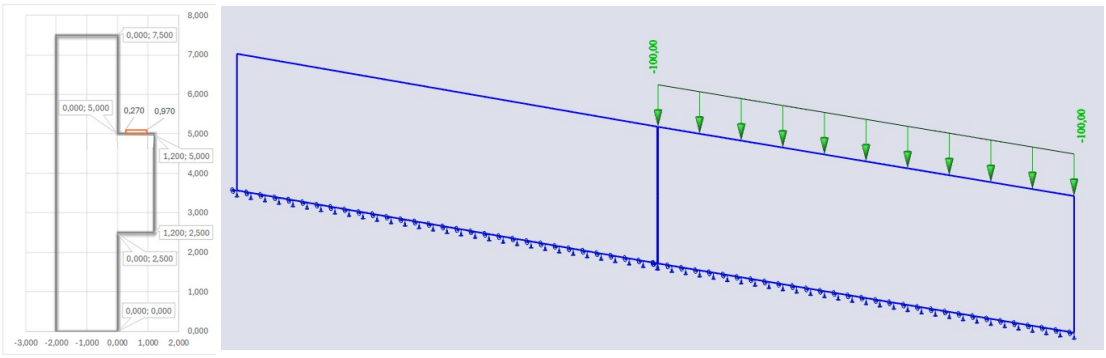

Figure E.7: Verification setup for 1D and 2D modeling of the shear key

Before the modelling approach of the shear key was incorporated into the full longitudinal model, the selected 1D modelling strategy was verified using a comparative 2D reference model. For this verification, an existing shear key design was modelled, as shown in Figure E.7. The shear key is connected to the inner walls of tunnel segments STD-09 (left) and STD-10 (right). Both walls are supported by line spring supports with stiffness properties corresponding to the vertical subgrade stiffness of the south support zone used for the STD tunnel segments in the UA3 longitudinal model.

The shear key has a thickness of 600 mm, corresponding to the thickness of both tunnel walls. In addition, the shear key is combined with a bearing block with a vertical stiffness of 1044 MN/m, derived from the corresponding force-displacement (F-u) relationship. To activate the deformation behavior of the shear key, the partition wall of STD-09 is subjected to a line load of 100 kN/m. Mesh sizes of 100 mm and 1000 mm were considered for both the 1D and 2D models. Concrete C35/45 was assigned to all structural elements. The comparison between the 1D and 2D models was performed to verify whether the deformation and force behavior of the simplified 1D representation is representative of the actual behavior of the shear key.

Both models use internal edges and rigid (line) links. The advantage of an internal edge is that, on a 2D element, the transfer of forces and deformations occurs along a predefined line, independent of the underlying mesh configuration. By combining an internal edge with a rigid link, the results at the nodes (forces and deformations) are coupled along the entire length of the internal edge. This avoids local deformation concentrations at point connections and distributes the deformation behavior of the member over the relevant height of the connection.

E.2.2. 2D reference model

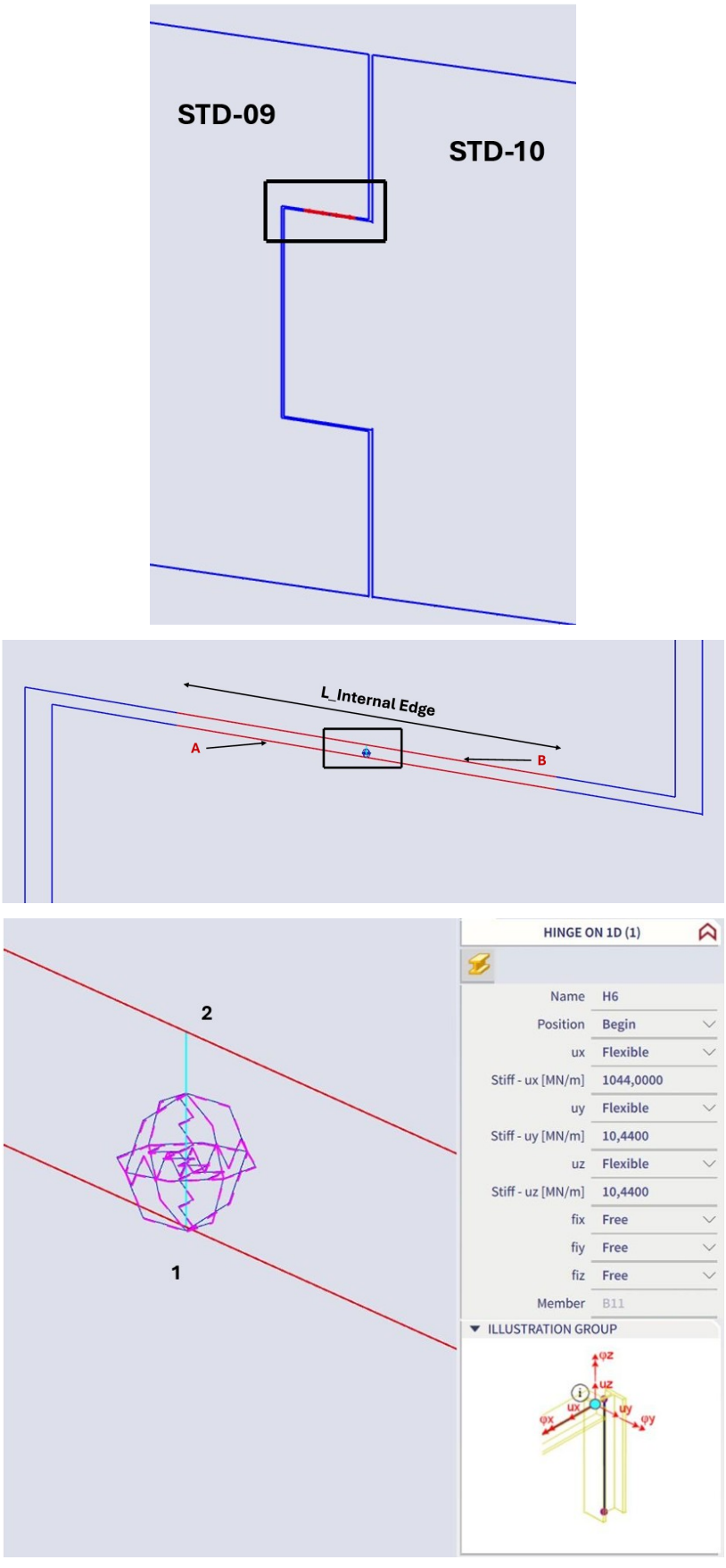

Figure E.8: 2D shear key reference model

The 2D reference model consists of two wall elements (shown in blue in Figure E.8). One wall represents the female segment with the opening, and the other represents the male segment with the shear key. At the center of the bearing block, the walls are connected by a rigid rod with a length equal to the joint width, in this case 50 mm (light blue). To ensure negligible deformation of the rod, its cross-section is multiplied by a factor of 1000. As a result, the deformation of the rod does not influence the behavior of the shear key connection. Point 1 is connected to Internal Edge A by a rigid line link, while Point 2 is connected to Internal Edge B by a rigid line link. Both internal edges are positioned at the bearing block location and have a length of $L_{\text{Internal Edge}} = 700$ mm. This ensures that the forces are transferred from the rigid rod to the walls across the full width of the bearing block.

To represent the actual behavior of the bearing block, a hinge is applied at one end of the rigid rod. This hinge prevents the transfer of bending moments through the connection. A translational spring is defined in the longitudinal direction of the rod to represent the stiffness of the bearing block. In the two transverse directions, the stiffness is taken as 1/100 of the longitudinal stiffness, representing the frictional resistance.

E.2.3. 1D Model

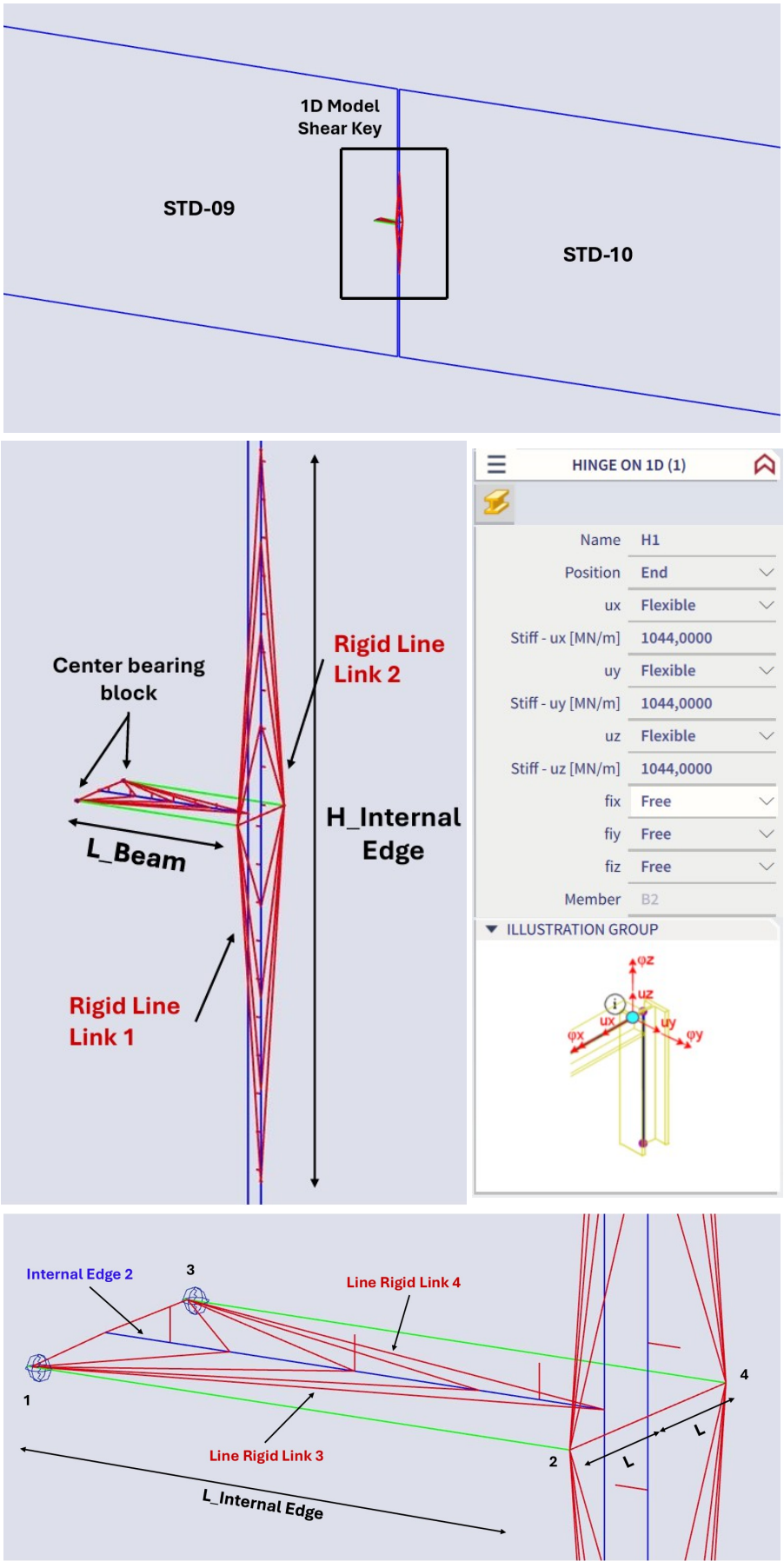

Figure E.9: 1D shear key model with hinged beam elements and rigid coupling to the 2D wall.

The 1D model of the shear key consists of two beam elements (green in Figure E.9) that are representing the half of the shear key cross-section (300 × 2500 mm) each. This approach is adopted to allow the beam elements to be positioned eccentrically outside the wall plane (L = 150 mm). This eccentric positioning is required to avoid unrealistic deformations and force transfer that would occur if the beam elements intersected the wall plane. If a single beam element were modeled through the wall, large forces would be concentrated at the node where the beam intersects the wall, resulting in non-physical behavior. By dividing the console into two beam elements, these effects are avoided and the force transfer is distributed more realistically. For consistency, this modeling approach is applied to both the inner and outer walls. Although eccentric positioning is inherently required for the outer wall due to the geometric location of the shear key, two beam elements are also used for the inner wall to maintain a consistent modeling approach.

The beam elements extend from the wall surface to the center of the bearing block (L_{Beam} = 620 mm). Nodes 2 and 4 are connected to the 2D wall element of tunnel segment STD-10 by means of rigid line links connected to an internal edge. This internal edge extends over the full height of the console ($H_{\text{Internal Edge}}$ = 2500 mm). As a result, the imposed displacements are distributed uniformly over the entire height of the connection, preventing local deformation concentrations.

Nodes 1 and 3 are likewise connected to an internal edge through rigid line links (Line Rigid Link 3 and Line Rigid Link 4, respectively). The length of this internal edge equals the beam length minus the joint width of 50 mm ($L_{\text{Internal Edge}}$ = 570 mm). The internal edge extends from the wall surface to the center of the bearing block. This ensures that the forces are transferred into the wall over the full inward length of the connection, preventing unrealistic stress concentrations and non-physical force transfer. Furthermore, it allows the forces to be applied at the correct location, namely at the center of the bearing block, consistent with the physical representation of the connection.

At both ends of the beam elements (node 1 and 3), a hinge is applied with the same parameters as in the 2D reference model, preventing the transfer of bending moments. A translational spring is defined in the longitudinal direction to represent the stiffness of the bearing block, with the stiffness corresponding to that of the actual support. In the two transverse directions, the stiffness is taken as 1/100 of the longitudinal stiffness, representing the frictional component.

E.2.4. Results

Table E.7: Overview of results

		1D-model	**2D-model**
Vertical displacement u_z	[mm]	4.61	4.61
Rotation φ_y	[mrad]	0.345	0.355
Shear force	[kN]	322.18	312.08

Table E.7 provides an overview of the results of the 1D and 2D modeling. The vertical displacement u_z and rotation φ_y are consistent in both models, indicating that the overall vertical stiffness of the console is correctly represented in the 1D modeling. The calculated shear force in the connection is also of the same order of magnitude for both models. Based on these results, it is concluded that the chosen 1D modeling is suitable for application in the full structural model.

E.2.5. Final shear key model

The final shear key model applied to the connections between tunnel segments STD-10 to STD-13 differs geometrically from the verification model. The verification model was developed to validate the proposed 1D modelling approach using a simplified geometry. The console has dimensions of 2000 mm in height, 600 mm in the transverse direction, and 1100 mm in the longitudinal direction. In addition, a bearing block with a width of 350 mm and a length of 450 mm is applied. As a result of this modified geometry, several dimensions and distances within the model differ from those of the verification model. The material properties, mesh size, and positioning of the rigid line links and internal edges remain unchanged. Table E.8 provides an overview of all dimensions and model parameters applied in the final shear key model.

Table E.8: Shear key model parameters

Parameter	Value
Number of beam elements	2
Beam cross-section (per beam)	300×2000 mm
Total shear key cross-section	600×2000 mm
Beam length (L_{Beam})	675 mm
Eccentricity inner wall (L)	150 mm
Eccentricity outer wall (L)	50 and 350 mm
Internal edge height ($H_{\text{Internal Edge}}$)	2000 mm
Internal edge length ($L_{\text{Internal Edge}}$)	625 mm
Distance floor to beam center	3875 mm
Distance roof to beam center	3875 mm
Translational spring stiffness	1044 MN/m
Frictional stiffness component	10.44 MN/m
Beam material	C35/45 Cracked

E.3. Collar Construction Model

For the modeling of the collar structure, the shear key in the tunnel floor from the original design was not included, as the collar construction is not used in combination with floor shear keys. The collar structure is represented by multiple 1D beam elements that connect the floor and roof across the width of the tunnel segment, as shown in Figure E.10.

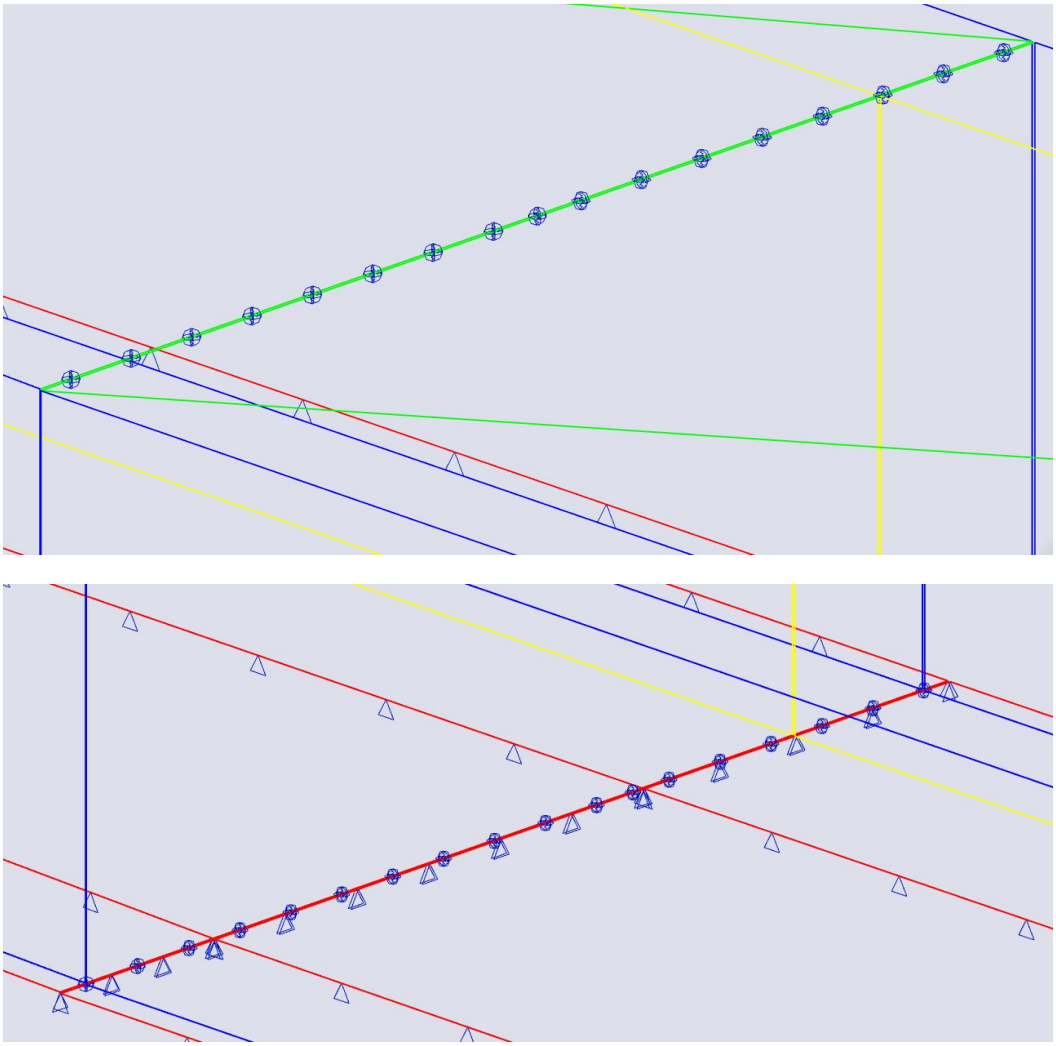

Figure E.10: Collar construction model

The collar structure is represented by multiple 1D beam elements (light blue in Figure E.12 and E.11) connecting the floor and roof across the width of the structure. The beam elements in the roof have a cross-section of 1000 × 1250 mm, while the beam elements in the floor have a cross-section of 1000 × 1500 mm. The beam elements are assigned the same material properties as the surrounding floor and roof elements, namely cracked concrete C35/45.

A hinge is applied at the end of each beam element located on the tunnel segment with the lowest STD number. For example, for the connection between tunnel segments STD-10 and STD-11, the hinges are located on the STD-10 side of the beam. The stiffness of the bearing block is incorporated into the hinge through a nonlinear force-displacement relationship in the vertical direction. This nonlinear relationship governs the shear force transfer and is defined using the stiffness of the bearing block (1044 MN/m). In the two transverse directions, linear translational springs are applied with a stiffness equal to 1/100 of the bearing block stiffness, representing the frictional resistance.

The nonlinear force-displacement relationships assigned to the hinges are required because the shear forces in the floor and roof cannot act in the same direction simultaneously. By applying these nonlinear hinge properties, only the physically correct shear force transfer mechanism is activated. As a result, the floor and roof elements can transfer shear forces only in the directions that are consistent with the structural behavior of the collar construction.

Figure E.11 shows the nonlinear spring function that is applied to all the beam elements between the floor elements that allows only downward shear force transfer on the left side of the connection. Figure E.12 shows the nonlinear spring function that is applied to all the beam elements between the roof elements that allows only upward shear force transfer on the left side of the connection. Together these nonlinear functions ensure that the collar structure behaves in accordance with the intended structural force-transfer mechanism.

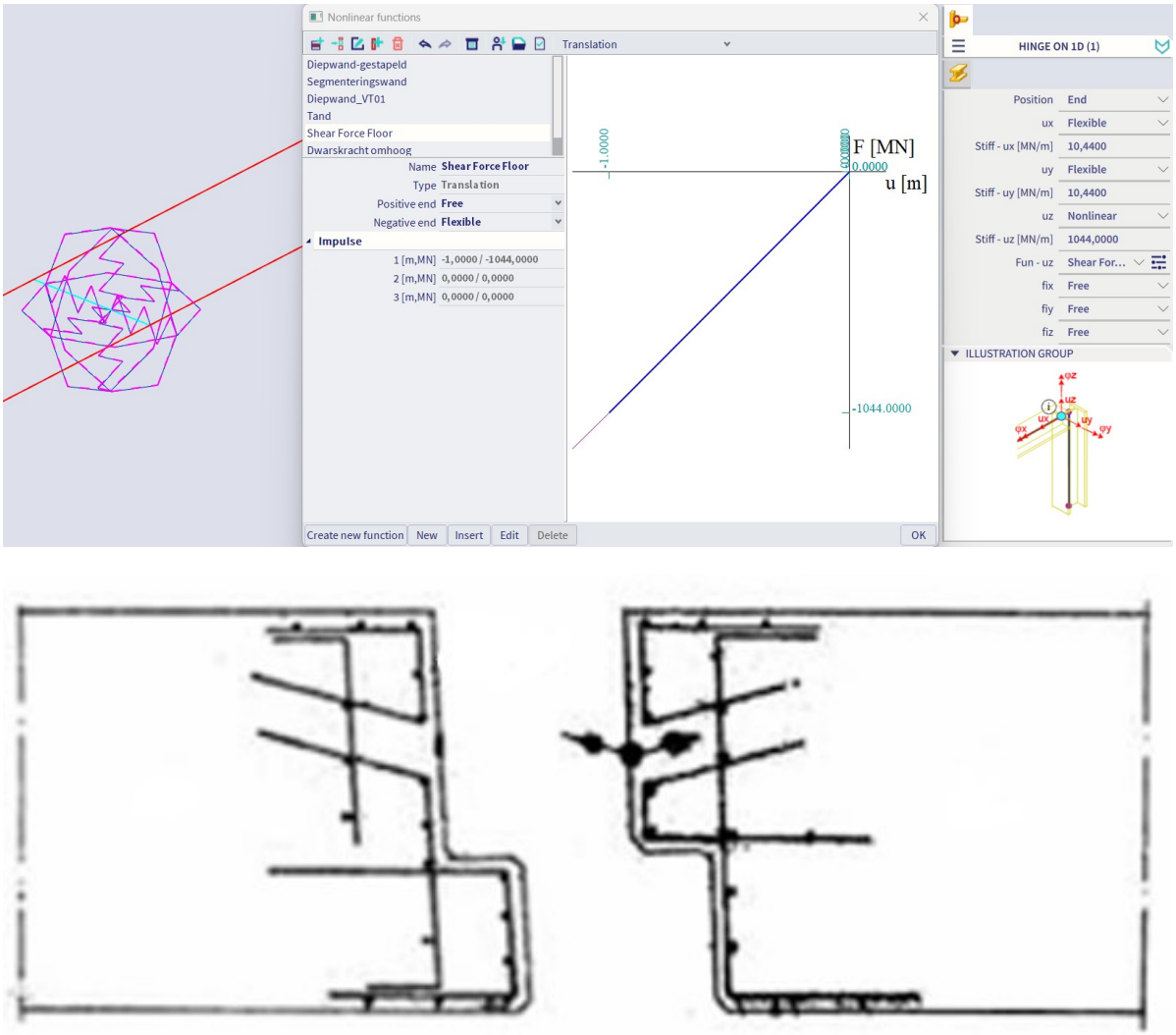

Figure E.11: Nonlinear spring behavior for the floor element allowing downward shear force transfer only, in accordance with the design

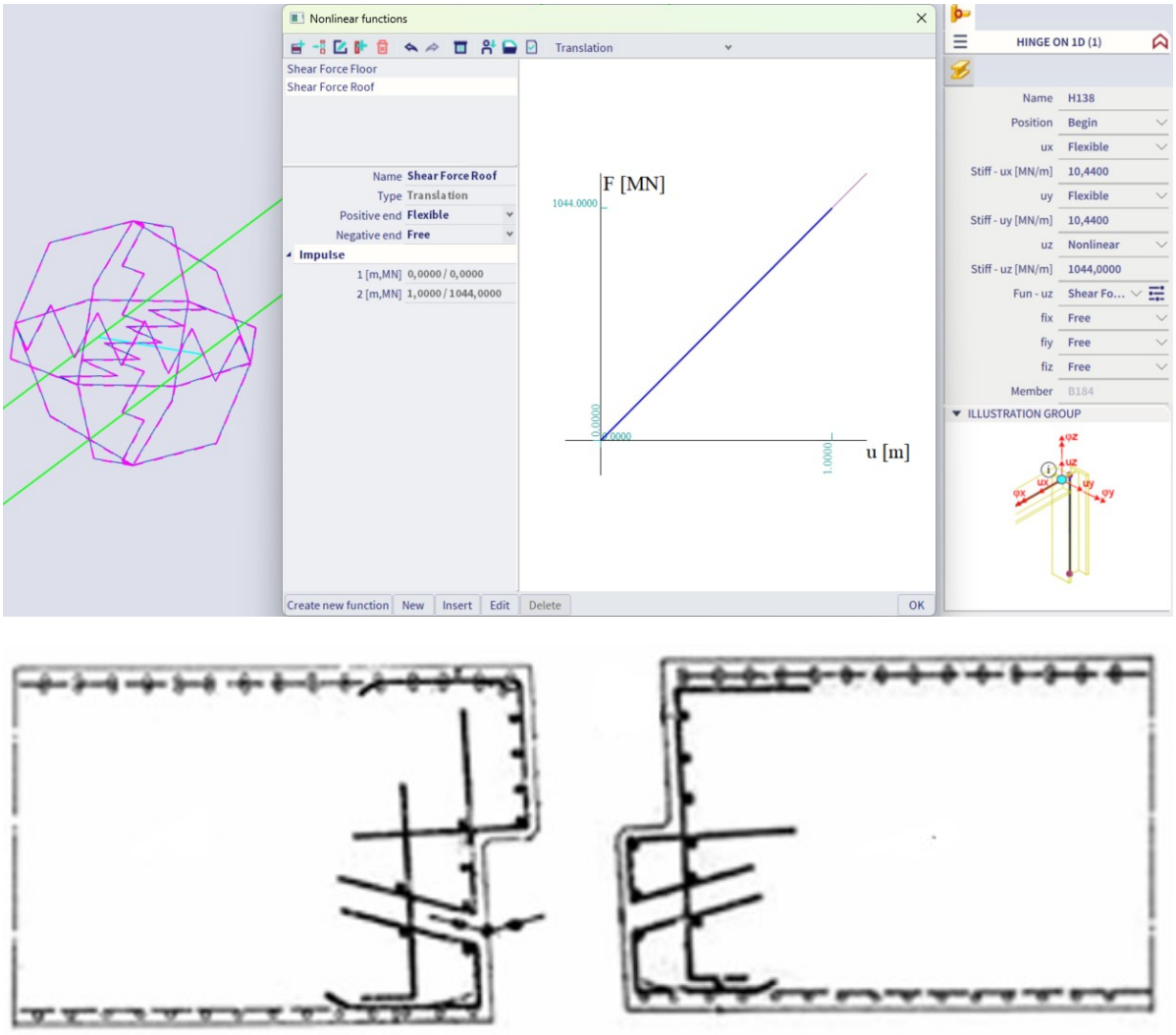

Figure E.12: Nonlinear spring behavior for the roof element allowing upward shear force transfer only, in accordance with the design

E.4. Dowel Connection Model

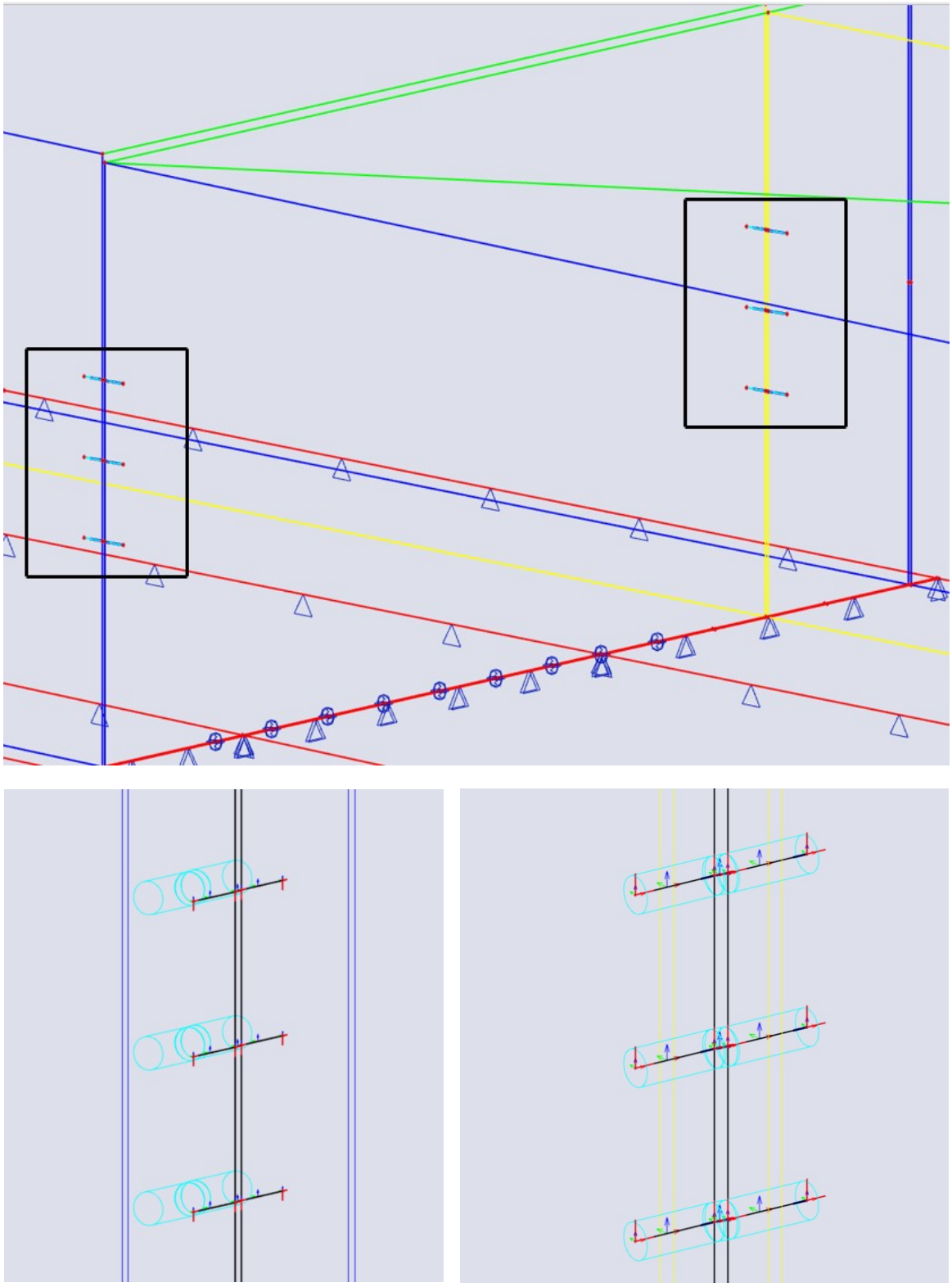

Figure E.13: Finite element representation of the DSDQ dowel model applied in the outer wall (left) and inner wall (right)

For the modeling of the DSDQ 450 dowel (Section 4.4) connection, a simplified representation was chosen in which a single 1D beam element is used per connection. The center of the element is located at the center of the DSDQ connection. For the outer walls, this means that the elements are modeled eccentrically with respect to the wall. The 1D elements serve only to determine the transverse forces occurring in the connection and are not intended for detailed stress analyses of the dowel itself. The cross-section of the element is equivalent to the combined cross-sections of the two dowels (77.3 mm). The material is S355 steel, with a modulus of elasticity corresponding to that of stainless steel. As a result, the bending stiffness is representative of the two dowels. The length and geometry of the 1D element correspond to the design of the DSDQ dowel and are summarized in Table E.9.

Table E.9: DSDQ 450 dowel model parameters

Parameter	Value
Dowel diameter	77.3 mm
Steel grade	S355
Total beam length	690 mm
Embedment length in concrete	320 mm
Joint width	50 mm
Distance from dowel center to floor	2875 mm
Distance from dowel center to roof	2875 mm
Center-to-center distance between dowels	1000 mm

As a conservative assumption, the 1D element is fully moment-restrained within the concrete. Longitudinal displacements in the direction of the joint are allowed, while transverse displacements and rotations are prevented. In the actual situation, the DSDQ dowel allows for limited transverse displacement and rotation in addition to longitudinal displacement. Due to this modeling choice, the connection is modeled as stiffer than in reality, resulting in higher calculated shear forces. This modeling choice is therefore conservative and leads to a safe design value for the shear force, which is adopted in the design of the connection.

E.5. Free-Settlement Joint Model

For the elaboration of the connection without structural coupling, it is necessary to determine the global displacements and rotations of the STD tunnel segments. In the model, the tunnel segments are structurally decoupled, meaning that no force transfer occurs between adjacent segments. As a result, the segments can move freely relative to each other, allowing the relative displacements to be directly derived from the model. At the locations of the axis lines of the tunnel segments (see Figure E.14), the displacements of both adjacent tunnel segments are determined for the design.

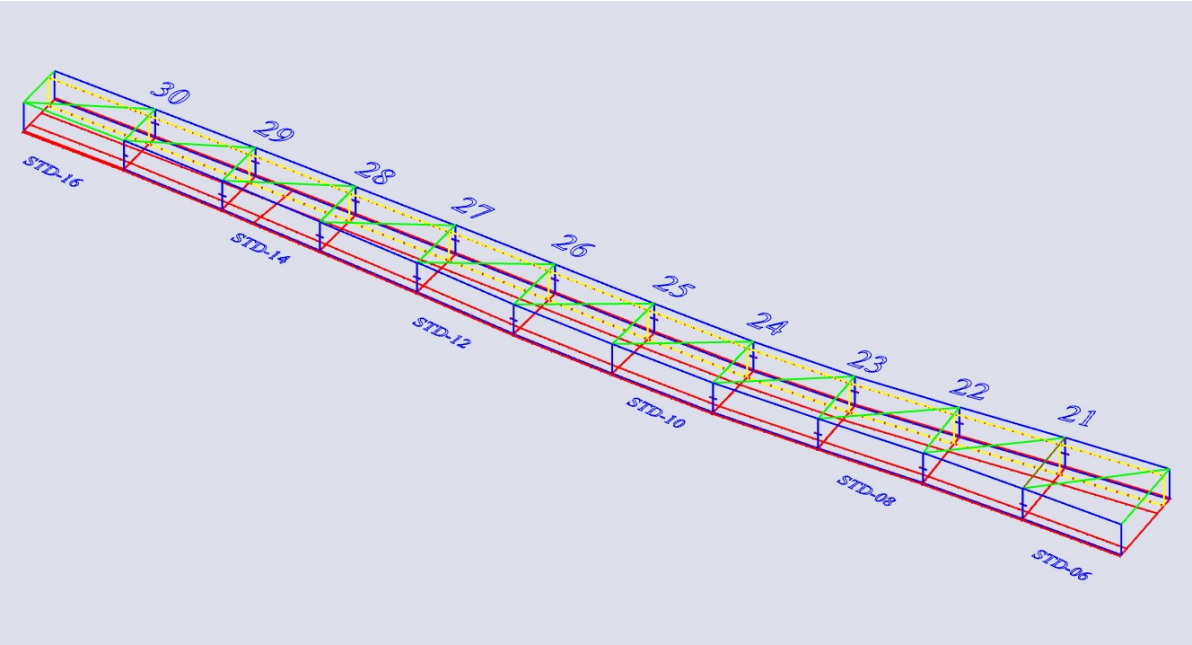

Figure E.14: Model for determining settlements and rotations of the tunnel segments

F

Strut and Tie Models

In this appendix, the strut-and-tie models (STM) developed for the reinforcement design of the shear key and collar construction variants are presented. Because this calculation has to be performed multiple times, a spreadsheet was developed for this research. The following strut-and-tie models have been established:

- Male part of the shear key
- Female part of the shear key
- Inner collar – floor
- Inner collar – roof

The STM modeling has been carried out in accordance with NEN-EN 1992-1-1 (EC2). The STM models are used to determine the required reinforcement capable of resisting the shear forces obtained from the SCIA longitudinal models, including the associated friction component. This friction component depends on the magnitude of shrinkage and temperature variations, the type of bearing material, and the magnitude of the vertical force. The VBC recommends adopting a friction coefficient of 0.2 for rubber bearings [47].

For this study, only the reinforcement required for the transfer of forces from the connection into the surrounding structure is considered, consisting of the tension ties and the hanger reinforcement. The load is applied as a concentrated vertical force F_z, combined with a horizontal force F_h, acting at the center of the bearing pad. The adopted strut-and-tie models are shown in Figures F.5, F.6, F.3, and F.4. The following assumptions are adopted:

- The load is transferred to the surrounding structure through a compression strut
- The angle of the compression strut satisfies the requirement $45° \leq \theta \leq 68.2°$ (NEN-EN 1992-1-1, J.3)
- Nodes are modeled as CCT nodes, with allowable stresses in accordance with EC2
- Tensile forces are resisted by reinforcement, consisting of horizontal tension ties and vertical hanger reinforcement
- Force equilibrium is considered in both horizontal and vertical directions

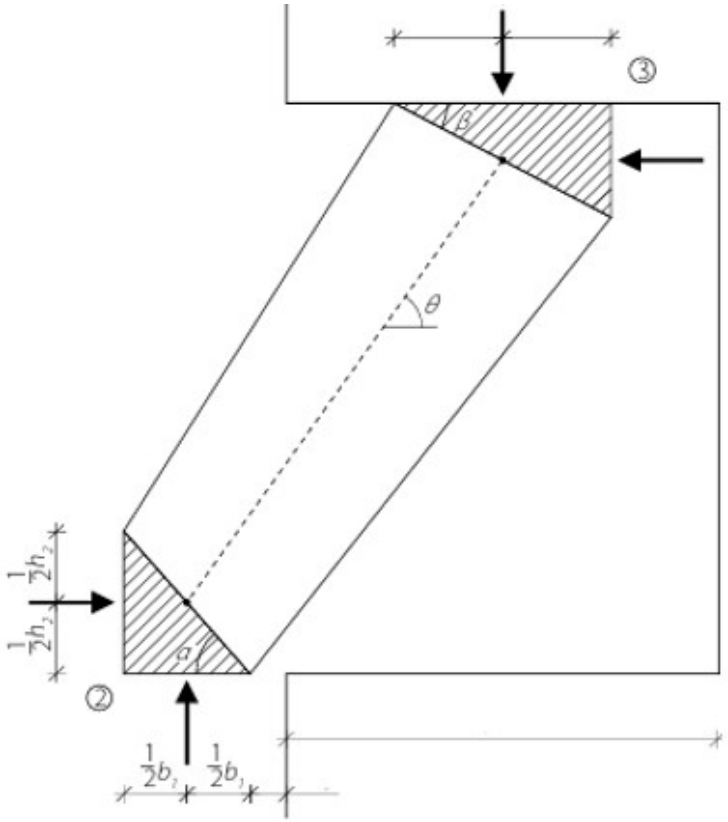

Figure F.1: Compressive strut between node 2 and 3 with angle θ [48]

For the angle (θ), an initial value is assumed to determine the dimensions of node 2. Subsequently, this angle is verified and checked, after which the remaining forces are determined based on the resulting geometry and equilibrium conditions. The following requirements are verified:

- Stresses in the nodes and the compression strut comply with the requirements in the ultimate limit state (ULS)
- Sufficient reinforcement is provided to resist the tensile forces (ULS)
- The crack width complies based on the resulting steel stresses and bar spacing, depending on the value of the maximum allowable crack width $w_{\max}$ (SLS)

Table 7.3N of NEN-EN 1992-1-1 provides reinforcement spacings for maximum crack widths of 0.20 mm and 0.30 mm. Since a maximum crack width of 0.25 mm is allowed for the connection, linear interpolation is performed between these values.

The forces in the tension and compression members of the strut-and-tie models are initially determined analytically based on equilibrium conditions. For verification, these models are also implemented in SCIA Engineer, where the truss is modeled using bar elements with axial force only as the FEM type.

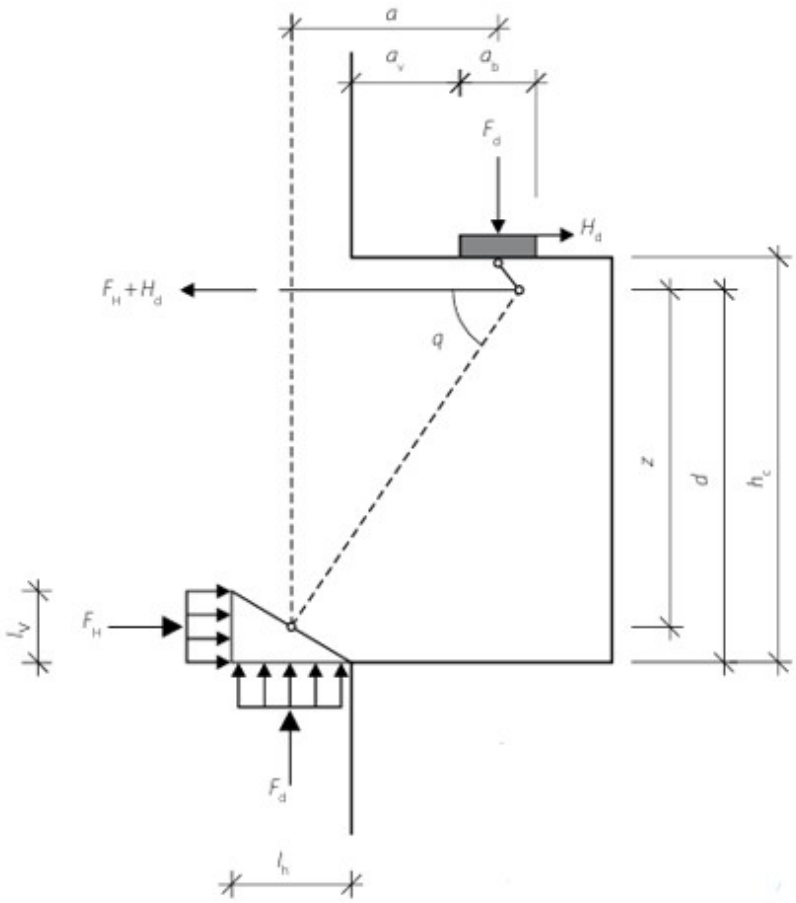

Figure F.2: Geometry Console [48]

To control cracking in the web of the console, horizontal side reinforcement distributed uniformly over the height must be provided on each face. The area of the splitting reinforcement shall be at least 25% of the tensile reinforcement required for strength, provided that a short console is considered. In this study, the splitting reinforcement is not included in the comparison between the variants. A console is classified as short if the following condition is satisfied (EC2 Art. J.3):

$$\frac{a_c}{h_c} = \frac{a_v + \frac{1}{2}a_b}{h_c} < 0.5 \tag{F.1}$$

If this condition is not satisfied, the console is classified as a long console and closed vertical stirrups must be provided when $F_d > V_{Rd,c}$. In the case of the shear key, only the female part is subjected to this condition and therefore requires the application of stirrups.

Data

Console				Concrete properties	
L	1100 mm	Concrete grade	C35/45 mm	fck =	35 MPa
B	600 mm	cover	60 mm	fcd =	23,3 MPa
H	2000 mm	Steel grade	B500B mm	fctm =	3,2 MPa
a	450 mm	Crack width wmax	0,25 mm	Ecm =	34077 MPa

Bearing block	
l	450 mm
b	350 mm

Load	SLS		ULS	
F_z	1150 kN (SLS)	$F_{z,Ed}$	1785 kN (ULS)	
F_h	230 kN (SLS)	$F_{h,Ed} = 0{,}2 * F_{z,Ed}$	357 kN (ULS)	
θ	0 mrad (SLS)	θ	0 mrad (ULS)	

Strut and node verification **(EC2-1 art. 6.5)**

Design value node types

$\sigma_{1Rd,max} = k_1 \times n' \times f_{cd}$	20,07 MPa	k_1	1	(CCC-node)	
$\sigma_{2Rd,max} = k_2 \times n' \times f_{cd}$	17,06 MPa	k_2	0,85	(CCT-node)	
$\sigma_{3Rd,max} = k_3 \times n' \times f_{cd}$	15,05 MPa	k_3	0,75		
		n'	0,86		

Node 3

σ_{Ed}	11,33 Mpa ≤	17,06			OK
$b_{3,min} = F_{Ed} / B * \sigma_{RD,max}$	174,4186 mm				

Compression strut verification		Angle verification	(EC2-1 art. J.3)			
θ (assumption)	68 °	θ	67,86 °	≤	68,20	OK
$F_{z,Ed} / \sin(\theta)$ =	1925,18 kN	Δx	769,06 mm			
$b_{strut,min} = F_{strut} / B * \sigma_{RD,max}$	188,12 mm	Δz	1890 mm			

Node 2

$b_{2,min} = F_{strut} / B * \sigma_{RD,max}$	188,12 mm
h_2	100 mm

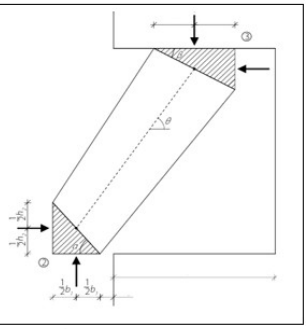

Strut and Tie model

Angles	
θ	68 °
α	46 °
β	58 °
γ	45 °

Length	
a	735 mm
b	1806 mm
c	2900 mm
d	2900 mm
e	2974 mm

ULS	
Tensile reinforcement	1083,33 kN
Hanger reinforcement	2178,03 kN

SLS (crack width)	
Tensile reinforcement	694,63 kN
Hanger reinforcement	1403,21 kN

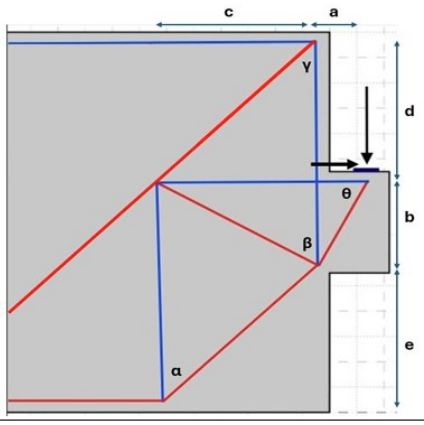

Tensile reinforcement **(EC2-1 art. 6.5)**

Quantity	3 -				
Diameter ø	40 mm				
A_s =	3770 mm^2				
f_{yd} =	435 MPa				
Tensile tie capacity (ULS)					
$F_{Rd} = A_s \times f_{yd}$	1640 kN >		1083 kN	U.C = 0,66	OK
Crack width check (EC2-1 art. 7.3N)					
σs	184 Mpa				
Steel spacing	160 mm <	Steel spacing Table 7.3N =	220 mm	U.C = 0,73	OK

Hanger reinforcement **(EC2-1 art. 6.5)**

Quantity	5 -				
Diameter ø	40 mm				
A_s =	6283 mm^2				
f_{yd} =	435 MPa				
Tensile tie capacity					
$F_{Rd} = A_s \times f_{yd}$	2733 kN >		2178 kN	U.C = 0,80	OK
Crack width check (EC2-1 art. 7.3N)					
σs	223,3277 Mpa				
Steel spacing	96 mm <	Steel spacing Table 7.3N =	171 mm	U.C = 0,56	OK

Controle console

$a_c = a_y + 1/2\, a_b$

a_c / h_c	0,3375 <	0,5	**Short Console**

Figure F.3: Strut-and-tie model and verification results for shear key (male part)

Data

Console						Concrete properties	
L	1100	mm	Concrete grade	C35/45	mm	fck =	35 MPa
B	600	mm	cover	60	mm	fcd =	23,3 MPa
H	2900	mm	Steel grade	B500B	mm	fctm =	3,2 MPa
a	200	mm	Crack width wmax	0,25	mm	Ecm =	34077 MPa
Bearing block							
t	450	mm					
b	350	mm					
Load	SLS			ULS			
F_z	1150	kN (SLS)	$F_{z,Ed}$	1785	kN (ULS)		
F_h	230	kN (SLS)	$F_{h,Ed} = 0,2 * F_{z,Ed}$	357	kN (ULS)		
θ	0	mrad (SLS)	θ	0	mrad (ULS)		

Strut and node verification **(EC2-1 art. 6.5)**

Design value node types							
$\sigma_{1Rd,max} = k_1 \times n' \times f_{cd}$	20,07	MPa	k_1	1	(CCC-node)		
$\sigma_{2Rd,max} = k_2 \times n' \times f_{cd}$	17,06	MPa	k_2	0,85	(CCT-node)		
$\sigma_{3Rd,max} = k_3 \times n' \times f_{cd}$	15,05	MPa	k_3	0,75			
			n'	0,86			
Node 3							
σ_{Ed}	11,33	Mpa ≤		17,06	Mpa		OK
$b_{3,min} = F_{Ed} / B * \sigma_{RD,max}$	174,4186	mm					
Compression strut verification			Angle verification	(EC2-1 art. J.3)			
θ (assumption)	68	°	θ	67,81	° ≤	68,20	OK
$F_{z,Ed} / \sin(\theta) =$	1925,18	kN	Δx	519,06	mm		
$b_{strut,min} = F_{strut} / B * \sigma_{RD,max}$	188,12	mm	Δz	1272,82	mm		
Node 2							
$b_{2,min} = F_{strut} / B * \sigma_{RD,max}$	188,12	mm					
h_2	100	mm					

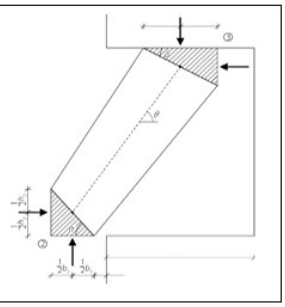

Strut and Tie model

Angles		
θ	68	°
α	57	°
β	64	°
γ	45	°
Length		
a	485	mm
b	2450	mm
c	1591	mm
d	1189	mm
e	2450	mm
f	2450	mm
ULS		
Tensile reinforcement	1084,92	kN
Hanger reinforcement As1	1622,77	kN
Hanger reinforcement As2	1785,00	kN
SLS (crack width)		
Tensile reinforcement	677,27	kN
Hanger reinforcement As1	1045,48	kN
Hanger reinforcement As2	1150,00	kN

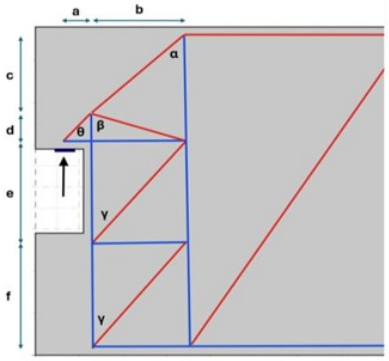

Tensile reinforcement	(EC2-1 art. 6.5)						
Quantity	3	-					
Diameter ø	40	mm					
A_s =	3770	mm²					
f_{yd} =	435	MPa					
Tensile tie capacity (ULS)							
$F_{Rd} = A_s \times f_{yd}$	1640	kN >		1085	kN	U.C = 0,66	OK
Crack width check (EC2-1 art. 7.3N)							
σs	180	Mpa					
Steel spacing	160	mm <	Steel spacing Table 7.3N =	225	mm	U.C = 0,71	OK

Hanger reinforcement	(EC2-1 art. 6.5)						
Quantity	4	-					
Diameter ø	40	mm					
A_s =	5027	mm²					
f_{yd} =	435	MPa					
Tensile tie capacity							
$F_{Rd} = A_s \times f_{yd}$	2187	kN >		1785	kN	U.C = 0,82	OK
Crack width check (EC2-1 art. 7.3N)							
σs	228,7852	Mpa					
Steel spacing	120	mm <	Steel spacing Table 7.3N =	164	mm	U.C = 0,73	OK

Controle console						
$a_c = a_s + 1/2\, a_b$						
a_c / h_c	0,875	≥	0,5	**Long Console**		
Shear capacity console						
$C_{Rd,c} = 0,18 / \gamma_c$	0,12	-				
d = 0,9H	2610	mm				
k	1,276818	-				
ρ_l	0,002407	-				
b_w	600	mm				
f_{ck}	35	Mpa				
$V_{Rd,c}$	488,2451	kN	V_{Ed}	1785	kN	**Not OK**
Stirrups						
s	200	mm	φ_{cw}	1	-	
Diameter ø	16	mm	v_1	0,6	-	
Asw	402	mm²	f_{cd}	23,3	Mpa	
z=0,9d	2349	mm	tanθ	1	-	
Fyw	435	Mpa				
Cot θ	1	-				
$V_{Rd,s}$	2054,481	kN <	$V_{Rd,max}$	9865,8	kN	**OK** U.C
$V_{Rd,s}$	2054,481	kN ≥	V_{Ed}	1785	kN	**OK** 0,87

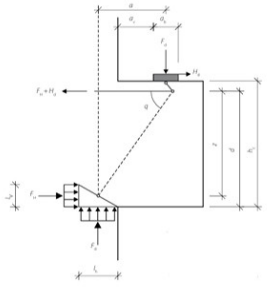

Figure F.4: Strut-and-tie model and verification results for the the shear key (female part)

Data

Floor						Concrete properties	
H	1500	mm	Concrete grade	C35/45	mm	fck =	35 MPa
B	1000	mm	cover	60	mm	fcd =	23,3 MPa
			Steel grade	B500B	mm	fctm =	3,2 MPa
			Crack width wmax	0,25	mm	Ecm =	34077 MPa
Console			Bearing block				
L	500	mm	l	250	mm		
B	1000	mm	b	600	mm		
H	750	mm					
Load	SLS			ULS			
F_z	2870	kN (SLS)	$F_{z,Ed}$	4336	kN (ULS)		
F_h	574	kN (SLS)	$F_{h,Ed} = 0,2 * F_{z,Ed}$	867	kN (ULS)		
θ	0	mrad (SLS)	θ	0	mrad (ULS)		

Strut and node verification **(EC2-1 art. 6.5)**

Design value node types							
$\sigma_{1Rd,max} = k_1 \times n' \times f_{cd}$	20,07	MPa	k_1	1	(CCC-node)		
$\sigma_{2Rd,max} = k_2 \times n' \times f_{cd}$	17,06	MPa	k_2	0,85	(CCT-node)		
$\sigma_{3Rd,max} = k_3 \times n' \times f_{cd}$	15,05	MPa	k_3	0,75			
			n'	0,86			
Node 3							
σ_{Ed}	8,67	Mpa ≤		17,06			OK
$b_{3,min} = F_{Ed} / B * \sigma_{RD,max}$	254,2115	mm					
Compression strut verification			Angle verification				
θ (assumption)	57	°	θ	56,94	°	≤ 45	OK
$F_{c,Ed} / \sin(\theta)$ =	5170,09	kN	Δx	410,00	mm	≤ 68,20	OK
$b_{strut,min} = F_{strut} / B * \sigma_{RD,max}$	303,11	mm	Δz = H - 2*cover	630	mm		
Node 2							
$b_{2,min} = F_{strut} / B * \sigma_{RD,max}$	303,11	mm					
h_2	120	mm					

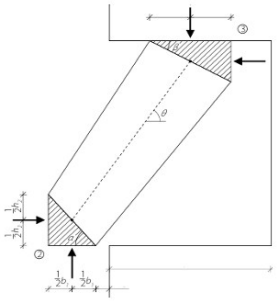

Strut and Tie model

Angles		
θ	57	°
Φ	45	°
β	50	°
γ	45	°
Length		
a	410	mm
b	750	mm
c	630	mm
d	630	mm
e	750	mm
ULS		
Tensile reinforcement	3689,04	kN
Hanger reinforcement	6020,13	kN
SLS (crack width)		
Tensile reinforcement	2441,78	kN
Hanger reinforcement	3984,72	kN

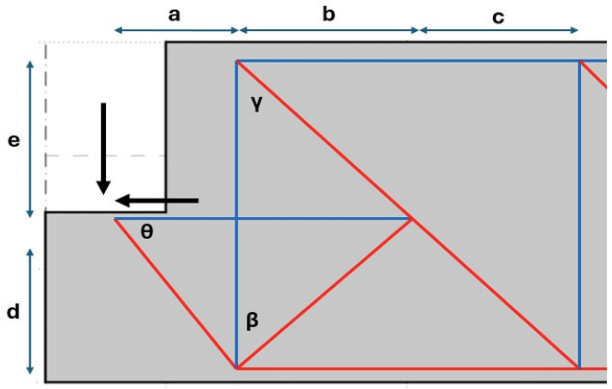

Tensile reinforcement	(EC2-1 art. 6.5)						
Quantity	7	-					
Diameter ø	40	mm					
A_s =	8796	mm^2					
f_{yd} =	435	MPa					
Tensile tie capacity (ULS)							
$F_{Rd} = A_s \times f_{yd}$	3826	kN >		3689	kN	U.C = 0,96	OK
Crack width check (EC2-1 art. 7.3N)							
σs	278						
Steel spacing	125,7143	mm <	Steel spacing Table 7.3N =	153	mm	U.C = 0,82	OK
Hanger reinforcement	(EC2-1 art. 6.5)						
Quantity	12	-					
Diameter ø	40	mm					
A_s =	15080	mm^2					
f_{yd} =	435	MPa					
Tensile tie capacity							
$F_{Rd} = A_s \times f_{yd}$	6560	kN >		6020	kN	U.C = 0,92	OK
Crack width check (EC2-1 art. 7.3N)							
σs	264,2453						
Steel spacing	73,33333	mm <	Steel spacing Table 7.3N =	120	mm	U.C = 0,61	OK

Figure F.5: Strut-and-tie model and verification results for the inner floor collar construction

Data

Roof						Concrete properties	
H	1250	mm	Concrete grade	C35/45	mm	f_{ck} =	35 MPa
B	1000	mm	cover	60	mm	f_{cd} =	23,3 MPa
			Steel grade	B500B	mm	f_{ctm} =	3,2 MPa
			Crack width wmax	0,25	mm	E_{cm} =	34077 MPa
Console			Bearing block				
L	500	mm	b	250	mm		
B	1000	mm	l	1000	mm		
H	625	mm					
Load	SLS			ULS			
F_z	1028	kN (SLS)	$F_{z,Ed}$	1555	kN (ULS)		
F_h	206	kN (SLS)	$F_{h,Ed} = 0{,}2 * F_{z,Ed}$	311	kN (ULS)		
θ	0	mrad (SLS)	θ	0	mrad (ULS)		

Strut and node verification (EC2-1 art. 6.5)

Design value node types

$\sigma_{1Rd,max} = k_1 \times n' \times f_{cd}$	20,07	MPa	k_1	1	(CCC-node)		
$\sigma_{2Rd,max} = k_2 \times n' \times f_{cd}$	17,06	MPa	k_2	0,85	(CCT-node)		
$\sigma_{3Rd,max} = k_3 \times n' \times f_{cd}$	15,05	MPa	k_3	0,75			
			n'	0,86			

Node 3

σ_{Ed}	3,11	Mpa ≤	17,06				OK
$b_{3,min} = F_{Ed} / B * \sigma_{RD,max}$	91,1667	mm					

Compression strut verification			Angle verification				
θ (assumption)	59	°	θ	58,46	°	≤ 68,20	OK
$F_{z,Ed} / \sin(\theta)$ =	1814,11	kN	Δx	310,00	mm		
$b_{strut,min} = F_{strut} / B * \sigma_{RD,max}$	106,36	mm	Δz = H - 2*cover	505	mm		

Node 2

$b_{2,min} = F_{strut} / B * \sigma_{RD,max}$	106,36	mm
h_2	120	mm

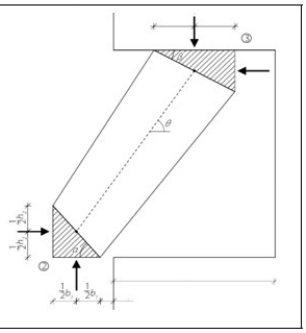

Strut and Tie model

Angles

θ	59	°
β	51	°
γ	45	°

Length

a	310	mm
b	625	mm
c	505	mm
d	505	mm
e	625	mm

ULS		
Tensile reinforcement	1245,34	kN
Hanger reinforcement	2120,58	kN
SLS (crack width)		
Tensile reinforcement	823,28	kN
Hanger reinforcement	1401,90	kN

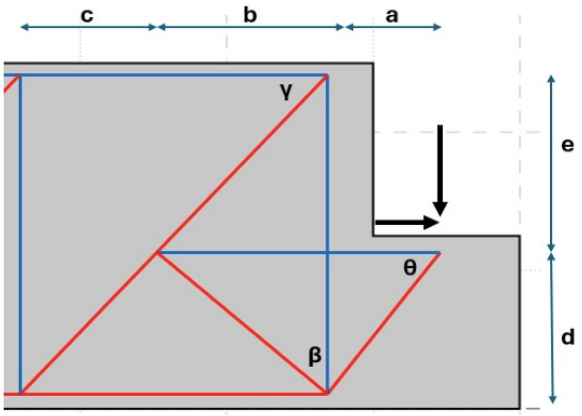

Tensile reinforcement (EC2-1 art. 6.5)

Quantity	6	-					
Diameter ø	32	mm					
A_s =	4825	mm²					
f_{yd} =	435	MPa					
Tensile tie capacity (ULS)							
$F_{Rd} = A_s \times f_{yd}$	2099	kN >		1245	kN	U.C = 0,59	OK
Crack width check (EC2-1 art. 7.3N)							
σs	171	Mpa					
Steel spacing	146,6667	mm <	Steel spacing Table 7.3N =	237	mm	U.C = 0,62	OK

Hanger reinforcement (EC2-1 art. 6.5)

Quantity	6	-					
Diameter ø	40	mm					
A_s =	7540	mm²					
f_{yd} =	435	MPa					
Tensile tie capacity							
$F_{Rd} = A_s \times f_{yd}$	3280	kN >		2121	kN	U.C = 0,65	OK
Crack width check (EC2-1 art. 7.3N)							
σs	185,9329	Mpa					
Steel spacing	146,6667	mm <	Steel spacing Table 7.3N =	218	mm	U.C = 0,67	OK

Figure F.6: Strut-and-tie model and verification results for the inner roof collar construction

G

Fatigue Spreadsheet Reinforcement

In this appendix, the fatigue verification of the reinforcement for the shear key and collar construction is presented. Both concrete connection concepts were assessed for fatigue in accordance with NEN-EN 1992-1-1, Article 6.8, considering both the tensile reinforcement and the hanger reinforcement. To determine the stress ranges, the load combination specified in Article 6.8.3 was applied:

$$\sum_{j\geq 1} G_{k,j} + P + \psi_{1,1} Q_{k,1} + \sum_{i>1} \psi_{2,i} Q_{k,i} + Q_{fat} \tag{G.1}$$

Within the tunnel segments considered, traffic loading is the only variable load and therefore the sole contributor to fatigue. The fatigue load, Q_{fat}, was determined in accordance with Fatigue Load Model 1 (BM1$_{fat}$) specified in NEN-EN 1991-2. This load model has the same configuration as the characteristic Load Model 1 (LM1), but incorporates reduced load magnitudes. The axle loads are multiplied by a factor of 0.7, while the uniformly distributed load is multiplied by a factor of 0.3:

$$Q_{ik,\mathrm{fat}} = 0.7\, Q_{ik} \quad q_{ik,\mathrm{fat}} = 0.3\, q_{ik} \tag{G.2}$$

Based on these load combinations, the minimum and maximum forces in both the tensile reinforcement and the hanger reinforcement were determined. Subsequently, the corresponding stress ranges were calculated and verified against the fatigue strength of the reinforcing steel in accordance with NEN-EN 1992-1-1, Article 6.8.4. For both the shear key and the collar connection, the reinforcement was classified as straight bars in accordance with Table 6.3N. In the shear key, however, the anchorage zones are formed by bent bars. Therefore, a reduction factor was applied when assessing the fatigue strength of these bent sections:

$$\zeta = 0.35 + 0.026 \frac{D}{\phi} \tag{G.3}$$

For both connection concepts the governing reinforcement bars were verified for fatigue as shown in Figures G.1 and G.2.

Fatigue assessment Reinforcement

Project	Thesis Research Oosterweelknoop
Date	20-7-2026
Autor	Wouter Wagenaars
Conform	NEN-EN 1992-1-1 art. 6.8 Eurocode 2: Design of concrete strucures

Reinforcement Shear Key — art. 6.8.4

Hanger reinforcement - Male part	5ø 40	A_s	6283	mm²
Tensile Reinforcement - Male part	3ø 40	A_s	3770	mm²
Hanger reinforcement - Female part	4ø 40	A_s	5027	mm²
Tensile reinforcement - Female part	3ø 40	A_s	3770	mm²

Table 6.3N Straight bars

Reinforcement Type	B500B	-	
$\gamma_{F,fat}$	1,00	-	art. 2.4.2.3(1)
$\gamma_{S,fat}$	1,15	-	art. 2.4.2.4(1)
k_1	5	-	
k_2	9	-	
D = 5ø	200	mm	
ζ=0,35 + 0,026 * (D / ø)	0,48	-	
$\Delta\sigma_{Rsk}$	130	Mpa	
$\Delta\sigma_{Rsk,red} = \zeta * \Delta\sigma_{Rsk}$	54,26	Mpa	
N*	2000000	Cycles	

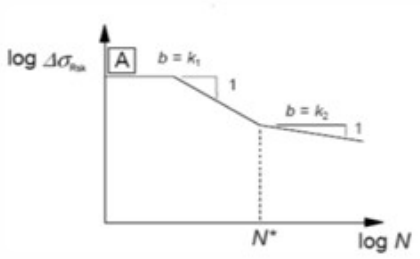

	Male		Female	
	Hanger	Tensile	Hanger	Tensile
SCIA Results	**Force [kN]**	**Force [kN]**	**Force [kN]**	**Force [kN]**
F_{min}	0	0	0	0
F_{max}	148	68	121	73
	Stress [Mpa]	**Stress [Mpa]**	**Stress [Mpa]**	**Stress [Mpa]**
σ_{min}	0,0	0,0	0,0	0,0
σ_{max}	23,6	18,0	24,1	19,4

$$\Delta\sigma_{Ed} < \Delta\sigma_{Rsk,\mathrm{red}} \qquad \Delta\sigma_{Ed} > \Delta\sigma_{Rsk,\mathrm{red}}$$

$$N = N^* \left(\frac{\Delta\sigma_{Rsk,\mathrm{red}}}{\Delta\sigma_{Ed}}\right)^{k_2} \qquad N = N^* \left(\frac{\Delta\sigma_{Rsk,\mathrm{red}}}{\Delta\sigma_{Ed}}\right)^{k_1}$$

Description	n_{Ei} [cycles]	$\sigma_{i,min}$ [MPa]	$\sigma_{i,max}$ [MPa]	$\Delta\sigma_{Ei}$ [MPa]	k_i [-]	N_{Ri} [cycles]	D_i [-]
Q_{fat}	200.000.000	0,0	24,1	24,1	9	3004492366	0,07
Total	200.000.000	cycles					

Damage number according to Palmgren-Miner = U.C. = $D_{d,T} = \Sigma D_i$ = **0,07** **≤ 1,0** **OK**

Figure G.1: Fatigue assessment of reinforcement shear key according to EN 1992-1-1, Section 6.8.4

Reinforcement Collar Construction — art. 6.8.4

Ophangwapening - Floor	7ø 40	A_s	8796	mm^2
Trekwapening - Floor	12ø 40	A_s	15080	mm^2
Ophangwapening - Roof	6ø 40	A_s	7540	mm^2
Trekwapening - Roof	6ø 32	A_s	4825	mm^2

Table 6.3N

Wapeningstype	B500B	-	
$\gamma_{F,fat}$	1,00	-	art. 2.4.2.3(1)
$\gamma_{S,fat}$	1,15	-	art. 2.4.2.4(1)
k_1	5	-	
k_2	9	-	
$\Delta\sigma_{Rsk}$	113,04	Mpa	
N*	2000000	wisselingen	

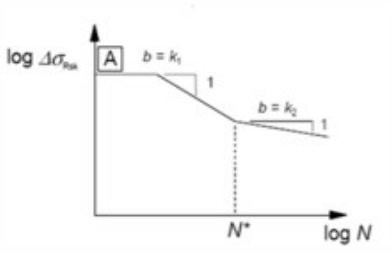

	Floor		Roof	
	Hanger	Tensile	Hanger	Tensile
SCIA Results	**Force [kN]**	**Force [kN]**	**Force [kN]**	**Force [kN]**
F_{min}	0	0	0	0
F_{max}	14	9	5	8

	Stress [Mpa]	Stress [Mpa]	Stress [Mpa]	Stress [Mpa]
σ_{min}	0,0	0,0	0,0	0,0
σ_{max}	1,6	0,6	0,7	1,7

$$\Delta\sigma_{Ed} < \Delta\sigma_{Rsk,\mathrm{red}} \qquad \Delta\sigma_{Ed} > \Delta\sigma_{Rsk,\mathrm{red}}$$

$$N = N^* \left(\frac{\Delta\sigma_{Rsk,\mathrm{red}}}{\Delta\sigma_{Ed}}\right)^{k_2} \qquad N = N^* \left(\frac{\Delta\sigma_{Rsk,\mathrm{red}}}{\Delta\sigma_{Ed}}\right)^{k_1}$$

Description	n_{Ei} [cycles]	$\sigma_{i,min}$ [MPa]	$\sigma_{i,max}$ [MPa]	$\Delta\sigma_{Ei}$ [MPa]	k_i [-]	N_{Ri} [cycles]	D_i [-]
Q_{fat}	200.000.000	0,0	1,7	1,7	9	63723484520667800000000	0,00
Total	200.000.000	cycles					

Damage number according to Palmgren-Miner = U.C. = $D_{d,T} = \Sigma D_i$ = **0,00** **≤ 1,0** **OK**

Figure G.2: Fatigue assessment of reinforcement collar construction based on EN 1992-1 art.6.8.4

H

Elastomer Bearing Block

In this appendix, the spreadsheet used for the design verification of the elastomer bearing block in the shear key connection is presented.

Bearing blocks according to NEN-EN 1337

Date 10-6-2026
Author WAA Wagenaars

Rectangular laminated bearing block with at least 2 steel plates

- Type B: Laminated bearing fully covered with elastomer comprising at least two steel reinforcing plates.

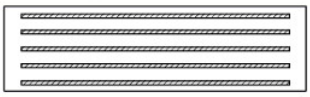

Bearing block data

a =	350	mm	block width (// to span)	T_q =	41	mm	total rubber thickness
b =	450	mm	block length (⊥ to span)	a' =	340	mm	steel plate width
t_b =	57	mm	total thickness of bearing block	b' =	440	mm	steel plate length
t_l =	12	mm	rubber layer thickness	G =	0,9	N/mm²	shear modulus rubber
n =	3	-	number of rubber layers	f_y =	235	N/mm²	yield strength steel
t_s =	4	mm	steel plate thickness	A_1 =	149.600	mm²	steel plate area
n_s =	4	-	number of steel plates	l_p =	1560	mm	perimeter steel plate
$t_{o/b}$ =	2,5	mm	cover layer thickness top and bottom	E_b =	2.000	N/mm²	compression modulus
$t_{i/r}$ =	5	mm	cover layer thickness sides	A =	157.500	mm²	block area
$k_{v,blok}$ =	1044	MN/m	vertical spring stiffness bearing block	$k_v = 1 / (t_l * n / A_1 * 10^3 * (1 / (5 * G * S_1^2) + 1 / E_b))$			
$k_{h,blok}$ =	3,94	MN/m	horizontal spring stiffness bearing block	$k_h = 1 / (T_e * 10^3 / (A * G))$			

Loads, translations and rotations

							Explanation	Article nr.
$F_{z,d,max}$ =	2000	kN	max. vertical load	$\varepsilon_{u,k}$ =	7	- allowable characteristic strain	ULS = 7	5.3.3
$F_{z,d\,min}$ =	1500	kN	min. vertical load	K_L =	1	- load type factor		Appendix C
$F_{x,d}$ =	0	kN	load in x direction (// span)	γ_m =	1	- material factor		5.3.3
$F_{y,d}$ =	0	kN	load in y direction (⊥ span)	K_p =	1,3	- correction factor stress		5.3.3.5
$v_{x,d}$ =	0	mm	translation in x direction (// span)	K_h =	1	- correction factor tensile stress	Without holes K_h = 1	5.3.3.5
$v_{y,d}$ =	15	mm	translation in y direction (⊥ span)	$K_{r,d}$ =	3	- rotation limit factor		Appendix B
$\alpha_{a,d}$ =	0,0001	rad	max. rotation in direction a	K_f =	0,6	- Friction factor	0,6 for concrete	5.3.3.6
$\alpha_{b,d}$ =	0	rad	max. rotation in direction b	K_s =	78,657	- moment restoring factor	Depends on a/b ratio	5.3.3.7 (Table 4)
$v_{x,d,tot}$ =	0,0	mm	translation in x direction (due to Fx,d + vx,d)		C35/45	concrete quality substructure		
$v_{y,d,tot}$ =	15,0	mm	translation in y direction (due to Fy,d + vy,d)		C35/45	concrete quality superstructure		
$v_{xy,d,tot}$ =	15,0	mm	combined translation					
$F_{xy,d,tot}$ =	59,1	kN	max. resulting horizontal force due to displacements vx,d and vy,d					

Check deformations (strain) - article 5.3.3

Shape factor - art. 5.3.3.1

$t_{e,inner}$ =	t_l =	12	mm	effective rubber thickness
$t_{e,outer}$ =	ti =	2,5	mm	effective rubber thickness
S_{inner} =	$A_1 / (l_p * t_{e,inner})$ =	8,0	-	shape factor for inner rubber layer
S_{outer} =	$A_1 / (l_p * t_{e,outer})$ =	38,4	-	shape factor for outer rubber layer

Compression due to maximum compressive force - art. 5.3.3.2

A_r =	$A_1 * (1-(v_{x,d} / a') - (v_{y,d} / b'))$ =	144.500	mm²	reduced effective bearing block area
$\varepsilon_{c,d}$ =	$1,5 * F_{z,d} / (G * A_r * S)$ =	2,89	-	

Shear due to horizontal translations - art. 5.3.3.3

$\varepsilon_{q,d}$ =	$v_{xy,d} / T_q$ =	0,37	<	1,00	**OK**

Deformation due to rotations - art. 5.3.3.4

$\varepsilon_{a,d}$ =	$(a'^2 * \alpha_{a,d} + b'^2 * \alpha_{b,d}) * t_l / (2 * \Sigma (t_l^3))$ =	0,01	-		

Maximum combined deformation - art. 5.3.3

$\varepsilon_{t,d}$ =	$K_L * (\varepsilon_{c,d} + \varepsilon_{q,d} + \varepsilon_{a,d})$ =	3,27	-		
$\varepsilon_{u,d}$ =	$\varepsilon_{u,k} / \gamma_m$ =	7	-		
$\varepsilon_{t,d} / \varepsilon_{u,d}$ < 1,00	UC =	0,47	<	1,00	**OK**

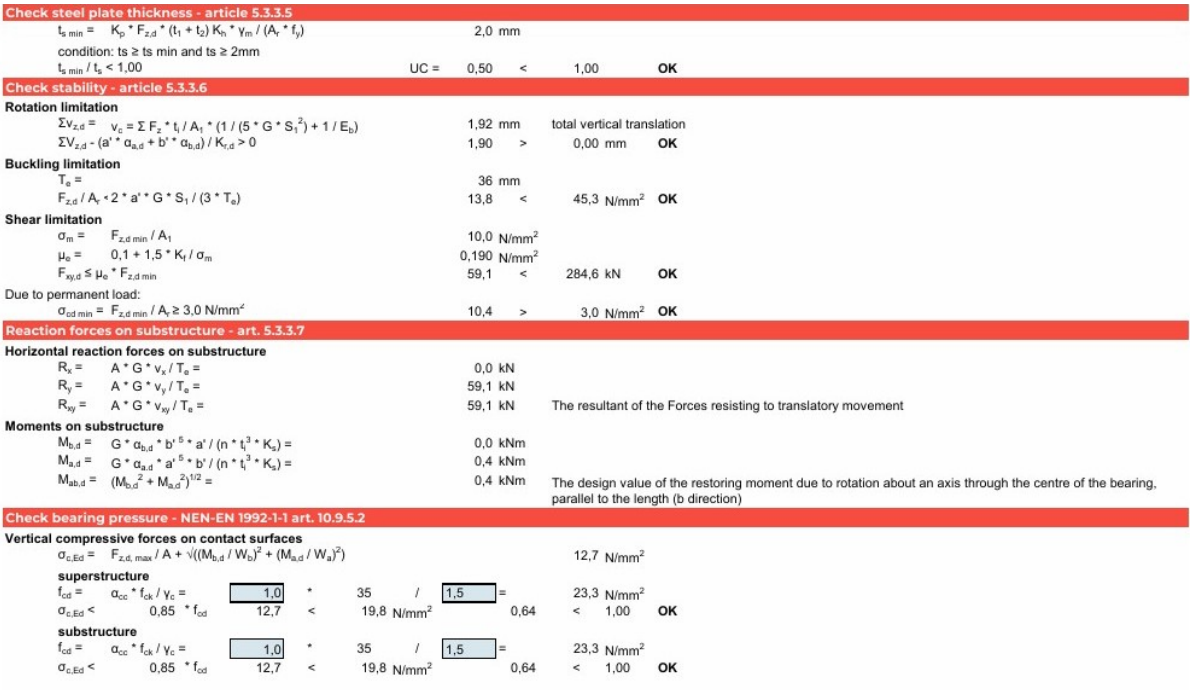

Check steel plate thickness - article 5.3.3.5

$t_{s\,min} = K_p * F_{z,d} * (t_1 + t_2) K_h * \gamma_m / (A_r * f_y)$ = 2,0 mm

condition: ts ≥ ts min and ts ≥ 2mm

$t_{s\,min} / t_s < 1{,}00$ UC = 0,50 < 1,00 **OK**

Check stability - article 5.3.3.6

Rotation limitation

$\Sigma v_{z,d} = v_c = \Sigma F_z * t_i / A_1 * (1 / (5 * G * S_1^2) + 1 / E_b)$ = 1,92 mm total vertical translation

$\Sigma V_{z,d} - (a' * \alpha_{a,d} + b' * \alpha_{b,d}) / K_{r,d} > 0$ 1,90 > 0,00 mm **OK**

Buckling limitation

T_e = 36 mm

$F_{z,d} / A_r < 2 * a' * G * S_1 / (3 * T_e)$ 13,8 < 45,3 N/mm² **OK**

Shear limitation

$\sigma_m = F_{z,d\,min} / A_1$ = 10,0 N/mm²

$\mu_e = 0{,}1 + 1{,}5 * K_f / \sigma_m$ = 0,190 N/mm²

$F_{xy,d} \leq \mu_e * F_{z,d\,min}$ 59,1 < 284,6 kN **OK**

Due to permanent load:

$\sigma_{cd\,min} = F_{z,d\,min} / A_r \geq 3{,}0$ N/mm² 10,4 > 3,0 N/mm² **OK**

Reaction forces on substructure - art. 5.3.3.7

Horizontal reaction forces on substructure

$R_x = A * G * v_x / T_e$ = 0,0 kN

$R_y = A * G * v_y / T_e$ = 59,1 kN

$R_{xy} = A * G * v_{xy} / T_e$ = 59,1 kN The resultant of the Forces resisting to translatory movement

Moments on substructure

$M_{b,d} = G * \alpha_{b,d} * b'^5 * a' / (n * t_i^3 * K_s)$ = 0,0 kNm

$M_{a,d} = G * \alpha_{a,d} * a'^5 * b' / (n * t_i^3 * K_s)$ = 0,4 kNm

$M_{ab,d} = (M_{b,d}^2 + M_{a,d}^2)^{1/2}$ = 0,4 kNm The design value of the restoring moment due to rotation about an axis through the centre of the bearing, parallel to the length (b direction)

Check bearing pressure - NEN-EN 1992-1-1 art. 10.9.5.2

Vertical compressive forces on contact surfaces

$\sigma_{c,Ed} = F_{z,d,\,max} / A + \sqrt{((M_{b,d} / W_b)^2 + (M_{a,d} / W_a)^2)}$ 12,7 N/mm²

superstructure

$f_{cd} = \alpha_{cc} * f_{ck} / \gamma_c$ = 1,0 * 35 / 1,5 = 23,3 N/mm²

$\sigma_{c,Ed} < 0{,}85 * f_{cd}$ 12,7 < 19,8 N/mm² 0,64 < 1,00 **OK**

substructure

$f_{cd} = \alpha_{cc} * f_{ck} / \gamma_c$ = 1,0 * 35 / 1,5 = 23,3 N/mm²

$\sigma_{c,Ed} < 0{,}85 * f_{cd}$ 12,7 < 19,8 N/mm² 0,64 < 1,00 **OK**

Figure H.1: Bearing block assessment according to NEN-EN 1337

I

Detailing of Hanger Reinforcement in Consoles

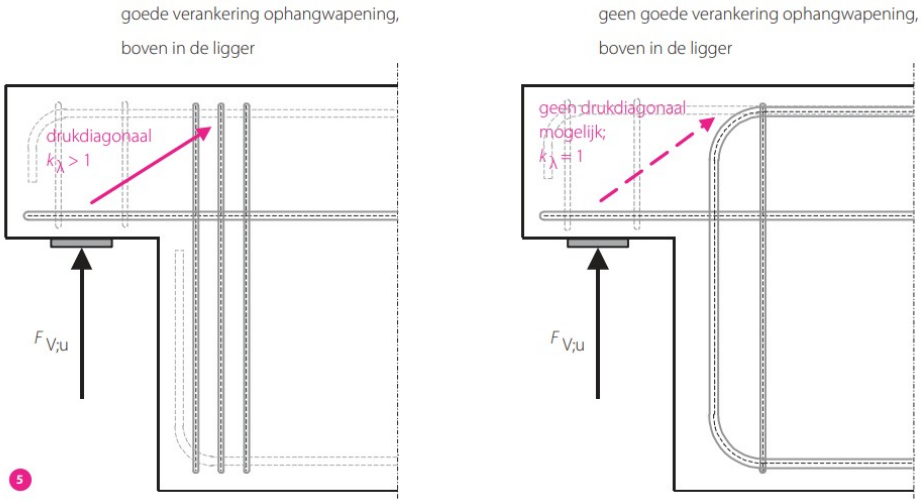

Figure I.1: Hanger reinforcement detailed as stirrups (left) and as bent reinforcement at the top of the beam, extending towards the span (right) [49]

This appendix presents the background information used for the reinforcement detailing of the collar connection. The recommendations of Kleiman (2006–2009) regarding hanger reinforcement in shear key supports were used as a basis for the development of the reinforcement configuration [20]. In the traditional design approach according to NEN 6720 (VBC 1995), shear key supports are often treated as deep beams or short consoles. In this approach, it is assumed that a compression strut can develop between the applied load and the support, allowing for an increased shear capacity through the enhancement factor for shear resistance, k_λ. In practice, the hanger reinforcement is often realized by bending up the longitudinal reinforcement of the beam, assuming that this reinforcement provides force transfer towards the top of the beam. Within this approach, it is assumed that the hanger reinforcement acts as a rigid support against which the compression strut can bear.

Experimental research by Kleiman has shown that this classical approach often leads to an overestimation of the load-bearing capacity of shear key supports. Full-scale tests demonstrate that cracking and failure occur at loads significantly lower than those predicted by deep beam theory. In addition, the failure mechanism deviates from the assumed strut-and-tie behavior. Instead of a well-developed compression strut with tensioned hanger reinforcement, a crack pattern often develops along the bent reinforcement, where the reinforcement does not function as a tension tie but rather as a local shear transfer element [20].



Figure I.2: Failure pattern VBC nok (left) and KN-nok (left) [20]

Recent insights confirm that the detailing of the hanger reinforcement is critical for the behavior of the shear key support. The hanger reinforcement must not only be capable of transferring the shear force to the top of the beam, but must also form a node in which the forces from the compression strut and the tension ties can be brought into equilibrium [49].

If this node is not properly formed, the concrete compression strut cannot develop in a physically consistent manner. As a result, the point of application of the forces shifts and the direction of the compression strut changes, leading to an unfavorable force distribution and an increase in forces in, among others, the horizontal tension tie. Consequently, the effective load-bearing capacity of the shear key support decreases, and the use of an increased shear capacity through the factor k_λ is not justified.

A possible solution lies in a detailing approach in which the hanger reinforcement is bent such that the concrete compression strut can directly reach the bend. When the hanger reinforcement is bent in the plane of Figure I.1 (left), the compression strut can bear against the inner side of this bend, allowing a node to form within this region. This results in a force mechanism that is consistent with the assumed strut-and-tie model, in which the forces are transferred in a clear and physically consistent manner.

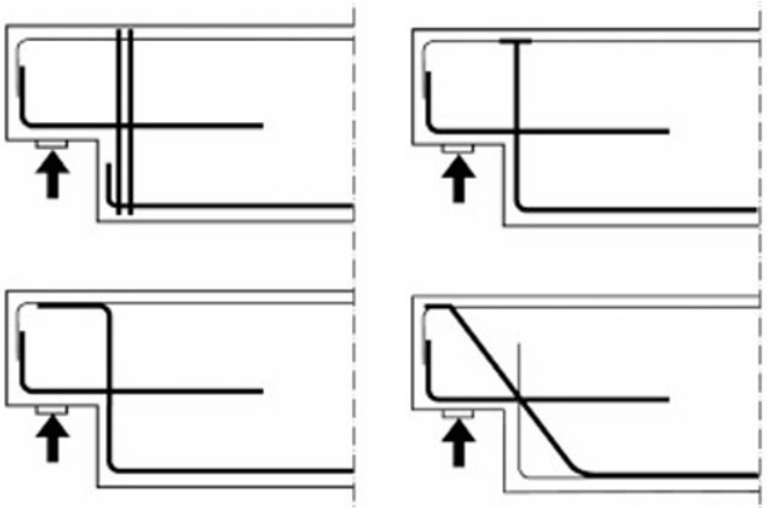

Figure I.3: Possible hanger reinforcement configurations [50]

J

Fatigue Spreadsheet Dowels

In this appendix, the fatigue verification of the dowel connection is presented.

Fatigue assessment dowels

Project	Thesis Research Oosterweelknoop
Date	22-6-2026
Autor	Wouter Wagenaars
Conform	NEN-EN 1993-1-9 Eurocode 3: Design of steel structures - Part 1-9: Fatigue

Fatigue strength (normal stress) — art. 7.1 (3)

Detail category	$\Delta\sigma_c$	80	MPa	Table 8.1 to 8.10
Reference cycles	N_C	2,00E+06	cycles	
Slope	m_1	3	-	
Slope	m_2	5	-	
Partial factor	γ_{Mf}	1,35	-	Table 3.1 ('Safe-life + High consequences)
Yield strength	f_y	355	MPa	
Red.factor geometric effect	k_s	1,00		

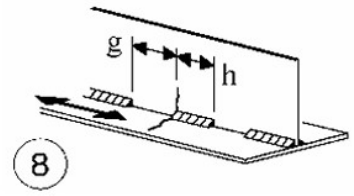

$\Delta\sigma_R$ [N/mm²]	N_R [cycles]	m [-]	
346,55	1,00E+04	3	
59,26	2,00E+06	3	$\Delta\sigma_C$; N_C
43,66	5,00E+06	3	$\Delta\sigma_D$; N_D
27,10	1,00E+08	5	$\Delta\sigma_L$; N_L
27,10	1,00E+09	-	

$\Delta\sigma_C = k_s \cdot \Delta\sigma_C / \gamma_{Mf}$

$$\Delta\sigma_R(N) = \Delta\sigma_{C,d}\left(\frac{N_C}{N}\right)^{1/m}$$

Stress cycles normal stress (Miner damage number) — Appendix A

SCIA Results BM1fat	Moment [kNm]
min	-0,33
max	0,35

Diameter 65 mm

Description	n_{Ei} [cycles]	$\sigma_{i,min}$ [MPa]	$\sigma_{i,max}$ [MPa]	$\Delta\sigma_{Ei}$ [MPa]	m_i [-]	N_{Ri} [cycles]	D_i [-]
BM1fat	200.000.000	-12,2	13,0	25,2	-	∞ (< $\Delta\sigma_L$)	0,00
Total	200.000.000	cycles					

Damage number according to Palmgren-Miner = U.C. = $D_{d,T} = \Sigma D_i$ = **0,00** ≤ **1,0** **OK**

Formulas

$$\sigma_M = \frac{M}{W} = \frac{32M}{\pi d^3}$$

$\Delta\sigma_{Ei} = \sigma_{i,max} - \sigma_{i,min}$

Als $\Delta\sigma_{Ei} \geq \Delta\sigma_D$ $N_{Ri} = N_C \times (\Delta\sigma_{Ei} / \Delta\sigma_C)^{-m}$
Boven de knik m = 3

Als $\Delta\sigma_{Ei} < \Delta\sigma_D$ $N_{Ri} = N_D \times (\Delta\sigma_{Ei} / \Delta\sigma_D)^{-m}$
Onder de knik m = 5

Uiteindelijk
$D_i = n_{Ei} / N_{Ri}$

Fatigue strength (Shear stresses) — art. 7.1 (3)

Detail category	$\Delta\sigma_c$	80	MPa	Table 8.1 to 8.10
Reference cycles	N_C	2,00E+06	cycles	
Slope	m_1	5	-	
Partial factor	γ_{Mf}	1,35	-	Table 3.1 ('Safe-life + High consequences)
Yield strength	f_y	355	MPa	

$\Delta\tau_i$ [N/mm²]	N_i [cycles]	m [-]
170,99	1,00E+04	5
59,26	2,00E+06	5
27,10	1,00E+08	-
27,10	1,00E+09	-

$\Delta\tau_C$; N_C $\quad \Delta\tau C = \Delta\tau_C / \gamma_{Mf}$

$\Delta\tau_L$; N_L

$$\Delta\tau_R(N) = \Delta\tau_{C,d}\left(\frac{N_C}{N}\right)^{1/m}$$

Stress cycles shear stress (Miner damage number) — Appendix A

SCIA Results BM1fat	Shear Force [kN]
min	-20,03
max	15,31

Diameter 65 mm
Area 3318,307 mm

Description	n_{Ei} [cycles]	$\tau_{i,min}$ [MPa]	$\tau_{i,max}$ [MPa]	$\Delta\tau_{Ei}$ [MPa]	m_i [-]	N_{Ri} [cycles]	D_i [-]
BM1fat	200.000.000	-8,05	6,15	14,20	-	∞ (< $\Delta\tau_L$)	0,00
Total	200.000.000	cycles					

Damage number according to Palmgren-Miner = U.C. = $D_{d,T}$ = ΣD_i = 0,00 ≤ 1,0 OK

Formulas

$$\tau_{max} = \frac{4V}{3A}$$

$\Delta\tau_{Ei} = \tau_{i,max} - \tau_{i,min}$

$N_{Ri} = N_L \times (\Delta\tau_{Ei} / \Delta\tau_L)^{-m}$

$D_i = n_{Ei} / N_{Ri}$

Figure J.1: Fatigue assessment of DSDQ dowels based on S–N curves according to EN 1993-1-9

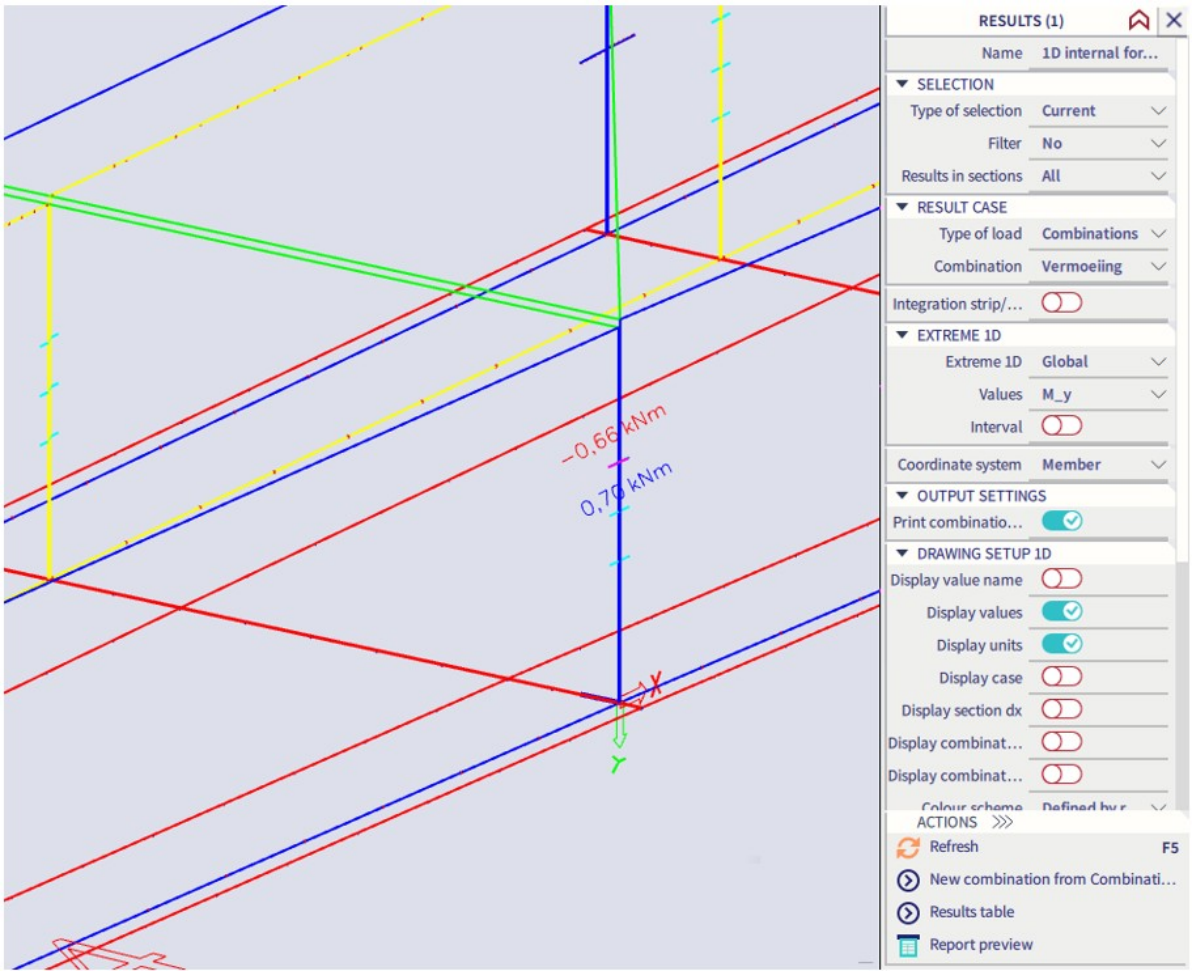

Figure J.2: SCIA results of the bending moment used for fatigue assessment DSDQ dowels

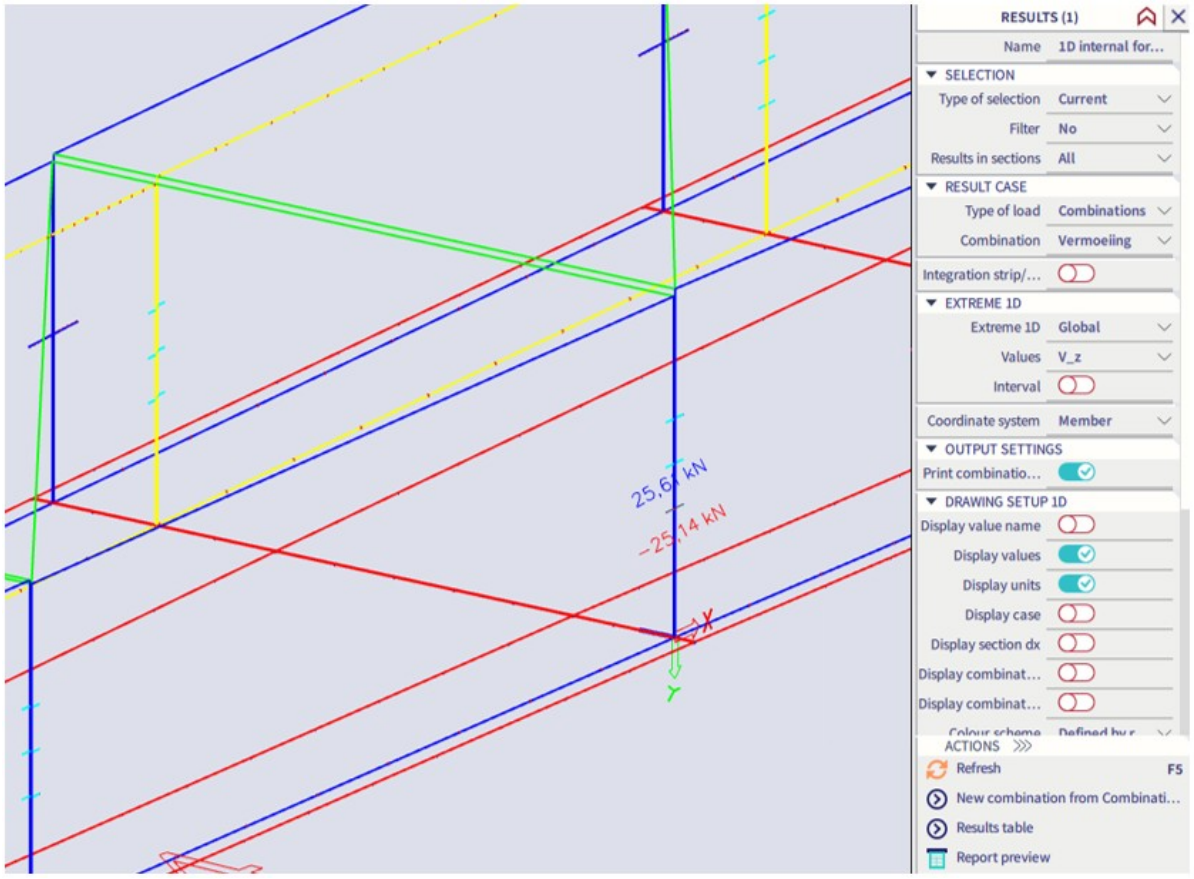

Figure J.3: SCIA results of the shear force used for fatigue assessment DSDQ dowels

To determine the stresses in the steel connection, a detailed model is developed for the governing dowel connection between tunnel segments STD-12 and STD-13. The original bar element with an equivalent diameter is replaced by two separate steel elements with a diameter of 65 mm each, corresponding to the geometry of the DSDQ-450 dowels.

K

Design Dowel Connection

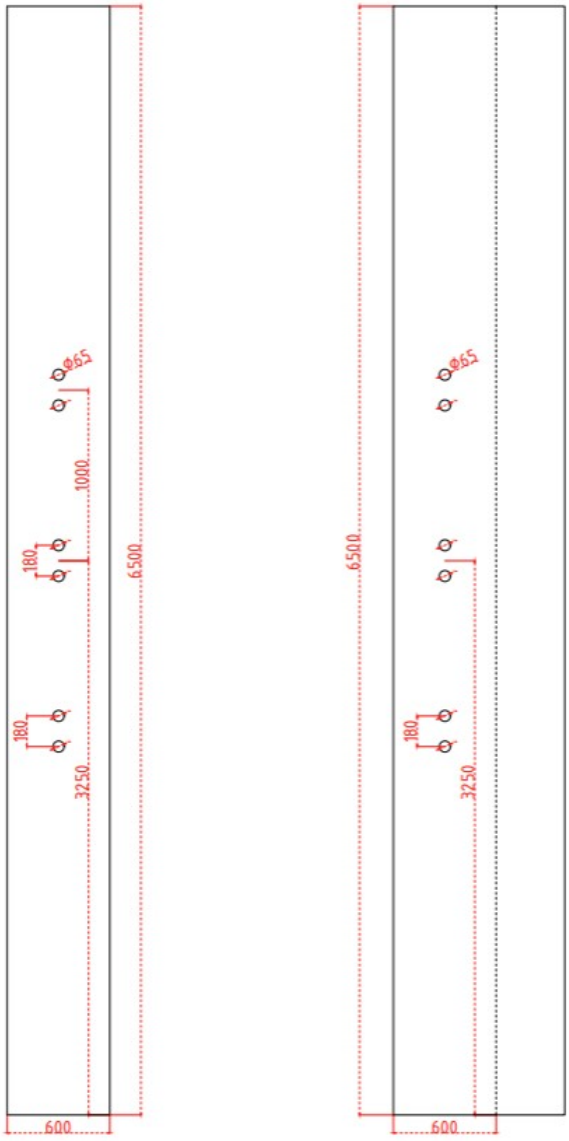

Figure K.1: Side view of the DSDQ-450 dowel connection in the inner wall (left) and outer wall (right)

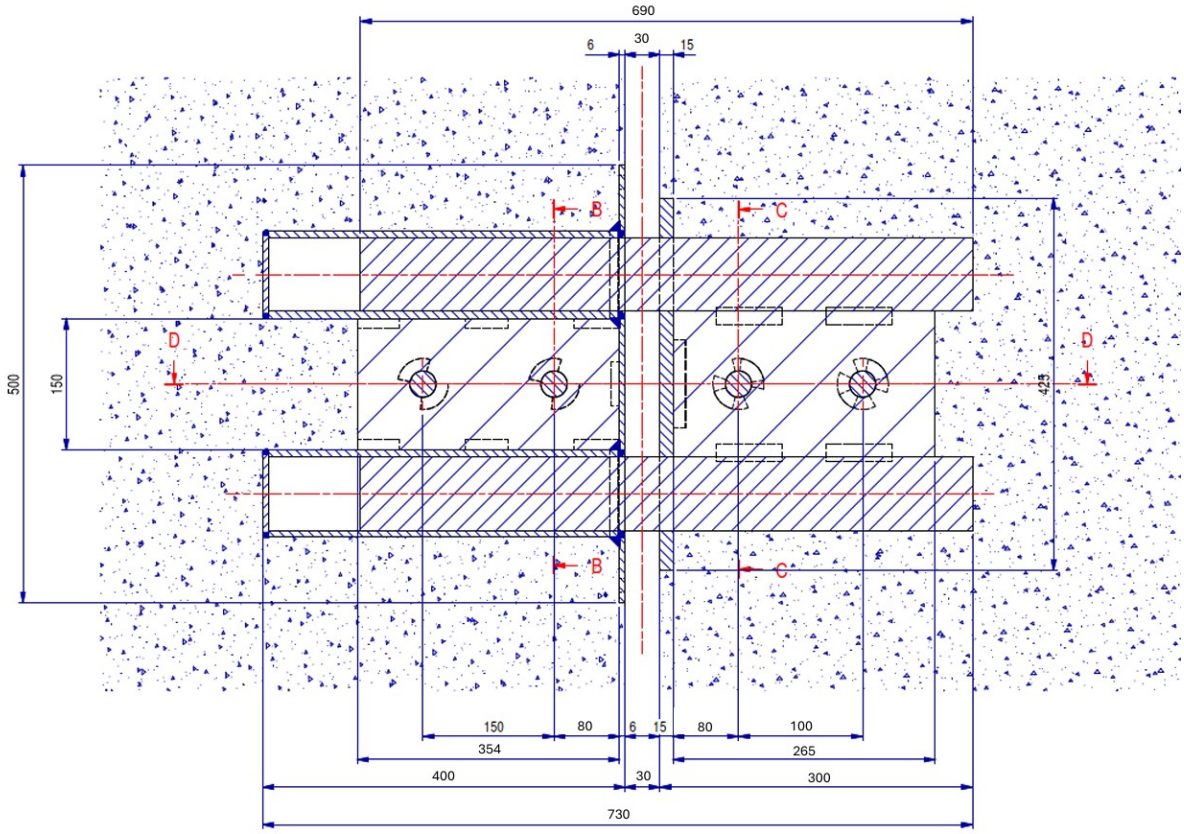

Figure K.2: Side view DSDQ-450 dowel

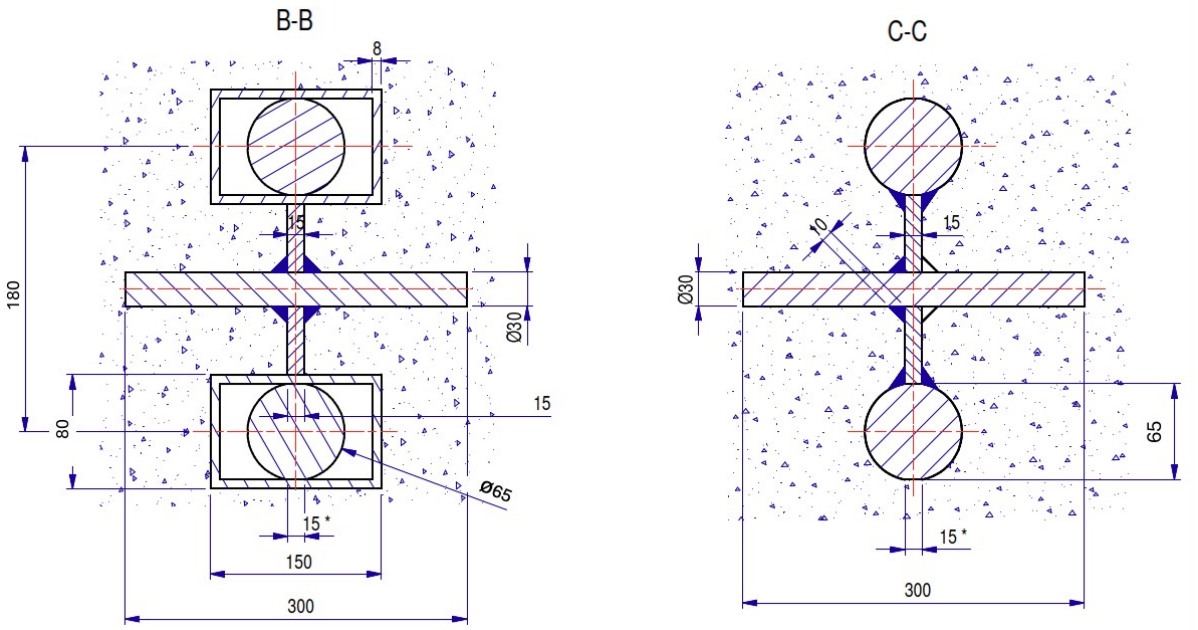

Figure K.3: Cross-sectional views (B–B and C–C) DSDQ-450 dowel

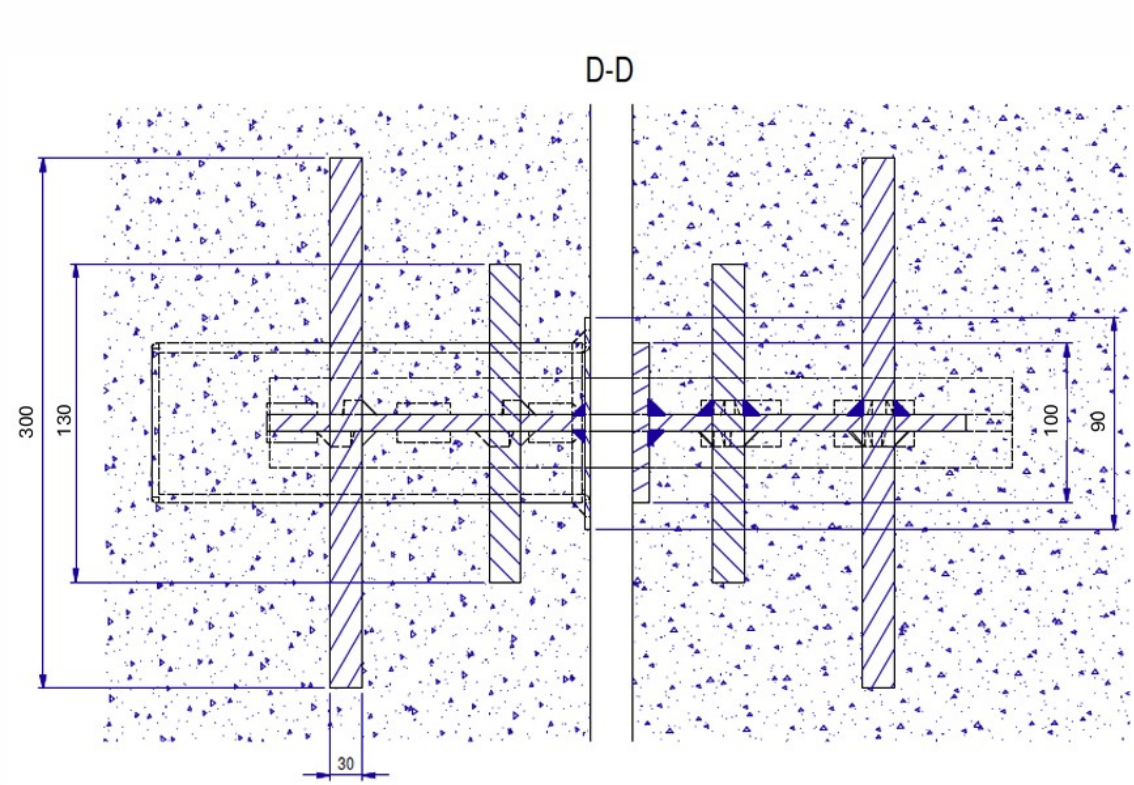

Figure K.4: Plan view of the DSDQ-450 dowel

To transfer the load from the dowel connection to the hanger reinforcement, additional reinforcement is required around the dowel. The design of the hanger reinforcement indicates that four ∅40 bars are required. This reinforcement was designed for the maximum load-bearing capacity of the DSDQ-450 dowel connection of 915 kN. A standard reinforcement layout consisting of ∅16 U-bars at a centre-to-centre spacing of 150 mm was assumed for the tunnel wall.

Additional transverse reinforcement is required to transfer the shear forces to the hanger reinforcement. When determining the required amount of transverse reinforcement it was assumed that the shear force spreads through the concrete at an angle of 45°. Based on this assumption a strut-and-tie model was developed to determine the forces in the additional reinforcement. Since the dowel can transfer shear force in both directions the reinforcement was detailed to accommodate loading in either direction. The adopted load transfer mechanism is shown in Figure K.5.

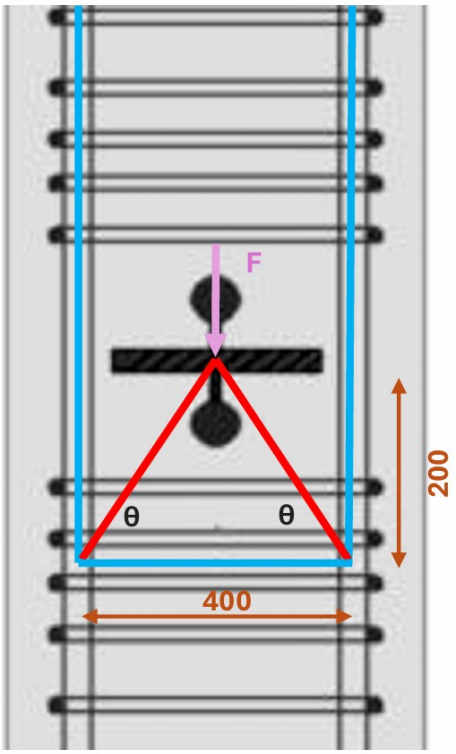

Figure K.5: Assumed load transfer mechanism and corresponding strut-and-tie model around the dowel connection.

When developing the reinforcement layout, the minimum clear bar spacing requirements specified in NEN-EN 1992-1-1 Art. 8.2 were taken into account. For the reinforcement considered, the minimum clear spacing between two parallel bars must be at least equal to the largest value specified by Equation K.1.

$$a_{\min} = \max\left(\phi,\ d_g + 5\ \text{mm},\ 20\ \text{mm}\right) \tag{K.1}$$

where d_g represents the maximum aggregate size. In accordance with the project-specific design assumptions, a nominal aggregate size of 31.5 mm was adopted [21].

Based on these boundary conditions, the final reinforcement detail consists of four ∅20 U-bars around each dowel. The resulting reinforcement detail is shown in Figures K.6 and K.7.

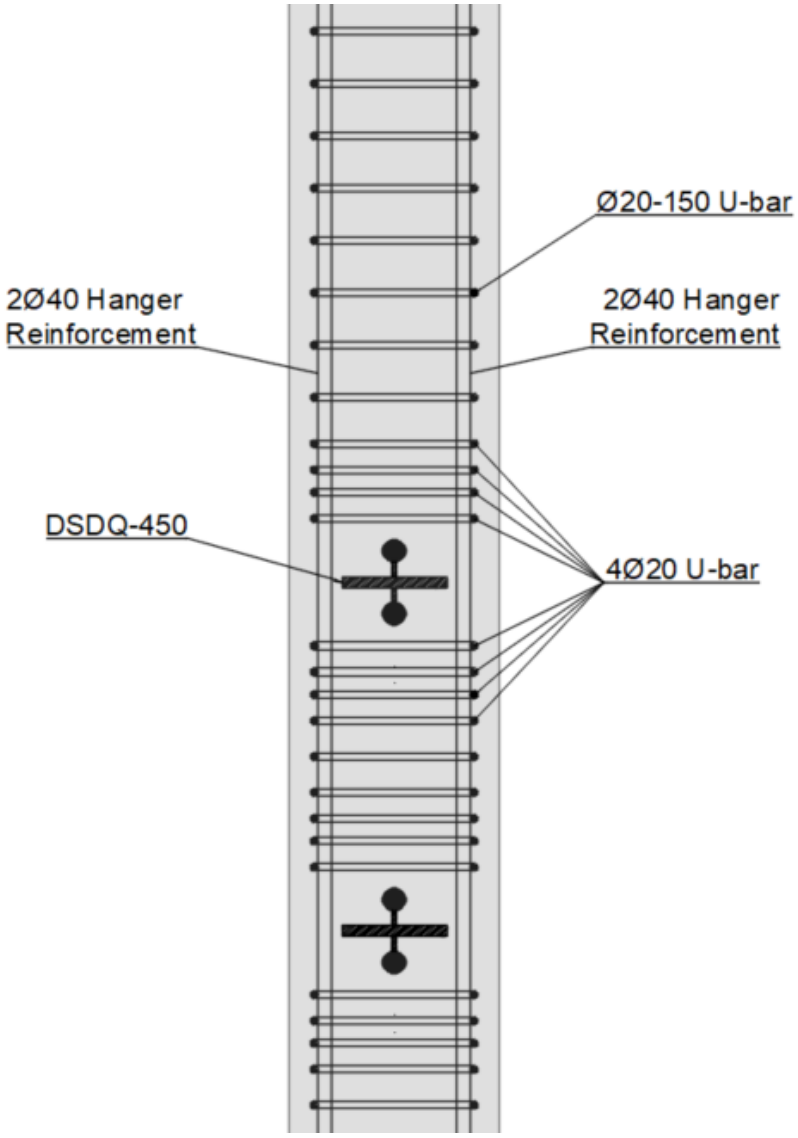

Figure K.6: Front view of the dowel connection reinforcement detailing

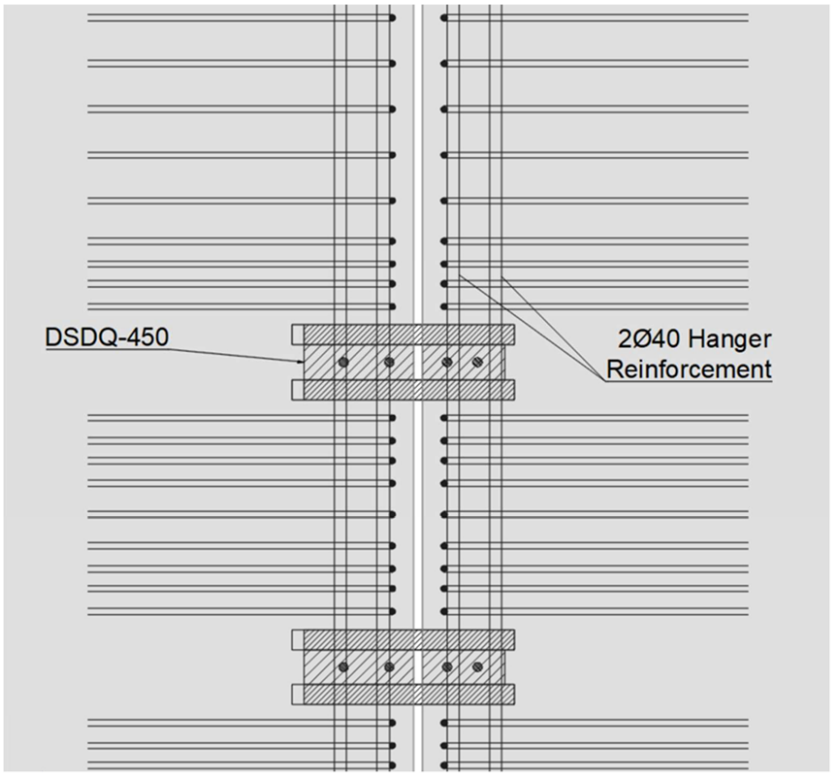

Figure K.7: Side view of the dowel connection reinforcement detailing.

L

Joint Displacements without Structural Connection

For designing the free-settlement joint, the horizontal (U_x) and vertical (U_z) displacements between the STD tunnel segments are calculated and evaluated. These displacements are verified against the requirements specified in SB260.

Based on the literature review (Section 2.3.2), it follows that, for connections without structural coupling and without the application of a transition slab, the relative displacements must be fully accommodated by the joint system. For the serviceability limit state (SLS), the boundary condition is that the relative displacements, in both horizontal and vertical directions, are limited to a maximum of $0.005\ \mathrm{m}$ in the quasi-permanent load combination. This load combination does not include traffic loads ($\psi_2 = 0$). In addition, the total settlement of the tunnel segments shall not exceed $0.05\ \mathrm{m}$.

The horizontal (U_x) and vertical (U_z) displacements are determined by local and global effects using SCIA analyses and hand calculations. The SCIA longitudinal model, as described in Appendix E.5, is used for the global effects. The following effects are considered:

Global effects

- Settlement due to permanent loads
- Rotations of the tunnel segments as a result of differential settlements

Local effects

- Shortening due to shrinkage
- Shortening and elongation due to temperature

The appendix concludes with an investigation into the influence of traffic loads on the joint displacements.

L.1. Vertical Displacements

The vertical displacements of the tunnel segments are determined based on the average settlement at the center of the floor at the ends of each segment. Local deformations of the floor, such as uplift displacements caused by wall–floor interaction, are considered a secondary effect. Since these deformations occur uniformly over the tunnel segments, they have a limited influence on the relative displacements between the tunnel segments and are therefore not explicitly taken into account.

The vertical displacements are obtained from the global SCIA longitudinal model and are evaluated in the SLS quasi-permanent load combination. The vertical displacements are extracted at the considered axis numbers from the model. The resulting differential settlement between adjacent tunnel segments is determined as the difference in vertical displacement between two consecutive segments. The calculated settlements and differential settlements for the considered STD tunnel segments are presented in Table L.1. The location of the considered cross-sections is shown in Figure L.1. The results show that the settlements and differential settlements remain within the limits of the requirements specified in SB260.

Table L.1: Settlements and differential settlements of tunnel segments

Segment	Section	Settlement [mm]	Connection	Δz [mm]
STD-10	23D	19.23		
STD-10	24D	19.53	STD-10 – STD-11	1.92
STD-11	24D	17.61		
STD-11	25D	17.44	STD-11 – STD-12	4.20
STD-12	25D	13.24		
STD-12	26D	13.68	STD-12 – STD-13	3.42
STD-13	26D	10.27		
STD-13	27D	10.64		

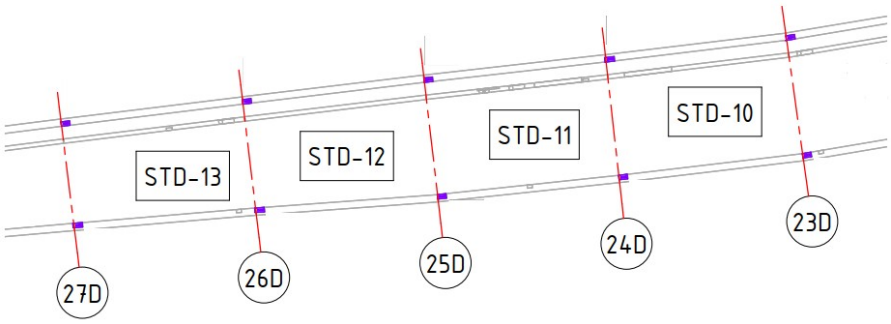

Figure L.1: Location of sections

L.2. Horizontal Displacements

Rotation

The rotations of the STD tunnel segments are derived from the vertical displacements of the three walls in the SCIA model, determined in the SLS quasi-permanent load combination. The resulting displacement is taken as the average of the vertical displacements of the three walls at both ends of the tunnel segment. Based on the differences in vertical displacements between the walls, the rotation per tunnel segment is calculated. The use of wall displacements is justified as they are less sensitive to local deformations compared to the roof and floor. Table L.2 presents the rotations of the STD tunnel segments. A positive rotation indicates that the bottom side (floor) of the segment opens relatively further, while a negative rotation indicates that the top side (roof) of the segment opens.

Table L.2: Rotation of STD tunnel segments

Segment	φ [mrad]
STD-10	0.01
STD-11	0.01
STD-12	-0.01
STD-13	-0.01

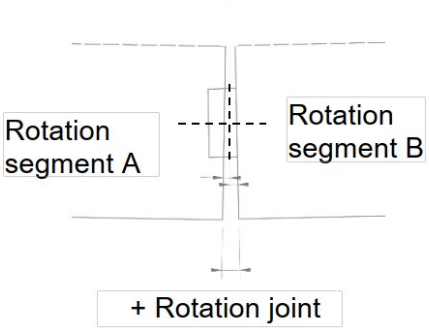

Figure L.2: Definition of positive rotation of tunnel segments

The rotation center of the tunnel segments is assumed to be located at half the wall height. This results in a distance of approximately $4.35\ \mathrm{m}$ to the underside of the floor, determined as $6.5/2 + 1.1\ \mathrm{m}$ (half the wall height including the floor thickness). The horizontal displacement due to rotation can be approximated by:

$$\Delta x_{\text{rot}} = \varphi \cdot h \tag{L.1}$$

where φ represents the rotation and h the distance to the rotation center. The calculated rotations are very small, on the order of magnitude of ± 0.01 mrad. This results in a horizontal displacement of:

$$\Delta x_{\text{rot}} \approx 0{,}01 \cdot 10^{-3} \cdot 4{,}35 \approx 0{,}04\ \text{mm} \tag{L.2}$$

It follows that the contribution of rotation to the relative horizontal displacement between the tunnel segments is negligible compared to the direct longitudinal displacements (Δx). For this reason, the effects of rotation are not considered in the further assessment of the joint displacements.

Shrinkage

Shrinkage is divided into a short-term component (t_0), consisting of the first 60 days, and a long-term component from 60 days to the end of the service life (t_∞). For the Oosterweel project, three types of shrinkage are distinguished: hardening shrinkage, autogenous shrinkage, and drying shrinkage. These effects are combined into a total strain factor ε_{tot} for both asphalt and concrete. The values of ε_{tot} are obtained from Section 2.3.2.

For the evaluation of horizontal displacements due to shrinkage, the full contribution between t_0 and t_∞ is considered for concrete. For asphalt, only the shrinkage contribution after 60 days is taken into account. The longitudinal shortening of the tunnel results in an opening of the asphalt joint profile. This shortening is determined by:

$$\Delta x = \varepsilon_{tot} \cdot L \tag{L.3}$$

where ε_{tot} is the total shrinkage strain and L is the considered length. The values for the strain are derived from the design assumptions. For the asphalt structure:

$$\Delta x_{\text{asphalt}} = 200 \cdot 10^{-6} \cdot 12\,500 = 2{,}5\,\text{mm} \tag{L.4}$$

with:

- $\varepsilon_{tot} = 200\,\mu\varepsilon$ (resulting shrinkage after 60 days)
- $L = 12{,}5\,\text{m}$ (half of the tunnel segment length)

For the concrete cross-section:

$$\Delta x_{\text{concrete}} = 220 \cdot 10^{-6} \cdot 12\,500 = 2{,}75\,\text{mm} \tag{L.5}$$

with:

- $\varepsilon_{\text{tot}} = 220\,\mu\varepsilon$ (including an initial contribution of $20\,\mu\varepsilon$ at t_0)
- $L = 12{,}5\,\text{m}$

The initial strain results in a short-term shortening of $0{,}25\,\text{mm}$, while the long-term contribution amounts to $2{,}75\,\text{mm}$. The calculated shortening results in an increase of the joint opening of the same order of magnitude.

Temperature

In addition to shrinkage, temperature variations result in longitudinal deformations of the tunnel segments. For the present assessment, only the uniform temperature component is considered.

The longitudinal deformation due to temperature is determined as:

$$\Delta L = \alpha_T \cdot L \cdot \Delta T_N \tag{L.6}$$

where:

- α_T = coefficient of thermal expansion
- L = considered length
- ΔT_N = uniform temperature change

In accordance with Section 2.3.2 $\Delta T_N = 20\,^\circ\text{C}$ is adopted. The coefficient of thermal expansion is taken as:

$$\alpha_T = 1.0 \cdot 10^{-5}\,^\circ\text{C}^{-1} \tag{L.7}$$

Using a considered length of $L = 12.5\,\text{m}$, the resulting longitudinal deformation equals:

$$\Delta L = 1.0 \cdot 10^{-5} \cdot 12{,}500 \cdot 20 = 2.5\,\text{mm} \tag{L.8}$$

The calculated uniform temperature deformation results in a change of the joint opening between adjacent tunnel segments of the same magnitude.

L.3. Traffic Contribution

In some projects, clients impose additional or alternative requirements for the assessment of joint deformations. In such cases, the quasi-permanent load combination is not always used and the contribution of traffic loading is also taken into account. To investigate the influence of this approach, an additional exploratory analysis was carried out in which the deformations caused by traffic loading were considered. For this purpose, the SCIA k20 longitudinal model was used (Appendix E).

The same procedure as used for the permanent loads was applied to determine the vertical and horizontal displacements. For each section, the average vertical displacement of the tunnel floor was determined. Based on these results, the differential settlements between adjacent tunnel segments and the rotation of each tunnel segment were calculated. The resulting differential settlements between the tunnel segments are presented in Table L.3.

Table L.3: Differential settlements of tunnel segment connections due to traffic loading

Tunnel segment	Δz [mm]	
	min	max
STD-10 - STD-11	-0.01	2.51
STD-11 - STD-12	-0.01	2.55
STD-12 - STD-13	0.02	2.53

The contribution of the traffic loads is added to the settlements caused by the permanent loads. The results are presented in Table L.4.

Table L.4: Settlements, rotations and joint displacements of tunnel segments with traffic and permanent loads combined

Tunnel segment	Length	Settlements	Rotation	Joint	Settlement difference	Horizontal displacement
	[m]	[mm]	[mrad]		[mm]	[mm]
STD-10	25.05	19.06 21.82	-0.11	STD-10 - STD-11	4.38	0.06
STD-11	24.95	17.44 19.85	-0.10	STD-11 - STD-12	6.76	0.09
STD-12	24.95	13.09 16.00	-0.12	STD-12 - STD-13	5.89	0.01
STD-13	24.95	10.11 12.93	-0.11			

The maximum vertical joint displacement increases from 4.20 mm to 6.76 mm while the maximum horizontal joint displacement increases from 10.50 mm to 10.59 mm. This exceeds the maximum allowable differential settlement of 5 mm specified in SB260.

The ULS displacements are 12.71 mm in the horizontal direction and 8.11 mm in the vertical direction. The resulting displacement is $V_r = 15.08$ mm. This displacement remains within the capacity of both the FMS350 and ACME35 profiles. The Nosing Joint Type 1.2a2 applied in the asphalt can accommodate joint movements of $\Delta z = \pm 10$ mm and $\Delta x = \pm 50$ mm. Therefore, the profile can also accommodate the ULS displacements.

Despite the increase in joint displacements due to traffic loading, the resulting deformations remain within the available displacement capacity of the joint profiles. However, the increase in vertical displacement is expected to result in more frequent maintenance and earlier replacement of the pavement section.

M

Properties Joint

Familie 1. Nosing joints

Familiedefinitie	*Factsheet concept 1.2a2*
Voegovergang met stalen randprofielen met of zonder overgangsbalken van beton, kunsthars of elastomeer. De voegspleet tussen de randprofielen wordt gevuld met een flexibele niet verkeerdragende voegafdichting.	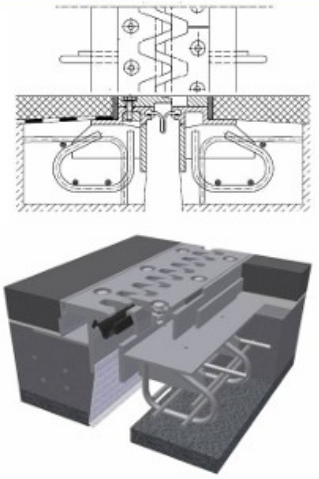
Beschrijving concept	
In constructie verankerde stalen randprofielen met ingeklemde voegprofielen zonder overgangsbalken met geluidreducerende voorzieningen.	

Functionele eisen		
	Functionele eis 1	
Bewegingsvrijheid	Δx= +/- 50 mm Δy= varieert per leverancier: van +/-4mm tot +/- 40 mm Δz= +/- 10 mm	
Kruisingshoek	65 tot 100 gon	
	Functionele eis 2	
Mechanische weerstand belasting uit constructie	Goed, er kunnen geen opspankrachten worden opgebouwd.	
	Functionele eis 3	
Mechanische weerstand belasting uit verkeer	Redelijk, op lange termijn schade mogelijk op intensief bereden wegen (schade aan sinusplaten, loskomen boutverbindingen)	
	Functionele eis 4	
Oneffenheid	Redelijk, door de geluidreducerende afdekplaten ontstaat een geleidelijkere overgang waardoor deze comfortabeler wordt ervaren dan bij een rechte voegspleet.	
Stroefheid	Goed. Niet relevant in verband met beperkte breedte bereden oppervlak.	
	Functionele eis 5	
Geluid	**Bovenzijde kunstwerk**	De GeluidsLabelWaarden voor een kruisingshoek van 100 gon: snelheid: 80 | 90 | 100 | 110 | **120** | 130 GLW: 77,5 | 78,7 | 79,8 | 80,8 | 81,7 | 82,6 De geluidmaatregel bij randprofielvoegen bestaat meestal uit het toepassen van sinusvormige platen.
	Onderzijde kunstwerk	Mogelijk zijn er geluidbeperkende maatregelen nodig. De vlakheid is bepalend voor de geluidproductie.
	Functionele eis 6	
Waterdichtheid	Goed.	

Figure M.1: Properties of noising joint type 1.2a2 [23]

Kwaliteit (RAMS)	
	Betrouwbaarheid
Levensduur	Vervangbare delen: Afdichtingsprofiel: 10 jaar; Geluidreducerende afdekplaten: 40 jaar. Niet vervangbare delen: aanvankelijk 40 jaar. Onderbouw is zeer geschikt voor modificatie.
Uitvoerings-ongevoeligheid	Redelijk. Robuust ontwerp, waarbij de vlakke aansluiting en correcte bevestiging van de geluidreducerende maatregelen een belangrijk aandachtspunt is. Op dit punt bestaat een zekere kans op fouten met gevolgen voor met name geluid en de gebruiksveiligheid. Belangrijkste risico's: - Onjuiste afstelling (maatvoering) voegconstructie (ook in langrichting van de voegovergang in verband met bewegingen in y-richting); - Geen vlakke aansluiting tussen geluidreducerende afdekplaten en onderbouw ; - Onjuiste voorspanning en onvoldoende borging van de bevestiging tussen geluidreducerende afdekplaten en onderbouw; - Niveauverschillen met aansluitend asfalt bij achteraf aanbrengen van het asfalt - Onvoldoende verdichting asfalt tegen de voeg aan bij achteraf aanbrengen van het asfalt (met schade tot gevolg) - Beschadiging van conserveringslagen in het bereden oppervlak bij achteraf aanbrengen van asfalt
Slijtvastheid	Goed. Betreft slijtage conservering in bereden oppervlak, is niet van invloed op het functioneren.
Aantasting-ongevoeligheid	Redelijk. Aantasting van de conservering kan leiden tot corrosie in niet bereden oppervlakken (in bijzonder de conservering in het klauwprofiel). De rubberafdichting veroudert en verliest in loop der tijd zijn elasticiteit. Door de geluidbeperkende maatregelen ontstaat een sterkere vervuiling waardoor snellere aantasting van de stalen randprofielen plaats kan vinden.
	Beschikbaarheid
Beschikbaarheid	Matig in verhouding tot de overige concepten, zie niet-beschikbaarheidsindex.
	Onderhoudbaarheid (binnen WBU)
Vast onderhoud	Goed. De afdichtingen dienen minimaal eenmaal per jaar (na de winter) gereinigd te worden. Vast onderhoud is mogelijk in WBU-uren en omvat enkele uren.
Variabel onderhoud vervangen onderdelen	Goed. Dit betreft het vervangen van de voegprofielen na 10 jaar. Thermisch verzinkte uitvoering heeft geen onderhoud nodig. De maatregel is mogelijk binnen de WBU.
Variabel onderhoud vervangen voegovergang	Slecht. Het vervangen van de voegovergang na 40 jaar betreft slechts het vervangen van het aan het asfalt grenzende stalen deel (bovenbouw) in verband met aantasting (corrosie). Het vervangen van de voegovergangen is niet mogelijk binnen de WBU. Indicatie benodigde uitvoeringstijd: 32-40 uur.
	Veiligheid
Risico op letselschade	Matig, kans op letselschade bij falen van de fixatie van de geluidreducerende afdekplaten.

Figure M.2: Properties of noising joint type 1.2a2 [23]

N

Pairwise Comparison

This appendix presents the pairwise comparison matrix used to determine the criteria weights in the MCDA model. The matrix is established based on the Saaty scale, with input derived from both literature and engineering expertise within WSP. This is consistent with existing literature which states that criteria in AHP applications are typically derived from prior studies and that no universal ranking exists. This aligns with practical observations where weightings in decision matrices and models are partly subjective. The weighting of the criteria is therefore dependent on the context of the problem and the judgment of experts [51].

In this study, subjective judgment is therefore considered an integral part of the methodology. The pairwise comparisons are established based on the key question of which criterion has the greatest influence on the quality and performance of the considered connection. The final consistency of the comparisons is verified using the consistency ratio (CR), which assesses the extent to which the pairwise evaluations are logically consistent [52].

Table N.1: Pairwise comparison MCDA decision model for connection variants

Pairwise Matrix	Robustness	Feasibility	Costs	Durability	Sustainability	Modeling Reliability
Robustness	1	1	4	4	7	7
Feasibility	1	1	4	4	7	7
Costs	1/4	1/4	1	1	3	4
Durability	1/4	1/4	1	1	2	3
Sustainability	1/7	1/7	1/3	1/2	1	2
Modeling Reliability	1/7	1/7	1/4	1/3	1/2	1

Robustness and feasibility are considered the most influential criteria. Together with the structural validation of the connection variants, these aspects form the essential boundary conditions for the performance of the joint between tunnel segments, as the design must fundamentally be safe, reliable, and feasible. If these conditions are not met, the solution cannot be regarded as applicable. Experience from the Oosterweelknoop project highlights in particular the importance of feasibility. In practice, the main challenges are related to the feasibility of the connection. Shear key connections, in particular, often only meet safety requirements when large amounts of reinforcement are applied, which leads to complex and critical construction conditions.

The criteria cost and durability are important for the economic and technical performance of the structure but play a less dominant role in the initial design choices. These aspects are highly project-dependent and are often governed by boundary conditions and client-driven optimizations. The Oosterweelknoop project demonstrates that cost reduction through design optimization is a key consideration.

The sustainability criterion is considered an integral part of the design process. Although its importance is increasing, current infrastructure practice shows that it is generally not a decisive factor in the selection of a specific structural solution.

Finally, modeling reliability is considered relatively limited. Throughout the design process, safety margins are applied, which account for a significant portion of the uncertainties. As a result, the influence of this criterion on the final evaluation is smaller compared to the other criteria.

Table N.2: AHP weights

Criterion	$w_{\textbf{mean}}$	**Weight [%]**	λ_i
Robustness	0.35	34.97%	6.20
Feasibility	0.35	34.97%	6.20
Costs	0.11	11.32%	6.10
Durability	0.10	9.81%	6.13
Sustainability	0.05	5.21%	6.02
Modeling Reliability	0.04	3.72%	6.03

Table N.2 presents the resulting relative weights of the evaluation criteria, as determined based on the pairwise comparisons. These values are obtained by normalizing the comparison matrix and calculating its eigenvector. In addition, the value λ_i is determined for each criterion, which is used to calculate the maximum eigenvalue λ_{max} of the matrix. Based on this, the consistency of the pairwise evaluations is verified.

Table N.3: Consistency check of the AHP matrix

Parameter	**Value**
Number of criteria (n)	7
Random index (RI)	1.35
$\lambda_{\max}$	7.20
Consistency index (CI)	0.034
Consistency ratio (CR)	0.025
Conclusion	**CR $\leq$ 0.10 $\rightarrow$ Consistent**

Table N.3 shows that the consistency ratio (CR) satisfies the required threshold value of 0.10. This indicates that the pairwise comparisons are sufficiently consistent. Consequently, the derived relative weights of the evaluation criteria can be considered reliable and suitable for further use in the decision model. The following formulas are used to calculate the consistency ratio.

$$\lambda_i = \frac{(A \cdot w)_i}{w_i} \qquad \lambda_{\max} = \frac{1}{n} \sum_{i=1}^{n} \lambda_i$$

$$CI = \frac{\lambda_{\max} - n}{n - 1} \qquad CR = \frac{CI}{RI} \tag{N.1}$$

O

Criteria Scoring

This appendix presents the qualitative and quantitative scoring of the connection variants included in the MCDA model. For each criterion and subcriterion, the assigned scores and the underlying justification are provided.

O.1. Robustness

O.1.1. Redundancy

Table O.1: Qualitative scoring of redundancy

Variant	Score
Shear key	2
Collar construction	2
Dowel connection	4
Free-settlement joint	3

Within this criterion, redundancy is defined as the degree to which a connection can continue to carry load after local failure through redistribution via alternative load transfer mechanisms. Based on this definition, the qualitative scores for the four variants are presented in Table O.1.

The shear key connection is assigned a score of 2. Experimental research shows that shear stresses concentrate at the interface zones where cracking occurs at the corners of the console. This indicates a highly localized stress field and a lack of alternative load transfer mechanisms. The joint resistance is provided primarily by the shear key resulting in a single load path. In case of local failure load redistribution is limited which results in low redundancy [26].

The collar construction is also assigned a score of 2. Shear forces are primarily transferred through the concrete collar construction in the floor and roof segments. Literature shows that high local stresses can develop within the collar itself and that the connections between the wall and the floor or roof may act as critical regions under increased loading. There is also no reinforcement that is continued across the joint. This reduces the ability to redistribute loads [10, 20].

The dowel connection is assigned a score of 4. The connection consists of multiple dowels acting in parallel to transfer the shear force. Local failure of a single dowel does not immediately lead to loss of the entire load transfer mechanism. The remaining dowels can continue to transfer the shear force through redistribution of the load among the remaining load-carrying components.

The free-settlement joint is assigned a score of 3. The joint is designed to accommodate differential settlements and rotations. If the deformation capacity of the joint is exceeded or the joint becomes damaged, these deformations can no longer be accommodated by the joint itself. In such a situation, stresses are transferred to the surrounding concrete. This creates a secondary load-transfer mechanism, but it may also lead to local stress concentrations that exceed the available capacity.

O.1.2. Tolerance sensitivity

Table O.2: Qualitative scoring of tolerance sensitivity

Variant	Score
Shear key	4
Collar construction	3
Dowel connection	2
Free-settlement joint	5

Tolerance sensitivity is defined as the degree to which the connection is sensitive to tolerances. The assessment examines whether there is room for tolerances in the design and how these tolerances affect the stress in the connection and the connection's capacity.

For the shear key connection and collar construction, the reinforcement detailing governs the load-carrying capacity of the connection. Evaluation of the strut-and-tie models shows that the detailing directly influences the reinforcement forces in the detail and therefore the load-carrying capacity of the connection. Geometric deviations result in changes to the internal force flow. This may increase the reinforcement forces and reduce the load-carrying capacity [27].

The shear key connection provides greater design flexibility due to the larger depth of the corbel. As a result, geometric deviations lead to relatively small changes in the reinforcement forces and sufficient allowance for tolerances remains available within the design. In the collar construction, this design flexibility is more limited due to the restricted depth available within the floor and roof structures. Consequently, geometric deviations have a greater influence on the reinforcement forces and the available load-carrying capacity of the detail.

The dowel connection is assigned a score of 2, as the stresses in the dowels are highly sensitive to joint width and load eccentricity. Design charts (Figure O.1) show that the shear capacity of the DSDQ connection decreases with increasing joint width. In addition, load eccentricity has a direct impact on the stress distribution in the dowels. Small variations in joint width and alignment can therefore lead directly to changes in stresses within the connection [12].

Finally, the free-settlement joint is assigned a score of 5, as tolerances in the installation of the joint system do not significantly affect its performance. Vertical tolerances can be accommodated within the asphalt layer and the thickness of the steel plates. In the horizontal direction, geometric deviations do not result in additional deformation or failure of the system.

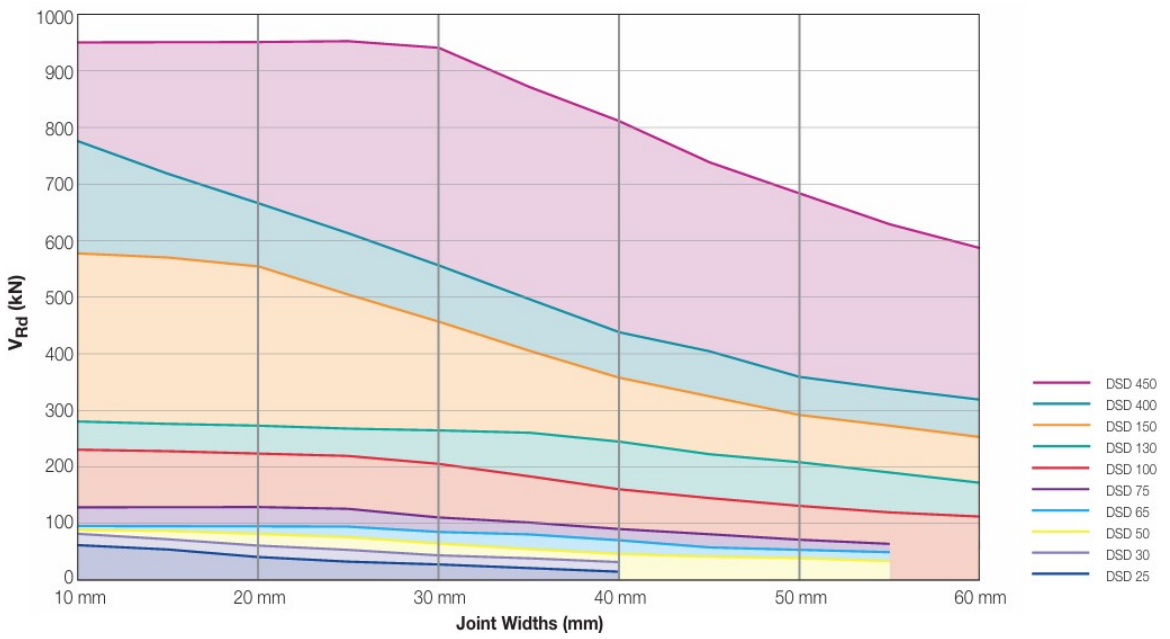

Figure O.1: DSD Design Resistance (kN) for various widths (mm) at the maximum Slab thickness (1000 mm)

O.1.3. Accidental load resistance

Table O.3: Qualitative scoring of accidental load resistance

Variant	Score
Shear key	4
Collar construction	4
Dowel connection	5
Free-settlement joint	2

Within this criterion sensitivity under exceptional loading conditions like fire is defined. High temperatures lead to rapid degradation of material properties with the connection acting as the weakest link in the structure.

According to European guidelines a tunnel must retain its load-bearing capacity for at least 2 hours in the event of fire [2]. Fire protection measures are therefore implemented in the Oosterweelknoop project. An additional concrete layer with polypropylene fibers is applied to the roof and walls to protect the tunnel elements. Fire-resistant sheeting is installed at the joints to ensure that the joint transition is also protected.

Because of the fire-resistant sheets, the shear key, collar, and dowel connections have low fire sensitivity. The dowel connection is fully embedded in the concrete which provides additional protection. The low thermal conductivity of concrete limits the temperature increase of the steel dowels during fire exposure [28].

In the floor there are no additional fire protection measures. The asphalt pavement acts as the protective layer. At the location of the joint there is no protection. Therefore the elastomer joint profile will degrade rapidly when exposed to fire [29]. This causes the joint to lose its watertightness. Failure of the joint does not directly affect structural safety due to its non-structural function. However, the joint profile must be replaced after fire exposure.

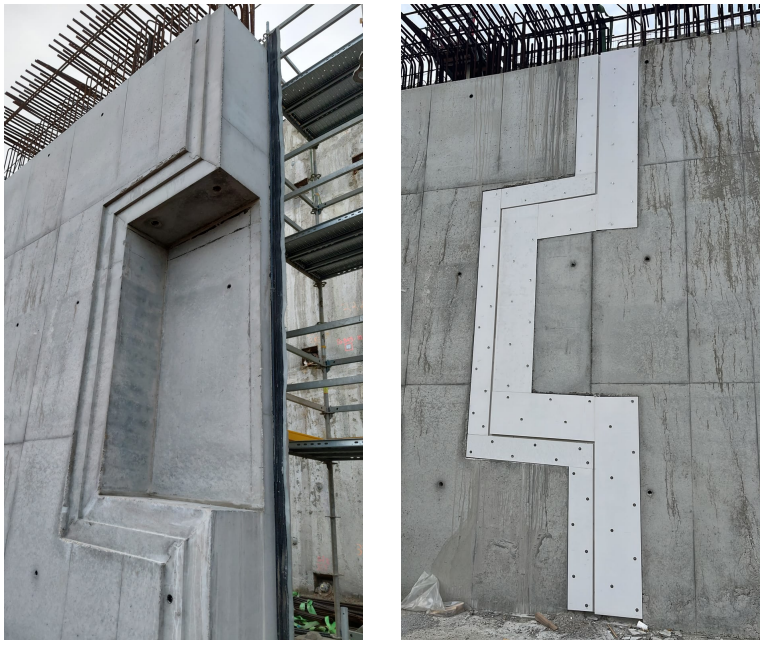

Figure O.2: Fire-resistant sheets applied at tunnel segment joints in the Oosterweelknoop project

O.1.4. Failure behavior

Table O.4: Qualitative scoring of failure behavior

Variant	Score
Shear key	4
Collar construction	3
Dowel connection	4
Free-settlement joint	4

Within this criterion, failure behavior is defined as the manner in which a connection fails and the degree to which this behavior is gradual. A distinction is made between the level of ductility and the consequences of failure for the functionality of the connection and the tunnel as a whole. Based on these aspects, the qualitative scores are presented in Table O.4.

The shear key connection is assigned a score of 4. Failure is characterized by cracking in the concrete followed by plastic deformation of the reinforcement which results in ductile behavior. The dowel connection shows similar behavior with plastic deformation of the steel dowels leading to a ductile failure mechanism. Local concrete damage may occur around the dowels [31].

The joint transitions also exhibit ductile behavior. The failure behavior is mainly governed by gradual material degradation, wear, and reduced adhesion to the substrate. In contrast to structural connections, failure of a joint transition does not immediately result in a loss of structural capacity, but rather in a loss of functional performance, such as watertightness and driving comfort [23].

The collar construction is assigned a score of 3. Although ductile behavior is also observed here due to cracking and plastic deformation of the reinforcement, failure of the collar can directly lead to a loss of watertightness of the tunnel. Crack formation may result in water ingress, corrosion, and leakage of the tunnel structure, with potential functional and safety consequences [10].

O.2. Modeling Reliability

O.2.1. Modeling accuracy

Table O.5: Qualitative scoring of modeling accuracy

Variant	Score
Shear key	4
Collar construction	3
Dowel connection	3
Free-settlement joint	5

Accuracy is defined as the extent to which the modeled variants in SCIA Engineer represent the actual behavior of the connection. The following aspects are considered:

- **Representation of physical behavior**: The extent to which the model accurately describes the actual behavior of the connection taking into account available verification and validation models.
- **Modeling assumptions and simplifications**: The presence and impact of assumptions and simplifications within the model.
- **Sensitivity and robustness**: The sensitivity of the model to variations in modeling choices, such as mesh size and model parameters.
- **Complexity and risk of errors**: The complexity of the model and the associated likelihood of modeling errors.

Based on these aspects, the qualitative scores are presented in Table O.5. The scores are based on the modeling approach and verification as described in Appendix E.

The shear key connection is assigned a score of 4, as the simplified 1D model has been verified against a 2D reference model. The results of both models show good agreement in terms of displacements, rotations, and shear forces. However, the modeling approach remains relatively complex and time-consuming.

The collar construction is assigned a score of 3. Although a verification between 1D and 2D models is also performed with good agreement in both displacements and forces, the modeling depends on nonlinear functions in the hinges. As a result of numerical effects in the finite element model, small residual forces occur in the opposite direction of the intended load transfer. These forces are very small in magnitude (on the order of 0.01 kN) and are considered negligible.

The dowel connection is assigned a score of 3. The model is relatively simple and based on conservative assumptions with rotations and slip not represented. The dowel is modeled as a single element with an equivalent diameter rather than as two separate dowels. A more detailed representation using a 3D solid finite element model would allow for a more accurate determination of forces and stresses.

The free-settlement joint is assigned the highest score of 5, as no load transfer between segments is modeled and the behavior is directly derived from the global deformations of the tunnel model. As a result, no additional modeling assumptions are required for the connection, and the likelihood of modeling uncertainties is minimized.

O.3. Feasibility

O.3.1. Construction complexity

Table O.6: Qualitative scoring of construction complexity

Variant	Score
Shear key	2
Collar construction	1
Dowel connection	4
Free-settlement joint	5

Construction complexity is determined by the geometric configuration, the reinforcement ratio and detailing, and the degree of prefabrication. Together, these aspects define the overall technical difficulty of construction.

For both the shear key connection and the dowel connection reinforcement must be integrated into the existing tunnel wall reinforcement. In practice [32] this results in reinforcement layouts that are difficult to place and access. For the shear key additional formwork is required and the large diameter reinforcement bars further increase the construction complexity, as illustrated by the VT tunnel segments (Figure O.3). For the dowel connection less reinforcement is required and the dowels can be placed directly in the wall formwork.

The collar construction has a high level of execution complexity. At the interface between wall and floor, high stress concentrations occur, resulting in a very high reinforcement ratio. Due to the limited available space, this leads to highly congested and complex reinforcement layouts. In addition, extra formwork is required across the full width of both the roof and floor.

The free-settlement joint has the lowest execution complexity. This is because the system is largely delivered as prefabricated components and can be easily integrated into the floor and roof.



Figure O.3: Design tensile reinforcement in the female part of the shear key for the Oosterweelknoop VT tunnel segments

O.3.2. Execution risk

Table O.7: Qualitative scoring of execution risk

Variant	Score
Shear key	4
Collar construction	4
Dowel connection	4
Free-settlement joint	4

Execution risk is defined as the extent to which external conditions, controllability and recoverability affect the successful execution of the connection.

All variants are similarly sensitive to external factors such as weather conditions. For example, the concrete quality in all connection types can be affected by high temperatures, which increase the risk of plastic shrinkage cracking, or by low temperatures, which slow down the hydration process and may result in insufficient strength development. To mitigate these risks, measures can be implemented such as cooling the concrete mix, covering the concrete surface, or heating the structure using systems such as hot water circulation.

In addition, modifications to the reinforcement, formwork, dowel positions or joint profiles can be made for all variants prior to concrete casting. After casting, corrective actions are only possible to a limited extent. Deviations often require time-consuming repair measures. As the possibilities for modifications and repairs are comparable for all variants, the controllability and recoverability of the construction process are considered equivalent.

O.3.3. Construction speed

Table O.8: Qualitative scoring of construction speed

Variant	Score
Shear key	2
Collar construction	1
Dowel connection	4
Free-settlement joint	5

Construction speed is defined as the time required to construct the connection, expressed as relative construction duration. The assessment focuses specifically on on-site activities required before and during the realization of the connection.

The dowel connection and the free-settlement joint can be executed relatively quickly. For both connection types, a large share of the components is delivered in prefabricated form. The DSDQ dowels are supplied as complete sets and can be directly integrated into the wall casting process, requiring only additional reinforcement locally around the dowels. For the free-settlement joint, the joint system is also prefabricated and can be incorporated directly into the casting of the floor and roof.

The execution of the shear key connection is significantly slower and is estimated to take approximately four times longer based on expert judgment [32]. This is mainly due to the need for custom formwork between the walls. The collar construction exhibits a similar but even more unfavorable situation, as it requires multiple casting stages and formwork operations, resulting in the lowest execution speed.

O.4. Sustainability

O.4.1. MKI value

To quantify the environmental impact of the four variants, the Milieu Kosten Indicator (MKI) is calculated. For this purpose, the software platform DuboCalc is used, which was developed by Rijkswaterstaat to assess the environmental impact of civil engineering and infrastructure projects. The tool operates on the basis of the required material quantities and combines these with environmental data from the National Milieu Database (NMD). Based on this information, the environmental impact of a design is converted into a single MKI value, expressed in euros [53].

The MKI is based on the Life Cycle Assessment (LCA) methodology, in which the environmental impact over the entire service life of a structure is considered. Distinction is made between the production phase (A1–A3), transport to the construction site (A4), construction activities on site (A5), the use and maintenance phase (B1–B5), the demolition and end-of-life processing phase (C1–C4), and the potential environmental benefits from reuse and recycling (D). For the four variants, the individual environmental impacts associated with these life-cycle phases are aggregated into a single MKI value [54].

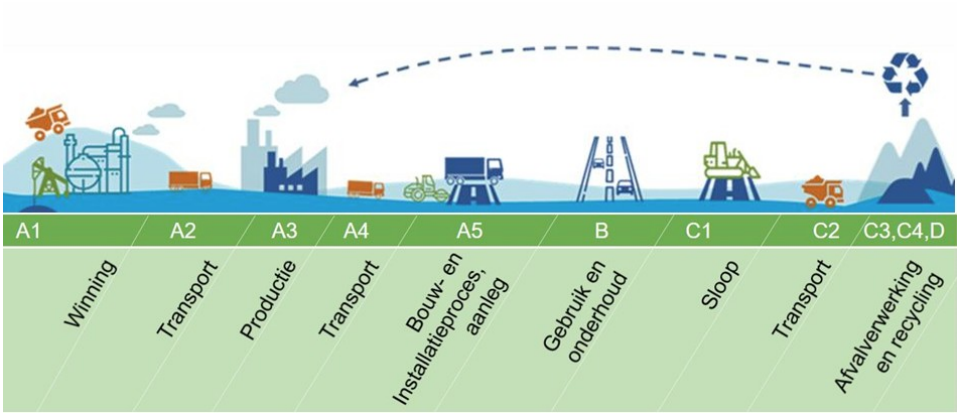

Figure O.4: Life cycle stages included in the MKI calculation according to the LCA methodology [54]

Shear Key

For the shear key connection, only the environmental impact of the reinforcement is considered. In total, six shear key connections are applied. Concrete is not included, as this connection variant does not require additional concrete compared to the reference variant without a structural connection between the tunnel segments.

Table O.9: Reinforcement quantities of the shear key

Component	Quantity	Unit
Male part tensile reinforcement	342	kg
Male part hanger reinforcement	300	kg
Female part tensile reinforcement	654	kg
Female part hanger reinforcement	832	kg
Female part shear reinforcement	55	kg
Total reinforcement per shear key	2183	kg
Number of shear keys	6	pcs
Total reinforcement	13.10	ton

MKI-waardes

MKI inclusief toeslag (totaal)		2,586.27
MKI exclusief toeslag		1,923.41
MKI Toeslag		662.86
Bijdrage		100 %
Productiefase	⌄	1,955.92
Bouwfase	⌄	179.42
Gebruiksfase	⌄	0
Sloop- en verwerkingsfase	⌄	-211.93
CO2 (kg CO2-eq)		18,955.51

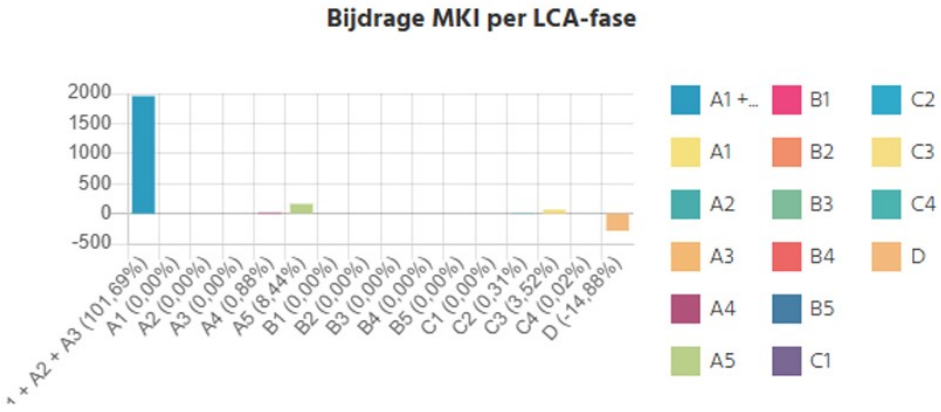

Figure O.5: Distribution of the MKI score of the shear key connection over the different LCA life cycle phases

Collar Construction

For the collar construction, both the additional concrete volume and the supplementary reinforcement are included in the calculation. At the outer wall locations, a locally thickened concrete section is applied in the floor with an additional thickness of 0.4 m. This thickening has a width of 3 meters and extends 2 meters on both sides of the joint in the longitudinal direction to ensure sufficient anchorage length of the collar.

The calculated reinforcement in both the floor and the roof is applied only at the outer wall locations. These consist of strips 3 meters wide per wall, in both the floor and the roof. Between these strips, minimum reinforcement is applied that does not differ from the standard detailing of the floor and roof. These zones are therefore not included in the calculation.

Table O.10: Material quantities of the collar construction

Component	Quantity	Unit
Concrete thickening (C35/45)	1.6	m^3/m
Floor tensile reinforcement	434	kg/m
Floor hanger reinforcement	336	kg/m
Roof tensile reinforcement	84	kg/m
Roof hanger reinforcement	288	kg/m
Total reinforcement per m	1142	kg/m
Total width	18	m
Total concrete volume	28.8	m^3
Total reinforcement	20.56	kg

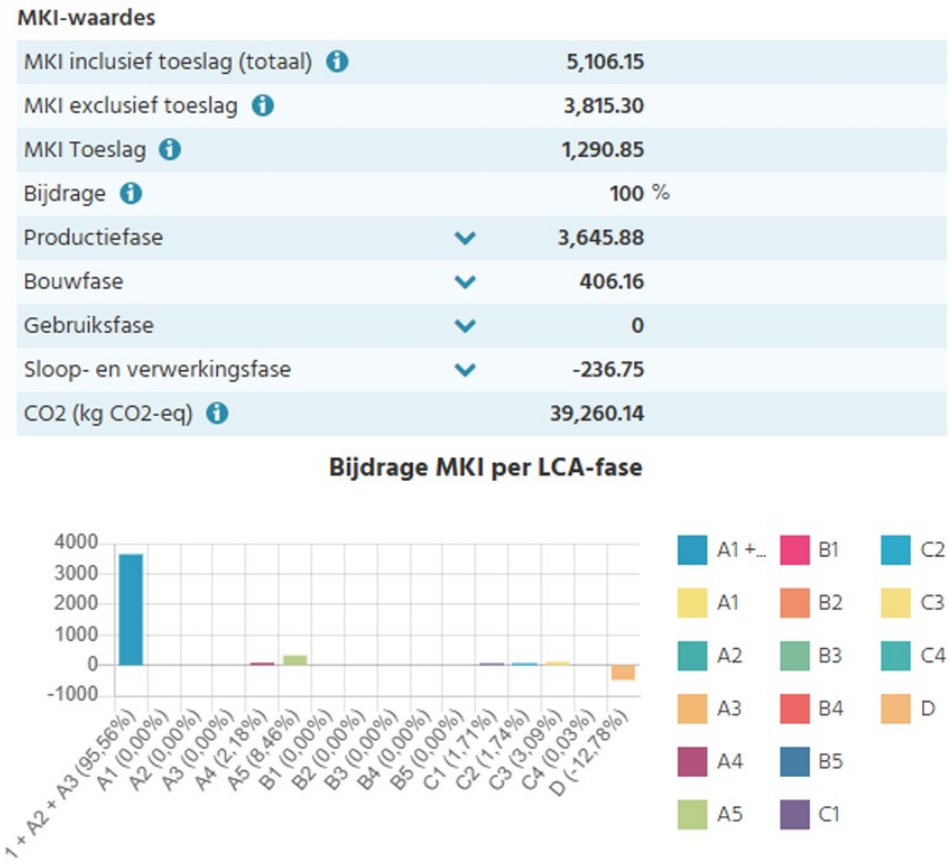

Figure O.6: Distribution of the MKI score of the collar construction over the different LCA life cycle phases

Dowel Connection

For the dowel connection, the environmental impact is determined based on the stainless steel (RVS) dowel system and the associated hanger reinforcement. The mass of the dowels is based on the product specifications of the DSDQ-450 connection. For additional components such as the sleeve and steel plates, an additional factor of 20% is included.

Table O.11: Material quantities of the dowel connection

Component	Quantity	Unit
RVS steel (per dowel)	45	kg
Number of dowels	18	pcs
Total RVS steel	810	kg
Reinforcement (per set)	400	kg
Number of sets	6	pcs
Total reinforcement	2.4	ton

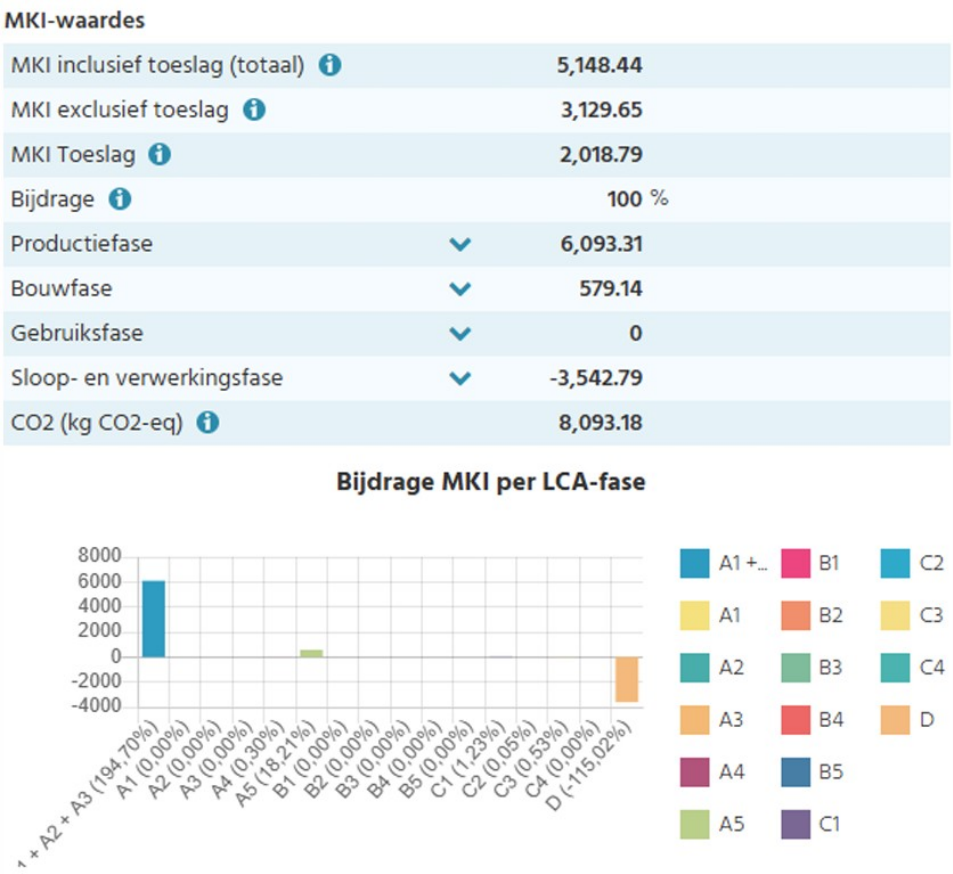

Figure O.7: Distribution of the MKI score of the dowel connection over the different LCA life cycle phases

Free-Settlement Joint

For the free-settlement joint, the environmental impact is determined based on the additional asphalt layer and a steel edge profile. To account for the maximum differential settlement of 5 mm, the asphalt quantity is calculated by multiplying the area of all traffic lanes by an additional asphalt thickness of 5 mm. The calculation considers three tunnel segments, each 25 m long and 13 m wide. The additional concrete required to maintain the clearance profile is considered negligible and is therefore not included in the calculation.

In addition, the steel edge profile forming part of the asphalt joint system is included. As no suitable MKI profile for the complete expansion joint system was available in DuboCalc, the environmental impact is approximated based on the steel edge profiles. A representative steel mass of 15 kg/m is assumed as a rule of thumb. Since the service life of the joint profile is approximately 40 years, the required steel quantity is multiplied by a factor of 2.5 to account for replacement during the 100-year design life of the tunnel.

Table O.12: Material quantities for the free-settlement joint

Component	Quantity	Unit
Asphalt layer thickness	0.005	m
Width per tunnel segment	13	m
Length per tunnel segment	25	m
Number of tunnel segments	3	pcs
Total asphalt mass	11.7	ton
Steel edge profile	15	kg/m
Total edge profile length	39	m
Total steel edge profile	1.46	ton

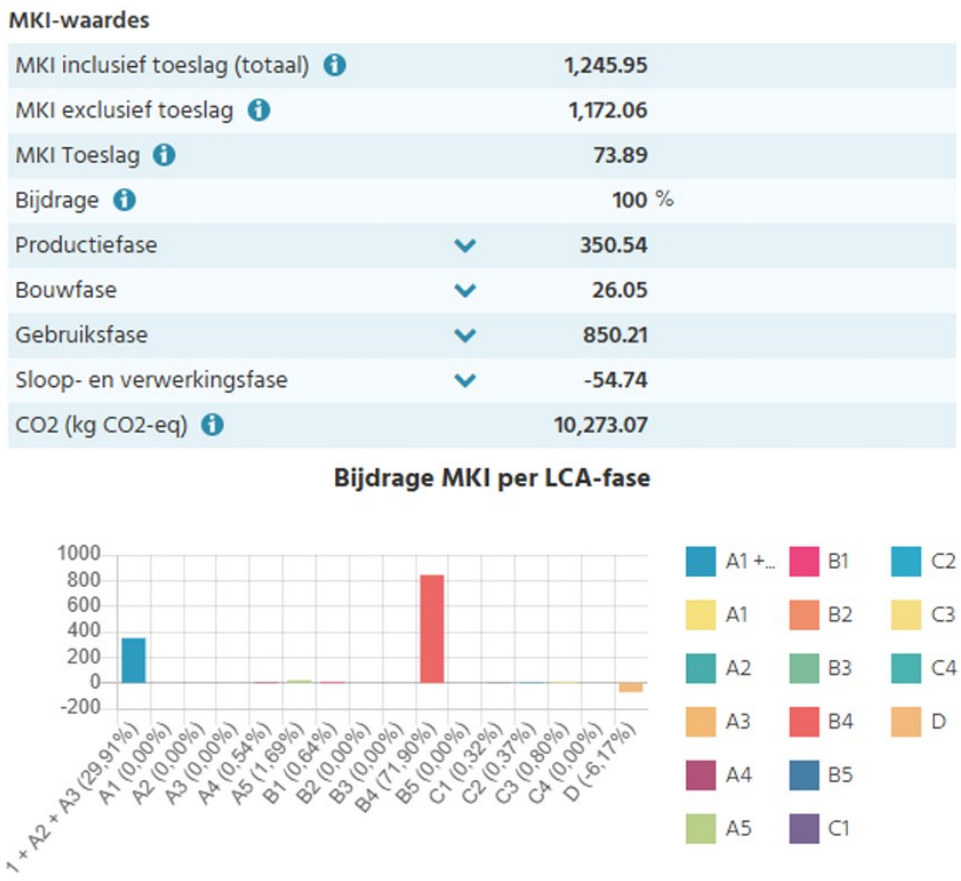

Figure O.8: Distribution of the MKI score of the free-settlement joint over the different LCA life cycle phases

O.4.2. Recycling opportunities

Table O.13: Qualitative scoring of recycling opportunities

Variant	Score
Shear key	2
Collar construction	2
Dowel connection	2
Free-settlement joint	2

Recycling opportunities are assessed based on the extent to which components can be separated into individual materials at the end of their service life and the potential for reuse of these materials.

Reinforced concrete is typically recycled by crushing, which allows recovery of reinforcing steel and reuse of concrete as aggregate. The effectiveness depends on the composition of construction and demolition waste (CDW) and the level of prior separation since both influence the quality of the recycled aggregates. Crushing and processing methods also affect the final properties and suitability for use in new concrete [34, 55].

The DSDQ dowels are cast into the concrete on one side. As a result, the dowels are not demountable and reuse is not possible. Furthermore, the dowels are subjected to cyclic loading throughout the service life of the tunnel. Although the fatigue verification demonstrates adequate performance during the design life, reuse of the dowels in a new structural application after demolition is considered unlikely. After demolition of the structure, the steel can be recovered and recycled into new steel products [35].

The same principle applies to the joint system. Since the steel edge profiles are cast into the concrete, they are not demountable and therefore have limited potential for reuse. In addition, reuse of the elastomer filler is uncommon, as this material has a relatively short service life and is typically replaced during maintenance or rehabilitation of the joint [32].

O.5. Durability

O.5.1. Service life

Table O.14: Quantitative scoring of service life

Variant	Score
Shear key	100 years
Collar construction	100 years
Dowel connection	100 years
Free-settlement joint	40 years

The shear key connection, collar construction, and dowel connection are designed for a service life of 100 years, in line with the design life of the tunnel structure. For these variants, parameters such as concrete cover, material selection, and detailing are designed to limit degradation over time. The dowels are made of stainless steel, ensuring that this type of connection also achieves a service life of 100 years [32].

The design service life of the free-settlement joint is approximately 40 years and is governed by the service life of the non-replaceable components, such as the steel edge profiles. In addition, the nosing joint system comprises multiple components with different service lives. The sealing profile has an expected service life of approximately 10 years and requires periodic replacement, while the noise-reducing cover plates have a service life of approximately 40 years. Although maintenance and replacement of wear-sensitive components are possible during operation, the design service life of the free-settlement joint remains limited to approximately 40 years [23]. This is inconsistent with SB260-21-5.1.1.1, which requires a design service life of 100 years for permanent structures. As a result, the free-settlement joint is considered less durable than the alternative connection concepts.

O.5.2. Inspectability

Table O.15: Quantitative scoring of inspectability

Variant	Score
Shear key	2
Collar construction	1
Dowel connection	1
Free-settlement joint	5

Inspectability is assessed based on the extent to which the condition of the connection can be determined during the service phase.

The concrete connections are covered by fire-resistant panels that provide protection against accidental fire loading. As a result, the connections and the associated bearing blocks are not directly visible during operation and can only be visually inspected after removal of the fire-resistant panels. Only the shear key connection in the inner wall remains partially visible from one side, as no fire protection panels are applied at that location.

The dowels are provided with a concrete cover of approximately 250 mm, which means the connection is fully embedded in the concrete after construction. This makes direct visual inspection of the dowels impossible during the service phase. Any degradation of the connection, such as corrosion of the dowels or wear of the sleeves, can only be identified indirectly through observations such as excessive deformations, cracking or other signs of structural distress.

In contrast, the joint system is directly accessible from the asphalt surface. Due to the open configuration of the detail, both the elastomer material and the steel edge profile can be visually inspected.

O.6. Costs

O.6.1. Initial costs

The initial costs of the different connection variants are determined based on the required materials and the corresponding unit prices [36, 32]. This cost estimate does not include modeling or construction costs. The material quantities are based on the calculations from the MKI analysis, as included in this appendix. An overview of the resulting costs is presented in Table O.16.

Table O.16: Initial costs of all connection variants

Variant	Component	Unit	Quantity	Unit price	Total cost
Shear key	Reinforcement	kg	13,098	€1.85	€24,231
	Total				**€24,231**
Collar construction	Concrete	m^3	28.8	€165	€4,752
	Reinforcement	kg	20,556	€1.85	€38,029
	Total				**€42,781**
Dowel connection	DSDQ-450 dowels	st	18	€1,500	€27,000
	Reinforcement	kg	2,400	€1.85	€4,440
	Total				**€31,440**
Free-settlement joint	Prefabricated joint	m	75	€2,000	€150,000
	Total				**€150,000**

O.6.2. Maintenance costs

The shear key connection, collar construction, and dowel connection are designed for a service life of 100 years and are not accessible for inspection. As a result, no maintenance or replacement costs are associated with these variants during the service life. In contrast, the free-settlement joint requires periodic maintenance and replacement of components. In particular, the sealing profile must be replaced approximately every 10 years. This replacement requires a complete closure of the tunnel. In an urban context such as Antwerp, this results in costs in the order of €150,000 to €200,000 per closure. These costs dominate the maintenance costs of this variant.

The free-settlement joint therefore requires periodic maintenance and replacement of components, especially the sealing profile with an approximate replacement interval of 10 years. In theory, this results in multiple replacement events over a 100-year service life. In practice, these activities can partly be combined with scheduled maintenance interventions of the infrastructure, such as the replacement of the asphalt layer.

It is therefore assumed that approximately three separate closures are required specifically for the joint. The cost of such a highway closure in Antwerp is in the order of €150,000 to €200,000 per intervention. This results in a total maintenance cost of approximately €525,000 over a service life of 100 years [32].

P

Decision Model A3

TU Delft	**MCDA decision model for connection variants between tunnel segments STD-10 through STD-13**
	Author Wouter Wagenaars
	Date 20-7-2026

Variant	**Shear Key**	**Collar Conncetion**	**Dowel Connection**	**Free-Settlement Joint**
Variant Description	Connection consisting of a concrete key (male part) and an opening (female part) in the inner and outer wall. Transfers shear forces in two directions using a bearing block.	Connection consisting of an inner and outer collar in the floor and roof. Transfers shear forces in one direction using a bearing block.	Connection with three DSDQ-450 steel dowels per wall in both the inner and outer wall, where each dowel consists of two stainless steel bars that only transfer shear forces. Through the application of a sliding sleeve, displacements in both longitudinal and transverse directions are enabled.	Joint without structural coupling (noising joint) that can accommodate displacements in longitudinal direction (±40 mm) and vertical direction (±10 mm), without transfer of shear forces.
Photo for design clarification	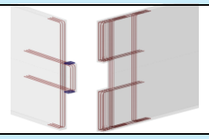	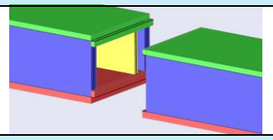	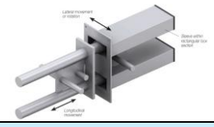	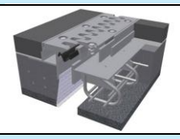

Qualitative criteria legend

1	Very unfavorable performance with significant deficiencies	2	Unfavorable performance with multiple shortcomings	3	Neutral performance meeting minimum requirements	4	Favorable performance with limited shortcomings	5	Very favorable performance with excellent characteristics

MCDA Method

The MCDA method combines the AHP and TOPSIS methods. Using the AHP methodology, the relative weighting of the main criteria is determined based on pairwise comparisons according to the Saaty scale (1-9). Subsequently, the variants are evaluated using the TOPSIS methodology. Qualitative criteria are scored on a scale of 1 to 5, and quantitative criteria are assessed based on project-specific input data. Based on this, a ranking is established using the TOPSIS methodology. Qualitative criteria are scored on a scale of 1 to 5, and quantitative criteria are assessed based on project-specific input data. Based on this, a ranking is established.

Robustness **Weight : 0,35**	**Clarification**	**Rating**	**Clarification**	**Rating**	**Clarification**	**Rating**	**Clarification**	**Rating**
Redundancy Weight 0,09	Concentrated stress field and single load path; limited redistribution in case of local failure	2	Load transfer via one dominant mechanism; no alternative load path in case of failure	2	Multiple load paths through parallel working dowels allowing redistribution	4	Secondary load transfer through surrounding concrete after joint failure, but with local stress concentrations	3
Tolerance Sensitivity Weight 0,09	Sensitive to geometry and reinforcement, but sufficient design space is available to accommodate tolerances	4	Sensitive to geometry and reinforcement. Limited design space results in a greater influence of tolerances on the force distribution and capacity	3	Highly sensitive to joint width and eccentricity; deviations directly lead to capacity loss	2	Tolerances do not hinder the joint system; vertical deviations can still be corrected in the asphalt layer	5
Accidental Load Resistance Weight 0,09	Protected against fire by fire-resistant sheetings	4	Protected against fire by fire-resistant sheetings	4	Protected against fire by fire-resistant sheetings and extra cover through cast-in concrete	5	Joint in floor not protected against high temperatures; elastomer degrades and loss of watertightness	2
Failure Behavior Weight 0,09	Concrete cracking followed by plastic behavior of reinforcement; ductile behavior	4	Concrete cracking followed by plastic behavior of reinforcement; ductile behavior with possible degradation to functional performance	3	Plasticization of dowels; ductile failure mechanism; local concrete damage possible around dowels	4	Ductile behavior; material degradation, wear and reduced bond to the substrate	4
Relative Performance - Robustness		**0,78**		**0,66**		**0,85**		**0,79**
Modeling Reliability **Weight : 0,04**	**Clarification**	**Rating**	**Clarification**	**Rating**	**Clarification**	**Rating**	**Clarification**	**Rating**
Modeling Accuracy Weight = 0,04	1D model verified with 2D model; good agreement in deformations, rotations and shear force; complex modeling	4	1D and 2D verification with good agreement; dependent on non-linear functions; numerical residual forces present	3	Simple model with conservative assumptions; rotations in transverse direction and slip not modeled	3	Load transfer does not need to be modeled; behavior directly derived from global deformations	5
Relative Performance - Modeling Reliability		**0,80**		**0,60**		**0,60**		**1,00**
Feasibility **Weight : 0,35**	**Clarification**	**Rating**	**Clarification**	**Rating**	**Clarification**	**Rating**	**Clarification**	**Rating**
Construction complexity Weight 0,12	Complex geometry due to the cantilevered key profile; high reinforcement ratio	2	High reinforcement ratio at wall locations; additional formwork required over entire width of floor and roof	1	Prefabricated; locally extra reinforcement around dowel	4	Prefabricated; no additional formwork and limited reinforcement complexity.	5
Execution risks Weight 0,12	Risks before and during pouring manageable through execution measures	4	Risks before and during pouring manageable through execution measures	4	Risks before and during pouring manageable through execution measures	4	Risks before and during pouring manageable through execution measures	4
Construction speed Weight 0,12	Custom formwork and challenging rebar placement	2	Multiple pouring phases and additional formwork; complex rebar placement at wall locations	1	Prefabricated dowels that can be easily placed in the formwork; locally challenging rebar placement	4	Prefabricated joint system; no additional pouring required	5
Relative Performance - Feasibility		**0,60**		**0,47**		**0,87**		**1,00**
Sustainability **Weight : 0,05**	**Clarification**	**Rating**	**Clarification**	**Rating**	**Clarification**	**Rating**	**Clarification**	**Rating**
MKI Score Weight 0,03		€ 2590		€ 5110		€ 5150		€ 1250
Recycling opportunities Weight 0,03	Not demountable; recycling via crushing, steel recoverable and concrete reusable as aggregate	2	Not demountable; recycling via crushing, steel recoverable and concrete reusable as aggregate	2	Not demountable due to cast-in; steel only recoverable after demolition	2	Steel edge profiles cast-in and elastomer not reusable	2
Relative Performance - Sustainability		**0,83**		**0,51**		**0,50**		**1,00**
Durability **Weight : 0,10**	**Clarification**	**Rating**	**Clarification**	**Rating**	**Clarification**	**Rating**	**Clarification**	**Rating**
Service Life Weight 0,05		100 years		100 years		100 years		40 years
Inspectability Weight 0,05	Not visible due to fire-resistant cladding; shear key in inner wall visible on one side	2	Fully covered by fire-resistant cladding; connection not visually inspectable	2	Fully embedded in concrete; inspection only possible indirectly via deformations or damage	1	Directly accessible from roadway when closed off; joint profile and steel construction visually inspectable	4
Relative Performance - Durability		**0,75**		**0,75**		**0,63**		**0,70**
Costs **Weight : 0,11**	**Clarification**	**Rating**	**Clarification**	**Rating**	**Clarification**	**Rating**	**Clarification**	**Rating**
Initial costs Weight 0,06		€ 24231		€ 42781		€ 31440		€ 150000
Maintenance costs Weight 0,06		€ 0		€ 0		€ 0		€ 525000
Relative Performance - Costs		**1,00**		**0,93**		**0,97**		**0,00**
Total score	**0,51**		**0,41**		**0,67**		**0,57**	

Q

MCDA Method Validation

This appendix describes the validation tests that were performed to assess the robustness of the applied MCDA methodology. The decision model combines the Analytic Hierarchy Process (AHP) method and the Technique for Order Preference by Similarity to Ideal Solution (TOPSIS) method. Four validation tests were performed:

- Sensitivity analysis of the AHP-derived weights
- Replacement of AHP by the Preference Selection Index (PSI)
- Replacement of TOPSIS by the Weighted Sum Model (WSM)
- Replacement of TOPSIS by the VIKOR method

The objective of these validation tests is to assess the extent to which the final ranking of the alternatives depends on the selected weighting method and ranking method. For each analysis, the same alternatives and assessment scores from the original decision model were used.

Q.1. Sensitivity Analysis

To assess the influence of the applied AHP weights on the final ranking, a sensitivity analysis was performed. Several weighting scenarios were considered for this purpose. Table Q.1 provides an overview of the weights applied in each scenario. The corresponding results are presented in Table Q.2.

Table Q.1: Weighting scenarios applied in the sensitivity analysis

Scenario	Robustness	Modeling Reliability	Feasibility	Sustainability	Durability	Costs
Equal weights	16.67%	16.67%	16.67%	16.67%	16.67%	16.67%
Costs dominant	18.31%	3.44%	17.94%	5.20%	11.41%	43.71%
Durability dominant	18.31%	3.44%	17.94%	5.20%	43.71%	11.41%
Sustainability dominant	18.74%	3.44%	18.49%	41.82%	11.67%	5.84%
Feasibility dominant	22.92%	3.93%	41.21%	5.92%	12.23%	13.78%
Robustness dominant	41.21%	3.93%	22.92%	5.92%	12.23%	13.78%
Modeling reliability dominant	18.21%	42.55%	18.59%	4.41%	6.42%	9.81%

Table Q.2: Results of the sensitivity analysis for the alternative weighting scenarios

Scenario	Shear Key	Collar Connection	Dowel Connection	Free-Settlement Joint
Equal weights	**0.67**	0.55	0.59	0.46
Costs dominant	0.85	0.80	**0.86**	0.19
Durability dominant	0.54	0.51	0.45	**0.58**
Sustainability dominant	0.58	0.27	0.35	**0.73**
Feasibility dominant	0.52	0.42	**0.70**	0.57
Robustness dominant	0.60	0.51	**0.65**	0.47
Modeling reliability dominant	0.55	0.33	0.40	**0.66**

Q.2. AHP Replaced by PSI

The Preference Selection Index (PSI) is an objective weighting method in which the criterion weights are derived directly from the normalized decision matrix. Unlike the AHP method, no expert judgments are required. Criteria with a high discriminating power between the alternatives are automatically assigned a higher weight [7]. After normalizing the assessment criteria, the preference variation is determined for each subcriterion:

$$PV_j = \sum (r_{ij} - \bar{r}_j)^2 \tag{Q.1}$$

The preference deviation is determined as follows:

$$\delta_j = 1 - PV_j \tag{Q.2}$$

The resulting preference deviations are used to determine the criterion weights:

$$w_j = \frac{\delta_j}{\sum \delta_j} \tag{Q.3}$$

The resulting PSI weights were applied within the TOPSIS methodology. The results are presented in Table Q.3.

Table Q.3: Comparison between AHP-TOPSIS and PSI-TOPSIS results

Variant	AHP + TOPSIS	PSI + TOPSIS
Shear Key	0.51	0.51
Collar Connection	0.41	0.40
Dowel Connection	0.67	0.54
Free-Settlement Joint	0.57	0.59

Q.3. TOPSIS Replaced by WSM

The Weighted Sum Model (WSM) is a widely used MCDA method in which the final score of an alternative is determined by the weighted sum of all assessment criteria. The criteria are first normalized (r_{ij}) and subsequently multiplied by the AHP weights (w_i) to determine the weighted score for each subcriterion.

$$v_{ij} = w_i \cdot r_{ij} \tag{Q.4}$$

The final score of each alternative was then determined by summing the weighted scores:

$$S_j = \sum w_i \cdot r_{ij} \tag{Q.5}$$

The results of the WSM analysis are presented in Table Q.4.

Table Q.4: Results of the AHP-WSM analysis

Variant	AHP + WSM
Shear Key	0.67
Collar Connection	0.56
Dowel Connection	0.74
Free-Settlement Joint	0.70

Q.4. TOPSIS Replaced by VIKOR

The VIKOR method is an MCDA method that identifies a compromise solution based on both the overall performance of an alternative and its worst-performing criterion [7]. For each criterion, the best and worst performance values were first determined (f_i^* and f_i^-). The weighted distance to the ideal solution was then calculated for each alternative. Based on these values, the Utility Measure (S_j) and Regret Measure (R_j) were determined:

$$\begin{aligned} d_{ij} &= w_i \frac{f_i^* - f_{ij}}{f_i^* - f_i^-} \\ S_j &= \sum d_{ij} \\ R_j &= \max(d_{ij}) \end{aligned} \tag{Q.6}$$

The best and worst values of the Utility Measure and Regret Measure (S^*, S^-, R^*, and R^-) were then determined. Based on these values, the Q-index was calculated:

$$Q_j = v \left(\frac{S_j - S^*}{S^- - S^*} \right) + (1 - v) \left(\frac{R_j - R^*}{R^- - R^*} \right) \tag{Q.7}$$

A value of 0.5 was adopted for the parameter v. This represents an equal balance between the overall performance of an alternative (Utility Measure) and its worst-performing assessment criterion (Regret Measure). The alternative with the lowest Q-value is considered the preferred alternative [7]. The results of the VIKOR analysis are presented in Table Q.5.

Table Q.5: Results of the AHP-VIKOR analysis

Variant	Q-index
Shear Key	0.18
Collar Connection	1.00
Dowel Connection	0.00
Free-Settlement Joint	0.05

The VIKOR score cannot be interpreted in the same way as the TOPSIS or WSM score. The Q-index only reflects the ranking of the alternatives and does not indicate the quality of the alternatives.

Q.5. Conclusion

Table Q.6: Summary of MCDA validation results

Method	Shear Key	Collar	Dowel	Free-Settlement
AHP + TOPSIS	0.51	0.41	0.67	0.57
AHP + WSM	0.67	0.56	0.74	0.70
PSI + TOPSIS	0.51	0.40	0.54	0.59
AHP + VIKOR*	0.18	1.00	0.00	0.05

* VIKOR scores represent the Q-index and are only used to determine the ranking of the alternatives.

The sensitivity analysis and PSI analysis demonstrate that the criterion weights have influence on the final ranking of the alternatives. This is not considered a limitation of the decision model, but rather an inherent characteristic of the applied MCDA methodology. The objective of the model is not to identify a single objectively best tunnel connection, but to determine which alternative best aligns with the project priorities.

The tests show that the preferred alternative changes when the relative importance of the criteria changes. The dowel connection performs best when feasibility and robustness are assigned a high importance, whereas the free-settlement joint becomes the preferred alternative when sustainability, durability or modeling reliability are prioritized. These results confirm that the criterion weights effectively translate project priorities into the decision-making process and therefore have a meaningful influence on the final ranking.

The comparison between TOPSIS, WSM, and VIKOR shows that the choice of ranking method has only a limited influence on the results. The ranking of the two validation analyses is the same as the ranking from the decision model. This indicates that the final ranking is primarily driven by the scoring of the alternatives and the applied criterion weights rather than by the selected ranking method.

The validation tests show that the combination of AHP and TOPSIS provides a reliable methodology for the assessment of the tunnel segment connection concepts considered. The WSM and VIKOR analyses lead to largely consistent results. The PSI analysis and sensitivity analysis demonstrate the influence of alternative criterion weights. This indicates that the final ranking is robust with respect to the selected ranking method and that the influence of the weights is a logical consequence of incorporating project-specific priorities into the decision-making process.